

# **Surface Modification and Conjugation Strategies for Bioassay/ Biomaterial Applications**

A thesis submitted for the degree of Ph.D.

by

Chandra K. Dixit, M.Sc.,

Under the supervision of

Professor Colette McDonagh, Professor Richard O’Kennedy and  
Professor Brian D. MacCraith

Based on research work carried out at

School of Biotechnology,  
Centre for Bioanalytical Sciences,  
and  
National Biophotonics and Imaging Platform,  
Dublin City University,  
Dublin 9, Ireland.

November 2011



**Statement of integrity of work:**

I hereby certify that this material, which I now submit for assessment on the programme of study leading to the award of *Doctor of Philosophy* (Ph.D.) is entirely my own work, that I have exercised reasonable care to ensure that the work is original, and does not to the best of my knowledge breach any law of copyright, and has not been taken from the work of others save and to the extent that such work has been cited and acknowledged within the text of my work.

Signed: Chandra K. Dixit      (Candidate) ID No.: 57119287      Date: November 30, 2011

**Abstract:**

The aims of this research were to develop novel surface modification strategies that can be used on a range of solid supports including polymeric and metallic matrices, as these could have a significant impact on the performance of bio/sensors employing these surfaces. These approaches were used to develop methods for immobilizing biomolecular recognition elements, such as antibodies, on modified matrices, and to exploit these approaches for the generation of high sensitivity bio-assays. Human fetuin A, mouse immunoglobulin G, and horseradish peroxidase were employed as model analytes.

A silane-based surface modification strategy was designed and optimized for planar or flat surfaces such as polymeric sheets, chips or microtitre plates. These polymeric surfaces were activated prior to silane-functionalization using potassium hydroxide (aq.)-mediated mild oxidation (wet method) and oxygen-plasma etching. This novel surface activation strategy was further optimized in combination with surface functionalization and covalent immobilization of antibodies, for enhancing immunoassay sensitivities. Sensitivities obtained for immunoassays using antibodies immobilized with the developed and adsorption-based conventional strategies were 39 and 625 pg/mL, respectively, for human fetuin A. The strategy was demonstrated to be generic in nature and could be employed to activate a wide range of polymeric and metallic surfaces. In addition, highly sensitive detection of human fetuin A was achieved with antibodies captured in an oriented manner on covalently immobilized protein A ( $EC_{50}$  3.7 ng/mL) in comparison to randomly captured antibodies ( $EC_{50}$  5.8 ng/mL).

High-brightness NIR664 dye-doped silica nanoparticles were employed to probe various activation states of platelets. These NPs were functionalized with silanes (*viz.* amine and carboxy-terminal) followed by conjugation to a platelet surface biomarker-specific antibody (anti-CD41) and successfully employed for probing platelet activation. The antibody-NP conjugates were found to be highly sensitive (>95%) and specific ( $\approx$ 100%). In addition, aggregation of NPs was minimized by controlling their surrounding chemical environment and their stability after antibody conjugation.

## Table of contents

Chapter	Section	Page Number
	Abbreviations	i
	Analytical units	v
	Patents, IDFs, Publications and Conference presentations and posters	vi
<b>1</b>	<b>Introduction: Strategies for immobilizing antibody molecules</b>	<b>1</b>
	1.1 Introduction	2
	1.2 Overview of the available immobilization strategies and their implications for conformation-associated functionality	3
	1.2.1 Adsorption of antibody on chemically active surfaces	3
	1.2.2 Covalent immobilization of antibody on functionalized surfaces	16
	1.2.2.1 Direct chemistries for antibody capture	16
	1.2.2.2 Linker-mediated strategies to capture antibody	23
	1.2.3 Site-specific immobilization of antibody	27
	1.2.3.1 Affinity tag-based site directed antibody capture	27
	1.2.3.2 Enzyme-substrate reaction-based site-directed antibody capture	33
	1.2.4 Site-specific orientation-based antibody capture	38
	1.3 Conclusions and Perspectives	39
	1.4 References	48
	1.5 Aims and Approach	71
<b>2</b>	<b>Development of a modified high sensitivity rapid sandwich ELISA procedure with picogram sensitivity</b>	<b>72</b>
	2.1 Abstract	73
	2.2 Introduction	74
	2.3 Materials	75
	2.4 Experimental Section	77
	2.4.1 Microtitre plate functionalization with amine silane and anti-human fetuin A antibody immobilization	77
	2.4.2 ELIA on anti-human fetuin A antibody-immobilized microtitre plates	78
	2.5 Results and Discussion	79
	2.5.1 Developed ELIA and conventional ELISA formats for human fetuin A detection	79
	2.5.2 Generic nature of the developed sandwich ELISA procedure on different substrates	83
	2.6 Conclusions	85
	2.7 References	85

<b>3</b>	<b>Evaluation of apparent non-specific protein loss due to adsorption on sample tube surfaces and/ or altered immunogenicity</b>	<b>88</b>
3.1	Abstract	89
3.2	Introduction	90
3.3	Materials	91
3.4	Experimental	92
3.4.1	Tube blocking	92
3.4.2	Sampling	93
3.4.3	Analytical techniques	93
3.4.4	Theory and analysis	94
3.5	Results	97
3.5.1	Evaluation of protein loss in unblocked polypropylene tubes	97
3.5.2	Effect of tube blocking on protein analyte loss	102
3.5.3	Evaluation of the contribution of human fetuin A fraction with conformation-related impaired immunogenicity	103
3.5.4	Evaluation of the signal loss due to the nature of the tube material	106
3.6	Conclusion	108
3.7	References	108
<b>4</b>	<b>Effect of antibody immobilization strategies on the analytical performance of a surface plasmon resonance-based immunoassay</b>	<b>114</b>
4.1	Abstract	115
4.2	Introduction	116
4.3	Materials	118
4.4	Methods	120
4.4.1	Surface cleaning of SIA Au chip and APTES functionalization	120
4.4.2	EDC activation of anti-HFA antibody	121
4.4.3	Immobilization of anti-HFA antibody	121
4.4.4	Covalent-CM5-dextran immobilization strategy	122
4.4.5	HFA-detection	123
4.4.6	Complete regeneration of the APTES-functionalized gold surface	123
4.4.6.1	Siloxane bond lysis by acid treatment and O <sub>2</sub> -plasma	123
4.4.6.2	SPR-based HFA immunoassay procedure	124
4.4.6.3	SPR-based reproducibility analysis of antibody immobilization on the regenerated Au chips	125
4.5	Results	125
4.5.1	Comparison of antibody immobilization strategies as a function of antibody immobilization density	125
4.5.2	Comparison of antibody immobilization strategies as a function of HFA capture densities	131

4.5.3	Regeneration studies of the APTES-functionalized Au surface	133
4.6	Conclusion	138
4.7	References	139
<b>5</b>	<b>Development of conjugates of dye-doped silica nanoparticles and anti-CD41 antibody for efficient platelet probing</b>	<b>145</b>
5.1	Abstract	146
5.2	Introduction	147
5.3	Materials	148
5.4	Methods	149
5.4.1	Synthesis of dye-doped nanoparticles	149
5.4.2	Amine-silanization of the nanoparticles	150
5.4.3	Bioassay performance to determine the efficiency of the antibody- nanoparticle conjugation	150
5.4.4	Characterization of the aminated nanoparticles	151
5.4.4.1	Zeta potential measurement	151
5.4.4.2	Fourier Transform Infra Red spectroscopic studies	151
5.4.4.3	Miscellaneous physical characterization approaches	152
5.4.5	Antibody conjugation to nanoparticles and characterization	152
5.5	Results	153
5.5.1	Zeta potential measurement to measure surface charge	153
5.5.2	Confirmation of the amine-functionalization of silica nanoparticles by Fourier Transform Infra Red spectroscopic measurement	154
5.5.3	Antibody conjugation and bioassay performance	158
5.6	Conclusion	160
5.7	References	161
<b>6</b>	<b>Analysis and reduction of process-induced aggregation of NIR-664 dye-doped silica nanoparticles</b>	<b>165</b>
6.1	Abstract	166
6.2	Introduction	167
6.3	Materials	169
6.4	Methods	169
6.4.1	Defining aggregation tendency in terms of zeta potential	169
6.4.2	Nanoparticle functionalization	170
6.4.2.1	Functionalization with amino-silane	170
6.4.2.2	Functionalization with carboxy-silane	170
6.4.3	Storage stability	171
6.4.3.1	Effect of solvent	171
6.4.3.2	Effect of nanoparticle incubation at different pHs	171
6.4.3.3	Effect of antibody cross-linking strategy and surface blocking methods	171
6.4.3.3.1	Amine surface blocking strategy for antibody-cross-linked-amine-functionalized nanoparticle adducts	171
6.4.3.3.2	Carboxy surface blocking strategy for antibody-cross-linked-carboxy-functionalized nanoparticle adducts	172

6.4.4	Characterization of nanoparticle stability using Surface charge (zeta potential) measurement	173
6.5	Results and Discussion	174
6.5.1	Effect of solvent	174
6.5.2	Effect of pH	177
6.5.3	Effect of antibody crosslinking	179
6.6	Conclusion	182
6.7	References	184
<b>7</b>	<b>Conclusions and future work</b>	<b>188</b>
7.1	Conclusions	189
7.1	Sorting nanoparticles as a function of their charge using a self-developed sorter	191
7.2	Replacing ethylenediamine (EDA) with ethanolamine (EA)	192
7.3	Gradual centrifugation as an aggregate sorting procedure	192
<b>8</b>	<b>Appendix I – Publication list</b>	<b>193</b>

## Abbreviations

Ab	Antibody
AFM	Atomic force microscopy
Ag	Antigen
APTES	Aminopropyltriethoxysilane
AU	Arbitrary unit
Au	Gold
Au NP	Gold nanoparticle
BMS	Bristol Myers Squibb
BSA	Bovine serum albumin
CA	Cellulose acetate
CBD	Chitin-binding domain
CD	Cluster of differentiation
CHOP	Chinese hamster ovary protein
CM	Carboxy methyl
CV	Coefficient of variation
Cy5	Cyanine 5 fluorescent dye
DIW	Deionized water (18 mega ohms)
DLVO	Derjaguin, Landau, Verwey and Overbeek (in DLVO theory)
DRP	Domain recognition protein
DTT	Dithiothreitol
EC <sub>50</sub>	Half-maximal effective concentration

EDA	Ethylenediamine
EDC	1-ethyl-3-[3-dimethylaminopropyl]carbodiimide
EDTA	Ethylenediamine tetra-acetic acid
ELIA	Enzyme-linked immunoassay
ELISA	Enzyme-linked immunosorbent assay
ELP	Elastin-like polypeptide
Fc	Fragment constant region (of antibody)
FIA	Fluorescence immunoassay
FCS	Fluorescence correlation spectroscopy
FLCS	Fluorescence lifetime correlation spectroscopy
FT-IR	Fourier transform infrared spectroscopy
hAGT	Human O <sup>6</sup> -alkylguanine transferase
H <sub>2</sub> O <sub>2</sub>	Hydrogen peroxide
H <sub>2</sub> SO <sub>4</sub>	Sulfuric acid
HBS	HEPES-buffered saline
HCl	Hydrochloric acid
HEPES	2-[4-(2-hydroxyethyl)-1-piperazinyl]ethanesulfonic acid
HFA	Human fetuin A
HRP	Horseradish peroxidase
Ig	Immunoglobulin
IgG	Immunoglobulin G
IR	Infrared
<i>k<sub>L</sub></i>	Kappa-light

KOH	Potassium hydroxide
KPR	KOH to polymer ratio
LOB	Limit of blank
LOD	Limit of detection
MES	2-(N-morpholino)ethanesulfonic acid
N	Avogadro's number ( $6.02 \times 10^{23} \text{ mol}^{-1}$ )
NaCl	Sodium chloride
NHS	N-hydroxysuccinimide
N/S	Noise to signal ratio
NTA	Nitriloacetic acid
PBS	Phosphate buffered saline
PC	Polycarbonate
PEG	Polyethylene glycol
PHA	Polyhydroxyalkanoate
PLL	Poly-L-lysine
PMMA	Polymethylmethacrylate
PNA	Peptide nucleic acid
PrA	Protein A
PS	Polystyrene
PSA	Pressure sensitive adhesive
PSBD	Polyhydroxyalkanoate depolymerase substrate-binding domain
QCM	Quartz crystal microbalance
$r^2$	Correlation coefficient

RBS	Rutherford back scattering
RT	Room temperature
$\rho$	Immobilization density
RU	Response unit (SPR studies)
SA	Streptavidin
scFv	Short chain fragment variable (of antibody)
SAM	Self-assembled monolayer
SD	Standard deviation
Si	Silica
SIA	Surface interaction analysis
Si NP	Silica nanoparticle
S/N	Signal to noise ratio
SNHS	Sulfo-N-hydroxysuccinimide
SPR	Surface plasmon resonance
TCEP	Tris(2-carboxyethyl)phosphine
TGase	Transglutaminase
TMB	3,3',5,5'-tetramethyl benzidine
UPW	Ultra pure water
UV	Ultra violet
Vis	Visible
ZnX	Zeonex

## **Analytical Units**

<b>Abbreviation</b>	<b>Full detail</b>
s	Second (time)
min	Minute (time)
h	Hour (time)
psi	Pounds per square inch (pressure)
J	Joule (energy)
mJ	milli-Joule (energy)
M	Molarity (concentration)
N	Normality (concentration)
µg/mL	Microgrammes per millilitre (concentration)
ng/mL	Nanogrammes per millilitre (concentration)
mm <sup>2</sup>	Millimetre square (area)
cm	Centimetre
Ω	Ohms (resistance)

## **Patents**

1. **Modified ELISA plate technology** (Published patent number: **WO2010/044083 A2**; DCU Ref: 2008/07/DCU/BT/CBAS): ‘Product and method relating to the multi-well plate for biological assays, in particular, the invention relates to a multiwall plate for enzyme linked immunosorbent assays and a method for preparing such plates’. DCU Ref: 2008/07, **European Application No. 08394037.9** filing date 14 Oct, 2008.

**Contributors:** Sandeep K. Vashist, Stephen O’Sullivan, Feidhlim O’Neill, **Chandra K. Dixit**, Brian O’Reilly, Harry Holthofer.

## **PUBLICATIONS**

### **Published:**

1. **Chandra Kumar Dixit**, Sandeep Kumar Vashist, Feidhlim O’Neill, Brian O’Reilly, Brian MacCraith, and Richard O’Kennedy. Development of a high sensitivity rapid sandwich ELISA procedure and its comparison with the conventional approach *Analytical Chemistry* **2010**, 82, 7049–7052. (**IF: 5.84**)
2. Shibshekhar Roy, **Chandra Kumar Dixit**, Robert Wolley, Brian MacCraith, Richard O’Kennedy, and Colette McDonagh. Novel multiparametric approach to elucidate the surface amine-silanization reaction profile on fluorescent silica nanoparticles *Langmuir* **2010**, 26(23), 18125-18134. (**IF: 4.26**)
3. **Chandra Kumar Dixit**, Sandeep Kumar Vashist, Brian MacCraith, and Richard O’Kennedy. Evaluation of apparent non-specific protein loss due to adsorption on

- sample tube surfaces and/ or altered immunogenicity *Analyst* **2011**, 136(7), 1406-1411. (IF: 3.91)
4. **Chandra Kumar Dixit**, Sandeep Kumar Vashist, Brian MacCraith and Richard O’Kennedy. Multi-substrate compatible ELISA procedures for rapid and high sensitivity immunoassays *Nature Protocol* **2011**, 6, 439-445. (IF: 8.36)
  5. Ram Prasad Gandhiraman, Nam Le, **Chandra Kumar Dixit**, Cedric Volcke, Colin Doyle, Vladimir Gubala, Suresh Uppal, Richard O’Kennedy, Stephen Daniels, and David E Williams. Multi-layered plasma polymerized chips for SPR-based detection. *Applied Material Interfaces*. 2011. DOI: 10.1021/am201061k (IF: 2.92)
  6. Sandeep Kumar Vashist, **Chandra Kumar Dixit**, Brian McCraith, and Richard O’Kennedy. Effect of antibody immobilization strategies on the analytical performance of a surface plasmon resonance immunoassay. *Analyst* **2011**, 136(21), 4431-4436. (IF: 3.91)
  7. Shibshekhar Roy, **Chandra Kumar Dixit**, Robert Wolley, Richard O’Kennedy, and Colette McDonagh. Label-free optical characterization methods for detecting amine silanization-driven gold nanoparticle self-assembly. *Langmuir* **2011**, 27(17), 10421-10428. (IF: 4.26)

#### **PRESENTATIONS (\*) AND POSTERS**

1. \*Sandeep Kumar Vashist, Feidhlim O’Neill, **Chandra Kumar Dixit**, Brian O’Reilly, Barry Byrne, Gerard O’Donohoe, Richard O’Kennedy, and Brian MacCraith. Novel approaches for advanced bioanalytical platforms; *International Conference on Trends in Bioanalytical Sciences and Biosensors (ICTBSB)* **2009**, Dublin, Ireland, January 26-27.

2. **Chandra Kumar Dixit**, Sandeep Kumar Vashist, Brian MacCraith, and Richard O’Kennedy. Development of novel strategies for antibody immobilization on agarose beads; *NCSR 10<sup>th</sup> Anniversary symposium 2009* NCSR, Dublin City University, Dublin, Ireland, October 22.
3. **Chandra Kumar Dixit**, Sandeep Kumar Vashist, Brian O’Reilly, Brian MacCraith, and Richard O’Kennedy. Development of highly sensitive antibody-coated microarray platforms for diagnostics and bioanalytical applications; *International conference on sensors and related networks (SENNET) 2009*, VIT Univ. Vellore, India, December 8-10.
4. **Chandra Kumar Dixit**, Sandeep Kumar Vashist, Brian MacCraith, and Richard O’Kennedy. Novel gold (Au)-chip modification strategy to immobilize antibody for surface plasmon resonance (SPR)-based platforms; *EUROPT(R)ODE X - A conference on optical chemical sensors and biosensors 2010*, Prague, Czech Republic, March 28-31.
5. **Chandra Kumar Dixit**, Shibsekhar Roy, Robert Woolley, Una Prendergast, Richard O’Kennedy, Colette McDonagh, Dye-doped silica nanoparticles as high-brightness probes: A study with Platelet-CD41 as model antigen system; *3<sup>rd</sup> Bangalore Nano 2010*, JNCASR, Bangalore, India, December 8-9.

# **Chapter 1**

## **Introduction**

Strategies for immobilizing antibody  
molecules

## 1.1 Introduction

Antibodies are glycoproteins that belong to the immunoglobulin super family [1]. An antibody is a homo-dimer molecule composed of two heavy and two light chains with a molecular weight of approximately 150 kD. The heavy chains are attached together by disulfide bonds and a disulfide bond also links them to their corresponding light chains. Each antibody contains a constant domain (Fc) and an antigen-binding domain (Fab). The amino terminal region of the Fab domain is hyper-variable and responsible for antigen recognition and specificity. A typical antibody (IgG2) with all the available functional groups is depicted in **Figure 1.1**.

The antibody and its isotypes are important components of the immune system; they are present either in soluble form or as membrane-bound surface receptors on B-cells. These antibody molecules occur naturally in the plasma. However, with advances in molecular biology they can be also developed as recombinant antibodies in bacterial and expression systems.

A monoclonal antibody is highly specific and binds to a single defined region or epitope on an antigen; whereas, polyclonal antibody preparations consist of a mixture of antibodies and can recognize a wide range of antigens or multiple epitopes on a single antigen.

There are variants of antibody structure (other than IgG) such as Fab (fragment antigen-binding unit) and scFv (short chain fragment variable) which may be generated by chemical or genetic approaches [2-4]. A range of different 'antibody-like' entities, also known as nanobodies or single-domain antibodies, exist [5]. These single-domain antibodies are generally obtained from camels and fish, particularly shark. These are smaller in size in comparison to the naturally occurring whole antibodies and possess

comparative affinities for antigen molecules. These smaller sized variants could also provide certain advantages for immunoassays and for *in-vitro* studies.

Antibodies, due to their high antigen specificity and affinity, [6,7] can make excellent probes and, therefore, have multiple applications in many fields of biological research such as biosensors and diagnostics. The development of these bioanalytical detection systems requires antibody immobilization on various solid supports. Therefore, a precise knowledge of the chemical and functional properties of an antibody, along with the chemical nature of the solid supports that will be employed to capture antibody, is essential for designing a suitable immobilization strategy. Strategies that allow the retention of functional conformation of the antigen binding sites of antibody molecules are essential and can be achieved by site-specific and orientated presentation of the antibodies on the surface used for immobilization [3,8]. However, the information pertaining to the development of an understanding of controlled immobilization is limited. In addition, the susceptibility of antibody to the loss of functional conformation and specificity due to steric hindrance [9,10] or molecular flattening and spreading [11-16] have restricted the development of highly sensitive immunoassay strategies.

In this introduction, antibody immobilization strategies (Table 1.1 and 1.2), particularly tag-assisted [17,18] and domain-specific protein-mediated methodologies [19-21], will be critically analyzed in terms of their efficiency, capability of capturing antibody in a site-directed fashion and their suitability for immunoassay development.

## **1.2 Overview of the available immobilization strategies and their implications for conformation-associated functionality**

### **1.2.1 Adsorption of antibody on chemically active surfaces**

Adsorption is a process of adhesion of biomolecules on surfaces as a consequence of net free energy change ( $\Delta G$ ), which must be negative in magnitude. This  $\Delta G$  may be entropy

or enthalpy driven [24]. Entropy, which is governed by second and third law of thermodynamics, is a state function of a thermodynamic system that describes the

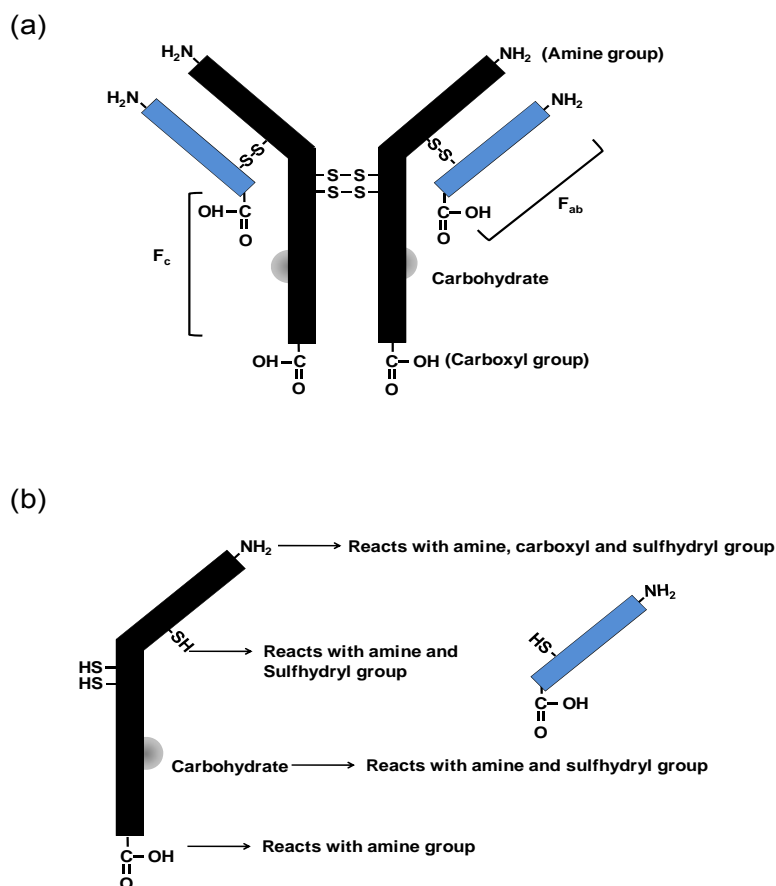


**Figure 1.1** (a) Model of a typical IgG with the available functional groups. An antibody consists of two heavy (black bars) and two light (blue bars) chains. Each chain has carboxyl (-COOH) and amine (-NH<sub>2</sub>) groups, which are contributed by terminal and internal amino acids. Both the heavy chains are linked together with two disulfide bridges at the hinge region. Similarly, each light chain is linked to its respective heavy chain through a disulfide bridge. (b) Reactive functional groups present on the heavy and light chains of an antibody. Amine and carboxyl groups are the only reactive functional groups present in an antibody in its native state. Sulfhydryl groups can be generated after reducing the disulfide bonds of an antibody with DTT or TCEP. Carbohydrates in the Fc section can be activated by periodate treatment [22,23].

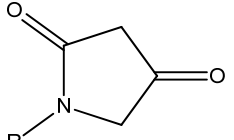
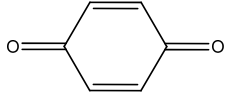
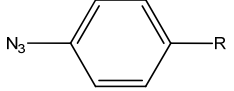
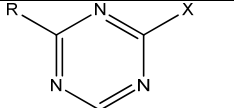
**Table 1.1.** Details of commonly employed antibody modification strategies for conjugation/ immobilization

Strategy for Antibody Modification	Target Functional Group/ Point of Modification	Reaction
Activation of carbohydrates by oxidation with sodium ( $\text{NaIO}_4$ )/potassium periodate ( $\text{KIO}_4$ )	Hydroxyls of carbons at position 3 and 4 in the sugar ring of carbohydrate, which is present in the Fc region of antibodies	$>\text{CH}(\text{OH}) - \text{C}(\text{OH})< \rightarrow 2(-\text{CHO})$
Alkylation by reduction	(a) disulfide bonds (-S-S-)  (b) amines of lysine (-NH <sub>2</sub> )	(a) <b>disulfide bonds:</b>  (Step 1) -S-S- (DTT/ TCEP) $\rightarrow$ -SH + -SH (Step 2) -SH + Alkylating agent $\rightarrow$ -S-alkane  (b) <b>lysine:</b>  -NH <sub>2</sub> + Alkylating agent $\rightarrow$ -NH-alkane
Acetylation	$\alpha$ -NH <sub>2</sub> of the protein located at the N-terminal	$\text{CH}_3\text{COOCH}_3 + \alpha\text{-NH}_2\text{-PROTEIN} \rightarrow \text{CH}_3\text{CO-NH-PROTEIN}$
(a) Chlorination/ tosylation (Tresyl and Tosyl chloride derivatives Fig. 1.4)	hydroxyl group (-OH)	$\text{CH}_3\text{C}_6\text{H}_4\text{SO}_2\text{Cl} + \text{PROTEIN-OH} \rightarrow \text{CH}_3\text{C}_6\text{H}_4\text{SO}_2\text{-O-PROTEIN} + \text{HCl}$
(b) Sulfonamidation (Tresyl and Tosyl chloride derivatives Fig. 1.4)	amine groups (-NH <sub>2</sub> 1°, 2°)	$\text{CH}_3\text{C}_6\text{H}_4\text{SO}_2\text{Cl} + \text{PROTEIN-NH}_2 \rightarrow \text{CH}_3\text{C}_6\text{H}_4\text{SO}_2\text{-NH-PROTEIN} + \text{HCl}$

**Table 1.2.** Available functional groups on the antibody and surface and their chemical reactivity toward each other.

<div> <div>Functional group on antibody</div> <div>Functional group on surface</div> </div>	Ab-NH <sub>2</sub>	Ab-SH	Ab-COOH	Ab-CHO	Ab-OH	Ab-Histidine	Ab-Tyr	Ab-Trp	Ab-Arg	Ab-Meth	Selectivity
RNH <sub>2</sub> Amine	×	×	×	+							
RNHNH <sub>2</sub> Hydrazine	×	×	×	+							
RN=NH Diazine	P	P	+		P		+				NS
$\text{R}-\overset{\text{O}}{\underset{\text{O}}{\text{C}}}-\text{Cl}$ chloride	+				+	H	H				
$\text{R}-\overset{\text{O}}{\underset{\text{O}}{\text{C}}}-\text{H}$ Aldehyde	+	+				+	+				
$\text{H}-\overset{\text{O}}{\underset{\text{O}}{\text{C}}}-\text{H}$ Formaldehyde	+	+				+	+	+	+		
									+		

$\begin{array}{c} \text{R}-\text{C}-\text{C}-\text{R} \\ \parallel \quad \parallel \\ \text{O} \quad \text{O} \end{array}$ Biacetyl											
$\begin{array}{c} \text{R}-\text{C}-\text{O}-\text{C}-\text{R} \\ \parallel \quad \parallel \\ \text{O} \quad \text{O} \end{array}$ Anhydride	+				+	H	H				
$\begin{array}{c} \text{R}-\text{C}-\text{CH}_2\text{X} \\ \parallel \\ \text{O} \end{array}$ Halo-ketone	+	+				+	+	+		+	
$\begin{array}{c} \text{R}-\text{SH} \\ \text{Thiol} \end{array}$	xx	x, +		+							
$\begin{array}{c} \text{O} \\ \parallel \\ \text{R}-\text{S}-\text{X} \\ \parallel \\ \text{O} \end{array}$ Sulfonyl halide	+	+				+	+	+			
$\begin{array}{c} \text{Ar}-\text{X} \\ \text{Argon halide} \end{array}$	+	+				+	+				
$\begin{array}{c} \text{O} \\ \diagup \quad \diagdown \\ \text{R}-\text{C} \quad \text{C} \\ \diagdown \quad \diagup \end{array}$ Epoxide	+	+	+		+	+	+				
$\begin{array}{c} \text{NH} \\ \diagup \quad \diagdown \\ \text{R}-\text{C} \quad \text{C} \\ \diagdown \quad \diagup \end{array}$ Aziridine	+	+								+	

 Pyrrolidine-2,4-dione	+				+	+					
 Benzoquinone	+	+			+			+			
 Azidobenzene	P	P			P	P	P	P			NS
 Triazine	+				+						

R Alkyl or aromatic group of the main carbon backbone

X halogen group

× Homo-bifunctional crosslinker required

×× Hetero-bifunctional crosslinker required

+ High reactivity towards each other

×, + High reactivity towards each other but can also react through a homobifunctional crosslinker

P Photoactivation required for reaction

NS Non-selective reaction

H Strong tendency for hydrolysis

Blank boxes indicate that no interaction is possible between the corresponding moieties

Prefix 'Ab' in the first row of table represents antibody followed by the functional group on the antibody involved in the reaction with the chemical groups listed in the first column of the table.

disorderliness or uncertainty within matter. In addition, entropy is a measure of the amount of energy that cannot be used to perform work. According to the laws governing thermodynamics, entropy of an isolated system can never decrease assuming the system is in its ground energy state. Therefore, thermodynamically a certain amount of entropy is always possessed by a system at any given time and this governs the reactivity of that system [25]. However, considering that matter is in dynamic state with its surroundings, the amount of entropy in a given system could either increase or decrease according to the nature of the body with which given system is interacting. The change in entropy ( $\Delta S$ ) describes the nature of the thermodynamic reaction undergone by the system in a dynamic state such that the given system is, either stabilized by losing its entropic contents, or destabilized by gaining entropy from the surroundings [26]. Enthalpy is the total energy content of a system that is required to maintain its physical and chemical form [26]. The change in enthalpy ( $\Delta H$ ) of a given system governs the conformational and functional stability of the proteins in the given surroundings. There is always a continuum between enthalpy and entropy, which is known as enthalpy-entropy compensation [25]. This compensation is the mathematical relation between both of these thermodynamic parameters and is described in the following equation as Gibb's free energy change ( $\Delta G$ ),

$$\Delta G = \Delta H - T \Delta S$$

where,

$\Delta G$ : Gibb's free energy change,  $\Delta H$ : enthalpy,  $T$ : temperature of the whole system, and  $\Delta S$ : entropy.

It can be seen from this equation that a linear rise in enthalpy and entropy will not change the free energy of the system and, therefore, no change in the chemical or physical parameters will be observed. However, an increase in enthalpy without

changing entropy of the system will introduce structural and chemical changes in the given system. Therefore, this enthalpy-entropy compensation is the most important and basic thermodynamic expression that governs every physical or chemical change that matter undergoes.

An antibody in solution continuously interacts with the solvent, the surface and other antibody molecules present in solution. Hydrophobic, van der Waals, and ionic interactions prevail in antibody-solvent interactions [27]. Hydrogen bonding could also be present depending on the chemical nature of the solvent [28,29]. These antibody-solvent interactions are in dynamic state, where new interactions are continuously formed replacing the previous interactions. On account of system thermodynamics, this interaction dynamics is directly regulated by  $\Delta S$  and  $\Delta H$ , as described previously [24]. Similarly, interaction of an antibody with other antibody molecules follows the ‘antibody-solvent’ type of interaction behaviour in terms of basic thermodynamics such that  $\Delta S$  and  $\Delta H$  govern the antibody self-interaction process. Hydrophobic, van der Waals, ionic and coordinate bonding types of interactions are predominant when an antibody interacts with a surface. Therefore, it could be inferred that antibody interactions are in dynamic state with their surroundings and are not isolated events. This suggests that the entropy of the antibody interactions with surface could therefore, either increase or decrease according to their surroundings such as temperature, pH, nature of solvent and nature of the chemicals used [30]. In addition, the chemical composition of an antibody also significantly affects its thermodynamic properties [31]. Therefore, adsorption of antibody could be either driven by enthalpy or entropy depending on which of these two components is predominant in the given system [31,32].

Entropy-based adsorption mainly favours hydrophobic interactions where the adsorption is achieved by the release of water of hydration [24,33]. Enthalpy-based adsorption

mainly leads to hydrophilic, weak van der Waals and electrostatic interactions along with hydrogen bonding [24]. All these interactions that play important roles in adsorption are mainly governed by the surface energy of either the solid support or the antibody. A subtle change in  $\Delta G$  can significantly change the surface energy of an antibody or solid support. This change in the surface energy affects the number of these interactions and hence the stability of the adsorption of an antibody molecule on the surface. The conformation of an antibody is stabilized by various weak interactions. Thermodynamically, a subtle change in the number of these weak interactions could lead to conformational and structural changes [12,13,34,35].

There are two different types of adsorption i.e. physisorption and chemisorptions, such that the critical energy threshold between binding energies of physisorption and chemisorptions is about 0.5 eV. Physisorption involves mainly weak van der Waals forces and hydrophobic interactions. As mentioned previously, these interactions may be entropic or enthalpic in origin. Hydrophobic interactions develop when hydrophobic pockets are generated around pendant non-polar groups of an antibody on their exposure to water in the solution [24] and are described elsewhere [36]. The exposure of non-polar groups to water results in repulsion of the non-polar groups due to hydrophobicity [37,38]. Similarly, the interaction of hydrophobic clusters on the surface of solid support also follows the same interaction behaviour. However, the hydrophobic clusters on the surface of solid support are rigid and therefore have a tendency to repel water without changing their position, whereas, an antibody is in a dynamic state with water and repulsion is experienced by both the interacting partners, i.e. antibody and water. The interaction with water of these non-polar groups on antibody and surface, therefore, creates hydrophobic pockets in the system. The generation of these pockets increases the entropy of the system because the bonds between water-to-water molecules, which

surround the system, have to rearrange in order to stabilize the system. Therefore, to reduce the overall entropy, the hydrophobic pockets on the antibody come together such that antibody comes into close proximity with the surface of the solid support. In addition, since antibody molecules have hydrophobic pockets, these pockets will also tend to interact with each other. The close proximity of antibody with the surface facilitates a range of interactions between them. However, the interaction of antibody molecules with each other may result in temporary self-aggregation. An increase in the number of these interactions thus, increases the enthalpy of the system following the entropy-enthalpy compensation law [25]. This increase in the enthalpy of the system decreases the entropy and favours the physisorption. Additionally, the interaction of non-polar groups of the antibody with the surface may lead to the loss of water of hydration from antibody, which could, in turn, adversely affect the overall structural stability of the antibody. These interactions are suitable for immobilizing antibody on hydrophobic surfaces such as polystyrene, fluorocarbon polymers etc.

Chemisorption is the process whereby an antibody is adsorbed on the surface by forming electrostatic interactions and/or dative bonds with it. The basic mechanism of chemisorption is similar to physisorption where the initial antibody-surface interaction is controlled by weak forces. However, in case of chemisorption, the major stabilization of antibody-surface interactions is achieved by chemical reactions performed in a specific  $\Delta G$  range, which is depicted as the chemisorption potential. Chemisorption also follows the previously explained rules of thermodynamics [24,39]. Antibody immobilization on positively charged surfaces, such as polyaniline or poly-L-lysine films, by the means of electrostatic interaction, is an example of an ionic ‘binding-type’ chemisorption (**Figure 1.2**). In addition, certain functional groups on an antibody (such as thiols (-SH) and amines (-NH<sub>2</sub>)) have an inherent capacity to make co-ordinate or dative bonds with

metals or metal-coated surfaces [40,41] and this is referred to as dative ‘chemistry-type’ chemisorption.

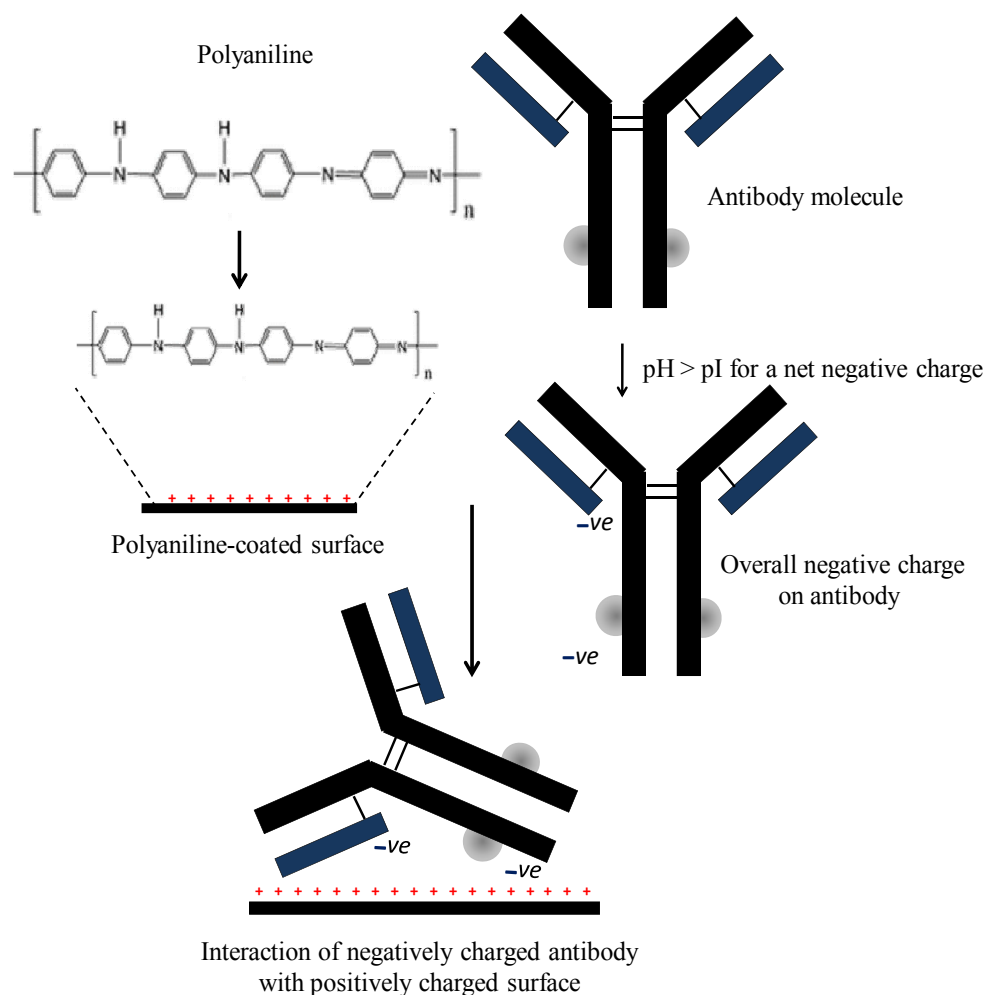


**Figure 1.2** Role of electrostatic interactions in antibody immobilization. An antibody will attain a net negative charge at a pH higher than its pI. A buffer, such as a carbonate buffer, with a pH of  $\sim 10$ , will introduce a net negative charge on the antibody. Antibody molecules may then be immobilized on positively charged surfaces by ionic/ electrostatic interactions. The polyaniline-coated surface in this figure represents a positively charged surface.

Adsorption is a complex phenomenon that is governed by numerous factors such as the shape, structural complexity and chemical properties of antibodies. The solubility and self-association of antibodies also plays an important role in achieving efficient adsorption [42,43]. Solubility of antibody in a given solvent strictly depends on the polarity of the solvent, where, solvents are categorised as polar, non-polar and neutral. Typically, antibodies present in highly polar solvents have a higher tendency to develop hydrophobic pockets in comparison to when in non-polar solvents. The higher the number of such hydrophobic pockets on the antibody, the higher will be the propensity of an antibody to develop hydrophobic interactions and, hence, the greater the adsorption of antibodies on the surface of the solid supports [24].

The chemical nature of the surface also plays an important role in adsorption-based antibody immobilization. Adsorption, being favoured by hydrophobic interactions, is better on hydrophobic surfaces. However, a few reports claim comparable adsorption of antibodies on hydrophilic and hydrophobic surfaces [44]. Short chain Fv (scFv) antibodies were also reported to be successfully adsorbed on hydrophilic polymer-coated glass slides [45] and custom-synthesized mesoporous silicates [46] with restricted loss of binding capacity. In addition, the physisorption of antibodies is partially reversible from hydrophilic surfaces when highly non-polar solvents are used. This is the case because a highly non-polar solvent can significantly reduce the number of hydrophobic pockets on an antibody following a conformational rearrangement [47]. This reversible antibody adsorption may also be controlled by other factors such as the introduction of water of hydration. The antibody after adsorption loses its water of hydration, which is initially bound to the biomolecules. However, non-polar solvents may re-introduce water in the adsorbed antibodies rendering them more hydrophilic. This hydration-induced hydrophilicity could play a crucial role in reversible adsorption.

Adsorption is a simple method of antibody immobilization, which makes it the preferential choice when developing certain immobilization-based immunoanalytical methods such as ELISA. However, there are some drawbacks associated with adsorption such as conformation-associated activity loss [13,34,48,49], and antibody leaching off the surface [50]. In addition, uncontrolled orientation, and random antibody packing on the surface, are other major drawbacks that may occur [51]. These processes are responsible for steric hindrance compromising antigen recognition ability of antibodies [52-54]. However, the problem of random orientation of antibody can effectively be overcome by employing an adsorbed sub-layer of capture proteins that leads to controlled and systematic capture of antibody molecules in an active binding orientation. Hence, a homogeneous molecular packaging of antibody over the surface can be achieved. The most commonly employed capture proteins include Fc-binding molecules such as protein A (prA) [55], G [56] and the *kappa*-light ( $k_L$ )-specific protein L [57], which can bind to specific regions on an antibody, and hence allowing them to be better orientated. Anti-antibodies could also serve as a capture stage for directed capture of a desired antibody on a given surface. Anti-tag capture methods also employ anti-tag antibodies such as anti-HIS antibody [58] and others, which are listed in **Table 1.3** (page 40 et seq). In addition, hapten-conjugated antibody/fragments could be immobilized on anti-hapten-antibody-pre-adsorbed surfaces [19].

Protein exchange [59] is another phenomenon observed in adsorbed antibody systems. Adsorbed antibody has a tendency to interact with proteins present in solution. These interactions of an antibody with other proteins favour conformational rearrangements in order to attain a stable state. The change in conformation might disrupt some of the antibody-surface interactions. This will result in leaching of antibody from the surface.

In addition, a protein with a higher tendency to interact with the surface can replace a physisorbed antibody/fragment [24].

Biosensor-based applications require well designed strategies for immobilization of antibodies onto the appropriate surfaces. Since adsorption is a complex process, the design of a highly repeatable adsorption-based immobilization strategy is a very important, if laborious, task. Some of the problems associated with adsorption-based immobilization strategies may be overcome by covalent methods, which are discussed in the next section.

### **1.2.2 Covalent immobilization**

In covalent immobilization antibody molecules react chemically with the functional groups of the surface via free reactive groups such as amine or carboxyl groups. Covalent strategies are generally categorized on the basis of the chemical reaction approaches used. The importance of covalently immobilized antibody systems for achieving high sensitivity assays has already been demonstrated with various diagnostic platforms [60-63]. Improved analyte sensitivity may be attributed at least in part to reduced protein losses due to antibody leaching and antibody exchange, which could increase the antibody surface coverage [60,61].

#### **1.2.2.1 Direct chemistries for antibody capture**

In this approach at least one of the reacting functional groups involved, on either the antibody molecule or the surface, readily reacts with the other without any activation or use of mediators. These strategies are mainly single step immobilization procedures. The most common direct chemistries that have been used for immobilization include epoxide-, chloride-, and aldehyde-based strategies and several examples of such strategies are outlined.

In aldehyde-based strategies either the antibody or the binding surface can be activated to generate free aldehydes, which can subsequently be used to immobilize the antibody. Active aldehydes can be generated on an antibody by oxidizing hydroxyl (-OH) groups of carbohydrates present in the Fc region of an antibody using meta-periodates of highly reactive alkali metals such as sodium ( $\text{NaIO}_4$ ) or potassium ( $\text{KIO}_4$ ). The resulting activated diol-groups can be captured efficiently on amine-functionalized surfaces [22,23,64]. In addition, the oxidized antibody molecules could be conjugated to labels such as biotin [65] and subsequently, be immobilized on surfaces coated with avidin or streptavidin. However, the major drawback associated with oxidizing an antibody is that the chemicals used for oxidation are highly reactive and, apart from activating carbohydrates, they may oxidize amino acids such as methionine, tryptophan or histidine at different points on antibody [66-68]. Therefore, another approach is preferable where the native antibody can be immobilized on surfaces functionalized with aldehydes [69,70]. Polymeric, metallic and nanoparticle surfaces may be functionalized with aldehyde to capture antibodies for various bioanalytical applications [69,70].

Epoxide-grafted solid supports are also widely used for antibody immobilization. An epoxide is cyclic ether containing one oxygen atom in the ring and its strained structure makes it highly reactive in comparison to other ether molecules. It is highly reactive towards secondary amines of amino acids, particularly histidine, and sulfhydryls of an antibody/fragment (**Figure 1.3**) [23,71,72]. The strong reactivity of an epoxide toward amine groups allows the immobilization of an antibody via lysine-rich regions or poly-histidine (HIS) tags. In addition, either a full-length antibody or a fragment or genetic variants (e.g. scFv, Fab), with exposed sulfhydryl groups, could also be captured on epoxide-functionalized surfaces [23,71,72].

Another direct chemistry is based on surface activation of solid support using aromatic chlorides e.g. trisyl (2,4,6-triisopropylbenzenesulfonyl chloride) and tosyl chlorides (p-toluenesulfonyl chloride).

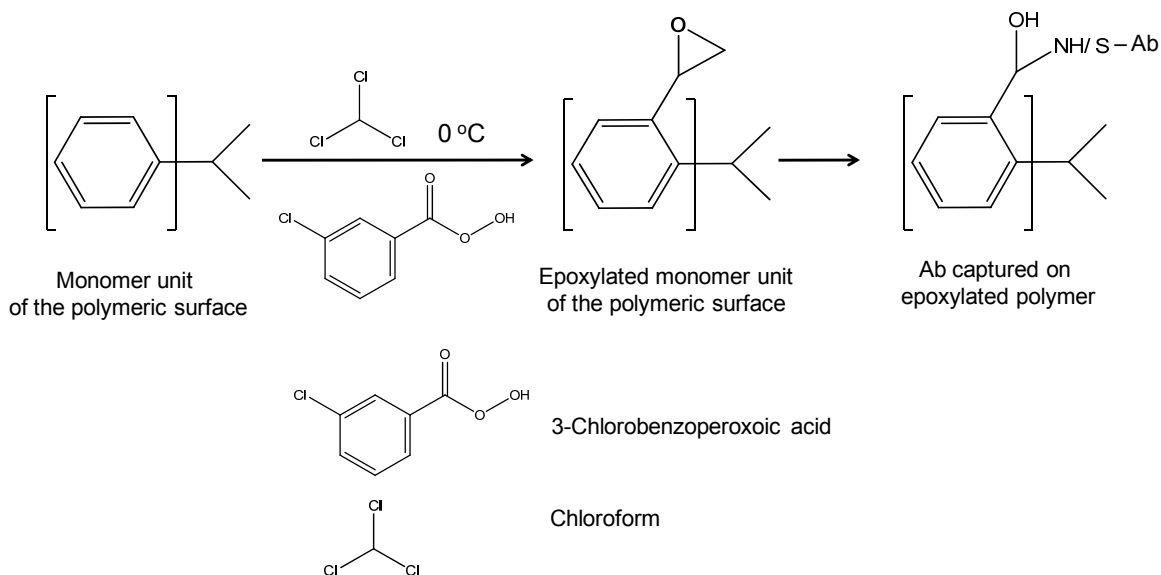


**Figure 1.3** A schematic representation of surface epoxylation and antibody immobilization. A typical organic polymer, such as polystyrene, is first epoxylated using 3-chlorobenzoperoxoic acid in the presence of chloroform at 0 °C. An antibody may then be immobilized on the epoxy-functionalized surface by the reaction of an amine or sulfhydryl group of the antibody and the epoxy group of the surface. 'NH—/ S—Ab' represents amine or sulfhydryl groups of an antibody that reacts with the epoxy groups of the surface. This is single step chemical reaction and no crosslinkers or intermediate molecules are required.

These aromatic chlorides are highly reactive toward hydroxyls and could easily be incorporated on the hydroxyls of the desired surface [73]. Such aromatic chloride-activated surfaces react with nucleophiles such as amine, sulfhydryl, imidazole, and hydroxyl groups of tyrosine that are present on an antibody (**Figure 1.4**) [74-77]. The only drawback of this strategy is that it is non-selective towards the previously mentioned functional groups. Therefore, the interaction of these chlorides with primary

amines of the antigen-recognition region on the antibody may lead to loss of antibody activity.

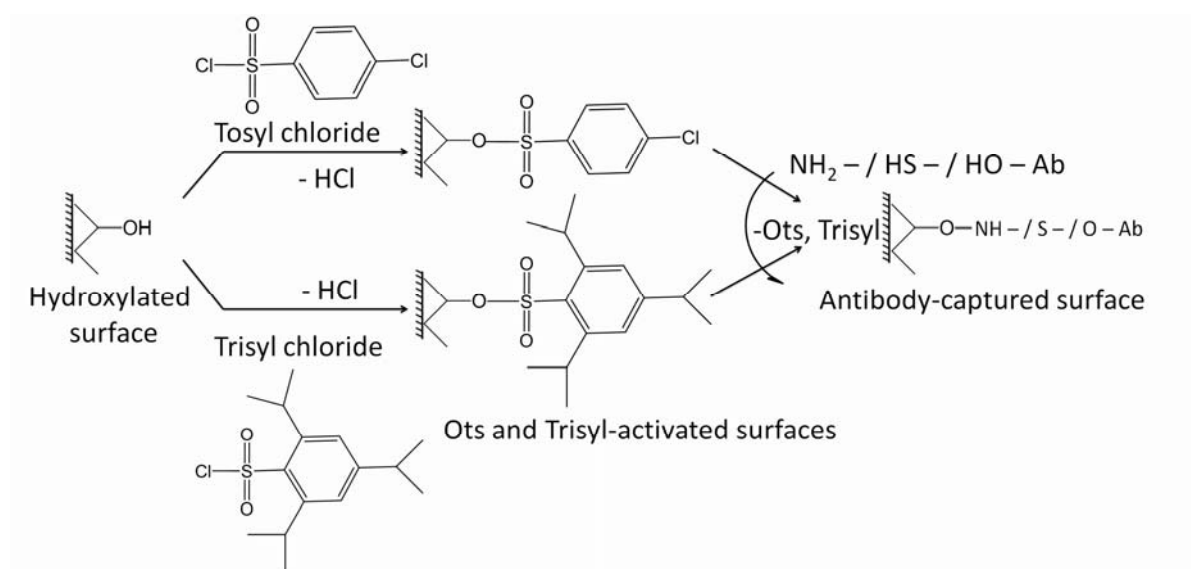


**Figure 1.4** Covalent immobilization of an antibody on a hydroxylated surface. Hydroxyl-functionalized surfaces, such as agarose, are activated with tosyl or trisyl chloride. The hydrogen 'H' of hydroxyl surface reacts with the chlorine moiety of tosyl/ trisyl chloride and generates HCl with subsequent attachment of these sulfonyl groups to the surface. The tosyl/ trisyl-activated surface then undergoes a displacement reaction such that the sulfhydryl, primary amine, hydroxyl group of tyrosine and imidazole groups of an antibody react with the surface displacing the tosyl/ trisyl group as shown. 'NH—/ S—/ O—Ab' represents binding of an amine, sulfhydryl or hydroxyl groups of an antibody bound to the sulfonate group of the trisyl or tosyl chloride-activated surface.

Immobilization of various protein molecules onto PEG-functionalized surfaces was demonstrated with Diels-Alder reactions and azide-alkyne [3+2] cycloadditions [78]. However, their use in antibody immobilization is restricted. In the associated reports customized PEG was synthesized with cyclopentadiene on one end at the 'α' carbon and biotin or protein A on the other end at 'ω' carbon (**Figure 1.5**). These customized PEG constructs were immobilized on a *N*-maleimide-functionalized surface (**Figure 1.5**) [79,80]. Subsequently, antibody was captured on the biotin or protein A present at 'ω'

carbon of the PEG chain. This strategy is advantageous as it generates homogeneous surface functionalization and results in highly specific antibody capture.

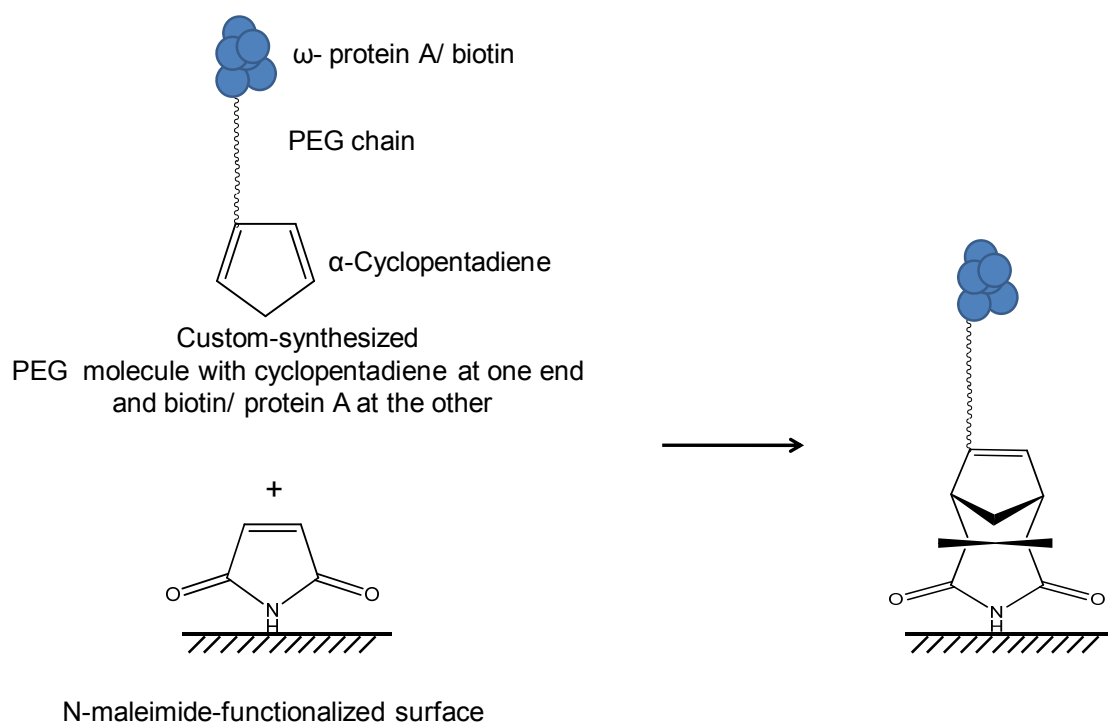


**Figure 1.5** Mechanism of covalent immobilization of Fc-binding and other proteins (including antibody) with Diels-Alder's [2+3] cyclo-addition reactions. Customized PEG was synthesized with cyclopentadiene at the 'α' carbon and biotin or protein A at the 'ω' carbon, which was immobilized on N-maleimide-functionalized surfaces. Similarly, an antibody molecule could also be bound directly to the 'ω' position of PEG replacing the biotin or protein A.

Since cycloaddition is specific to ringed structures, the surface functionalization is highly specific. In addition, protein A and biotin-based antibody capture can introduce a high degree of immobilization specificity and orientation. Moreover, the length of the PEG chain can be varied enabling control of the distance of the antibody from the surface and the degrees of freedom of movement of the immobilized antibody. The degrees of freedom are a measure of the independence of movement of an antibody in space with

respect to its surroundings. Immobilization of an antibody on a surface restricts this spatial freedom of motion in different directions such that the smaller the separation-distance between antibody and surface, the lower will be the degrees of freedom and vice-versa (**Figure 1.6**).

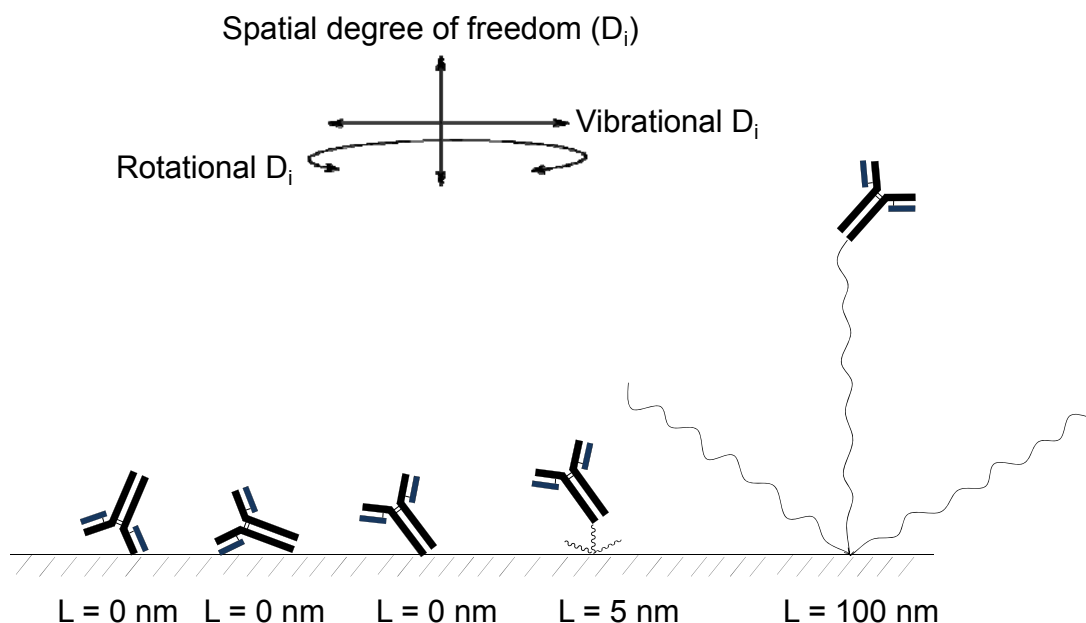


**Figure 1.6** Analysis of the effect of cross-linker length on degrees of freedom of immobilized antibody. The antibody is cross-linked to the functionalized surface via a crosslinker of variable length. The crosslinker length, as depicted, increases in the order of  $L = 0 \text{ nm} < 5 \text{ nm} < 100 \text{ nm}$ . With increasing crosslinker length the distance of the antibody from the surface also increases. Distance of the immobilized antibody from the surface governs the flexibility of antibody. At  $L = 0 \text{ nm}$ , the antibody is rigidly immobilized on the surface and possesses little or no flexibility whereas, at  $L = 100 \text{ nm}$ , antibody is highly flexible. In general, the greater the flexibility of immobilized antibody molecule the lower the steric strain on it, thus maintaining its functional conformation.

Therefore, shorter separation distances may result in higher steric stress, which may cause conformational changes and functionality loss. However, this strategy is very time

consuming and requires long preparatory phases to conjugate PEG with protein and cyclopentadiene, making it less attractive.

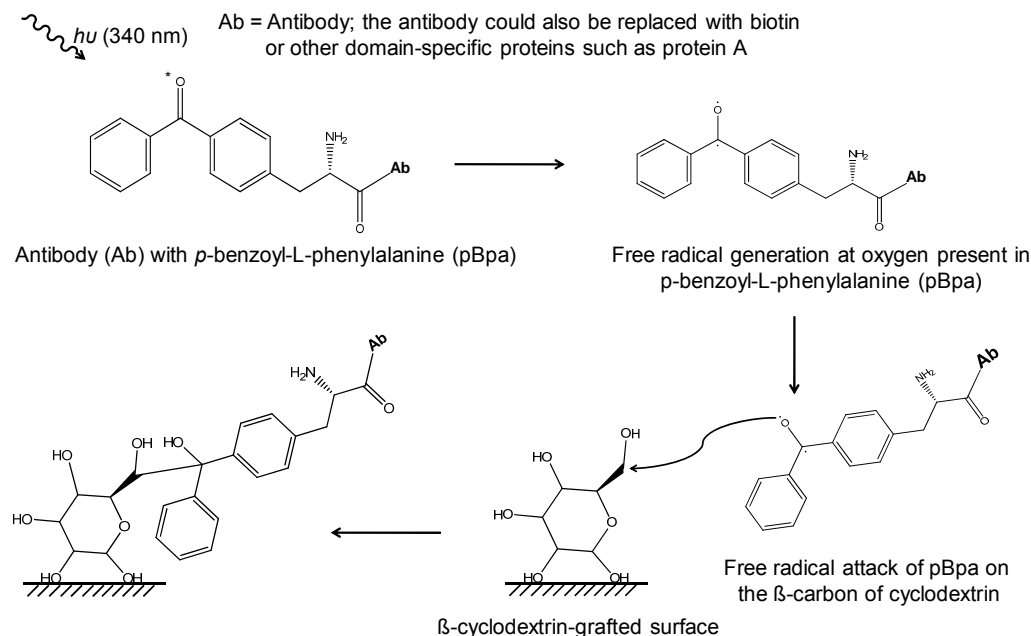


**Figure 1.7** Photoactivable cross-linking of antibody to a cyclodextrin-modified surface. The antibody, antibody fragment or an antibody-capturing protein is modified with *p*-benzoyl-L-phenylalanine (pBpa). The pBpa is photoactivated. This generates an oxygen radical on the benzoyl moiety. The oxygen radical attacks the hydroxyl-containing carbon centre of cyclodextrin with the subsequent formation of a covalent bond.

Photoactivation-based antibody immobilization is another potential approach. Recently, several groups [81,82] reported the successful immobilization of photoactive variants of amino acids such as *p*-benzoyl-L-phenylalanine (pBpa), attached to a modified antibody, on  $\beta$ -cyclodextrin ( $\beta$ CD)-modified surfaces, by irradiating the desired surface with ultraviolet (UV) light (340-360 nm). This mechanism of antibody immobilization is shown in **Figure 1.7**. However, unlike most other direct chemistries, it is highly selective in immobilizing antibodies on to a surface because the reaction will only take place at the

position where *p*Bpa is present on the antibody. In addition, *p*Bpa can be genetically introduced to the antibody at a desired position as explained in [83,84].

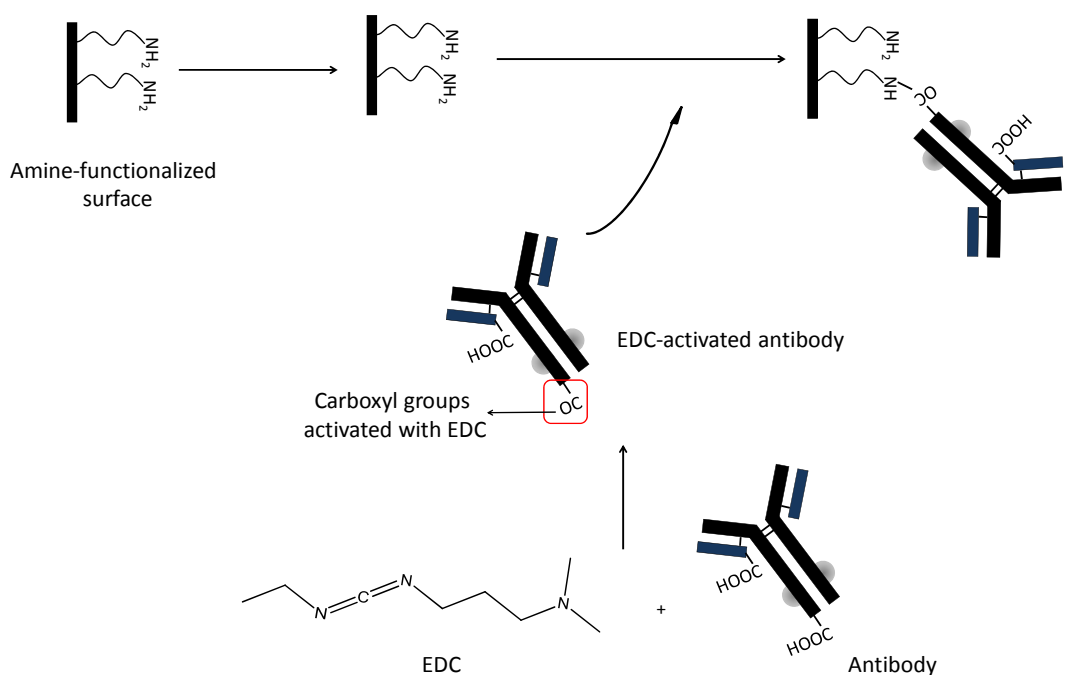
In addition to the direct chemistries, there is another important category for covalently immobilizing an antibody where linkers are employed. These linker types provide a range of choice for immobilization and may be easier to use than other covalent immobilization strategies.

#### **1.2.2.2 Linker-mediated strategies to capture antibody**

Linkers are chemical species that contain highly reactive moieties at one or both ends and, hence, are capable of creating bonds between given functional groups. These linkers facilitate the reaction of the desired functional groups of an antibody by creating highly reactive intermediates that can subsequently be bound to the functional groups of the surface. The linker choice strictly depends on the chemical reactivity of the selected functional groups on the antibody and the desired surface. These linkers may be categorized as homo- and hetero-bifunctional [85]. Homo-bifunctional linkers have the same chemically-reactive groups at both the ends and react with the same entities on the target molecules, whereas hetero-bifunctional linkers have two different chemically reactive centres at each end.

A variety of such cross-linkers is commercially available in different combinations [73,85] e.g. amine-amine and sulfhydryl-sulfhydryl homo-bifunctional, and amine-sulfhydryl and amine-carboxyl hetero-bifunctional linkers. Widely used cross-linkers representing homo- and hetero-bi-functional categories are glutaraldehyde and 1-ethyl-3-(3-dimethylaminopropyl) carbodiimide (EDC), respectively (**Figure 1.8**). Other specific bifunctional linkers such as sulfhydryl-hydroxy, amine-carbohydrate and sulfhydryl-carbohydrate are also available with specific chemistries and associated linkages.

### STRATEGY A



### STRATEGY B

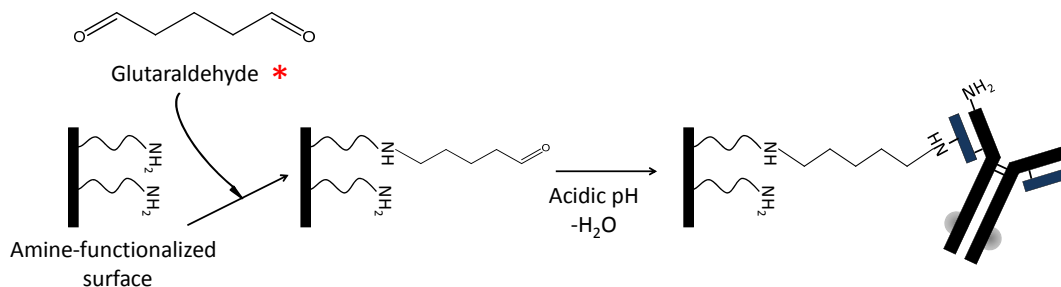


**Figure 1.8** Schematic reaction of carboxyl-amine (Strategy A), and amine-amine (Strategy B) cross-linkers. Carboxyl-amine crosslinkers represent hetero-bifunctional chemistry such as carbodiimide (EDC). The carboxyl group of the antibody reacts with the carbodiimide group of EDC to generate an intermediate urea derivative, which further reacts with the amine on the surface. Similarly, amine-amine coupling cross-linkers generally possess homo-bifunctional reaction centres reactive towards amines such as glutaraldehyde and react with an amine on the surface followed by amines on the antibody molecule.

\* Glutaraldehyde has a potential tendency to multimerize and it is advisable to distil and aliquot it prior to use [86].

Amine-targeting linkers possess functional moieties that react with amine groups. Such reactive centres mainly have esters of NHS/ imide and phenyl hydrazide or aldehyde that preferably bind to primary amines irrespective of their position [73]. Amine-targeting strategies may result in the loss of antibody activity [87]. However, the addition of ‘lysine-rich’ pockets at locations on the antibody away from the region associated with antigen-recognition may be employed for minimizing activity loss [88].

Hetero-bifunctional crosslinkers that target carboxyl groups mainly possess carbodiimide or azide reactive groups [73] and could be used as alternatives to the amine-targeting linkers. These linkers are probably the most commonly used in antibody immobilization over a modified surface because of their robustness in delivering cross-linking on a wide range of functionalized surfaces with amine, sulfhydryl and epoxy coatings.

Maleimide or vinyl sulfone-containing linkers are used for targeting sulfhydryl groups of the antibody or the surface [73,85]. These linkers are commercially available in various combinations and can cross-link sulfhydryl functional groups to amine, carbohydrate or sulfhydryls. The utility of sulfhydryl-based hetero-bifunctional cross-linkers in protein coupling is already proven [89]. However, their use in immobilization is fairly restricted to either amine-functionalized or gold-coated surfaces [89,90]. The major drawback of this approach is that either the antibody has to be chemically processed to introduce a thiol group on it or it must be modified genetically to introduce a cysteine. Cysteine, a sulfhydryl-containing amino acid, is also a widely exploited chemical species for immobilizing antibody molecules on amine or sulfhydryl-functionalized and gold-coated surfaces. A cysteine-tagged antibody can be captured on amine and sulfhydryl-functionalized surfaces with bi-functional cross-linkers, whereas, on gold surfaces it can be immobilized via co-ordinate bonds formed between the sulfhydryl group and gold in a chemical-free single step. Cysteine-based antibody/fragment immobilization using

chemical modifications such as cyanogen bromide-activated surfaces was also reported [91]. This strategy provides robustness to the approach with minimum antibody leakage [92]. However, introduction of cysteine in the basic antibody structure could introduce conformational changes leading to a non-functional antibody. This drawback could easily be controlled by the introduction of cysteine on the antibody/fragment away from the antigen recognition domains, using reduction and alkylation chemistries [93], which may enable the more efficient use of sulfhydryl linkers in solid phase immobilization [76,94-96] or by genetic approaches.

Photoswitchable linkers, which comprise the most advanced class of linkers, could also be employed for antibody immobilization [85]. These linkers mainly possess a photoactivable group at one terminal and a reactive chemical group at the other. The photoactivable group can be activated to either react with the surface or the antibody. However, photoactivable chemistry is not selective. Therefore, the linkers are mainly allowed to react first with the surface via their photoactivable terminal group and, subsequently, facilitating capture of the antibody through the other end of the cross-linker that possesses a reactive group e.g. NHS ester or maleimide.

These linker-based chemistries are important because these are easy to perform with minimum preparation. In addition, the most advantageous use of linkers is that they may be of variable length and can be used to control the distance of the immobilized antibodies from the surface. Hence, the linker arm-length could impact on antibody functionality by controlling the immobilization-associated steric stress on the antigen-binding site [97]. A spacer/linker of zero-length chemistry (e.g. carbodiimide (EDC)-succinimide (NHS)) immobilizes antibody on the surface with a rigid bond that minimizes the freedom of rotation (degrees of freedom) (**Figure 1.6, page 20**), which may result in 'functionally-challenged' antibody. However, this rigidity could

significantly be decreased by increasing the spacer arm-length. Therefore, in many cases the functional antibody density on the surface may be enhanced.

All the covalent strategies described have been used in the fabrication of different biosensor formats. The advantages of using covalent immobilization-based strategies are the higher density and homogeneous loading of the captured antibody on the surface along with leach-proof immobilization. However, the major drawback is the random immobilization of antibody as it may drastically affect the antibody functionality.

### **1.2.3 Site-specific Immobilization of antibody**

Site-directed immobilization is where an antibody can be captured specifically through a desired region. Many approaches are reported claiming strong site-directed antibody immobilization. These strategies include either the use of affinity biomolecules such as biotin-avidin, enzyme or domain-specific proteins (e.g. protein A) for antibody capture. A high degree of orientation can be introduced to the immobilized antibodies using this strategy and the antigen binding region of the antibody is always correctly positioned for antigen recognition.

#### **1.2.3.1 Affinity Tag-based site directed antibody capture**

Affinity is the strength of interaction between two molecules where the interaction may be stabilized by multiple bonds. In an antigen-antibody interaction, affinity can be described as the strength of interaction of an antigen with the single binding site of an antibody. If a tag has a strong affinity towards a certain molecule and binds with significantly high specificity, it is referred to as an 'affinity tag'. These tags are successfully used for affinity-based protein immobilization [17,98-100]. Tags can also be incorporated into the antibody either genetically or chemically [17,18]. There is an array of commercially available affinity tags but those used for the antibody immobilization are described.

In a polyhistidine tag [101] there is a long repeated sequence of histidine residues of varying numbers (ranging from six to ten). This tag has a strong affinity for divalent transition metal ions including divalent nickel ( $\text{Ni}^{+2}$ ) and copper ( $\text{Cu}^{+2}$ ) [102-104](**Figure 1.9**).

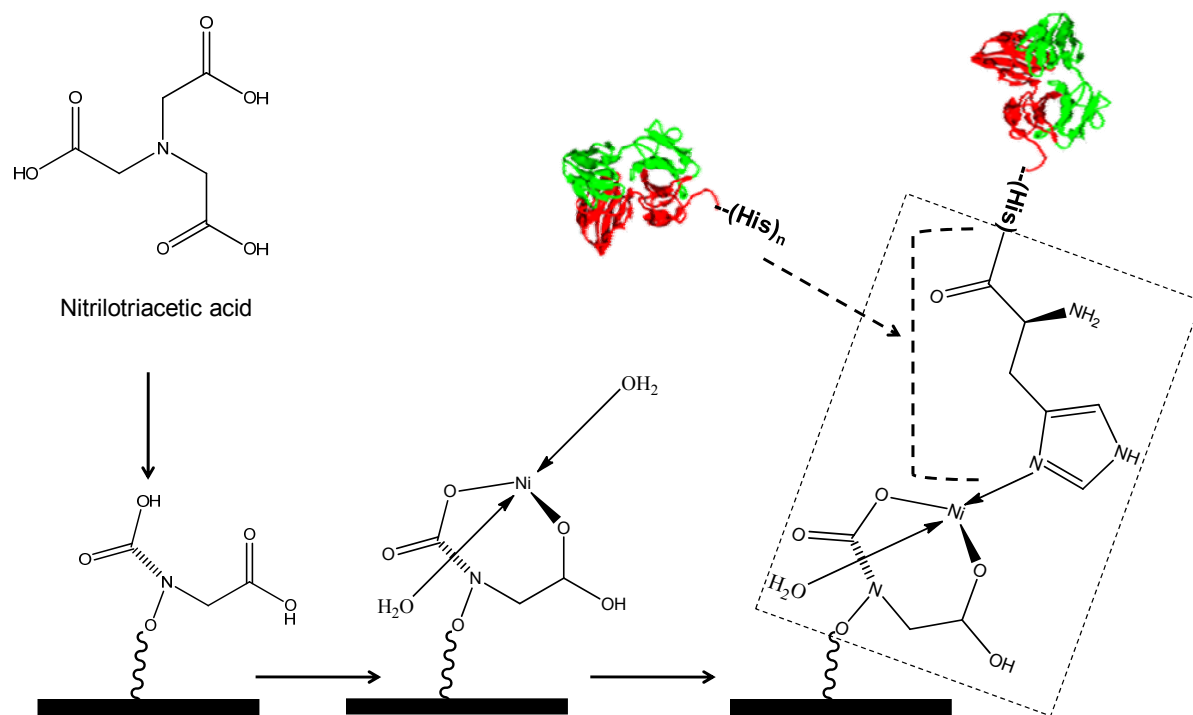


**Figure 1.9** Mechanism of ‘His-tag-mediated’ immobilization on a nitrilotriacetic acid (NTA)-modified surface. The NTA-functionalized surface is chelated with divalent metals such as  $\text{Ni}^{+2}$ . The histidine of the tag reacts with the hydrated  $\text{Ni}^{+2}$  via the nitrogen of the imidazole ring, thus immobilizing scFv or recombinant antibodies labelled with the His-tag.

The transition metal ions are chelated on the support layer, which consists of nitriloacetic acid (NTA) or iminodiacetic acid (IDA). They provide a matrix for the selective immobilization of tagged antibodies where this tag is genetically incorporated at either the *N*- or *C*-terminal of the antibody [105]. However, there are many drawbacks associated with this strategy. Non-homogenous antibody distribution on the NTA-grafted surface is the foremost [106,107]. The non-homogeneous distribution of antibody is due

to the immobilization of a mixture of functional and non-functional antibody on the NTA matrix. In addition, the selectivity of NTA to distinguish the HIS tagged antibody from other histidine-rich naturally occurring cellular proteins is very poor [108]. This will result in competition between tagged antibody and histidine-rich cellular proteins (e.g. histidine-rich glycoprotein (HRG) and histidine-rich calcium-binding protein (HRC) [109-111]) for binding with the NTA present on the surface and results in heterogeneous immobilization on the surface. There are several reports that describe the non-specificity associated with this system as an attribute of histidine's relatively low affinity toward metal ions ( $K_d$  in the order of 1-10  $\mu\text{M}$ ). However, a better affinity may be achieved either by increasing the number of histidine residues in the tag or employing two tandem tags [112,113].

Biotin is a water soluble vitamin known as vitamin B<sub>7</sub>. It is a fused ring structure composed of tetrahydroimidazolone and tetrahydrothiophene with valeric acid ( $\text{C}_5\text{H}_{10}\text{O}_2$ ) substitution on the thiophene ring. It is an important biomolecule and plays a critical role in gluconeogenesis. Biotin can act as an affinity tag if incorporated into the antibodies either genetically or chemically. These biotinylated antibodies then can easily be captured on avidin or streptavidin or genetically derived combinations of both proteins, which are conjugated with functionalized polymeric and metallic [114,115], silicate [116] and amino-polypyrrole-coated surfaces [117]. Initially, this tag was often used for histochemical diagnostics [118] but its commercial relevance in immobilization and purification was realized later. In addition, this approach was successfully employed in the development of microarrays [119] and optical sensors based on surface plasmon resonance [120]. However, due to the multivalency of avidin, which can accommodate four biotin molecules per avidin, high densities of the immobilized antibody molecules may be obtained. Such a high density of antibody may induce interactions between

closely bound antibody molecules that may lead to a high degree of steric hindrance [121]. In addition, endogenous biotin could also compete for the surface-bound avidin or streptavidin. This non-specific competition may reduce the overall binding efficiency of the immobilization procedure [122]. The strong affinity ( $K_d \approx 10^{-15}$  M) of the biotin to avidin is a major advantage and the interaction is effectively irreversible until a temperature-dependent regeneration method was developed using a hydro-thermostat [123]. However, this strong affinity may introduce steric hindrance in the immobilized antibodies, as an antibody bound through biotin loses freedom of rotation [124,125]. Reducing the affinity of biotin, using genetically-engineered variants of streptavidin or biomolecules mimicking the biotin-binding event with streptavidin could be used to minimize steric stress on antibody and improve the regenerative capacity of the bound antibody [126].

Use of peptide nucleic acids (PNAs) is another approach that was employed for antibody immobilization. The PNAs are chemically synthesized single stranded nucleic acid analogs. The backbone repeat unit of the PNA consists of an amino acid derivative of alkylamide and is shown in **Figure 1.10**. Nucleotide is attached to the PNA backbone repeat unit at the 4-oxoethyl position via an aminoethyl-glycine linkage. PNA is then synthesized by repeated addition of these nucleotide-functionalized amino acids via peptide bonds replacing the normal phosphodiester backbone [127,128]. Therefore, PNAs can interact with other nucleic acids in a highly specific manner forming PNA-PNA, PNA-RNA and PNA-DNA hybridization constructs similar to the hybridization of complementary DNA strands. In addition, PNAs are non-ionic and achiral molecules. Their non-ionic nature and achirality makes them resistant to enzymatic hydrolysis. Achirality also provides a high degree of thermal stability. These properties of PNA could be harnessed in developing efficient immobilization strategies such that the PNA-

conjugated antibody could be immobilized on surfaces grafted with the anti-sense oligonucleotide or PNA by hybridization (**Figure 1.10**) [129,130]. Subsequently, the distance between surface and antibody could be controlled by varying the number of PNA monomers in the backbone [131-134]. Although this strategy is not commonly used for antibody immobilization, it could be an efficient single-step approach that could provide high steric freedom to the captured antibodies, with strong site specificity and orientation. There are few reports pertaining to the use of complementary oligonucleotide tags[135], which are relatively simpler than PNAs. In addition, the hybridized oligonucleotide tags can be separated from their complementary strands grafted on the surface by a variation in either pH or divalent ion strength.

Elastin-like polypeptides (ELP) are a relatively novel category of small thermally responsive proteins [136,137]. They can easily be tagged on to various antibodies, antibody fragments or other proteins [138]. ELPs possess ‘biopolymer-like’ properties such that they polymerize in a temperature range of 4-37 °C. At temperatures above 37 °C these proteins precipitate out of the solution and below 4 °C they remain in solution phase. Therefore, ELP-tagged antibodies could efficiently be captured as a monolayer on a specifically tailored surface [139]. ELPs have been successfully used for antibody immobilization in microarrays and related applications [140].

FLAG<sup>R</sup> proteins, commercially available from Sigma Aldrich, may also be employed for immobilization. These are octa-peptides (NH<sub>2</sub>-DYKDDDDK-COOH) that could be genetically incorporated into antibodies and antibody fragments (Fabs and scFvs) [141]. Antibodies tagged with FLAG can be captured on the surfaces immobilized with monoclonal anti-FLAG antibody. Use of the FLAG tag introduces specificity and orientation for the immobilization [142-144].

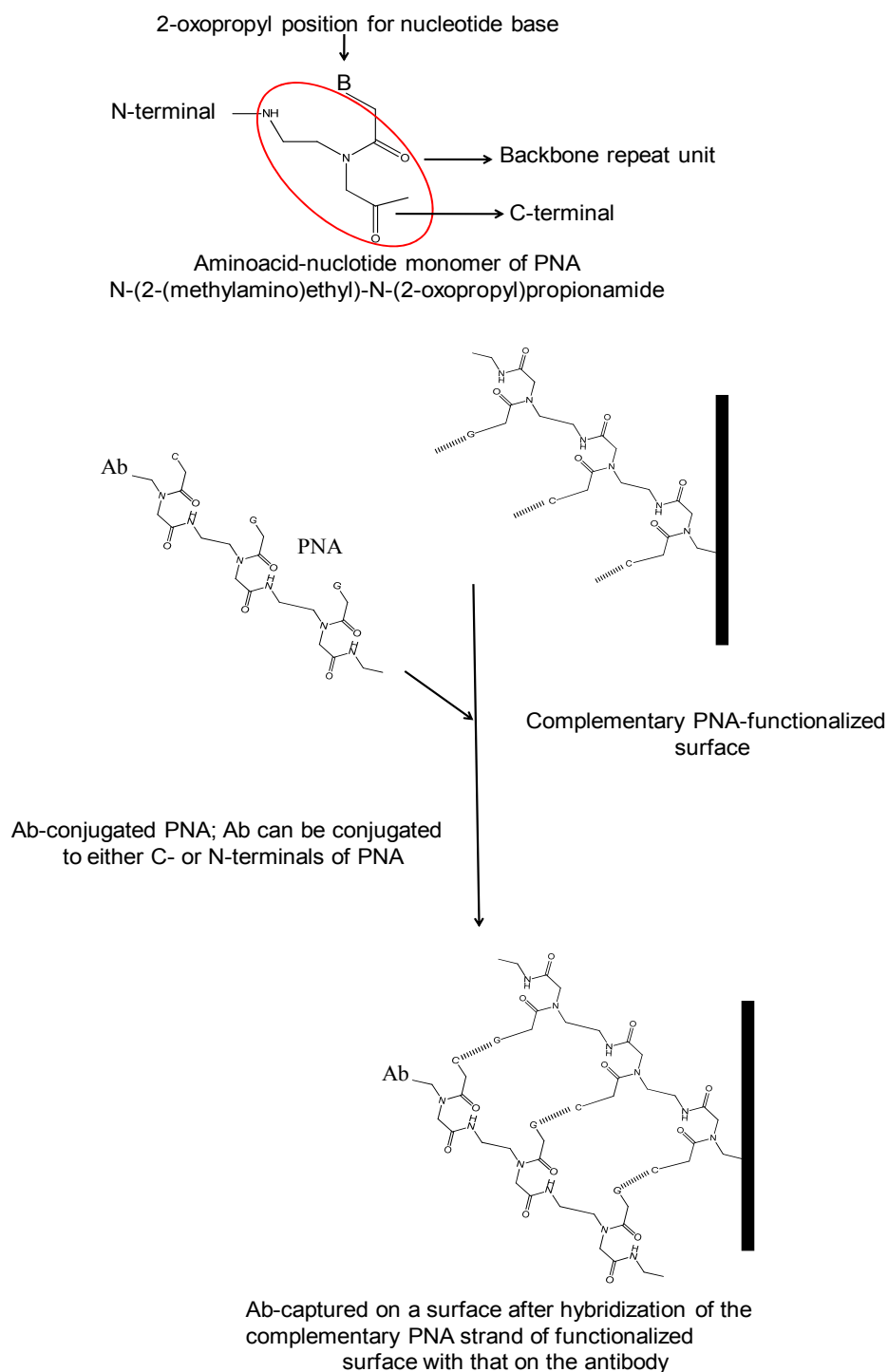


**Figure 1.10** Immobilization of an antibody-functionalized with a peptide nucleic acid (PNA) on a surface grafted with a complementary nucleotide base sequence. Antibody could be covalently linked to a PNA sequence. This PNA-functionalized antibody can be immobilized on a second PNA sequence that contains complementary nucleotide sequences, which easily hybridize directly to it.

### 1.2.3.2 Enzyme-substrate reaction-based site-directed antibody capture

Antibody immobilization using enzyme-mediated coupling is also feasible. There are many different enzyme-catalyzed reactions. The participating substrates react in the presence of the enzyme and products are formed. This very fundamental principle of enzymology can also be used for antibody immobilization. The enzyme-mediated reaction must be a ‘two substrate component’ system, where the enzyme facilitates the reaction of one substrate moiety with the other, as shown in **Figure 1.11**. An antibody can be conjugated to one substrate of the ‘two substrate component system’. This antibody-substrate complex can then be immobilized on the surface and grafted with the second substrate of the ‘two substrate component system’ via an enzyme-catalyzed reaction.

Antibody could also be conjugated to the active domain of an enzyme that is involved in catalyzing some reaction. These conjugates can subsequently be captured on the surfaces, grafted either with the substrate or their analogs. The enzyme’s substrate-binding domain interacts with the substrate (via interactions such as hydrogen bonding and electrostatic interactions, along with the formation of covalent bonds). Various examples of this strategy that are used for antibody immobilization are discussed in this section.

The immobilization of cutinase-conjugated calmodulin was one of the first demonstrations of this strategy. Cutinase-conjugated calmodulin was captured on the phosphonate inhibitor-functionalized thiolated self-assembled monolayer (SAM) on a gold surface [145]. Although, this report was not specific for antibody immobilization, its potential implications will be discussed.

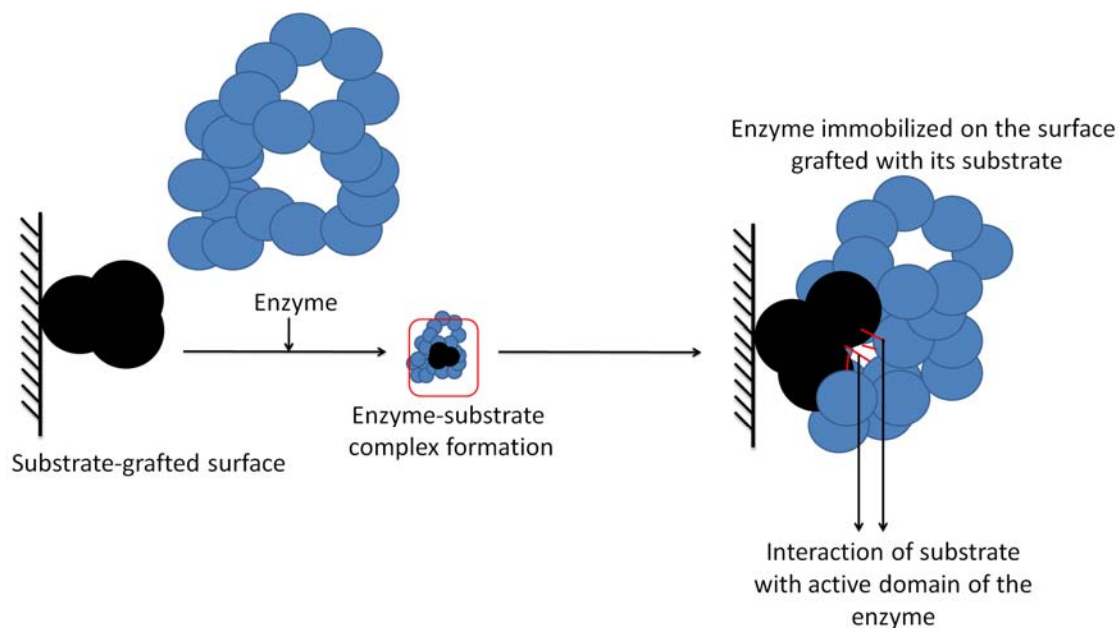


**Figure 1.11** Illustration of enzyme-mediated reaction of two substrates. Substrate 1 binds to the specific site on the enzyme forming enzyme-substrate 1 complex. This complex then binds to the second substrate. Enzyme catalyzes the reaction between the two substrates by forming a covalent bond between them. This strategy could be used to immobilize antibodies tagged with substrate 1 on the surfaces grafted with substrate 2.

Human O<sup>6</sup>-alkylguanine transferase (hAGT) plays important role in DNA repair during DNA synthesis. It binds to a DNA molecule at a specific error site and alkylates it by transferring an alkyl group from its substrate (**Figure 1.12**). Methyltransferase is one of the most important enzymes of this category. Immobilization of proteins tagged with this enzyme has already been demonstrated [146-149]. Similarly, the hAGT-fused antibody can be covalently captured on surfaces functionalized with benzylguanine. Fused hAGT enzyme replaces the guanine by covalently binding to a benzyl moiety. Immobilization of hAGT-fused glutathione S-transferase and tandem repeats of ‘immunoglobulin-type’ domains of a muscle protein, called titin, was demonstrated [150]. This technology is commercially available under the name SNAP-tag® with New England Biolabs. In addition, if the enzyme’s substrate is changed from benzylguanine to benzylcytosine then

it is known as a CLIP-tag™. These tags can be genetically incorporated in recombinant antibodies or chemically fused to full length antibodies [151]. There are many applications of these tags for specific and covalent immobilization of antibodies. Micropatterning of antibody is also feasible using these strategies [152].

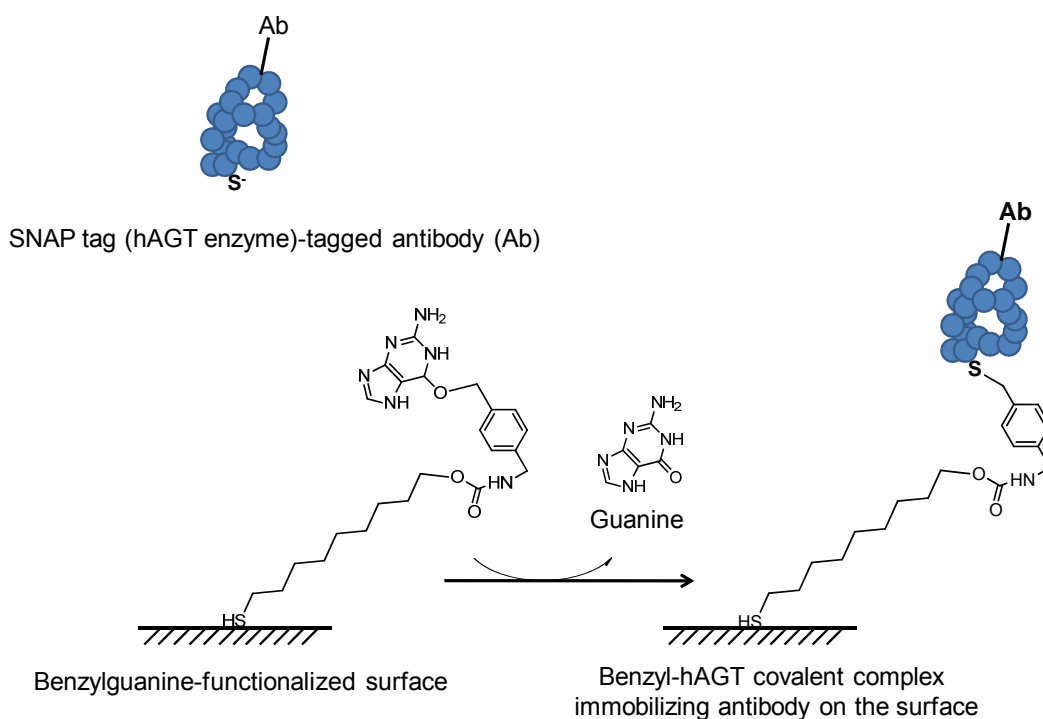


**Figure 1.12** Mechanism of SNAP-tag-mediated antibody immobilization. Antibody is tagged with human *O*<sup>6</sup>-alkylguanine transferase (hAGT), which is a DNA repair enzyme. This enzyme removes guanine and forms covalent bonds with the benzyl group of the benzylguanine that is grafted on the surface, thus immobilizing the tagged antibody by displacement catalysis of the benzylguanine group on the surface.

Transglutaminase (TGase) is another enzyme system, which specifically catalyzes the formation of covalent cross-linking of the peptide-bound glutamine with a primary amine. This enzyme is specific to a 12 peptide long sequence that is known as ‘glutamine-donor substrate’ sequence and is designated as T26 (HQS<sub>Y</sub>VDPWMLDH). Flank of (GGGS)<sub>3</sub> spacer is incorporated on either side of the T26 sequence prior to

molecular tagging onto the *N*- or *C*-terminal of the antibody fragment. This strategy was demonstrated for the immobilization of tagged anti-BSA antibody on aminated surfaces by inducing the TGase-mediated amine-T26 reaction [153]. The underlying mechanism of immobilization is shown in **Figure 1.13**. This technique is efficient as it involves no chemical modification of the antibody or fragment.

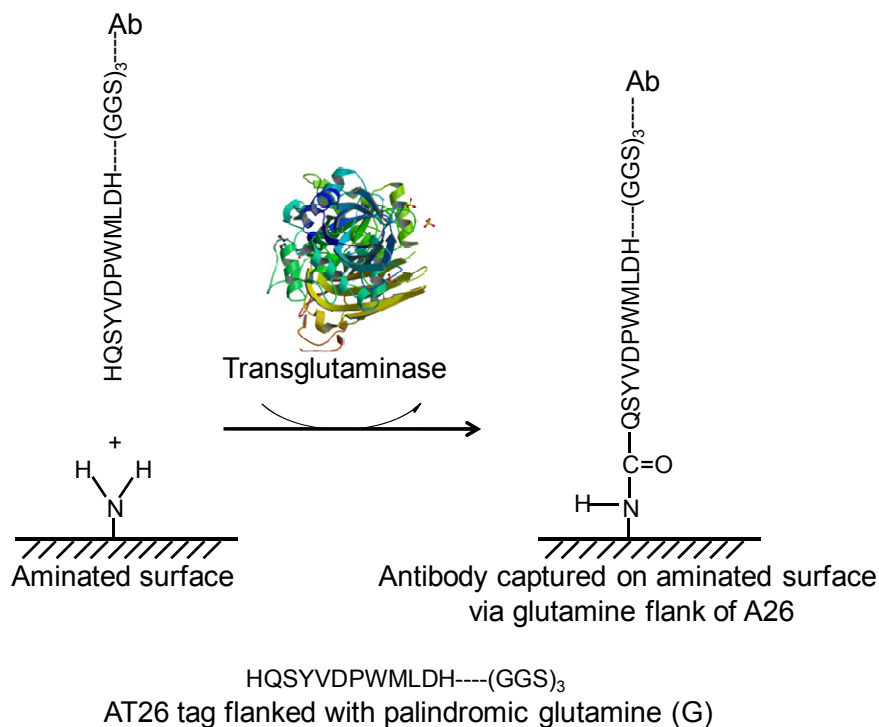


**Figure 1.13** Mechanism of transglutaminase-mediated antibody immobilization on aminated surfaces. Antibody tagged with T26 and glutamine spacer reacts with the amine of the surface in TGase-catalyzed acyl-transfer-mediated isopeptide bond formation by facilitating the reaction between carboxamide of glutamine and the amine of the side-chain of lysine on the surface.

The use of enzymes on poly-L-lysine (PLL) and polyethylene glycol (PEG)-grafted surfaces to capture cells and peptides had also been demonstrated. This strategy was also demonstrated for immobilizing antibodies with preserved functionality [154].

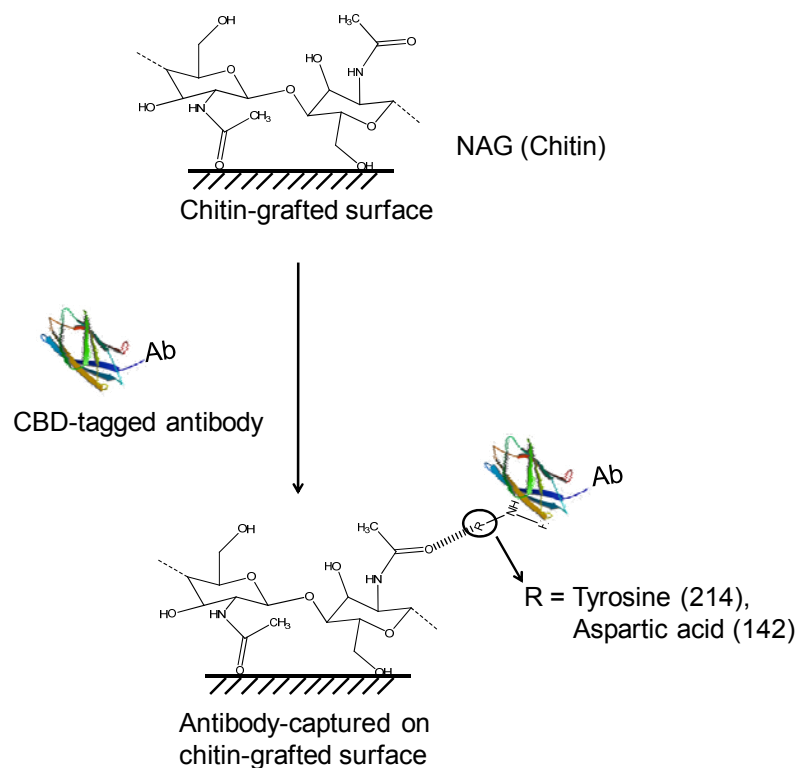


**Figure 1.14** Schematic representation of immobilization of an antibody conjugated to the substrate-binding domain of an enzyme on surfaces grafted with the substrate of the respective enzyme. Antibody tagged with chitin-binding domain (CBD) can interact with chitin via hydrogen bonds formed between the hydrogen of the aspartic acid (142) of the CBD and oxygen of the amide of the chitin, which is grafted on surface. Hydrophobic interactions between the tyrosine (214) of the CBD and N-acetylglucosamine of chitin also play a crucial role in this immobilization.

The chitin-binding domain (CBD), which is the hydrolase part of the enzyme chitinase, catalyses the hydrolysis of chitin polymers. These domains can be incorporated genetically into recombinant antibodies and can be chemically conjugated to full length antibodies. Immobilization of a CBD-conjugated antibody on the chitin-grafted surface is shown in **Figure 1.14**. An early use of CBD in immobilization was reported by Kuranda and co-workers [155]. Later, this strategy was employed for whole cell-based assay development whereby whole cells were immobilized on chitin-grafted surfaces via their

surface-expressed CBD [156]. This strategy is primarily used to immobilize antibodies on the chitin-functionalized chromatographic resins [157]. In addition, several CBD-antibody constructs were developed [158-160] to capture antibodies on chitin-coated surfaces for immunoassay-based applications [157,161,162]. Similarly, polyhydroxyalkanoate (PHA) depolymerase substrate-binding domain (PSBD) [163] was also reported for use in antibody immobilization-related applications.

#### **1.2.4 Site-specific orientation-based antibody capture**

Site specificity can be easily introduced using the tag-based strategies and enzyme-mediated methods (section 1.2.3, page 27-38). However, the orientation of immobilized molecules is of major importance for immunoassay development. Strategies based on domain-recognition proteins (DRPs), such as protein A, are widely used for immobilizing antibody molecules. These DRPs have high avidity toward specific domains on the antibody and bind strongly to them introducing strong directed orientation to the antibodies when immobilized (**Figure 1.15**). In addition, the covalent immobilization of these DRPs on a surface could certainly achieve a homogenous distribution of antibody over the surface [164,165] minimizing leaching and protein exchange-associated variability in assays [166]. However, DRPs must be correctly orientated on the surface to provide proper orientation to the antibody molecules. Use of DRPs with multiple antibody-binding domains, such as protein A with five antibody-binding domains, may minimize the concerns associated with the orientation of these DRPs. The applications of these orientated antibodies could be enzyme immunoassays (ELISA) [166], surface plasmon resonance (SPR), microdevices such as QCM [167,168] and chromatography [169].

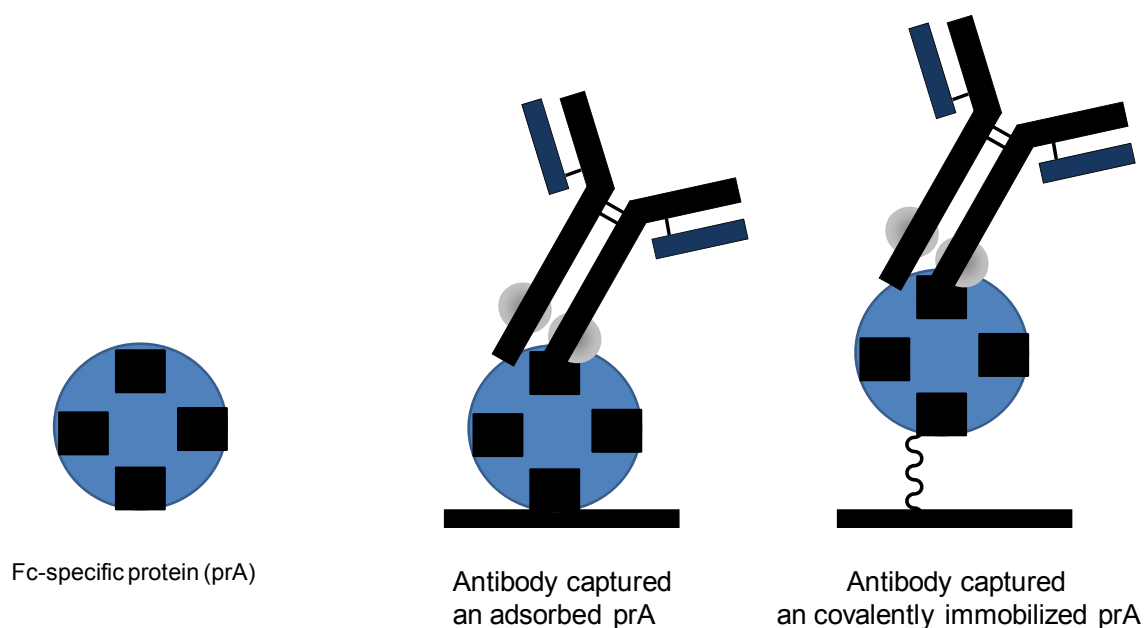


**Figure 1.15** Orientation of an immobilized antibody by capture on a sub-layer of protein A, which is either adsorbed or covalently captured on the surface.

### 1.3 Conclusions and Perspective

Adsorption of antibody is very commonly used approach for immobilization. This is a cost-effective and simple method with no expertise required for its use. However, it has many drawbacks. These is no control over the (a) amount and packing density of the antibody, (b) antibody distribution on the surface, (c) site-specificity, orientation and conformation of the antibody [13,34,48,49], and (d) susceptibility of the antibody to leaching and protein exchange [24,59]. Introduction of capture stages that include a sub-layer of Fc-binding proteins or anti-antibody molecules may introduce a higher degree of orientation with a controlled antibody packing [170]. However, this will significantly increase the time and cost involved for immunoassay development. Tag-assisted strategies could be employed to address some of these issues, such as site-specificity and

improved control over the active conformation of the immobilized antibody. However, stability of the interaction of the tag with its affinity ligand is strictly dependent on various physical and chemical parameters such as temperature, solvent polarity, pH and salt concentration. Therefore, a slight change in the optimum conditions may introduce leaching [171,172] and activity loss. In addition, the homogeneous distribution of the tagged-antibody is dependent on the distribution of the affinity ligand on the surface. Therefore, a strategy is required that could provide an approach to respond to most of these drawbacks whilst maintaining the cost-effectiveness of the immunoassay development. Employing covalent strategies could deal with most of the previously mentioned drawbacks. Covalently-captured antibodies have least susceptibility for leaching and protein exchange. In addition, a high degree of site-specificity and orientation could be introduced to the antibody by employing enzyme-mediated covalent strategies. However, covalent immobilization may require activation of the antibody prior to immobilization. This may result in self-conjugation of antibodies forming multimeric complexes. This multimerization could be a drawback in the case of antibody-based imaging, whereas in assay development, this multimerization may mask the active site of antibody along with the introduction of conformational stress. This multimerization can be restricted by optimizing the molar ratios of antibody to cross-linker. This could also be addressed by employing direct chemistries. Strong orientation could also be employed by capturing antibody on a covalently-immobilized sub-layer of Fc-binding proteins [165]. A summary of all the available techniques, along with their advantages and drawbacks, is given in Table 1.3.

Theoretically, covalent strategies offer great potential to tag-assisted strategies in terms of the cost and time involved. Introduction of a tag is performed either by using recombinant molecular biological approaches or by chemical methods. Therefore, in this

thesis, covalent immobilization-based strategies will be employed for developing immunoassays.

This thesis covers the development and optimization of a mild surface activation and modification method that could be employed on most of the polymeric surfaces irrespective of their chemical nature. In addition, the various available chemistries will be critically analyzed for their immobilization efficiency with the aim of developing high-sensitivity immunoassays on various bioanalytical platforms including microtiter plates and nanoparticles.

**Table 1.3**

Strategy	Overview	Advantages (+) Disadvantages (-)
<b>Physisorption (Section 1.2.1)</b>	Antibody (Ab) (+) immobilization with physical interactions between Ab and surface. Involves hydrophobic and electrostatic interactions with hydrophobic and charged surfaces, respectively.	<div data-bbox="1029 932 1435 1199">           (+)            i. could be used for any type of antibody            ii. 'Label-free' and 'reagent-free' (no Ab modification or surface modification required)         </div> <div data-bbox="1029 1171 1435 1713">           (-)            i. Highly susceptible to protein-exchange and leaching            ii. Conformational instability of the adsorbed antibody (denaturation) due to the underlying processes such as molecular spreading or flattening            iii. Random molecular distribution (non-homogenous density of Ab on surface and no control over functional orientation of the molecules)         </div>

**Covalent immobilization**  
**(Section 1.2.2)**  
**Linker-mediated**  
**chemistries**

Linker length plays important role in minimizing the coupling-related conformational stress

**EDC-mediated (Figure 1.8 (a))**

- For surfaces with amine or carboxy-functionalization
- A classical example of heterobifunctional cross-linking (carboxy to amine)

The EDC linker activates the carboxyl group followed by transferring the activated carboxyl adduct to primary amine  
 Immobilization on amine-functionalized surfaces: Ab should be activated prior cross-linking

- (+)
- No leaching after cross-linking
  - No Ab modification required (could be performed with native proteins)
  - Commercially available from all major suppliers

Immobilization on carboxyl-functionalized surfaces: the carboxy groups of surface should be activated first

- (-)
- High susceptibility of EDC toward hydrolysis
  - Random orientation
  - Activated Ab molecules are susceptible to multimerization (could be minimized by optimizing the molar ratio of antibody to EDC and using a pH at which only carboxyl groups will interact with EDC)
  - Ab functionality may be compromised in few cases if amine groups of the antibody are conjugated to the carboxyl groups of the functionalized surfaces

**Glutaraldehyde (Figure 1.8 (b))**

- For surfaces with amine functionalization
- A classical example of homobifunctional cross-linking (amine to amine)

Glutaraldehyde activates amine groups irrespective of their position on Ab

- (+)
- Strong coupling, hence 'leach-proof'
  - No Ab modification required
  - Commercially available
- (-)
- Multimerization of Ab (this could be compensated by activating the amine-

functionalized surface with glutaraldehyde prior to Ab cross-linking)

- ii. Ab functionality may be compromised (if the amine-rich regions of antigen recognition portion of the Ab get involved in cross-linking)
- iii. No specificity
- iv. High degree of randomness in immobilized Ab molecules
- v. Inappropriate cross-linking

### **Sulfhydryl-targeting linkers**

Primarily contains maleimide (+)

or vinyl sulfone as reactive centres which target the sulfhydryl group

These could be either homo- (SH-SH) or heterobifunctional (SH-NH<sub>2</sub>) (-)

- i. Site specific immobilization in the case of cysteine-tagged Ab
- ii. Commercially available
- i. Generation of thiol groups is required on the antibody either by converting pendant amino groups of Ab into sulfhydryl (this may change the amines of the antigen recognition domain of the Ab causing compromised Ab functionality) or by reducing disulfide bonds to generate free sulfhydryl groups with chemical agents such as DTT, TCEP etc.

### **Direct chemistries**

#### **Epoxide-mediated (Figure 1.3)**

Epoxide-functionalized surface (+)

Epoxide ring opens up following the reaction of oxygen species with amine or sulfhydryl

- i. 'Leach-proof' immobilization
- ii. No Ab modification required
- iii. 'Reagent-free', 'label-free' single-step immobilization
- iv. Commercial availability
- (-)
- i. An epoxide functionalization

		of the surface is required
		ii. Randomly-orientated Ab
<b>Aldehyde-mediated</b>	Aldehyde-functionalized surface	(+)
	Aldehyde reacts with amino group that results in an imine group between surface and Ab	i. No Ab modification required (native Ab)
	Reduction of imine to amine should be performed in order to stabilize the bond	ii. Single step strategy iii. 'Label-free' and 'reagent-free'
		(-)
		i. Reversible imine-bond formation (require additional step of reduction for stabilization of the imine bond)
		ii. No site-specificity
		iii. Uncontrolled orientation
<b>Amine-mediated</b>	Amine-functionalized surface	(+)
	Ab oxidation activates the diol of the sugar moieties on the Fc region, which reacts with amine of the surface to form imine bond	i. Highly site-specific
		(-)
		i. Oxidation of Ab is required (uncontrolled oxidation)
		ii. Restricted to full-length Ab which has sugar moiety
<b>Aromatic sulfonate chloride-mediated (Figure 1.4)</b>	Tosyl and trisyl chlorides are widely used	(+)
	Aromatic chloride activates hydroxyl of the surface and conjugates it to the sulfhydryl, primary amine, imidazole and tyrosine hydroxyl of the Ab	i. Covalent attachment ii. Robust approach (could couple a variety of Ab's functional groups) iii. Site-selective iv. Single-step method v. Commercially available
		(-)
		i. Non-orientated immobilization
<b>Diels-Alder cyclo-addition (Figure 1.5)</b>	PEG-functionalized with ligand such as biotin or domain-specific protein A at $\omega$ -carbon and cyclopentadiene at $\alpha$ -carbon. PEG grafted through the	(+)
		i. Covalent attachment with higher steric freedom (PEG chain length can control the steric freedom of the captured Ab)

	cyclopentadiene on the maleimide-functionalized surface	<i>N</i> - ii. Orientated capture of Ab on protein A or biotin iii. Site-specific iv. 'Label-free' and 'reagent-free' v. Single-step procedure to generate functionalized surface
<b>Photoactive chemistry (Figure 1.7)</b>	$\beta$ -cyclodextrin-functionalized surfaces genetically-incorporated benzoyl-L-phenylalanine ( <i>p</i> Bpa) Ab	(+) <ul style="list-style-type: none"> <li>i. Covalently captured Ab</li> <li>ii. Site-specific</li> <li>iii. 'Label-free' and 'reagent-free' single step procedure</li> <li>iv. Commercially available</li> </ul> (-) <ul style="list-style-type: none"> <li>i. Incorporation of <i>p</i>Bpa may introduce conformational changes in Ab fragments such as scFv and Fab</li> </ul>
<b>Site-specific immobilization (Section 1.2.3)</b>		
<b>Affinity tags</b>		
<b>PolyHistidine (His-tag) (Figure 1.9)</b>	Nitrilotriacetic acid (NTA) or iminodiacetic acid (IDA)-functionalized surface Imidazole of histidine forms a metal co-ordination complex	(+) <ul style="list-style-type: none"> <li>i. Single step methodology</li> <li>ii. Non-covalent co-ordination complex formation</li> <li>iii. Site-specific</li> <li>iv. Reusable</li> <li>v. Commercial availability</li> </ul> (-) <ul style="list-style-type: none"> <li>i. Poor ligand affinity (histidine repeats could be increased to 6 to 10 in number to obtain higher affinity)</li> <li>ii. Leaching (it could be minimized with multimeric histidine tags)</li> <li>iii. Low selectivity (metal-</li> </ul>

		functionalized surface does not discriminate tag from the endogenous histidine-rich proteins)
<b>Biotin-Avidin system</b>	Avidin/streptavidin-functionalized surface Chemical conjugation or genetic incorporation of biotin to the Ab	(+) i. Strong specificity and selectivity (-) i. Conformational stress could be introduced due to Ab congestion on avidin surface (tetrameric molecule)
<b>Peptide-Nucleic Acid (PNA) tags</b> (Figure 1.10)	Surface-functionalized with complementary nucleic acid sequence PNA could be incorporated to Ab in a selective way either by its carboxyl end or amine end using routine EDC chemistry	(+) i. High stability over a thermal and pH range ii. Single step, 'reagent-free' and 'label-free' method iii. High degree of steric freedom by varying length of the backbone
<b>Elastin-like polypeptides (ELP)</b> <b>Thermally responsive protein</b>	ELP-functionalized surface ELP-fused Ab or fragments	(+) i. Reversible temperature-dependent immobilization ii. Highly selective (-) i. Immobilized system must be stored in a temperature range 2-37 °C (below which the ELP depolymerises and above which it precipitates)
<b>Enzyme-mediated O<sup>6</sup>-alkylguanine transferase (AGT) SNAP-tag</b> (Figure 1.12)	Benzylguanine-functionalized surface AGT-fused Ab	(+) i. Covalent immobilization ii. Site-specific iii. Commercially available
<b>Transglutaminase (TGase)</b> (Figure 1.13)	T26 tagging on <i>N</i> - or <i>C</i> -terminal of Ab with a flank of (GGGS) <sub>3</sub>	(+) i. Site-specific and covalent immobilization

- |                              |  |
|------------------------------|--|
| Amine-functionalized surface | ii. 'Reagent-free' and 'label-free' single step immobilization |
|------------------------------|--|

### Site-specific orientation-based (Section 1.2.4)

#### Enzyme domains

- |  |   |  |
|--|---|--|
| <b>Chitin-binding domain (CBD)</b><br>(Figure 1.14)                            | Chitin-functionalized surface<br>CBD-fused Ab | (+)<br>i. High selectivity and site specificity<br>ii. Covalently-captured Ab (enzyme domain interact covalently with substrate)<br>(-)<br>i. Enzyme domain could be susceptible to conformational change in different physiological conditions    |
| <b>Polyhydroxyalkanoate (PHA) depolymerase substrate-binding domain (PSBD)</b> | PHA-functionalized surface<br>PSBD-fused Ab   | (+)<br>iii. High selectivity and site specificity<br>iv. Covalently-captured Ab (enzyme domain interact covalently with substrate)<br>(-)<br>ii. Enzyme domain could be susceptible to conformational change in different physiological conditions |

#### Proteins specific to Ab domains (Figure 1.15)

- |   |  |                              |
|---|--|------------------------------|
| Fc-specific<br>Protein A (prA), protein G (prG) and recombinant | Immobilization of Fc-specific protein on surface | (+)<br>i. Strong orientation |
|---|--|------------------------------|

protein A/G (prA/G)		ii. Site-specific and high selectivity iii. Ab captured in its native state iv. Strong binding (-) i. Could only be used on Ab with Fc domain
$k_L$ -specific Protein L (prL)	prL immobilized on surface	(+) i. Strong orientation ii. Site-specific and high selectivity iii. Ab captured in its native state iv. Strong binding (-) i. Could only be used on Ab with $k_L$ domain

---

#### 1.4 References

1. Roux KH: Immunoglobulin structure and function as revealed by electron microscopy. *Int Arch Allergy Immunol* 1999, 120(2):85-99.
2. Holliger P, Hudson PJ: Engineered antibody fragments and the rise of single domains. *Nat Biotechnol* 2005, 23(9):1126-1136.
3. Blazek D, Celer V: The production and application of single-chain antibody fragments. *Folia Microbiol (Praha)* 2003, 48(5):687-698.
4. Ono K, Kamihira M, Kuga Y, Matsumoto H, Hotta A, Itoh T, Nishijima K, Nakamura N, Matsuda H, Iijima S: Production of anti-prion scFv-Fc fusion proteins by recombinant animal cells. *J Biosci Bioeng* 2003, 95(3):231-238.
5. Muyldermans S, Baral TN, Retamozzo VC, Baetselier PD, Genst ED, Kinne J, Leonhardt H, Magez S, Nguyen VK, Revets H, Rothbauer U, Stijlemans B, Tillib S,

- Wernery U, Wyns L, Hassanzadeh-Ghassabeh G, Saerens D: Camelid immunoglobulins and nanobody technology. *Vet Immunol Immunopathol* 2009, 128(1-3):178.
6. Schramm W, Paek S, Voss G: Strategies for the immobilization of antibodies. *Immunomethods* 1993, 3(2):93-103.
7. Saerens D, Ghassabeh GH, Muyldermans S: Antibody technology in proteomics. *Brief Funct Genomic Proteomic* 2008, 7(4):275-282.
8. Steinhauer C, Wingren C, Hager AC, Borrebaeck CA: Single framework recombinant antibody fragments designed for protein chip applications. *BioTechniques* 2002, 33Sup:38-45.
9. Danczyk R, Krieder B, North A, Webster T, HogenEsch H, Rundell A: Comparison of antibody functionality using different immobilization methods. *Biotechnol Bioeng* 2003, 84(2):215-223.
10. Jung Y, Jeong JY, Chung BH: Recent advances in immobilization methods of antibodies on solid supports. *Analyst* 2008, 133(6):697-701.
11. Lee CS, Belfort G: Changing activity of ribonuclease A during adsorption: a molecular explanation. *Proc Natl Acad Sci U.S.A.* 1989, 86(21):8392-8396.
12. Norde W, Favier JP: Structure of adsorbed and desorbed proteins. *Colloids Surf* 1992, 64(1):87-93.
13. Haynes CA, Norde W: Structures and stabilities of adsorbed proteins. *J Colloid Interf Sci* 1995, 169(2):313-328.

14. Kwok KC, Yeung KM, Cheung NH: Adsorption kinetics of bovine serum albumin on fused silica: population heterogeneities revealed by single-molecule fluorescence microscopy. *Langmuir* 2007, 23(4):1948-1952.
15. Rabe M, Verdes D, Zimmermann J, Seeger S: Surface organization and cooperativity during nonspecific protein adsorption events. *J Phys Chem, B* 2008, 112(44):13971-13980.
16. Raffaini G, Ganazzoli F: Protein adsorption on a hydrophobic surface: a molecular dynamics study of lysozyme on graphite. *Langmuir* 2010, 26(8):5679-5689.
17. Arnau J, Lauritzen C, Petersen GE, Pedersen J: Current strategies for the use of affinity tags and tag removal for the purification of recombinant proteins. *Protein Expr Purif* 2006, 48(1):1-13.
18. Nogi T, Sangawa T, Tabata S, Nagae M, Tamura-Kawakami K, Beppu A, Hattori M, Yasui N, Takagi J: Novel affinity tag system using structurally defined antibody-tag interaction: application to single-step protein purification. *Protein Sci* 2008, 17(12):2120-2126.
19. Decker RH, Ling C, Overby LR: Hapten conjugated antibody for antibody or antigen detection. USA Patent 1980, 05/932394(4230683).
20. Holthues H, Pfeifer-Fukumura U, Hartmann I, Baumann W: An immunoassay for terbutryn using direct hapten linkage to a glutaraldehyde network on the polystyrene surface of standard microtiter plates. *Fresenius J Anal Chem* 2001, 371(7):897-902.

21. Seurnynck-Servoss SL, Baird CL, Miller KD, Pefaur NB, Gonzalez RM, Apiyo DO, Engelmann HE, Srivastava S, Kagan J, Rodland KD, Zangar RC: Immobilization strategies for single-chain antibody microarrays. *Proteomics* 2008, 8(11):2199-2210.
22. Weiping Q, Bin X, Lei W, Chunxiao W, Zengdong S, Danfeng Y, Zuhong L, Yu W: Orientation of antibodies on a 3-aminopropyltriethoxysilane-modified silicon wafer surface. *J Inclusion Phenom macrocyclic Chem* 1999, 35(1):419-429.
23. de Boer A, Hokke C, Deelder A, Wuhler M: Serum antibody screening by surface plasmon resonance using a natural glycan microarray. *Glycoconj J* 2008, 25(1):75-84.
24. Lvov Y, Mohwald H: Protein Architecture: Interfacing Molecular Assemblies and Immobilization Biotechnology (ed. 1). Marcel & Dekker, Inc. U.S.A:2000;4-12.
25. Cornish-Bowden A: Enthalpy–entropy compensation: a phantom phenomenon. *J Biosci* 2002, 27(2):121-126.
26. Howard IK: H is for enthalpy, thanks to Heike Kamerlingh Onnes and Alfred W. Porter. *J Chem Educ* 2002, 79(6):697.
27. Pace CN, Fu H, Fryar KL, Landua J, Trevino SR, Shirley BA, Hendricks MM, Iimura S, Gajiwala K, Scholtz JM, Grimsley GR: Contribution of hydrophobic interactions to protein stability. *J Mol Biol* 2011, 408(3):514.
28. Pace CN: Energetics of protein hydrogen bonds. *Nat Struct Mol Biol* 2009, 16(7):681-682.
29. Petukhov M, Rychkov G, Firsov L, Serrano L: H-bonding in protein hydration revisited. *Protein Sci* 2004, 13(8):2120-2129.

30. Scholtz JM, Grimsley GR, Pace CN: Solvent denaturation of proteins and interpretation of their m-values. *Methods Enzymol* 2009, 466:549-565.
31. Liao H, Yeh W, Chiang D, Jernigan RL, Lustig B: Protein sequence entropy is closely related to packing density and hydrophobicity. *Protein Eng Des Sel* 2005, 18(2):59-64.
32. Schymkowitz JWH, Rousseau F, Serrano L: Surfing on protein folding energy landscapes. *Proc Natl Acad Sci U.S.A.* 2002, 99(25):15846-15848.
33. Fernandez-Escamilla AM, Cheung MS, Vega MC, Wilmanns M, Onuchic JN, Serrano L: Solvation in protein folding analysis: Combination of theoretical and experimental approaches. *Proc Natl Acad Sci U.S.A.* 2004, 101(9):2834-2839.
34. Haynes CA, Norde W: Globular proteins at solid/liquid interfaces. *Colloids Surf, B* 1994, 2(6):517-566.
35. Ball V, Huetz P, Elaissari A, Cazenave JP, Voegel JC, Schaaf P: Kinetics of exchange processes in the adsorption of proteins on solid surfaces. *Proc Natl Acad Sci U.S.A.* 1994, 91(15):7330-7334.
36. Petukhov M, Cregut D, Soares CM, Serrano L: Local water bridges and protein conformational stability. *Protein Sci* 1999, 8(10):1982-1989.
37. Sancho J, Serrano L, Fersht AR: Histidine residues at the N- and C-termini of  $\alpha$ -helices: perturbed pKas and protein stability. *Biochemistry (NY)* 1992, 31(8):2253-2258.

38. Petukhov M, Uegaki K, Yumoto N, Yoshikawa S, Serrano L: Position dependence of amino acid intrinsic helical propensities II: Non-charged polar residues: Ser, Thr, Asn, and Gln. *Protein Sci* 1999, 8(10):2144-2150.
39. Pace G, Venanzi M, Castrucci P, Scarselli M, De Crescenzi M, Palleschi A, Stella L, Formaggio F, Toniolo C, Marletta G: Static and dynamic features of a helical hexapeptide chemisorbed on a gold surface. *Mater Sci Eng , C* 2006, 26(5-7):918-923.
40. Hammer B, Morikawa Y, Nørskov JK: CO chemisorption at metal surfaces and overlayers. *Phys Rev Lett* 1996, 76(12):2141-2144.
41. Berkebile S, Ules T, Puschnig P, Romaner L, Koller G, Fleming AJ, Emtsev K, Seyller T, Ambrosch-Draxl C, Netzer FP, Ramsey MG: A momentum space view of the surface chemical bond. *Phys Chem Chem Phs* 2011, 13(9):3604-3611.
42. Liu J, Gustafsson A, Breimer ME, Kussak A, Holgersson J: Anti-pig antibody adsorption efficacy of  $\alpha$ -Gal carrying recombinant P-selectin glycoprotein ligand-1/immunoglobulin chimeras increases with core 2  $\beta$ 1, 6-N-acetylglucosaminyltransferase expression. *Glycobiology* 2005, 15(6):571-583.
43. Dixit CK, Vashist SK, MacCraith BD, O'Kennedy R: Evaluation of apparent non-specific protein loss due to adsorption on sample tube surfaces and/or altered immunogenicity. *Analyst* 2011, 136(7):1406-1411.
44. Wang X, Wang Y, Xu H, Shan H, Lu JR: Dynamic adsorption of monoclonal antibody layers on hydrophilic silica surface: a combined study by spectroscopic ellipsometry and AFM. *J Colloid Interf Sci* 2008, 323(1):18-25.

45. Ghatnekar-Nilsson S, Dexlin L, Wingren C, Montelius L, Borrebaeck CA: Design of atto-vial based recombinant antibody arrays combined with a planar wave-guide detection system. *Proteomics* 2007, 7(4):540-547.
46. Hu X, Spada S, White S, Hudson S, Magner E, Wall JG: Adsorption and activity of a domoic acid binding antibody fragment on mesoporous silicates. *J Phys Chem B* 2006, 110(37):18703-18709.
47. Bee JS, Chiu D, Sawicki S, Stevenson JL, Chatterjee K, Freund E, Carpenter JF, Randolph TW: Monoclonal antibody interactions with micro- and nanoparticles: Adsorption, aggregation, and accelerated stress studies. *J Pharm Sci* 2009, 98(9):3218-3238.
48. Butler JE, Ni L, Brown WR, Joshi KS, Chang J, Rosenberg B, Voss EW, Jr: The immunochemistry of sandwich ELISAs--VI. Greater than 90% of monoclonal and 75% of polyclonal anti-fluoresceinyl capture antibodies (CAbs) are denatured by passive adsorption. *Mol Immunol* 1993, 30(13):1165-1175.
49. Van Tassel PR, Talbot J, Tarjus G, Viot P: Kinetics of irreversible adsorption with a particle conformational change: A density expansion approach. *Phys Rev E* 1996, 53(1):785-798.
50. Fleminger G, Hadas E, Wolf T, Solomon B: Oriented immobilization of periodate-oxidized monoclonal antibodies on amino and hydrazide derivatives of Eupergit C. *Appl Biochem Biotechnol* 1990, 23(2):123-137.

51. Xu H, Lu JR, Williams DE: Effect of surface packing density of interfacially adsorbed monoclonal antibody on the binding of hormonal antigen human chorionic gonadotrophin. *J Phys Chem B* 2006, 110(4):1907-1914.
52. Kusnezow W, Jacob A, Walijew A, Diehl F, Hoheisel JD: Antibody microarrays: An evaluation of production parameters. *Proteomics* 2003, 3(3):254-264.
53. Kusnezow W, Hoheisel JD: Solid supports for microarray immunoassays. *J Mol Recognit* 2003, 16(4):165-176.
54. Guo A, Zhu XY: In functional protein microarrays in drug discovery (ed. 1). Ed. Predki PF. Boca Raton, CRC Press, Florida, US; 2007:53-71.
55. Ljungberg UK, Jansson B, Niss U, Nilsson R, Sandberg BE, Nilsson B: The interaction between different domains of staphylococcal protein A and human polyclonal IgG, IgA, IgM and F(ab')<sub>2</sub>: separation of affinity from specificity. *Mol Immunol* 1993, 30(14):1279-1285.
56. Akerstrom B, Bjorck L: A physicochemical study of protein G, a molecule with unique immunoglobulin G-binding properties. *J Biol Chem* 1986, 261(22):10240-10247.
57. Kastern W, Sjobring U, Bjorck L: Structure of peptostreptococcal protein L and identification of a repeated immunoglobulin light chain-binding domain. *J Biol Chem* 1992, 267(18):12820-12825.
58. Sasakura Y, Kanda K, Yoshimura-Suzuki T, Matsui T, Fukuzono S, Han MH, Shimizu T: Protein microarray system for detecting protein-protein interactions using an anti-His-tag antibody and fluorescence scanning: effects of the heme redox state on

- protein-protein interactions of heme-regulated phosphodiesterase from *Escherichia coli*. *Anal Chem* 2004, 76(22):6521-6527.
59. Huetz P, Ball V, Voegel J, Schaaf P: Exchange kinetics for a heterogeneous protein system on a solid surface. *Langmuir* 1995, 11(8):3145-3152.
60. Corso CD, Dickherber A, Hunt WD: An investigation of antibody immobilization methods employing organosilanes on planar ZnO surfaces for biosensor applications. *Biosens Bioelectron* 2008, 24(4):811-817.
61. Das RD, Maji S, Das S, RoyChaudhuri C: Optimization of covalent antibody immobilization on macroporous silicon solid supports. *Appl Surf Sci* 2010, 256(20):5867.
62. Dixit CK, Vashist SK, O'Neill FT, O'Reilly B, MacCraith BD, O'Kennedy R: Development of a high sensitivity rapid sandwich elisa procedure and its comparison with the conventional approach. *Anal Chem* 2010, 82(16):7049-7052.
63. Darain F, Gan K, Tjin S: Antibody immobilization onto polystyrene substrate-on-chip immunoassay for horse IgG based on fluorescence. *Biomed Microdevices* 2009, 11(3):653-661.
64. Shmanai V, Nikolayeva T, Vinokurova L, Litoshka A: Oriented antibody immobilization to polystyrene macrocarriers for immunoassay modified with hydrazide derivatives of poly(meth)acrylic acid. *BMC Biotechnol* 2001, 1(1):4.
65. Abuknesha RA, Jeganathan F, Wu J, Baalawy Z: Labeling of biotin antibodies with horseradish peroxidase using cyanuric chloride. *Nat Protocols* 2009, 4(4):452-460.

66. Andersen BR, Abele DC, Vannier WE: Effects of mild periodate oxidation on antibodies. *J Immunol* 1966, 97(6):913-924.
67. Wei Z, Feng J, Lin H, Mullapudi S, Bishop E, Tous GI, Casas-Finet J, Hakki F, Strouse R, Schenerman MA: Identification of a single tryptophan residue as critical for binding activity in a humanized monoclonal antibody against respiratory syncytial virus. *Anal Chem* 2007, 79(7):2797-2805.
68. Zamani L, Andersson, FO, Edebrink P, Yang Y, Jacobsson, SP: Conformational studies of a monoclonal antibody, IgG1, by chemical oxidation: Structural analysis by ultrahigh-pressure LC-electrospray ionization time-of-flight MS and multivariate data analysis. *Anal Biochem* 2008, 380(2):155-163.
69. Caballero D, Samitier J, Bausells J, Errachid A: Direct patterning of anti-human serum albumin antibodies on aldehyde-terminated silicon nitride surfaces for hsa protein detection. *Small* 2009, 5(13):1531-1534.
70. Shen G, Zhang Y: Highly sensitive electrochemical stripping detection of hepatitis B surface antigen based on copper-enhanced gold nanoparticle tags and magnetic nanoparticles. *Anal Chim Acta* 2010, 674(1):27.
71. Elia G, Silacci M, Scheurer S, Scheuermann J, Neri D: Affinity-capture reagents for protein arrays. *Trends Biotechnol* 2002, 20(12):s19-s22.
72. Ehlers J, Rondan NG, Huynh LK, Pham H, Marks M, Truong TN: Theoretical study on mechanisms of the epoxy-amine curing reaction. *Macromolecules* 2007, 40(12):4370-4377.

73. Thermo Scientific Pierce Protein Research Products: Cross-linking reagents: A technical handbook. 2006.
74. Nilsson K, Mosbach K: Immobilization of ligands with organic sulfonyl chlorides. *Methods Enzymol* 1986, 104:56-69.
75. Hermanson GT, Mallia AK, Smith PK: Immobilized affinity ligand techniques (ed.1). Academic Press, San Diego, US; 1992;66-155.
76. Kim HS, Hage DS: Immobilization methods for affinity chromatography. In Handbook of affinity chromatography (ed,1). Ed. Hage DS. CRC press, Florida, US; 2006:37-78.
77. Uttamchandani M, Wang J, Yao SQ: Protein and small molecule microarrays: Powerful tool for high-throughput proteomics. *Mol Bio Syst* 2006, 2:58-68.
78. Sun X, Stabler CL, Cazalis CS, Chaikof EL: Carbohydrate and Protein Immobilization onto Solid Surfaces by Sequential Diel-Alder and Azide-Alkyne Cycloadditions. *Bioconjug Chem* 2006, 17(1):52-57.
79. Sun XL, Yang L, Chaikof EL: Chemoselective immobilization of biomolecules with aqueous Diel-Alders and PEG chemistry. *Tetrahedron Lett* 2008, 49(16):2510-2513.
80. Colombo M, Bianchi A: Click chemistry for the synthesis of RGD-containing integrin ligands. *Molecules* 2010, 15(1):178-197.
81. Jullian V, Courtois F, Bolbach G, Chassaing G: Carbon-carbon bond ligation between  $\beta$ -cyclodextrin and peptide by photo-irradiation. *Tetrahedron Lett* 2003, 44(34):6437-6440.

82. Jensen RL, Stal' de LW, Wimmer R, Stensballe A, Duroux M, Larsen KL, Wingren C, Duroux L: Direct site-directed photocoupling of proteins onto surfaces coated with  $\beta$ -cyclodextrins. *Langmuir* 2010, 26(13):11597-11604.
83. Hino N, Hayashi A, Sakamoto K, Yokoyama S: Site-specific incorporation of non-natural amino acids into proteins in mammalian cells with an expanded genetic code. *Nat Protocols* 2007, 1(6):2957-2962.
84. Wang F, Robbins S, Guo J, Shen W, Schultz PG: Genetic Incorporation of Unnatural Amino Acids into Proteins in *Mycobacterium tuberculosis*. *PLoS ONE* 2010, 5(2):e9354.
85. Wong SS: Conjugation of proteins to solid matrices. In Chemistry of protein conjugation and cross-linking (ed.1). Ed. Wong SS. Florida, CRC press, US; 1991:295-318.
86. Migneault I, Dartiguenave C, Bertrand MJ, Waldron KC: Glutaraldehyde: behavior in aqueous solution, reaction with proteins, and application to enzyme crosslinking. *Biotechniques* 2004,37:790–802..
87. Howell S, Kenmore M, Kirkland M, Badley RA: High-density immobilization of an antibody fragment to a carboxymethylated dextran-linked biosensor surface. *J Mol Recognit* 1998, 11(1-6):200-203.
88. Kweon D, Kim S, Han NS, Lee JH, Chung KM, Seo J: Immobilization of *Bacillus macerans* cyclodextrin glycosyltransferase fused with poly-lysine using cation exchanger. *Enzyme Microb Technol* 2005, 36(4):571-578.

89. Bain CD, Troughton EB, Tao YT, Evall J, Whitesides GM, Nuzzo RG: Formation of monolayer films by the spontaneous assembly of organic thiols from solution onto gold. *J Am Chem Soc* 1989, 111(1):321-335.
90. Bhatia SK, Shriver-Lake LC, Prior KJ, Georger JH, Calvert JM, Bredehorst R, Ligler FS: Use of thiol-terminal silanes and heterobifunctional crosslinkers for immobilization of antibodies on silica surfaces. *Anal Biochem* 1989, 178(2):408-413.
91. Morfill J, Blank K, Zahnd C, Luginbuhl B, Kuhner F, Gottschalk KE, Pluckthun A, Gaub HE: Affinity-matured recombinant antibody fragments analyzed by single-molecule force spectroscopy. *Biophys J* 2007, 93(10):3583-3590.
92. Kipriyanov SM, Little M: Affinity purification of tagged recombinant proteins using immobilized single chain Fv fragments. *Anal Biochem* 1997, 244(1):189-191.
93. Sun MMC, Beam KS, Cervený CG, Hamblett KJ, Blackmore RS, Torgov MY, Handley FGM, Ihle NC, Senter PD, Alley SC: Reduction and alkylation strategies for the modification of specific monoclonal antibody disulfides. *Bioconjug Chem* 2005, 16(5):1282-1290.
94. Chen LL, Rosa JJ, Turner S, Pepinsky RB: Production of multimeric forms of CD4 through a sugar-based cross-linking strategy. *J Biol Chem* 1991, 266(27):18237-18243.
95. Rao SV, Anderson KW, Bachas LG: Oriented immobilization of proteins. *Microchimica Acta* 1998, 128(3):127-143.
96. Brogan KL, Wolfe KN, Jones PA, Schoenfisch MH: Direct oriented immobilization of F(ab') antibody fragments on gold. *Anal Chim Acta* 2003, 496(1-2):73-80.

97. Wong SS: Reactive groups of proteins and their modifying agents. In *Chemistry of protein conjugation and cross-linking* (ed.1). Ed. Wong SS. Florida, CRC press, US; 1991:7-48.
98. Hedhammer M, Graslund T, Hober S: Protein engineering strategies for selective protein purification. *Chem Engineer Technol* 2005, 28(11):1315-1325.
99. Rusmini F, Zhong Z, Feijen J: Protein immobilization strategies for protein biochips. *Biomacromolecules* 2007, 8(6):1775-1789.
100. Camarero JA: Recent development in the site-specific immobilization of proteins onto solid supports. *Biopolymers* 2008, 90(3):450-458.
101. Darain F, Ban C, Shim YB: Development of a new and simple method for the detection of histidine-tagged proteins. *Biosens Bioelectron* 2004, 20(4):857-863.
102. Cha T, Guo A, Zhu XY: Enzymatic activity on a chip: the critical role of protein orientation. *Proteomics* 2005, 5(2):416-419.
103. Hochuli E: Large-scale chromatography of recombinant proteins. *J Chromatog* 1988, 444:293-302.
104. Gaberc-Porekar V, Menart V: Potential for using histidine tags in purification of protein at large scale. *Chem Engineer Technol* 2005, 28(11):1306-1314.
105. Paramban RI, Bugos RC, Su WW: Engineering green fluorescent protein as a dual functional tag. *Biotechnol Bioengineer* 2004, 86(6):687-697.

106. Halliwell CM, Morgan G, Ou C, Cass AEG: Introduction of a (poly)histidine tag in l-lactate dehydrogenase produces a mixture of active and inactive molecules. *Anal Biochem* 2001, 295(2):257-261.
107. Lin P, Weinrich D, Waldmann H: Protein biochips: Oriented surface immobilization of proteins. *Macromolecular Chem Phys* 2010, 211(2):136-144.
108. Wong LS, Khan F, Micklefield J: Selective covalent protein immobilization: strategies and applications. *Chem Rev* 2009, 109(9):4025-4053.
109. Fan G, Gregory KN, Zhao W, Park WJ, Kranias EG: Regulation of myocardial function by histidine-rich, calcium-binding protein. *Am J Physiol Heart Circ Physiol* 2004, 287(4):H1705-H1711.
110. Sadanandom A, Findlay K, Doonan JH, Schulze-Lefert P, Shirasu K: CHPA, a cysteine- and histidine-rich-domain-containing protein, contributes to maintenance of the diploid state in *Aspergillus nidulans*. *Eukaryotic Cell* 2004, 3(4):984-991.
111. Jones AL, Hulett MD, Parish CR: Histidine-rich glycoprotein: A novel adaptor protein in plasma that modulates the immune, vascular and coagulation systems. *Immunol Cell Biol* 2005, 83(2):106-118.
112. Khan F, He M, Taussig MJ: Double-hexahistidine tag with high-affinity binding for protein immobilization, purification, and detection on  $\text{Ni}^{+2}$  nitrilotriacetic acid surfaces. *Anal Chem* 2006, 78(9):3072-3079.
113. Steinhauer C, Wingren C, Khan F, He M, Taussig MJ, Borrebaeck CAK: Improved affinity coupling for antibody microarrays: Engineering of double-(His)<sub>6</sub>-tagged single framework recombinant antibody fragments. *Proteomics* 2006, 6(15):4227-4234.

114. Laitinen OH, Nordlund HR, Hytönen VP, Kulomaa MS: Brave new (strept)avidins in biotechnology. *Trends Biotechnol* 2007, 25(6):269.
115. Grunwald C: A brief introduction to the streptavidin-biotin system and its usage in modern surface based assays. *Zeitschrift für Physikalische Chemie* 2008, 222(5-6):789-821.
116. Chalkias NG, Giannelis EP: An avidin-biotin immobilization approach for horseradish peroxidase and glucose oxidase on layered silicates with high catalytic activity retention and improved thermal behavior. *Industrial Biotechnol* 2007, 3(1):82-88.
117. Torres-Rodríguez LM, Billon M, Roget A, Bidan G: A polypyrrole-biotin based biosensor: elaboration and characterization. *Synth Met* 1999, 102(1-3):1328-1329.
118. Jones CJ, Stoddart RW: A post-embedding avidin-biotin peroxidase system to demonstrate the light and electron microscopic localization of lectin binding sites in rat kidney tubules. *Histochem J* 1986, 18(7):371-379.
119. Pavlickova P, Hug H: A streptavidin-biotin-based microarray platform for immunoassays. *Methods Mol Biol* 2004, 264:73-83.
120. Pradier CM, Salmain M, Liu Z, Methivier C: Comparison of different procedures of biotin immobilization on gold for the molecular recognition of avidin: an FT-IRRAS study. *Surf Interface Anal* 2002, 34(1):67-71.
121. Kolenko P, Dohnalek J, Duskova J, Skalova T, Collard R, Hasek J: New insights into intra- and intermolecular interactions of immunoglobulins: crystal structure of mouse IgG2b-Fc at 2Å-0.1Å resolution. *Immunology* 2009, 126(3):378-385.

122. Burkhart KK, Beard D, Billingsley ML: Enhanced elimination of biotinylated antibodies by avidin-based hemoperfusion in rats. *J Pharmacol Exp Therapeutics* 1994, 270(1):356-361.
123. Holmberg A, Blomstergren A, Nord O, Lukacs M, Lundeberg J, Uhlen M: The biotin-streptavidin interaction can be reversibly broken using water at elevated temperatures. *Electrophoresis* 2005, 26(3):501-510.
124. Johnsson B, Lofas S, Lindquist G, Edstrom A, Hillgren RM, Hansson A: Comparison of methods for immobilization to carboxymethyl dextran sensor surfaces by analysis of the specific activity of monoclonal antibodies. *J Mol Recognit* 1995, 8(1-2):125-131.
125. Evans L, Hughes M, Waters J, Cameron J, Dodsworth N, Tooth D, Greenfield A, Sleep D: The production, characterisation and enhanced pharmacokinetics of scFv-albumin fusions expressed in *Saccharomyces cerevisiae*. *Protein Expr Purif* 2010, 73(2):113.
126. Piervincenzi RT, Reichert WM, Hellinga HW: Genetic engineering of a single-chain antibody fragment for surface immobilization in an optical biosensor. *Biosens Bioelectron* 1998, 13(3-4):305-312.
127. Nielsen P, Egholm M, Berg R, Buchardt O: Sequence-selective recognition of DNA by strand displacement with a thymine-substituted polyamide. *Science* 1991, 254(5037):1497-1500.
128. Egholm M, Buchardt O, Christensen L, Behrens C, Freier SM, Driver DA, Berg RH, Kim SK, Norden B, Nielsen PE: PNA hybridizes to complementary

oligonucleotides obeying the Watson–Crick hydrogen-bonding rules. *Nature* 1993, 365(6446):566-568.

129. Sheng H, Ye BC: Different strategies of covalent attachment of oligonucleotide probe onto glass beads and the hybridization properties. *Appl Biochem Biotechnol* 2009, 152(1):54-65.

130. Silva TAR, Ferreira LF, Souza LM, Goulart LR, Madurro JM, Brito-Madurro AG: New approach to immobilization and specific-sequence detection of nucleic acids based on poly(4-hydroxyphenylacetic acid). *Mat Sci Eng, C* 2009, 29(2):539-545.

131. Hook F, Ray A, Norden B, Kasemo B: Characterization of PNA and DNA Immobilization and Subsequent Hybridization with DNA Using Acoustic-Shear-Wave Attenuation Measurements. *Langmuir* 2001, 17(26):8305-8312.

132. Masuko M: Hybridization of an immobilized PNA probe with its complementary oligodeoxyribonucleotide on the surface of silica glass. *Nucleic Acids Res Suppl* 2003, 3:145-146.

133. Lim SY, Chung W, Lee HK, Park MS, Park HG: Direct and nondestructive verification of PNA immobilization using click chemistry. *Biochem Biophys Res Commun* 2008, 376(4):633-636.

134. Ray A, Norden B: Peptide nucleic acid (PNA): its medical and biotechnical applications and promise for the future. *FASEB J* 2000, 14(9):1041-1060.

135. Zhong M, Fang J, Wei Y: Site Specific and Reversible Protein Immobilization Facilitated by A DNA Binding Fusion Tag. *Bioconjug Chem* 2010, 21(7):1177-1182.

136. Meyer DE, Trabbic-Carlson K, Chilkoti A: Protein purification by fusion with an environmentally responsive elastin-like polypeptide: effect of polypeptide length on the purification of thioredoxin. *Biotechnol Prog* 2001, 17(4):720-728.
137. Trabbic-Carlson K, Meyer DE, Liu L, Piervincenzi R, Nath N, LaBean T, Chilkoti A: Effect of protein fusion on the transition temperature of an environmentally responsive elastin-like polypeptide: a role for surface hydrophobicity? *Protein Eng Des Sel* 2004, 17(1):57-66.
138. Ong SR, Trabbic-Carlson KA, Nettles DL, Lim DW, Chilkoti A, Setton LA: Epitope tagging for tracking elastin-like polypeptides. *Biomaterials* 2006, 27(9):1930-1935.
139. Floss DM, Schallau K, Rose-John S, Conrad U, Scheller J: Elastin-like polypeptides revolutionize recombinant protein expression and their biomedical application. *Trends Biotechnol* 2010; 28:37-45.
140. Gao D, McBean N, Schultz JS, Yan Y, Mulchandani A, Chen W: Fabrication of antibody arrays using thermally responsive elastin fusion proteins. *J Am Chem Soc* 2006, 128(3):676-677.
141. Zhang L, Liu Y, Chen T: Label-free amperometric immunosensor based on antibody immobilized on a positively charged gold nanoparticle/L-cysteine-modified gold electrode. *Microchimica Acta* 2009, 164(1):161-166.
142. Hopp TP, Prickett KS, Price VL, Libby RT, March CJ, Pat Cerretti D, Urdal DL, Conlon PJ: A short polypeptide marker sequence useful for recombinant protein identification and purification. *Nat Biotech* 1988, 6(10):1204-1210.

143. Nakajima H, Brindle PK, Handa M, Ihle JN: Functional interaction of STAT5 and nuclear receptor co-repressor SMRT: implications in negative regulation of STAT5-dependent transcription. *EMBO J* 2001, 20(23):6836-6844.
144. Butterfield DA, Bhattacharya D: Biofunctional membranes: site specifically immobilized enzyme arrays. In *New insights in membrane science and technology: polymeric and biofunctional membranes*. Edited by Butterfield DA, Bhattacharya D. Elsevier Science BV, Amsterdam, The Netherlands; 2003:233-240.
145. Hodneland CD, Lee Y, Min D, Mrksich M: Selective immobilization of proteins to self-assembled monolayers presenting active site-directed capture ligands. *Proc Natl Acad Sci U.S.A.* 2002, 99(8):5048-5052.
146. Juillerat A, Gronemeyer T, Keppler A, Gendreizig S, Pick H, Vogel H, Johnsson K: Directed evolution of o<sub>6</sub>-alkylguanine-dna alkyltransferase for efficient labeling of fusion proteins with small molecules in vivo. *Chemistry & Biology* 2003; 10:313-317.
147. Kindermann M, George N, Johnsson N, Johnsson K: Covalent and selective immobilization of fusion proteins. *J Am Chem Soc* 2003, 125(26):7810-7811.
148. Huber W, Perspicace S, Kohler J, Müller F, Schlatter D: SPR-based interaction studies with small molecular weight ligands using hAGT fusion proteins. *Anal Biochem* 2004, 333(2):280-288.
149. Engin S, Trouillet V, Franz CM, Welle A, Bruns M, Wedlich D: Benzylguanine Thiol Self-Assembled Monolayers for the Immobilization of SNAP-tag Proteins on Microcontact-Printed Surface Structures. *Langmuir* 2010, 26(9):6097-6101.

150. Kufer S, Dietz H, Albrecht C, Blank K, Kardinal A, Rief M, Gaub H: Covalent immobilization of recombinant fusion proteins with hAGT for single molecule force spectroscopy. *Eur Biophys J* 2005, 35(1):72-78.
151. Kampmeier F, Ribbert M, Nachreiner T, Dembski S, Beaufils F, Brecht A, Barth S: Site-specific, covalent labeling of recombinant antibody fragments via fusion to an engineered version of 6-o-alkylguanine dna alkyltransferase. *Bioconjug Chem* 2009, 20(5):1010-1015.
152. Iversen L, Cherouati N, Berthing T, Stamou D, Martinez KL: Templated protein assembly on micro-contact-printed surface patterns. use of the snap-tag protein functionality. *Langmuir* 2008, 24(12):6375-6381.
153. Sugimura Y, Ueda H, Maki M, Hitomi K: Novel site-specific immobilization of a functional protein using a preferred substrate sequence for transglutaminase 2. *J Biotechnol* 2007, 131(2):121-127.
154. Sala A, Ehrbar M, Trentin D, Schoenmakers RG, Voros J, Weber FE: Enzyme mediated site-specific surface modification. *Langmuir* 2010, 26(13):11127-11134.
155. Kuranda MJ: Immobilization and purification of fusion proteins using chitin-binding ability. U.S.A. Patent 303827(5258502).
156. Wang J, Chao Y: Immobilization of cells with surface-displayed chitin-binding domain. *Appl Environ Microbiol* 2006, 72(1):927-931.
157. Blank K, Lindner P, Diefenbach B, Plückthun A: Self-immobilizing recombinant antibody fragments for immunoaffinity chromatography: generic, parallel, and scalable protein purification. *Protein Expr Purif* 2002, 24(2):313.

158. Lindner P, Blank K, Diefenbach B, Plückthun A: Chitin binding domains for immobilizing antibody fragments in immunoaffinity chromatography. In *Proceedings of the 5th International Conference of the European Chitin Society. Volume VI*. Edited by K. M. Varum, A. Domard and O. Smidsrod. Norwegian University of Science and Technology, Trondheim: The European Chitin Society (EUCHIS); 2002:261-262.
159. Saerens D, Huang L, Bonroy K, Muyldermans S: Antibody fragments as probe in biosensor development. *Sensors* 2008, 8(8):4669-4686.
160. Reulen S, van Baal I, Raats J, Merkx M: Efficient, chemoselective synthesis of immunomicelles using single-domain antibodies with a C-terminal thioester. *BMC Biotechnol* 2009, 9(1):66.
161. Tjoelker LW, Gosting L, Frey S, Hunter CL, Trong HL, Steiner B, Brammer H, Gray PW: Structural and functional definition of the human chitinase chitin-binding domain. *J Biol Chem* 2000, 275(1):514-520.
162. Pavlickova P, Schneider EM, Hug H: Advances in recombinant antibody microarrays. *Clinica Chimica Acta* 2004, 343(1-2):17-35.
163. Park T, Park J, Lee S, Hong H, Lee S: Polyhydroxyalkanoate chip for the specific immobilization of recombinant proteins and its applications in immunodiagnostics. *Biotechnol Bioprocess Eng* 2006, 11(2):173-177.
164. Kausaite-Minkstimiene A, Ramanaviciene A, Kirlyte J, Ramanavicius A: Comparative study of random and oriented antibody immobilization techniques on the binding capacity of immunosensor. *Anal Chem* 2010, 82(15):6401-6408.

165. Vashist SK, Holthofer H, Leister K: A method of immobilising biological molecules to a support and products thereof. 2009, PCT / IE2008/ 000112 (WO/ 2009/ 066275).
166. Schmid AH, Stanca SE, Thakur MS, Thampi KR, Suri CR: Site-directed antibody immobilization on gold substrate for surface plasmon resonance sensors. *Sens Actuat, B: Chem* 2006, 113(1):297.
167. Carrigan SD, Scott G, Tabrizian M: Real-time QCM-D immunoassay through oriented antibody immobilization using cross-linked hydrogel biointerfaces. *Langmuir* 2005, 21(13):5966-5973.
168. Yuan Y, He H, Lee LJ: Protein A-based antibody immobilization onto polymeric microdevices for enhanced sensitivity of enzyme-linked immunosorbent assay. *Biotechnol Bioeng* 2009, 102(3):891-901.
169. Beyer NH, Hansen MZ, Schou C, Hojrup P, Heegaard NHH: Optimization of antibody immobilization for on-line or off-line immunoaffinity chromatography. *J Sep Sci* 2009, 32(10):1604.
170. Subramanian A, Velander WH: Effect of antibody orientation on immunosorbent performance. *J Mol Recognit* 1996, 9(5-6):528-535.
171. Darby RAJ, Hine AV: LacI-mediated sequence-specific affinity purification of plasmid DNA for therapeutic applications. *FASEB J*. 2005, 19(7):801-803.
172. Ueda EKM, Gout PW, Morganti L: Current and prospective applications of metal ion-protein binding. *J Chromat, A* 2003, 988(1):1.

## **1.5 Aims**

### **The aims of this research were:**

1. Development of a generic surface modification strategy which can be used over a variety of solid supports. This section was dedicated to develop an approach that, unlike labour-intense chemical methods of surface modification, would be easy to perform under ambient conditions/ routine laboratory set-ups and would be cost-effective at the same time. A strategy was developed based on KOH- and O<sub>2</sub>-plasma-based surface activation followed by silane-mediated functionalization. This strategy could be employed on surfaces that are hydrophobic, hydrophilic and chemically inert.
2. Development of high-sensitivity assays on the aforementioned modified surfaces. The bioanalytical platforms chosen were of commercial interest and included polymer-based microtitre plates for enzyme-linked and fluorescence immunoassays and fluorocap platforms (Bristol Myers Squibb, Syracuse, NY, USA, licensed platform) for fluorescence immunoassays. The other major analytical strategy involved custom-functionalized gold surfaces for surface plasmon resonance. This section was directed towards demonstrating the application of the activated surfaces following functionalization with silanes and employing them to immobilize antibodies for immunoassay development in direct (model antigen: IgG) and sandwich (model antigen: human fetuin A) formats. Fluorocap and chromatographic resin-based technologies were developed and transferred to Bristol Myers Squibb, Syracuse, NY, USA.
3. Development of antibody-conjugated nanoprobe using high brightness nanoparticles, developed within our group, for detection of activation phases of platelets. This section involved nanoparticle functionalization, optimization and conjugation to platelet-specific anti-CD41 antibody for surface marker probing.

## **Chapter 2**

Development of a modified high sensitivity  
rapid sandwich ELIA procedure with  
picogram sensitivity

(Published in Analytical Chemistry 2010, 82, 7049-7052)

## 2.1 Abstract

A highly sensitive and rapid sandwich enzyme-linked immunoassay (ELIA) procedure was developed for the detection of human fetuin A/AHSG ( $\alpha$ 2-HS-glycoprotein), a specific biomarker for hepato-cellular carcinoma and atherosclerosis. Anti-human fetuin A antibody was immobilized on aminopropyltriethoxysilane-mediated amine-functionalized microtitre plates using 1-ethyl-3-[3-dimethylaminopropyl]carbodiimide hydrochloride and N-hydroxysulfosuccinimide-based heterobifunctional cross-linking. The analytical sensitivity of the developed assay was 39 pg/mL, compared to 625 pg/mL for the conventional assay. The generic nature of the developed procedure was demonstrated by performing human fetuin A assays on different polymeric matrices i.e. polystyrene, poly(methyl methacrylate) and polycyclo-olefin (Zeonex), in a modified microtitre plate format. Thus, the newly developed procedure has considerable advantages over the existing method.

## 2.2 Introduction

Conventional enzyme-linked immunosorbent assay (ELISA) procedures have been followed for decades for the detection of analytes of importance in industrial, healthcare, and academic research. However, improvements on existing ELISA technologies are continuously attempted by many groups [1, 2]. The development of a high-sensitivity enzyme-linked immunoassay (ELIA)-based assay for human fetuin A (HFA), with lower detection limits and a higher sensitivity than commercially available assays is reported. The biological importance of HFA, a member of the cystatin superfamily, which is commonly present in the cortical plate of the immature cerebral cortex and hemopoietic matrix of bone marrow, is discussed elsewhere [3-10]. There are many commercially available ELISA kits for fetuin A, which are listed in **Table 2.1**. The assay was demonstrated on various commercially relevant solid supports. The developed ELIA is better than the conventional procedure in terms of greatly reduced overall assay duration, higher sensitivity, and greater reproducibility.

HFA was taken as the model analyte system to demonstrate the utility of the developed ELIA procedure since all the assay components were commercially available in kit form. This enables the performance of a robust and highly precise comparison of the developed ELIA with the commercially existing conventional ELISA procedures, as the same assay components were used under the same conditions. The developed procedure can be employed on any commercially relevant substrate. Therefore, this approach of immobilizing antibody on chemically-modified solid supports (**Figure 2.1**) has potential applications in many other assays and formats.

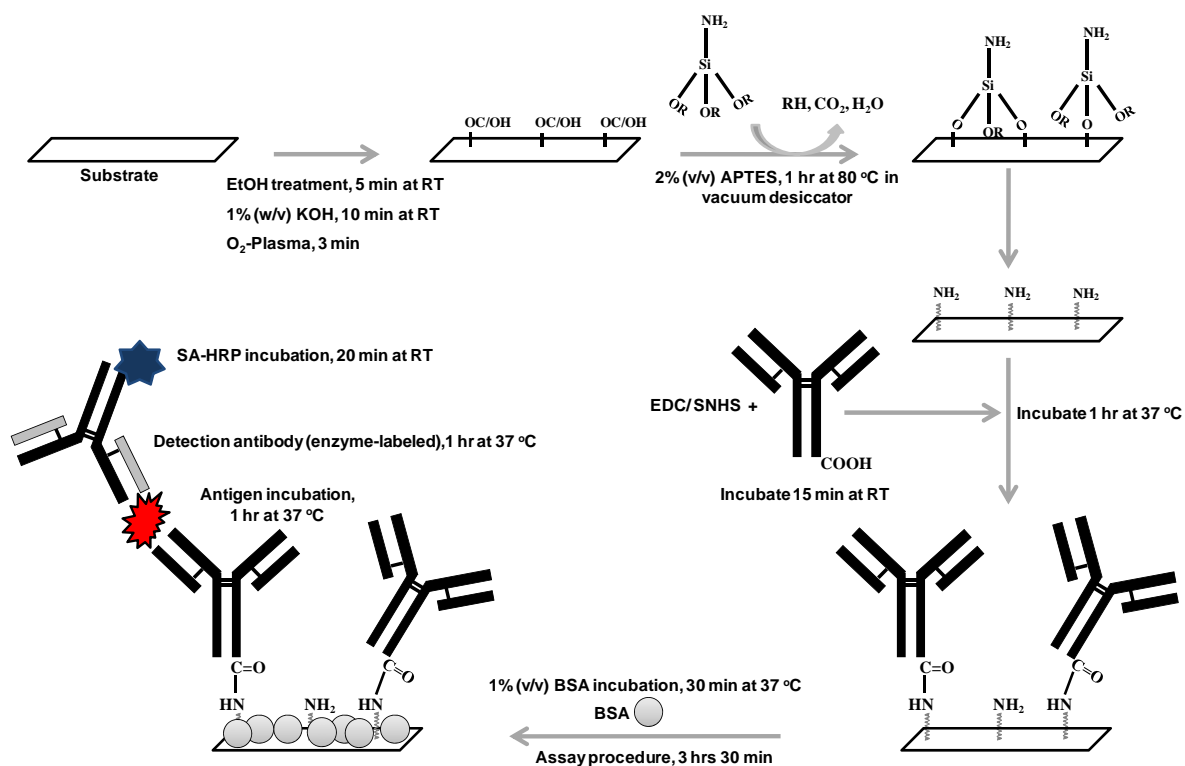


**Figure 2.1** Schematic of the developed sandwich ELISA procedure for the HFA assay. Plate functionalization was performed by treatment with 1% (w/v) KOH, treatment with oxygen (O<sub>2</sub>)-plasma and then silanization with 2% (v/v) APTES. KOH oxidizes the organic moiety of the polymer generating a carbonyl (-CO) or a hydroxyl (-OH) group according to the nature of the polymer. The alkoxy groups of APTES subsequently react with the carbonyl or hydroxyl groups of the surface in a hydrolysis-dependent reaction [11, 12]. Anti-HFA/ $\alpha$ -Herman Schmidt glycoprotein (AHSG) antibody was then activated using EDC and SNHS chemistry on the aminated 96-well plate, where the EDC-SNHS was used in a ratio of 1:100 with the antibody.

### 2.3 Materials

EDC, SNHS, phosphate buffered saline (PBS, 0.1M, pH 7.4), 2-(N-morpholino)ethanesulfonic acid (MES, pH 4.7), 3,3',5,5'-Tetramethylbenzidine (TMB) substrate kit and bovine-serum albumin (BSA) were purchased from Fisher Scientific (previously Pierce), Ballycoolin, Dublin, Ireland. Potassium hydroxide (KOH), 3-APTES,

absolute ethanol and Nunc 96-well polystyrene plates (P7491) were obtained from Sigma-Aldrich, Blessington, Co. Wicklow, Ireland. The HFA duoset kit, with all HFA assay components, was procured from RnD Systems, Abingdon, Oxon, UK. The capture antibody used was mouse anti-HFA/ $\alpha$ -Herman Schmidt glycoprotein (AHSG) while detection was achieved through the use of biotinylated goat anti-HFA/AHSG antibody and streptavidin-conjugated horseradish peroxidase (HRP).

**Table 2.1** A comparative analysis of various commercially available ELISA techniques with their respective formats and the high sensitivity modified ELISA procedure reported here.

<b>Manufacturer</b>	<b>Format of antibody capture</b>	<b>Sensitivity (ng/mL)</b>	<b>Refer to</b>
Covalent assay	Chemically cross-linked	0.03	Reported in Chapter 2
Passive assay	Passively adsorbed	0.31	Reported in Chapter 2
RnD systems	Passively adsorbed	0.37	<a href="http://www.rndsystems.com/pdf/DY1184.pdf">http://www.rndsystems.com/pdf/DY1184.pdf</a>
Biovendor	Passively adsorbed	0.35	<a href="http://www.biovend.com/product/immunoassays/fetuin-a-ahsg-human-elisa">http://www.biovend.com/product/immunoassays/fetuin-a-ahsg-human-elisa</a>
Alpco Diagnostics	Passively adsorbed	5.00	<a href="http://www.alpco.com/pdfs/43/43-NSEHU-E01.pdf">http://www.alpco.com/pdfs/43/43-NSEHU-E01.pdf</a>
Immunology Consultants Laboratory, Inc.	Passively adsorbed	6.25	<a href="http://www.life-sciences.com.br/pdf/icllab.pdf">http://www.life-sciences.com.br/pdf/icllab.pdf</a>
Genway Biotech, Inc.	Passively adsorbed	6.25	<a href="http://www.genwaybio.com/images/gw_tds/elisa_kits/40-374-130036.pdf">http://www.genwaybio.com/images/gw_tds/elisa_kits/40-374-130036.pdf</a>
Assay Pro	Passively adsorbed	6.25	<a href="http://www.assaypro.com/datasheet/eg3501_1.pdf">http://www.assaypro.com/datasheet/eg3501_1.pdf</a>

All assay components were reconstituted in 0.1M PBS, pH 7.4, with 1% (v/v) BSA. Buffers and solutions were prepared in Milli-Q deionised water (DIW). The dilutions of all HFA assay components and BSA were made in 0.1M PBS, pH 7.4, whereas KOH and 3-APTES were diluted in DIW. EDC and SNHS were reconstituted in 0.1M MES buffer, pH 4.7. Poly(methyl methacrylate) (PMMA), polystyrene (PS) and zeonex<sup>TM</sup> slides were purchased from Microfluidic Chip Shop GmbH, Jena, Germany. Pressure-sensitive adhesive (PSA) was obtained from Adhesive Research, Limerick, Ireland. Bottomless 96-well microtitre plates were purchased from Greiner Labortechnik, Germany. The Optec Micro-Master CO<sub>2</sub> Laser was procured from Optec S.A., Belgium. The assay temperature was maintained at 37 °C using a thermostat which was obtained from Labnet International Inc., Edison, NJ, USA.

## **2.4 Experimental Section**

### **2.4.1 Microtitre plate functionalization with amine-silane and anti-human fetuin A antibody immobilization**

Each well of the 96-well plate was treated with 100 µL of absolute ethanol for 5 min at 37 °C and washed five times with 300 µL of deionised water (DIW). Subsequently, each well was treated with 100 µL of 1.0% (w/v) KOH at 37 °C for 10 min followed by five washings with 300 µL of DIW. The KOH-treated wells were then treated with O<sub>2</sub>-plasma and were functionalized with amino groups by incubation with 100 µL of 2% (v/v) aminopropyltriethoxysilane (APTES) per well at 80 °C for 1 h inside a vacuum-desiccator, in order to achieve maximum silanization. It is important to mention here is that KOH-based chemical oxidation followed by O<sub>2</sub>-plasma treatment facilitates generation and stabilization of the surface functional groups. The reaction mechanism following the KOH

activation and APTES-based surface functionalization involves mild oxidation followed by a hydrolytic APTES polymerization on the oxidized surface through its alkoxy groups [11, 12]. The desiccator was equilibrated to room temperature for 20 min. The amine-functionalized plate was subsequently washed five times with 300  $\mu$ L of DIW in order to remove excess unbound 3-APTES from the surface. Afterward, the anti-HFA/AHSG (990  $\mu$ L of 4  $\mu$ g/mL) was incubated with 10  $\mu$ L of a pre-mixed solution of 1-ethyl-3-[3-dimethylaminopropyl]carbodiimide hydrochloride (EDC) (4 mg/mL) and N-hydroxysulfosuccinimide (SNHS) (11 mg/mL) for 15 min at 37°C. The resulting EDC cross-linked anti-HFA/AHSG antibody solution was added to each of the functionalized wells (100  $\mu$ L) and incubated for 1 h at 37°C. The anti-HFA/AHSG-coated wells were then washed five times with 300  $\mu$ L of PBS. The conventional ELISA was performed with the protocol supplied by the manufacturer.

#### **2.4.2 ELIA on anti-HFA/AHSG antibody-immobilized microtitre plates**

Plates with covalent and passively immobilized anti-HFA antibody were blocked with 1% (v/v) BSA diluted in 0.1M phosphate buffered saline (PBS), pH 7.4, for 30 min at 37 °C and subsequently washed five times with 300  $\mu$ L of PBS. Varying concentrations of HFA/AHSG (from 4.8 pg/mL to 20 ng/mL) were prepared in 0.1M PBS, pH 7.4, and 100  $\mu$ L of each of these concentrations were incubated in the antibody-coated plates for 1 h at 37 °C, and, subsequently washed five times with PBS. One hundred microliters of biotinylated anti-HFA/AHSG detection antibody (200 ng/mL) was added and incubated for 1 hr at 37 °C followed by five PBS washes. HRP-conjugated streptavidin (100  $\mu$ L per well), at a dilution of 1:200, was added and then incubated for 20 min at 37 °C followed by five washes with PBS. The 3,3',5,5'-tetramethylbenzidine (TMB) substrate was subsequently added (as per

the manufacturer's recommendations) and the reaction was stopped after 20 min by addition of 50  $\mu$ L of 0.5M H<sub>2</sub>SO<sub>4</sub>. The absorbance was recorded at a primary wavelength of 450 nm with a reference wavelength of 540 nm. The dual wavelength system of absorbance measurement in 96-well plates is designed to eliminate or greatly reduce the optical imperfections at the well-to-well level.

All the experiments were carried out in triplicate. The control for this study was zero ng/mL concentration of HFA in 0.1M PBS, pH 7.4, and the absorbance of the control was subtracted from all the assay values. The respective analytical sensitivity (detection limit) of the assay were determined where it was calculated using the formula [mean absorbance of blank + 3 $\sigma$  (standard deviation of the blank)]. Additionally, data sets obtained from the ELIA and conventional ELISA were analysed using standard curve analysis of Sigma Plot software, version 11.0.

## **2.5 Results and Discussion**

### **2.5.1 Developed ELIA and conventional ELISA formats for HFA detection**

The range of detection of HFA for the developed ELIA (**Figure 2.2**) was 9 to 20 pg/mL ( $r^2=0.99$ ). An analytical sensitivity of 39 pg/mL was recorded for the developed ELIA, where analytical sensitivity was calculated using the formula [average absorbance of blank + 3 (SD<sub>blank</sub>)]. Assay variability parameters for this high-sensitivity assay for HFA are described in **Table 2.2**, where intra-day assay variability was calculated from 5 repeats performed on a single day and inter-day assay variability from three repeats performed on three different days in triplicate.

The half-effective concentration (EC<sub>50</sub>) obtained from the dose-response curve [13], which is a measure of analyte-ligand interaction, was found to be on an average of 3.3 ng/mL. The

EC<sub>50</sub> for all the assay repeats was found to be in the range of 3-3.5 ng/mL. A lower EC<sub>50</sub> (3.3 ng/mL), which was obtained for the developed ELIA, suggests a strong interaction between HFA and anti-HFA antibody. This interaction behavior is attributed to the significant increase in the total amount of immobilized antibody achieved by using the covalent immobilization strategy, which increased the availability of anti-HFA antibody per HFA molecule, thus increasing the resultant HFA capture on the well surface.

**Table 2.2.** Comparison of assay performance parameters (precision and sensitivity) for conventional ELISA and developed ELIA

	<b>Intra-day precision range (CV%), (n=5)</b>	<b>Inter-day precision range (CV%), (n=3)</b>	<b>Sensitivity</b>
Developed ELISA	2.4-10.4	1.7-17.6	39 pg/mL
Conventional ELISA	4.7-17.4	3.6-20.0	312.0 pg/mL

*Intra-day precision was calculated from the five repeats (n=5) of the same assay on a single day but at different times while inter-day precision was calculated from assay repeats on three different days (n=3). All the assays were carried out in triplicate. Analytical sensitivity was determined using the formula [average absorbance of blank + 3 (SD<sub>blank</sub>)].*

Conversely, EC<sub>50</sub> for the conventional ELISA format was 23 ng/mL, ( $r^2=0.99$ ), which was significantly higher than the developed ELIA. This suggests a less sensitive conventional assay (**Table 2.3**). The most important factor that may be attributed to the enhanced sensitivity of the modified assay is the covalent immobilization of the anti-HFA/AHSG capture antibody, since the covalently-crosslinked antibodies should not leach out during the assay procedure in comparison to the use of passively-adsorbed antibodies, where leaching may occur more easily.

Performance of the developed sandwich ELIA procedure was compared with the conventional protocols (**Figure 2.2**), both involving passively adsorbed antibody on normal unmodified microtitre plates (one performed using the modified protocol and the other as per the manufacturer's recommendations). All the assays were performed simultaneously on the same day under same set of conditions in order to minimize variability, where variability was reported as percentage coefficient of variation (% CV).

**Table 2.3** Comparative analysis of the modified sandwich ELISA procedure which was developed for HFA/AHSG and the commercially used conventional sandwich ELISA procedure in terms of timings of various assay steps (**Table 2.2**).

<b>Immunoassay</b>	<b>Conventional HFA ELISA</b>	<b>Modified HFA ELIA</b>
<b>Steps and Parameters</b>	<b>(passively adsorbed Ab)</b>	<b>(covalently captured Ab)</b>
Immobilization of mouse anti-HFA	Overnight at room temp (RT)	2 hrs 30 min
Blocking buffer (BSA)	2 hrs at RT	30 min at 37° C
Recombinant HFA	2 hrs at RT	1 hr at 37° C
Incubation of biotinylated goat anti-HFA	2 hrs at RT	1 hr at 37° C
Binding of Streptavidin-HRP	20 min at RT	20 min at 37° C
TMB substrate assay	20 min at RT	20 min at 37° C
Total immunoassay duration	~ 20 hrs	~ 6 hrs
Detection limit	156 pg/mL	9.76 pg/mL
Sensitivity	624 pg/mL	39 pg/mL
Immobilization strategy applicable to many polymeric surfaces	Not possible	Possible

The technique employed here for chemically modifying the polymeric surface was developed and standardized by our group and a standard EDC-based cross-linking strategy was deployed to immobilize anti-HFA/AHSG antibody. The developed sandwich ELIA procedure decreased the overall assay duration from 20 h to 6 h, which is more than a 3-fold

decrease. Thus, the reported procedure is a rapid ELIA format having the additional benefit of being generic in nature, i.e. it can be used with sandwich ELISAs on different polymeric matrices for a range of different analytes. Hence, using the surface modification technique reported here, it is possible to develop rapid and high sensitivity assays on various categories of solid supports including those that are chemically inert.

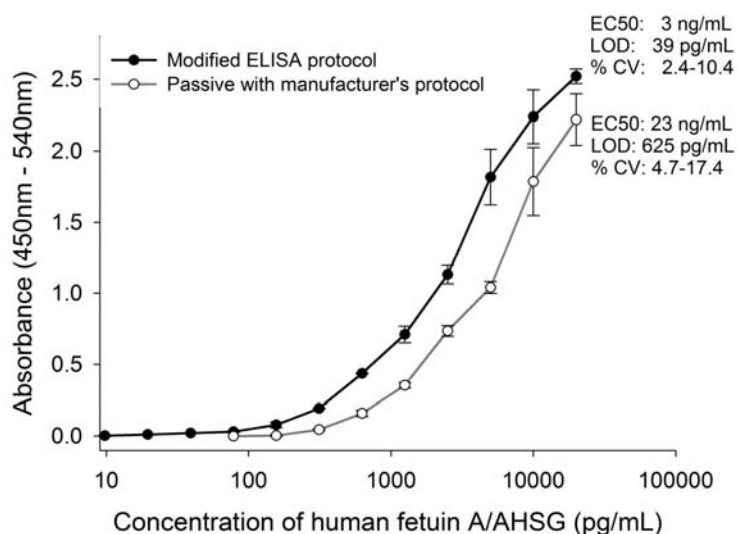


**Figure 2.2** Comparative analysis of developed sandwich ELISA (black circles) with conventional formats. Anti-human fetuin A (anti-HFA) antibody was covalently bound to the amine-modified surface in the developed ELISA, whereas antibody adsorbed on the unmodified surface was used in the conventional assay format. The assay was performed with the manufacturer-recommended protocol (white circles) and the protocol developed in this study (filled circles). The error bars represents the standard deviations.

As far as can be ascertained, this developed ELIA procedure is the most sensitive assay reported for the detection of HFA/AHSG (**Table 2.2**), which is based on the comparison between different commercially-available ELISA kits for HFA. The sensitivity of the assay may be attributed to the use of monoclonal antibody at the capture stage, which was

covalently immobilized on the surface, and a polyclonal antibody to detect the antigen. The covalently cross-linked monoclonal antibody that is used as capture antibody in this study was found to capture significantly higher amounts of HFA, which has improved the detection limit and the overall assay sensitivity of the developed ELIA procedure in comparison to other conventional formats. However, the commercially available ELISA kits, as described in **Table 2.1**, have different capture and detection antibody combinations that may be a factor in their reduced sensitivities [14]. The sensitivity and specificity of any immunoassay is dependent on the antigen capture efficiency of an antibody which is subsequently governed by the nature of antibody [15, 16] and accounts for the different assay sensitivities of the commercially-available kits employing different types of antibodies that are monoclonal or polyclonal at the capture stage in ELISA.

### **2.5.2 Generic nature of the developed sandwich ELIA procedure on different substrates**

Five different substrates were demonstrated for the use of the developed surface modification strategy and antibody immobilization followed by immunoassay performance (**Figure 2.3b**), whereas, three different types of commercially relevant substrates, polystyrene (PS) (hydrophobic), polymethyl methacrylate (PMMA) (hydrophilic) and cyclolefin polymer (zeonex) (inert), were demonstrated for the assay development (**Figure 2.3a**). The HFA assay was performed on these matrices in the modified microtitre plate format.

The HFA assays performed on different solid substrates could not be directly compared because of their different thicknesses. Theoretically, the optical path length contributes

toward the absorbance (A). Therefore, a thick solid support increases the path length and hence significantly changes the absorbance. However, generic nature of the developed strategy was successfully demonstrated (**Figure 2.3**).

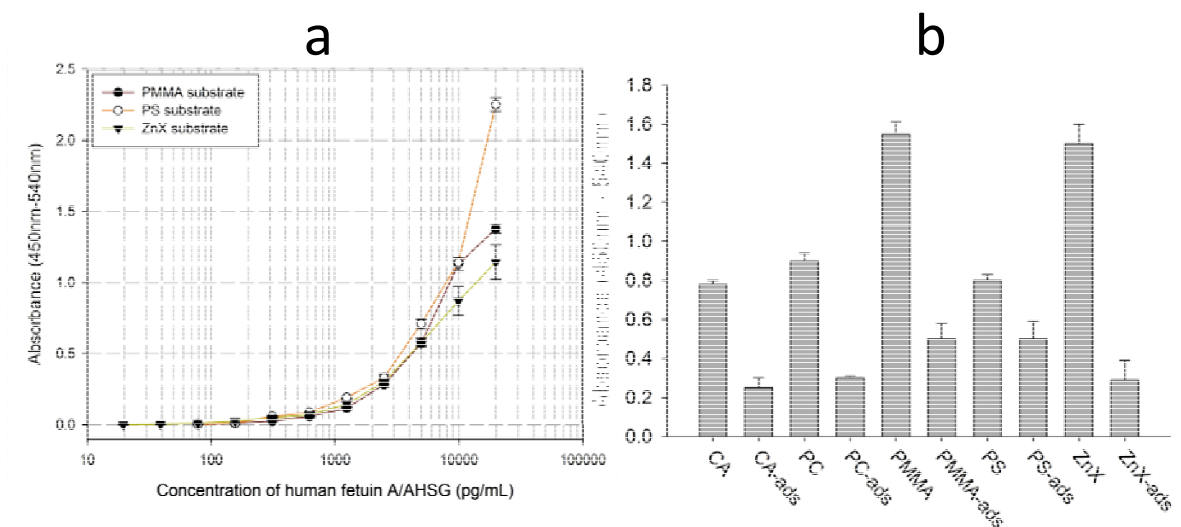


**Figure 2.3** Generic nature of the antibody immobilization procedure that enables performance of the developed sandwich ELIA for human fetuin A (HFA) on different solid support matrices. (a) ELIA performance on three categories of solid supports that were chosen on the basis of their chemical properties, namely polystyrene (PS) which is hydrophobic (white circles), polymethyl methacrylate (PMMA), a hydrophilic polymer (black circles) and polycycloolefin polymer, trade name Zeonex that is a neutral matrix (inverted black triangles). (b) Demonstration of ELIA on a range of various polymeric solid supports that have been regularly employed in biosensor development. The error bars represent the standard deviations.

The HFA assay performed on Zeonex support, which is an inert cyclic polyoolefin derivate, had an analytical sensitivity of 39 pg/mL, while for the assay performed on PS and PMMA, it was 78 pg/mL. The  $EC_{50}$  for the HFA assay performed on Zeonex and PMMA was approximately 7 ng/mL ( $r^2=0.98$ ) and for PS it was 9 ng/mL. The analytical sensitivities for the HFA assays and the dose-response, which determines the slope-dependent linearity

range of the assay, of HFA-anti-HFA for all the solid supports used in this study suggests that this modified protocol increases the overall assay sensitivity and is not confined to the nature of the solid support used for capturing antibody.

## **2.6 Conclusions**

A rapid sandwich ELISA procedure was developed for the detection of HFA/AHSG. It was based on the covalent immobilization of anti-HFA capture antibody on a 3-APTES functionalized microtitre plate and had an analytical sensitivity of 39 pg/mL of HFA/AHSG. The antibody immobilization procedure is generic in nature for capturing antibody on solid supports irrespective of their chemical nature of the support. This strategy can also be used in research for rapid assay development on various commercially relevant substrates and the screening of substrates for a particular biosensor/diagnostic application.

## **2.7 References**

1. Kaur J, Boro RC, Wangoo N, Singh KR, Suri CR: Direct hapten coated immunoassay format for the detection of atrazine and 2,4-dichlorophenoxyacetic acid herbicides. *Anal Chim Acta* 2008, 607(1):92-99.
2. Jia C, Zhong X, Hua B, Liu M, Jing F, Lou X, Yao S, Xiang J, Jin Q, Zhao J: Nano-ELISA for highly sensitive protein detection. *Biosens Bioelectron* 2009, 24(9):2836-2841.
3. Kalabay L, Graf L, Voros K, Jakab L, Benko Z, Telegdy L, Fekete B, Prohaszka Z, Fust G: Human serum fetuin A/alpha2HS-glycoprotein level is associated with long-term survival in patients with alcoholic liver cirrhosis, comparison with the Child-Pugh and MELD scores. *BMC Gastroenterol* 2007, 7(1):15-23.

4. Srinivas P, Wagner A, Reddy L, Deutsch D, Leon M, Goustin A, Grunberger G: Serum alpha 2-HS-glycoprotein is an inhibitor of the human insulin receptor at the tyrosine kinase level. *Mol Endocrinol* 1993, 7(11):1445-1455.
5. Mathews ST, Srinivas PR, Leon MA, Grunberger G: Bovine fetuin is an inhibitor of insulin receptor tyrosine kinase. *Life Sci* 1997, 61(16):1583-1592.
6. Kalabay L, Prohaszka Z, Fust G, Benko Z, Telegdy L, Szalay F, Toth K, Graf L, Jakab L, Pozsonyi T, Arnaud P, Fekete B, Karadi I: Human fetuin/alpha2HS-glycoprotein levels in sera of patients with liver disease. In *Liver Cirrhosis: New Research*. Ed. Chen TM. Nova Science, New York, USA; 2005:63-75.
7. Reynolds JL, Skepper JN, McNair R, Kasama T, Gupta K, Weissberg PL, Jahnchen-Dechent W, Shanahan CM: Multifunctional Roles for Serum Protein Fetuin-A in Inhibition of Human Vascular Smooth Muscle Cell Calcification. *J Am Soc Nephrol* 2005, 16(10):2920-2930.
8. Jethwaney D, Lepore T, Hassan S, Mello K, Rangarajan R, Jahnchen-Dechent W, Wirth D, Sultan AA: Fetuin-A, a Hepatocyte-Specific Protein That Binds *Plasmodium berghei* Thrombospondin-Related Adhesive Protein: a Potential Role in Infectivity. *Infect Immun* 2005, 73(9):5883-5891.
9. Ix JH, Shlipak MG, Brandenburg VM, Ali S, Ketteler M, Whooley MA: Association Between Human Fetuin-A and the Metabolic Syndrome: Data From the Heart and Soul Study. *Circulation* 2006, 113(14):1760-1767.

10. Hermans MMH, Brandenburg V, Ketteler M, Kooman JP, van der Sande FM, Boeschoten EW, Leunissen KML, Krediet RT, Dekker FW: Association of serum fetuin-A levels with mortality in dialysis patients. *Kidney Int* 2007, 72(2):202-207.
11. Park S, Jung W: Effect of KOH activation on the formation of oxygen structure in activated carbons synthesized from polymeric precursor. *J Colloid Interf Sci* 2002, 250(1):93-98.
12. Cass T, Ligler FS: Immobilized biomolecules in analysis: a practical approach (ed.1). Oxford University Press, New York, USA; 1998.
13. Armbruster D, Schwarzhoff R, Hubster E, Liserio M: Enzyme immunoassay, kinetic microparticle immunoassay, radioimmunoassay, and fluorescence polarization immunoassay compared for drugs-of-abuse screening. *Clin Chem* 1993, 39(10):2137-2146.
14. Wild D: Immunoassay troubleshooting guide. In *The Immunoassay Handbook* (ed.2). Ed. Wild D. New York, USA: Nature Publishing Group; 2001:483-518.
15. Byrne B, Stack E, Gilmartin N, O'Kennedy R: Antibody-based sensors: principles, problems and potential for detection of pathogens and associated toxins. *Sensors* 2009, 9(6):4407-4445.
16. Lacy A, Dunne L, Fitzpatrick B, Daly S, Keating G, Baxter A, Hearty S, O'Kennedy R: Rapid analysis of coumarins using Surface Plasmon Resonance. *J AOAC Intern* 2006, 89(3):884-892.

## **Chapter 3**

Evaluation of apparent non-specific protein  
loss due to adsorption on sample tube surface  
and/ or altered immunogenicity

(Published in the Analyst, 2011, 136(7), 1406-1411)

### **3.1 Abstract**

The non-specific loss of protein analytes can have a major effect on assay results particularly where the concentrations of such analytes are extremely low and the matrix is complex. This report assesses how the protein incubated in sample tubes may be lost due to adsorption. Use of proteins, such as bovine serum albumin (BSA), may be used to pre-treat tubes to reduce such losses. However, such losses may also be associated with structural perturbations leading to changes in immunogenicity (as a result of alterations in specific epitope-related conformations). This can lead to erroneous results or lack of comparability with a range of methodologies such as the bicinchoninic protein assay and immunoassays, or when surface plasmon resonance (SPR)-based approaches are used. A model system to evaluate these phenomena is proposed.

### 3.2 Introduction

Analytical techniques such as surface plasmon resonance (SPR) and enzyme-linked immunosorbent assay (ELISA) may involve sample preparation [1-5] and long incubation periods of analyte in sample tubes. Thus, there is a possibility of analyte loss due to non-specific binding to matrix-associated interferents or adsorption of protein molecules onto the surface of the sampling tubes or onto devices used in the preparation procedure [6-14]. This may result in a low analyte recovery and/or a considerable decrease in the signal obtained with specific techniques (e.g. antibody-based methods such as ELISA). Therefore, it is critically important to prevent such analyte loss, particularly for those antigens that are present at very low concentrations (such as cardiac troponins, tumor biomarkers or cytokines) [15]. The use of relevant controls and standards can be used to compensate for some losses due to this phenomenon. However, it can have very significant effects if the technique or assay used is no longer able to detect the low levels of the analyte present, due to the amount lost in the pre-analysis steps.

This report describes analyte losses both as a function of duration of incubation and due to the chemical nature of the tube material. The model analytes employed for this study were human fetuin A (HFA) and HRP-labeled mouse IgG. Analyte loss was characterized by comparative analysis of sampling performed in tubes that were either treated with blocking proteins such as BSA or were used without any prior treatment (untreated). Known quantities of the analyte were incubated in BSA-treated and untreated tubes made of polypropylene (PP) and low protein-adsorbing chrome-coated glass (GT) (customized for SPR studies) for 0, 0.5 and 12 h. The analyte loss was characterized as a function of

decrease in absorbance obtained with the bicinchoninic acid (BCA) assay (which is a direct method for calculation of total protein concentration in solution and hence, to quantitate protein recovery). After confirming protein analyte loss with the BCA assay, enzyme-linked immunoassay (ELIA) and surface plasmon resonance (SPR) were employed to determine the apparent concentration of the targeted analytes. Results indicated that in immunoassay-based analyses the reduction in concentration may be due to a combination of losses associated with non-specific adsorption and to structural changes that may result in altered epitope conformation, leading to reduced immunogenicity.

### **3.3 Materials**

1-ethyl-3-(3-dimethylaminopropyl)carbodiimide (EDC), sulfo-N-hydroxysuccinimide (SNHS), phosphate buffered saline (PBS, pH 4.7), tetramethylbenzidine (TMB) substrate kit, BCA assay kit and bovine serum albumin (BSA) were purchased from Fisher Scientific (Ireland), Ballycoolin, Dublin, Ireland. HRP-labeled mouse IgG, goat anti-mouse IgG, potassium hydroxide (KOH), 3-APTES, absolute ethanol, Nunc 96-well polystyrene plates (P7491) and Eppendorf polypropylene (PP) microtubes were obtained from Sigma-Aldrich, Blessington, Co. Wicklow, Ireland. SIA gold chips (BR-1004-05) and glass vials (BR-1002-09) were obtained from GE Healthcare, Buckinghamshire, HP7 9NA, UK. Human fetuin A/AHSG duoset kit, with all human fetuin A assay components, was procured from R&D Systems Europe, Abingdon, Oxon, UK. The kit consisted of the capture antihuman fetuin A/AHSG (anti-HFA) antibody from mouse, human fetuin A/AHSG standard, biotinylated goat anti-HFA detection antibody and streptavidin–HRP. All the assay components were reconstituted in 0.15 M PBS, pH 7.4, with 1% (w/v) BSA. All buffers and solutions were prepared using Milli-Q deionised water (DIW). The dilution of BSA was made in 0.15 M

PBS, pH 7.4, whereas KOH and 3-APTES were diluted in DIW. EDC and SNHS were reconstituted in 0.1 M MES buffer, pH 4.7.

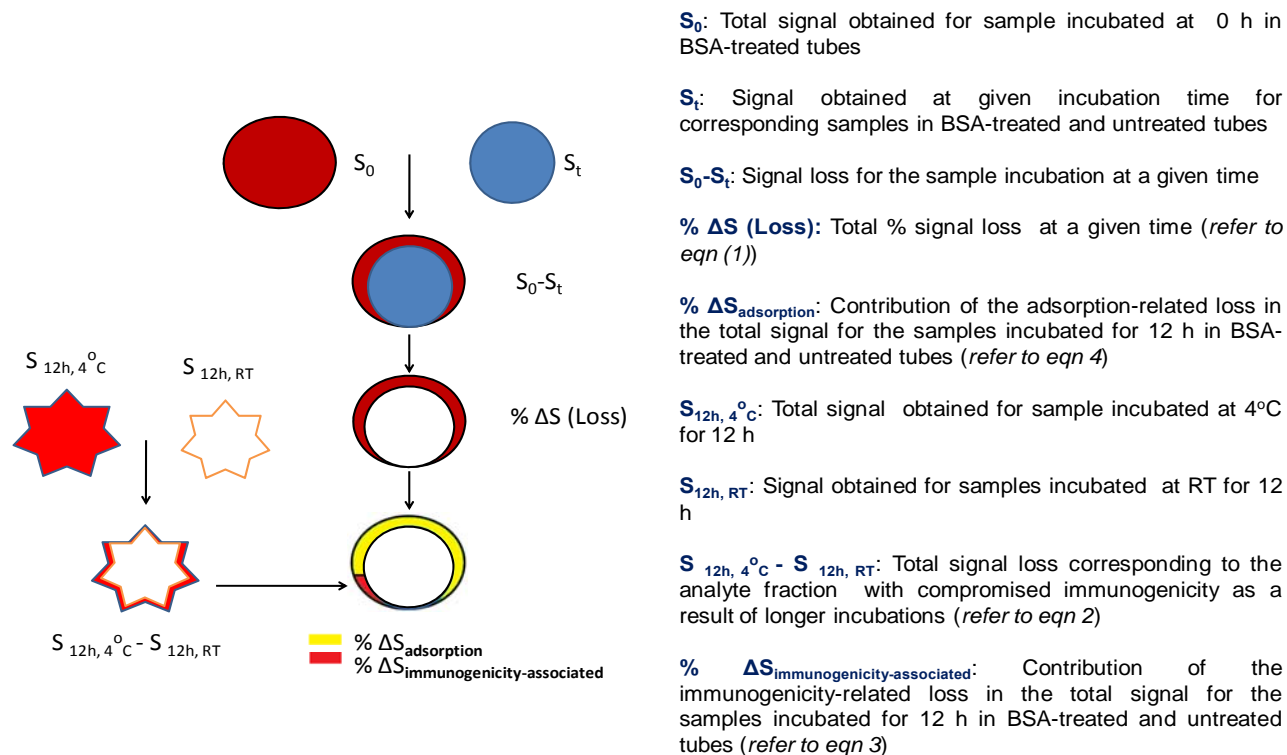


**Figure 3.1** This model is designed to illustrate that the losses in analyte (e.g. HFA) concentration, as determined by antibody-based methods, result from a combination of both adsorption on the tube surfaces and loss of conformation-related immunogenicity and that these increase over time of incubation and also are temperature dependent.

### 3.4 Experimental

#### 3.4.1 Tube blocking

Polypropylene (PP) and glass (GT) tubes were treated with 1% (w/v) BSA for 30 min followed by extensive washing with PBS (0.15 M, pH 7.4). The tubes were dried under nitrogen ( $N_2$ ).

### 3.4.2 Sampling

For initial experiments, HFA (2  $\mu\text{g/mL}$ ) and HRP-labeled mouse IgG (2  $\mu\text{g/mL}$ ) were employed. After performing all the analyses, HFA (0–20 000  $\text{pg/mL}$ ) and HRP-labeled mouse IgG (0–1210  $\text{ng/mL}$ ), reconstituted in 0.15 M PBS, pH 7.4, were employed for the immunoassay studies. All samples were incubated in BSA-treated and untreated tubes (PP and GT) for 0, 0.5 and 12 h at room temperature (RT). Additionally, HFA was also incubated in BSA (1% (w/v))-treated and untreated tubes at 4 °C for analysis essential to quantify the contribution of sample incubation conditions to the altered immunogenicity. ‘Blank’ controls for this study had zero analyte concentration and were incubated for 0 h in blocked PP and GT tubes. These controls also facilitate the detection of any BSA leaching into solution from the tube surfaces following blocking.

### 3.4.3 Analytical techniques

ELIA was performed over the stated concentration range of analytes for all sets of sampling, whereas the BCA and SPR assays were performed at concentrations of 10  $\text{ng/mL}$  and 300  $\text{ng/mL}$  for HFA and HRP-labeled mouse IgG, respectively. The BCA assay, performed according to the manufacturer’s instructions, was used to determine the HFA recovery in the samples incubated for different durations. ELIA was performed with covalently immobilized anti-HFA antibody, as previously described [16]. The microtiter plate wells were activated using 1% (w/v) KOH. The amine-functionalization was performed with 3-aminopropyltriethoxy silane (APTES). The anti-HFA antibody was conjugated to the aminated surface via EDC chemistry.

For SPR (Biacore 3000) analysis each flow-cell of the amine-activated gold chip had approximately 5000 response units of anti-HFA antibody immobilised, using EDC

chemistry. The sample buffer (HEPES, pH 7.0) was passed over all the flow-cells serving as a blank. Four different concentrations of HFA (1.25–10 ng/mL) in two sets were incubated in BSA-treated and untreated tubes and were then subjected to SPR analysis. The corresponding control values were subtracted from each signal value. The absorbance and RU signals obtained for ELIA and SPR were analysed and reported as the % analyte loss, where the % signal loss for each set of experiments was calculated as a loss relative to the 0 h sampling performed in blocked (B) tubes and discussed in detail in the Theory and analysis section. Similarly, goat anti-mouse IgG was immobilized on the chip and HRP-labeled mouse IgG was assayed at a concentration of 300 ng/mL (concentration just above the EC<sub>50</sub> value). SPR was performed on all samples that were used in the BCA assay and ELIA.

#### **3.4.4 Theory and analysis**

The model developed is an attempt to capture key elements that can impinge on the accuracy and potential sensitivity of an assay and to suggest approaches that may help to quantitate and minimise the sample loss. It is also the case that there are inherent limitations in the analytical methods used but the model attempts to take these into consideration.

The model describing various theoretical considerations is presented in **Figure 3.1**. The model follows the sequence of events according to the ‘A–B’ rule, where the contributing factors are calculated by deducting individual fractions at each step from the total. All the calculations performed with the results obtained from BCA, ELIA and SPR were based on an assumption that there was no significant analyte loss for the samples incubated in blocked tubes for 0 h incubation. The difference in signals obtained for samples incubated for various durations in blocked and unblocked tubes with respect to those in blocked tubes at 0

h quantifies the adsorption-based analyte loss (%  $\Delta S$ ). This is summarized as eqn (1).

$$\% \Delta S = [1 - (S_t / S_{0hB})] \times 100 \text{-----(1)}$$

where,

$S_t$ : Signal obtained for the HFA or HRP-labeled mouse IgG samples at a given incubation time

$S_{0hB}$ : Signal obtained for the HFA or HRP-labeled mouse IgG sample incubated in BSA-treated tubes at 0 h incubation (equivalent to 100% signal)

The loss was expressed as the relative percentage signal loss (Table 1, marked with \*), where the signal corresponds to the absorbance (for ELIA-based analysis) or response units (for SPR-based analysis) for each set of sampling performed in either PP or GT tubes.

Similarly, the signal loss contributed by the reduced analyte immunogenicity (%  $\Delta S_{\text{immunogenicity-associated}}$ ) was calculated as the difference in signals obtained with the samples incubated for 12 h in blocked tubes at RT with respect to those in blocked tubes for 12 h at 4 °C. This is shown in eqn (2). This assumption was based on the fact that when protein molecules in solution are adsorbed onto surfaces, their conformation may become more unstable and a loss of structural integrity can occur [17-21]. There may also be aggregation-dependent activity loss where the aggregation may either be due to solvent [22, 23] or temperature effects [24]. Additionally, an increase in protein adsorption occurs in the temperature range 20-40 °C. However, at lower temperatures there is a significant reduction in adsorption [25, 26].

For this study, the analyte samples were incubated in the BSA-treated tubes under two conditions (a) at RT and (b) at 4 °C with the same experimental set-up. The percentage

fraction of the signal loss relative to the samples incubated at 4 °C for 12 h was calculated using the following equation 2,

$$\% \Delta S_{\text{immunogenicity-associated}} = [\{(S_{0B} - S_{12h \text{ RT } B}) / S_{12h \text{ 4 } ^\circ \text{C } B}\} - \{1 - (S_{12h \text{ RT } B} / S_{12h \text{ 4 } ^\circ \text{C } B})\}] \times 100 \text{---(2)}$$

where,

$S_{12h \text{ RT}}$  : Signal of the HFA or HRP-labeled mouse IgG samples incubated for 12 h at RT and,

$S_{12h \text{ 4 } ^\circ \text{C } B}$  : Signal of corresponding sample incubated for 12 h at 4 °C in BSA-treated tubes (equivalent to the estimate of signal loss contributed mainly by adsorption in blocked tubes only)

This fraction, as exemplified by equation (2), corresponds to losses associated with altered immunogenicity in samples due to longer incubations. However, the total analyte loss (eq. 1) for 12 h incubation at RT consists of two different loss fractions corresponding to adsorption and altered immunogenicity. Therefore, in order to obtain how much the compromised immunogenicity (eq. 2; Table 2 marked with \*\*) contributes toward the total signal loss equation (3) may be devised.

$$\%(\Delta S / \Delta S_{\text{immunogenicity-associated}}) = [(B_n) \cdot (A_n)] \text{-----(3)}$$

where,

$B_n$ : altered immunogenicity-associated loss ( $\% \Delta S_{\text{immunogenicity-associated}}$ ) for ‘n’ h of incubation at RT,

$A_n$ : Total signal loss ( $\% \Delta S$ ) in the samples for corresponding incubation time (as calculated using eqn (1)).

Similarly, the adsorption-associated analyte loss can be obtained by deducting the altered immunogenicity fraction (eqn (3)) from the total analyte loss corresponding to

100% loss (eqn (1)). The percentage fraction of total signal loss corresponding to the loss due to non-specific adsorption (Table 1 marked with \*\*) was calculated using equation (4),

$$[(100 - B_n) \cdot A_n] \text{ -----(4)}$$

The fractions corresponding to loss due to adsorption and immunogenicity are listed in Table 1. Moreover, the immunogenicity-associated loss in untreated tubes could be determined by eqn (5) (Table 2), which is based on assumptions that adsorption is insignificant in blocked tubes and there is negligible immunogenicity-associated loss of analyte in blocked tubes incubated at 4°C.

$$\% \Delta S_{\text{immunogenicity-associated in untreated tubes}} = \left[ \left\{ (S_{0B} - S_{12h \text{ RT U}}) / S_{12h \text{ 4 } ^\circ \text{C B}} \right\} - \left\{ (S_{12h \text{ 4 } ^\circ \text{C B}} - S_{12h \text{ 4 } ^\circ \text{C U}}) / (S_{12h \text{ 4 } ^\circ \text{C B}} - S_{12h \text{ RT U}}) \right\} \right] \times 100 \text{ -----(5)}$$

Where,

$\{(S_{0B} - S_{12h \text{ RT U}}) / S_{12h \text{ 4 } ^\circ \text{C B}}\}$ : signal loss of analyte incubated in unblocked at RT relative to those incubated in blocked tubes at 4 °C,

$\{(S_{12h \text{ 4 } ^\circ \text{C B}} - S_{12h \text{ 4 } ^\circ \text{C U}}) / (S_{12h \text{ 4 } ^\circ \text{C B}} - S_{12h \text{ RT U}})\}$ : signal loss of analyte incubated in unblocked tubes at RT relative to those incubated in unblocked tubes at 4 °C eq.

### 3.5 Results and discussion

#### 3.5.1 Evaluation of protein loss in unblocked PP tubes

The loss of HFA (initial concentration ( $C_0$ )=10 ng/mL) and HRP-labeled mouse IgG (initial concentration ( $C_0$ )=300 ng/mL) over time was quantified by the BCA assay (**Figure 3.2**). The relative loss was calculated as a difference between the initial ( $C_0$ ) and

recovered ( $C_T$ ) concentrations of the analyte in solution  $[C_0 - C_T]$ . The analyte loss obtained with the BCA assay was also compared and correlated with SPR and ELIA (Figure 3.2, 3.3, Table 3.1). However, the analyte loss shown with the BCA assay was considerably lower than that found with SPR and ELIA.

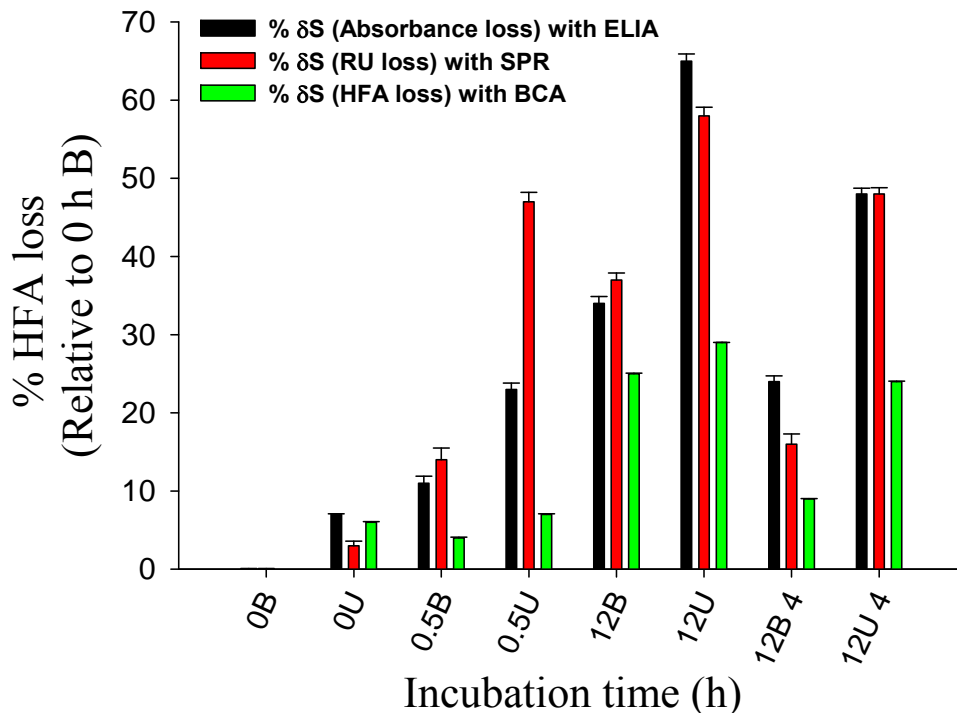


**Figure 3.2** Analysis of protein analyte (HFA) loss due to non-specific adsorption and conformation-related immunogenicity as a function of percentage signal loss. The BCA assay was employed initially to quantify HFA loss (initial concentration ( $C_0$ ) of 10 ng/mL) in the BSA-treated (B) and untreated (U) sample tubes (the numerical value before B and U correspond to the time of incubation in hours). The findings of the BCA assay were cross-validated to immunoassay formats with a sandwich ELIA and SPR. The ‘12B 4’ and ‘12U 4’ correspond to the 12 h incubation of HFA performed at 4 °C in BSA-treated and untreated tubes, respectively. Error bars represent the standard deviation. The % loss was expressed relative to the signal obtained for samples incubated in blocked tubes at 0 h incubation (equivalent to 100% signal) and was calculated using equation 1.

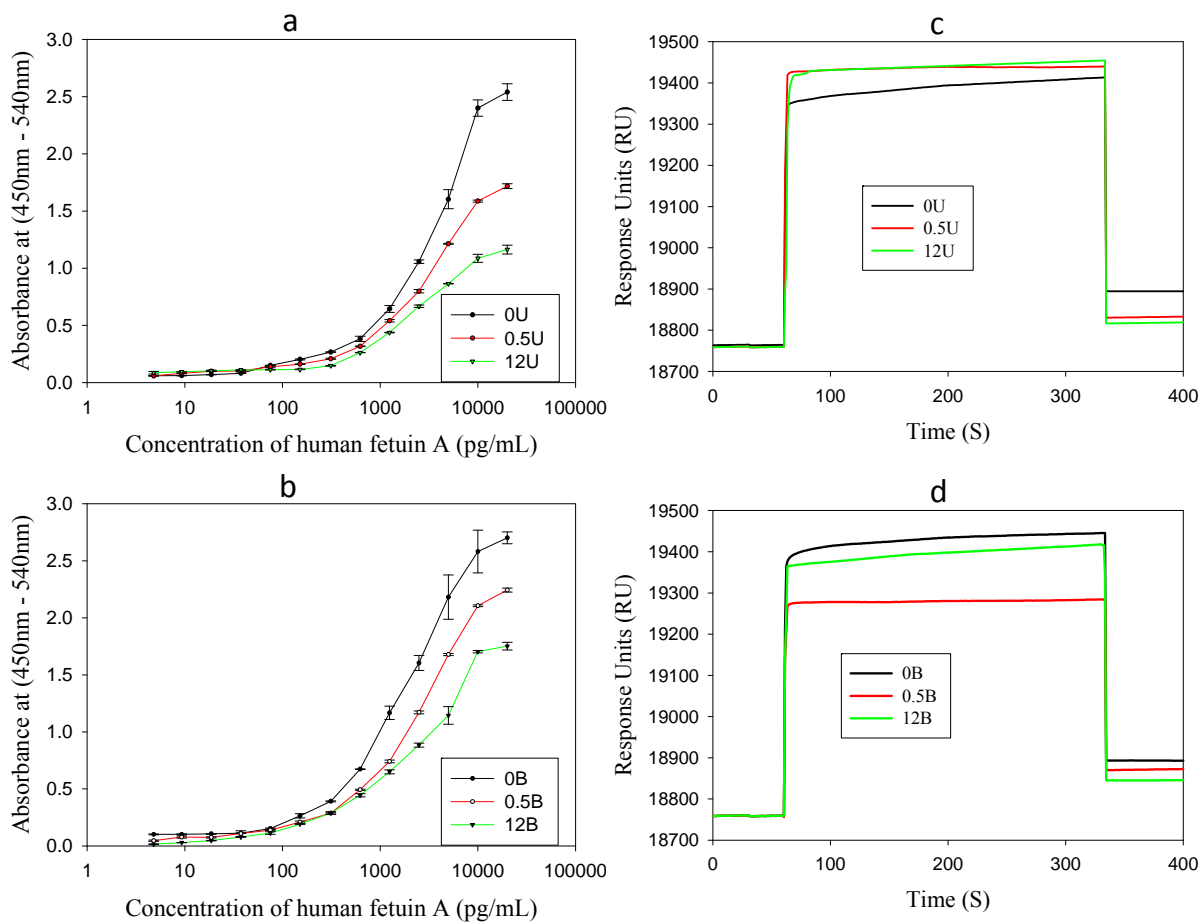


**Figure 3.3** Assay performance for the HFA samples incubated in BSA-treated (B) and untreated (U) PP tubes. ELIA was performed to analyze the effect of HFA loss on the assay performance with the sample incubated in untreated (a) and BSA-treated (b) PP tubes. It is evident that sampling performed in BSA-treated tubes efficiently reduces the adsorption-associated decline in absorbance. Similar results were obtained with the SPR assay performed with the samples incubated in BSA-treated (d), and untreated (c) PP tubes. A significant difference in assay signals obtained for incubation for 0.5h in BSA-treated and untreated tubes demonstrates the analyte loss as a function of incubation time as characterized by ELIA and SPR. Error bars in assay points correspond to standard deviations.

This difference in loss calculated using the BCA assay with respect to ELIA and SPR is due to the nature of the analytical approach. BCA measures the total protein content in the solution and does not distinguish the conformationally compromised analyte from its active form. Therefore only the protein loss attributed to adsorption is accountable in the case of BCA assay. However, ELIA and SPR are highly sensitive approaches and losses due to both adsorption and the analyte conformation changes are detectable. This results in a higher % signal loss due to analyte loss. There was no significant loss obtained with the BCA assay for the samples incubated in untreated tubes for 0h and 0.5 h. Whereas, a consistent increase in the percentage loss was obtained with ELIA and SPR as a function of increasing incubation time.

The protein loss was higher in GT tubes in comparison to PP tubes (**Figure 3.4**). This differential analyte loss behaviour was attributed to the chemical nature of the tube material used. The data obtained for HFA was validated with a HRP-labeled mouse IgG-based two component system (**Figure 3.5**). Similar results were obtained with the HRP-labeled mouse IgG and were in accordance with the previous reports on the loss of immunoglobulin from solution [27]. However, HFA (59 kDa) is a relatively smaller molecule in comparison to the HRP-labeled mouse IgG molecule (194 kDa). This significant size difference between HFA and the mouse IgG-HRP conjugate significantly changes the adsorption behaviour although the loss behaviour follows the same pattern for both analytes.

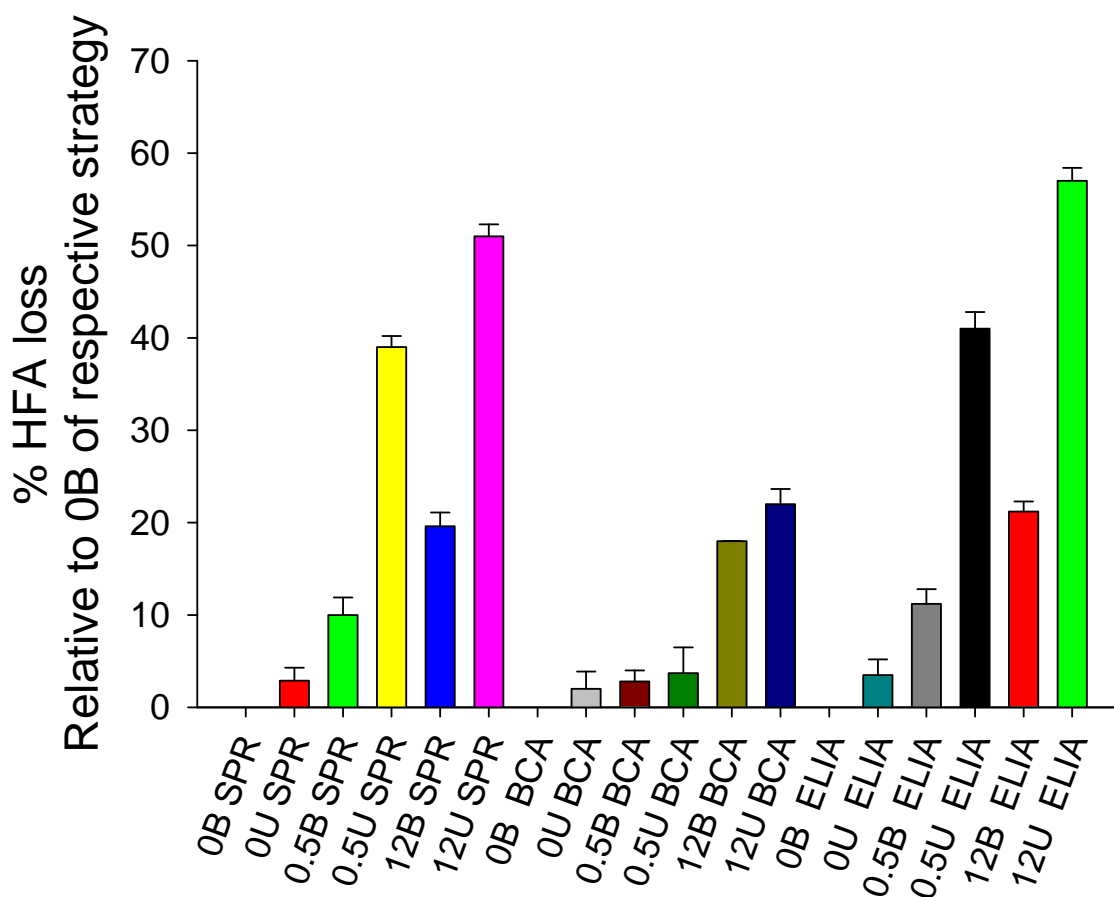


**Figure 3.4** Assay performance for the HFA samples incubated in BSA-treated (B) and untreated (U) glass tubes (GT tubes). The BCA assay was performed to analyze the total protein content available in solution. The protein loss can be quantified by relative analysis with respect to samples incubated in blocked tubes at 0h (0B). Results for the BCA assay are designated as ‘0B BCA’ to ‘12U BCA’. ELIA and SPR were performed to analyse the effect of HFA loss on assay performance with both sandwich and direct immunoassay detection approaches, respectively. The samples results corresponding to ELIA and SPR are suffixed as ‘ELIA’ or ‘SPR’ on the X-axis. Since losses due to adsorption and altered immunogenicity are determined in both the ELIA and SPR-based detection approaches, therefore, the percentage signal loss obtained for the HFA in all the sets of ELIA and SPR is higher than that obtained with the BCA assay. Error bars correspond to standard deviations.

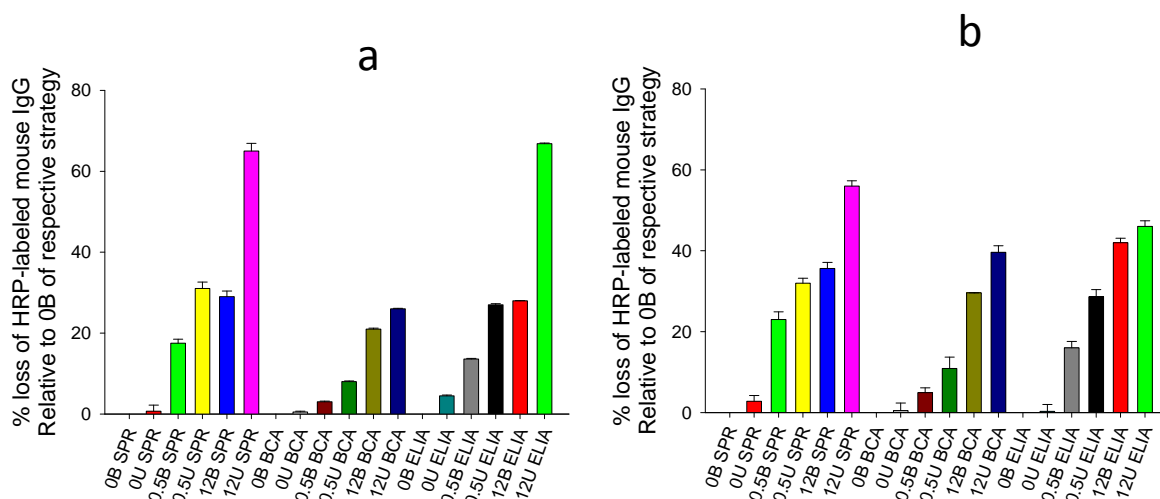


**Figure 3.5** Assay performance analysis for HRP-labeled mouse IgG incubated in BSA-treated (B) and untreated (U) (a) PP and (b) GT tubes. A similar analyte loss pattern was obtained for PP and GT tubes. This loss was higher with the use of GT tubes, as obtained with BCA assay. However, higher signal loss obtained in PP tubes relative to GT tubes corresponding to SPR and ELIA may be attributed to the losses due to impaired functionality of analyte. The symbols used are as in previous diagrams

### 3.5.2 Effect of tube-blocking on protein analyte loss

The tube surface was treated with 1% (w/v) bovine serum albumin (BSA), which is a routine blocking agent for various immunoassays. Tubes were incubated with 1% (w/v) BSA for 30 min followed by washing with 0.15M PBS, pH 7.4, and dried under N<sub>2</sub>.

The percentage signal loss (protein analyte loss) in the blocked tubes was analyzed using the same procedure as described previously for the untreated tubes. A comparative analysis was made for the analyte loss obtained for test samples incubated in BSA-treated and untreated tubes over a 12 h incubation period (**Figure 3.2**). A significant decrease ( $p \leq 0.05$ ) in the amount of protein loss was achieved by blocking the tubes

with 1% (w/v) BSA. However, it is advisable to optimize the surface blocking as a function of BSA concentrations and tube-treatment times for all type of polymers as the adsorption kinetics of the blocking proteins are dependent on the chemical nature of surface to be treated.

The tube treatment significantly improved the available antigen concentration in solution and, hence, various analytical features of the assays (**Table 3.2**). However, while a certain amount of analyte loss was observed in the BSA-treated tubes with 12 h incubation, it was significantly less ( $p \leq 0.05$ ), in comparison to the untreated tubes (**Figure 3.3a-d**). This signal loss in blocked tubes may be due to the nature of BSA, which has a tendency to bind reversibly to a variety of potential analytes thus, developing a dynamic interaction between the BSA adsorbed on the tube surface and the free analyte in solution [28, 29].

The effect of tube-blocking was also analyzed in a direct assay format by incubating HRP-labeled mouse IgG in the untreated and BSA-treated tubes, and assaying with immobilized goat anti-mouse IgG (**Figure 3.3**). The results obtained were found to correspond to those with HFA.

### **3.5.3 Evaluation of the contribution of HFA fraction with conformation-related impaired immunogenicity**

The loss of protein activity as a result of conformational changes on solid-liquid interfaces [29-32] or due to molecular flattening/spreading [33] have already been demonstrated. However, analysis of protein losses due to these phenomena and their effects on bio/ immunoassay performance have not been reported.

**Table 3.1.** Determination of total HFA loss due to non-specific adsorption and conformation-related immunogenicity changes

Incubation time (h)	Sample tube	Percentage signal loss* relative to samples of 0h B incubation time		Correlation studies
		ELIA	BCA	
0RT	BSA-treated PP	0	0	BSA-treated PP $r^2 = 1.00$ ( $p = 0.76$ )
	Untreated PP	7	5	
0.5RT	BSA-treated PP	11	2	Untreated PP $r^2 = 0.78$ ( $p = 0.48$ )
	Untreated PP	23	7	
12RT	BSA-treated PP	34 (24**)	24	
	Untreated PP	65 (49**)	30	
12 (4 °C)	BSA-treated PP	24***	9	
	Untreated PP	48***	24	

\*The percentage signal loss for each set of HFA samples at a defined incubation time was calculated using eq. (1). The control used for this study was blocking performed at 0h incubation.

\*\* The fraction of the total signal loss contributed by adsorption-based non-specific losses and calculated using eq. (4).

\*\*\*The percentage signal loss obtained for sampling performed at 12 h in BSA-treated and untreated tubes (\*\*) after subtracting the fraction corresponding to the immunogenicity loss (marked with\*\* in Table 3.3) corresponds closely with the percentage signal loss obtained for the samples incubated in BSA-treated and untreated tubes at 4 °C for 12 h. This indicates that immunogenicity-related losses in HFA samples were minimized for incubations at 4 °C.

PP stands for polypropylene tubes.

$r^2$  is the coefficient of determination of the techniques used for cross-validation and the  $p$ -value (at 95% confidence) represents the level of significance between the analysis performed with both the experimental approaches used. The  $r^2$  and  $p$ -values for this study were calculated using SigmaPlot software version 11.0.

**Table 3.2.** Effect of varying incubation time of analyte on the sensitivity of the immunoassay as observed by the increase in EC<sub>50</sub>.

Treatment ((Un)blocked) and Tube composition	*Increase in EC <sub>50</sub> values (ng/mL) over a period of 12 h of incubation (EC <sub>50</sub> <sup>12h</sup> - EC <sub>50</sub> <sup>0h</sup> )	Analytical error (% CV)
	Δ EC <sub>50</sub>	
Unblocked PP	87	24
BSA-blocked PP	31	2
Unblocked GT	85	19
BSA-blocked GT	11	3

*EC<sub>50</sub> for each set of assay was calculated using SigmaPlot version 11.0.*

*PP = polypropylene tubes; GT = glass tubes.*

*SD is standard deviation*

*% CV corresponds to the coefficient of variation in all the assay repeats and is calculated as (SD/ Mean of the obtained signal for all repeats) X 100.*

*\*EC<sub>50</sub> is a measure of assay performance and is described as the half-maximal effective concentration.*

It was shown that adsorption may be a potential source of conformational stress on protein molecules, which may result in compromised immunogenicity. Therefore, in this study an attempt was made to assess the contribution of immunogenicity loss to the loss of signal in samples incubated for 12 h at room temperature. This fraction of signal loss was quantified by calculating the difference in the signals obtained for samples incubated in BSA-treated and untreated tubes at room temperature and comparing them with samples incubated in BSA-treated tubes at 4 °C using the eqn (2). These

calculations were initially based upon previous reports stating that conformation-associated activity of a protein is retained at lower temperatures in order of  $4\text{ }^{\circ}\text{C} > \text{RT} > 37\text{ }^{\circ}\text{C}$  [34-38]. Therefore, the signal loss contributed by the fraction of HFA with impaired immunogenicity will be minimal for the samples incubated in BSA-blocked tubes at  $4\text{ }^{\circ}\text{C}$ . There was a substantial signal loss due to this phenomenon, which was significantly greater in the samples incubated in untreated tubes. As claimed in many studies the compromised immunogenicity loss may be a result of conformational stress/change induced either by solid-liquid interface or by molecular spreading of proteins in physisorbed systems that increases over the period of incubation [29-33].

The adsorption-associated loss ( $\%\Delta S_{\text{adsorption}}$ ) obtained for samples incubated at RT and the total loss ( $\%\Delta S$ ) in samples incubated at  $4\text{ }^{\circ}\text{C}$  was equivalent ( $p \leq 0.001$ ) for 12 h (**Table 3.1 and 3.3**). These findings justify our assumption that there were significant reductions in the losses due to the impaired immunogenicity of the HFA samples incubated at  $4\text{ }^{\circ}\text{C}$  for a duration of 12 h. One explanation may be that the kinetics of proteins in solution reduces significantly at lower temperatures. Therefore, with less movements in solution, the probability of analyte interactions with the surface is also reduced.

#### **3.5.4 Evaluation of the signal loss due to the nature of tube material**

The dependence of protein loss on the chemical composition of the sample tubes (PP and glass (GT)) was analyzed. The % signal losses obtained for HFA sampling in BSA-treated and untreated PP tubes were significantly lower than the corresponding values obtained in GT tubes even though GT tubes were customized for low protein adsorption.

**Table 3.3.** Determination of immunogenicity-associated loss for HFA samples incubated in BSA-treated and untreated PP tubes for 12 h at 4 °C

	<b>In BSA-treated tubes</b>	<b>In untreated tubes</b>
	eq. (2)	eq. (5)
$\% \Delta S_{\text{immunogenicity-associated}}$	30*	28*
Immunogenicity-associated loss as a % of total loss	10**	17**

\* *The calculations pertaining to immunogenicity-associated analyte loss were performed using either the eq. (2), as mentioned in the methods section, or modified version of eq. (2) as mentioned in eq. (5) (Theory & Analysis section)*

\*\* *Contribution of  $\% \Delta S_{\text{immunogenicity-associated}}$  toward total signal loss (Table 3.1 \*\*) was calculated using eq. 3.*

This protein adsorption behaviour strongly supports the previous reports, where hydrophilic self-assembled monolayers (SAMs) were found to be more active in terms of protein adsorption than hydrophobic SAMs [11, 39, 40]. A similar finding was also reported for silica-based nanoparticulate material [41]. However, the BSA-treatment significantly reduced the analyte losses due to non-specific adsorption in both types of tubes (**Figure 3.5**). Therefore, the use of pre-treated sample tubes significantly reduced analyte losses and this is of major significance to generate accurate assay results, minimise the loss of analytes and to yield greater reproducibility in immunoassays based on different assay/biosensor formats. The results obtained indicate that epitope-conformation changes and related immunogenicity alterations contribute significantly to the apparent loss of analytes during sample preparation and processing, and may be significantly minimized by using BSA-blocked tubes at 4 °C.

### 3.6 Conclusions

In the design of any assay involving protein analytes it is necessary to carefully select the tubes used and it may be necessary to pre-treat (block) them to minimize losses due to non-specific adsorption or alterations in the immunogenicity. Careful selection of temperature is also required. It is advisable to optimize these parameters in relation to each protein studied. A modeling-based approach was developed to assist in the rationale understanding of the issues involved.

### 3.7 References

1. Horie M, Nishio K, Fujita K, Endoh S, Miyauchi A, Saito Y, Iwahashi H, Yamamoto K, Murayama H, Nakano H, Nanashima N, Niki E, Yoshida Y: Protein adsorption of ultrafine metal oxide and its influence on cytotoxicity toward cultured cells. *Chem Res Toxicol* 2009, 22(3):543-553.
2. Krieter DH, Canaud B: High permeability of dialysis membranes: what is the limit of albumin loss? *Nephrol Dial Transplant* 2003, 18(4):651-654.
3. Tomisawa N, Yamashita A: Amount of adsorbed albumin loss by dialysis membranes with protein adsorption. *J Artif Organs* 2009, 12(3):194-199.
4. Walsh R, Coles M: Binding of IgG and other proteins to microfilters. *Clin Chem* 1980, 26(3):496-498.
5. Wu CC, Chen GC: Adsorption of proteins onto glass surfaces and its effect on the intensity of circular dichroism spectra. *Anal Biochem* 1989, 177(1):178-182.

6. Bark SJ, Hook V: Differential recovery of peptides from sample tubes and the reproducibility of quantitative proteomic data. *J Proteome Res* 2007, 6(11):4511-4516.
7. Dutta D, Sundaram SK, Teeguarden JG, Riley BJ, Fifield LS, Jacobs JM, Addleman SR, Kaysen GA, Moudgil BM, Weber TJ: Adsorbed proteins influence the biological activity and molecular targeting of nanomaterials. *Toxicol Sci* 2007, 100(1):303-315.
8. Haynes CA, Norde W: Globular proteins at solid/liquid interfaces. *Colloids Surf, B* 1994, 2(6):517-566.
9. Haynes CA, Norde W: Structures and stabilities of adsorbed proteins. *J Colloid Interf Sci* 1995, 169(2):313-328.
10. Menaa B, Torres C, Herrero M, Rives V, Gilbert ARW, Eggers DK: Protein adsorption onto organically modified silica glass leads to a different structure than sol-gel encapsulation. *Biophys J* 2008, 95(8):L51-L53.
11. Menaa B, Herrero M, Rives V, Lavrenko M, Eggers DK: Favourable influence of hydrophobic surfaces on protein structure in porous organically-modified silica glasses. *Biomaterials* 2008, 29(18):2710-2718.
12. Nakanishi K, Sakiyama T, Imamura K: On the adsorption of proteins on solid surfaces, a common but very complicated phenomenon. *J Biosci Bioengin* 2001, 91(3):233-244.
13. Waanders LF, Chwalek K, Monetti M, Kumar C, Lammert E, Mann M: Quantitative proteomic analysis of single pancreatic islets. *Proc Natl Acad Sci USA* 2009, 106(45):18902-18907.

14. Weib N, Wente W, Muller P: Note 180: Influence of vessel surface on the recovery rate of proteins. *Eppendorf Applications* 2008.
15. McDonnell B, Hearty S, Leonard P, O'Kennedy R: Cardiac biomarkers and the case for point-of-care testing. *Clin Biochem* 2009, 42(7-8):549-561.
16. Dixit CK, Vashist SK, O'Neill FT, O'Reilly B, MacCraith BD, O'Kennedy R: Development of a High Sensitivity rapid sandwich elisa procedure and its comparison with the conventional approach. *Anal Chem* 2010, 82(16):7049-7052.
17. Wahlgren M, Arnebrant T: Protein adsorption to solid surfaces. *Trends Biotechnol* 1991, 9(1):201.
18. Sui S, Wu H, Sheng J, Guo Y: Conformational changes of proteins at an interface induced by a supported planar phosphatidic acid monolayer. *J Biochem* 1994, 115(6):1053-1057.
19. Hlady V, Buijs J: Protein adsorption on solid surfaces. *Curr Opin Biotechnol* 1996, 7(1):72.
20. Moulin AM, O'Shea SJ, Badley RA, Doyle P, Welland ME: Measuring Surface-Induced Conformational Changes in Proteins. *Langmuir* 1999, 15(26):8776-8779.
21. Roach P, Farrar D, Perry CC: Interpretation of Protein Adsorption: Surface-Induced Conformational Changes. *J Am Chem Soc* 2005, 127(22):8168-8173.

22. Pérez-Rodriguez C, Montano N, Gonzalez K, Griebenow K: Stabilization of [alpha]-chymotrypsin at the CH<sub>2</sub>Cl<sub>2</sub>/water interface and upon water-in-oil-in-water encapsulation in PLGA microspheres. *J Controlled Release* 2003, 89(1):71.
23. Goyal K, Walton LJ, Tunnacliffe A: LEA proteins prevent protein aggregation due to water stress. *Biochem J* 2005, 388(1):151-157.
24. Capasso P, Aliprandi M, Ossolengo G, Edenhofer F, de Marco A: Monodispersity of recombinant Cre recombinase correlates with its effectiveness in vivo. *BMC Biotechnology* 2009, 9(1):80.
25. Satulovsky J, Carignano MA, Szleifer I: Kinetic and thermodynamic control of protein adsorption. *Proc Natl Acad Sci U S A* 2000, 97(16):9037-9041.
26. Azzam RMA, Rigby PG, Krueger JA: Kinetics of protein adsorption and immunological reactions at a liquid/solid interface by ellipsometry. *Phys Med Biol* 1977, 22(3):422-430.
27. Alves CM, Reis RL, Hunt JA: The competitive adsorption of human proteins onto natural-based biomaterials. *J Royal Soc Interf* 2010, 7(50):1367-1377.
28. Jeyachandran YL, Mielczarski JA, Mielczarski E, Rai B: Efficiency of blocking of non-specific interaction of different proteins by BSA adsorbed on hydrophobic and hydrophilic surfaces. *J Colloid Interf Sci* 2010, 341(1):136-142.
29. Kwok KC, Yeung KM, Cheung NH: Adsorption kinetics of bovine serum albumin on fused silica: population heterogeneities revealed by single-molecule fluorescence microscopy. *Langmuir* 2007, 23(4):1948-1952.

30. Lee CS, Belfort G: Changing activity of ribonuclease A during adsorption: a molecular explanation. *Proc Natl Acad Sci U S A* 1989, 86(21):8392-8396.
31. Norde W, Favier JP: Structure of adsorbed and desorbed proteins. *Colloids Surf* 1992, 64(1):87-93.
32. Rabe M, Verdes D, Zimmermann J, Seeger S: Surface organization and cooperativity during nonspecific protein adsorption events. *J Phys Chem, B* 2008, 112(44):13971-13980.
33. Raffaini G, Ganazzoli F: Protein adsorption on a hydrophobic surface: a molecular dynamics study of lysozyme on graphite. *Langmuir* 2010, 26(8):5679-5689.
34. Kiss E: Temperature dependence of bovine serum albumin adsorption onto a poly(ethylene oxide)-grafted surface. *Colloids Surf Physicochem Eng Aspects* 1993, 76:135-140.
35. Kondo A, Fukuda H: Effects of adsorption conditions on kinetics of protein adsorption and conformational changes at ultrafine silica particles. *J Colloid Interf Sci* 1998, 198(1):34-41.
36. Balamurugan S, Ista LK, Yan J, Lopez GP, Fick J, Himmelhaus M, Grunze M: Reversible protein adsorption and bioadhesion on monolayers terminated with mixtures of oligo(ethylene glycol) and methyl groups. *J Am Chem Soc* 2005, 127(42):14548-14549.
37. Cheng X, Canavan HE, Graham DJ, Castner DG, Ratner BD: Temperature dependent activity and structure of adsorbed proteins on plasma polymerized N-isopropyl acrylamide. *Biointerphases* 2006, 1(1):61-72.

38. Idenyi NE, Ekuma CE, Umahi AE: Effect of temperature and pH on the spectral and conformational distribution of adsorbed lysozyme. *Biotechnology* 2006, 5(4):429-435.
39. Silin V, Weetall H, Vanderah DJ: SPR studies of the nonspecific adsorption kinetics of human IgG and BSA on gold surfaces modified by self-assembled monolayers (SAMs). *J Colloid Interf Sci* 1997, 185(1):94-103.
40. Wang Q, Wang J, Geil PH, Padua GW: Zein Adsorption to hydrophilic and hydrophobic surfaces investigated by surface plasmon resonance. *Biomacromolecules* 2004, 5(4):1356-1361.
41. Menna B, Menna F, Aiolfi-Guimaraes C, Sharts O: Silica-based nanoporous sol-gel glasses: from bioencapsulation to protein folding studies. *Int J Nanotechnol* 2010, 7(1):1-45.

## **Chapter 4**

Effect of antibody immobilization strategies  
on the analytical performance of a surface  
plasmon resonance-based immunoassay

(Published in the Analyst, 2011, 136(21), 4431-4436)

#### **4.1 Abstract**

Antibody immobilization strategies (random, covalent, orientated and combinations of each) were examined to determine their performance in a surface plasmon resonance-based immunoassay using human fetuin A (HFA) as the model antigen system. The random antibody immobilization strategy selected was based on passive adsorption of anti-HFA antibody on 3-aminopropyltriethoxysilane (APTES)-functionalized gold (Au) chips. The covalent strategy employed covalent crosslinking of anti-HFA antibody on APTES-functionalized chips using 1-ethyl-3-[3-dimethylaminopropyl]carbodiimide (EDC) and sulfo-*N*-hydroxysuccinimide (SNHS). The orientation strategy used passive adsorption of protein A (PrA) on Au chips, with subsequent binding of the anti-HFA antibody in an orientated fashion via its fragment constant region (Fc) region. In the covalent-orientated strategy, PrA was first bound covalently, to the surface, which in turn, then binds the anti-HFA antibody in an orientated manner. Finally, in the most widely used strategy, covalent binding of anti-HFA antibody to carboxymethyl dextran (CM5-dextran) was employed. This immobilization strategy gave the highest anti-HFA antibody immobilization density, whereas the highest HFA response was obtained with the covalent-orientated immobilization strategy. Therefore, the covalent-orientated strategy was the best for SPR-based HFA immunoassay and can detect 0.6-20.0 ng/mL of HFA in less than 10 min.

## 4.2 Introduction

Immunoassays based on the immobilization of antibodies on a substrate have been widely used in different biosensing or bioanalytical techniques for the detection of specific antigens. Surface plasmon resonance (SPR)-based immunosensors are ‘real-time’ and ‘label-free’ rapid assay formats that provide highly useful information on biomolecular interactions [1, 2] and provide highly reproducible immunoassays.

The immobilization of antibodies on sensor chips plays a very important role in the analytical performance of a SPR-based immunoassay. The affinity, orientation and stability of the antibodies are often affected by the immobilization strategy employed [3, 4]. In addition, the size of the antibodies/fragments used and their surface distribution and the size of the analyte are of significance in relation to the minimization of steric hindrance, which may affect the immunoassay performance. Antibodies present in the solution phase have three dimensional freedom of movement and maintain their native structure. Immobilization of antibodies at an interface restricts their freedom of movement and may impact on their three dimensional conformation [5]. Therefore, a critical understanding of the interactions between macromolecular receptor and ligand is important [5].

A large number of chemistries are available for immobilizing antibodies on biosensor surfaces; however, those introducing orientation [6] and maintaining native antibody conformation [7] are of major importance. CM5-dextran is often used where the antibody is linked via its amine groups to the EDC-NHS-activated carboxyl groups of CM5 by heterobifunctional crosslinking and this chemistry leads to a high density of antibody immobilization. However, immobilization using this strategy can result in interference with

the antigen detection capability if the antibody is inadvertently captured via amine groups of or adjacent to the antigen binding site [8].

In another format, poly-histidine tagged antibodies are bound to nitriloacetic acid (NTA)-modified surfaces. However, problems may arise from the strong non-specific adsorption of other metal-binding proteins to the poly-histidine tag and continuous leaching of the bound ligand [9, 10]. Biotin-avidin systems have also been used for immobilization in SPR assays. Streptavidin-coated SPR chips are preferred for the site-directed immobilization of biotinylated antibodies. This strategy introduces steric freedom along with site-directed orientation. However, as with other proteins, immobilization of streptavidin on the surface may introduce conformational-stress that may reduce its binding affinity for biotin. This can also occur with other physical parameters such as temperature [11]. Conversely, strategies employing thiols, which can be immobilized on the gold surface with high-affinity and without any prior surface modification, provide strong site-directed orientation. This strategy is useful if the antibody naturally has free thiol groups. However, if the thiol group is introduced chemically, involving reaction with the antibody's amine groups, then this can affect activity.

A high degree of orientation for the capture antibody on a sensor surface can be attained with a sub-layer of proteins such as protein A or protein G [12]. These proteins are specific for binding the Fc region of the antibodies, which keeps the fragment antigen-binding (Fab) region free for antigen binding thus obviating the need of any chemical modification of the antibody. However, randomly immobilized Fc-binding protein molecules may affect the orientation of antibody to some degree but this is significantly lower in comparison to the degree of orientation actually achieved. Nevertheless, due to steric considerations, a

maximum of two antibodies may only be accommodated by each of these protein binding molecules [7]. Drawbacks associated with random immobilization and the introduction of conformational strain will not affect, to a significant degree, the antibody molecules captured on the sub-layer of Fc-binding proteins. Moreover, Fc-binding protein-antibody interaction is generally regenerative [13].

The present study is aimed at determining the effect of various antibody immobilization strategies, i.e. random, orientated, covalent, covalent-orientated and covalent-CM5-dextran on a SPR-based immunoassay for HFA (Figure 4.1). Recently we reported a multi-substrate compatible novel antibody immobilization strategy [14], which is based on the APTES functionalization of the surface and the covalent binding of antibodies to it by EDC-SNHS heterobifunctional crosslinking. The same strategy was employed for SPR immunoassays and the schematic representation of the strategy is depicted in Fig. 4.1. An alternative covalent-orientated strategy was also devised by introducing an additional step in the covalent strategy, where PrA was initially bound covalently and anti-HFA antibody was immobilized, thereafter, in an orientated manner. The random strategy employed the passive adsorption of anti-HFA antibody on APTES-functionalized chips, whereas the orientated strategy used the passive adsorption of PrA on SIA Au chips followed by the orientated immobilization of anti-HFA antibody. The covalent-CM5-dextran strategy employed the covalent binding of amino groups of anti-HFA antibody to the carboxyl groups of CM5-dextran using EDC-SNHS. Each strategy was compared on the basis of their SPR immunoassay performance, anti-HFA antibody immobilization density and mass-density of captured HFA. This study provides an insight as to how antibody orientation strategy may influence immunoassay performance.

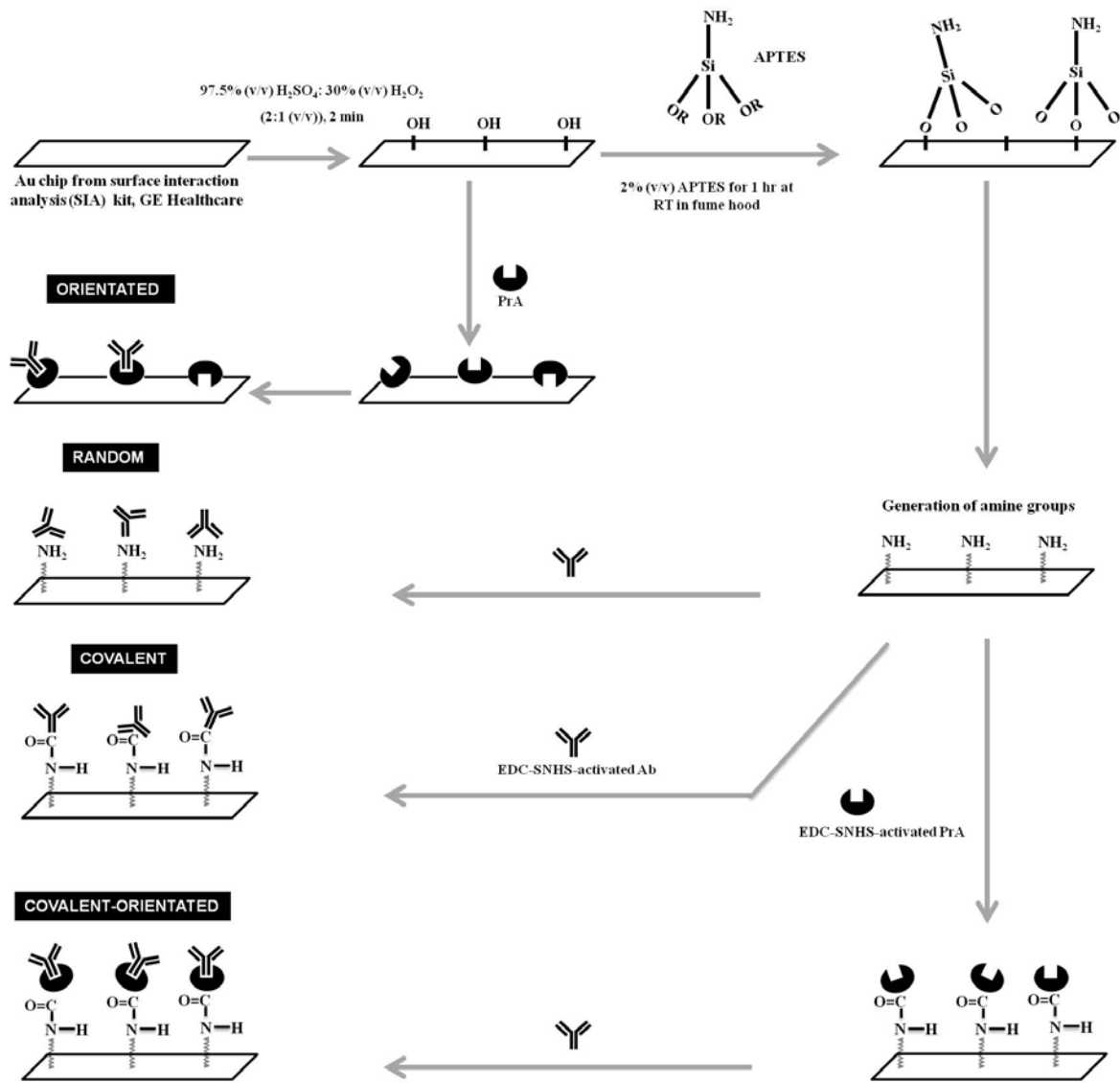


**Figure 4.1** Schematic representation of APTES functionalization of Au surface and effect of antibody immobilization strategies on the performance of immunoassays in surface plasmon resonance format.

### 4.3 Materials

EDC, SNHS and 2-(*N*-morpholino)ethane sulfonic acid (MES, pH 4.7) were purchased from Thermo Scientific. 3-APTES (purity 98%, w/v), 4-(2-hydroxyethyl)-1-piperazineethanesulfonic acid (HEPES), Tween 20,  $\text{H}_2\text{O}_2$  (30%, v/v),  $\text{H}_2\text{SO}_4$  (97.5%, v/v),

ethylenediaminetetraacetic acid (EDTA), NaCl, HCl and protein A (soluble, Cowan strain, recombinant, expressed in *Escherichia coli*) were procured from Sigma-Aldrich, Singapore. The human Fetuin A/AHSG kit with all the necessary components was obtained from R&D Systems Inc., USA. All buffers and solutions were prepared with 18M $\Omega$  Milli-Q ultrapure water (UPW) filtered through a 2- $\mu$ m filter. Oxygen-plasma cleaner was obtained from Harrick Plasma, Ithaca, New York, USA. UVISEL spectroscopic ellipsometer was obtained from Jobin Yvon Horiba, ChillyMazarin, France. Surface Plasmon Resonance was performed on BIAcore 3000 purchased from GE Healthcare, Uppsala, Sweden. The SIA kit (BR-1004-05) containing SPR Au chips, carboxymethyl dextran (CMD)-functionalized Au chips, and ethanolamine hydrochloride (1M, pH 8.5) were purchased from GE Healthcare, London, U.K.

The SPR Au chip was assembled according to the instructions supplied by the manufacturer. HEPES-buffered saline (HBS) buffer (10mM) pH 7.4, (running buffer for BIAcore) was made up, filtered through 0.2 $\mu$ m Millipore filter paper and degassed overnight in order to remove any air bubbles, which may cause interference with SPR analysis. All the sample dilutions were made in the running buffer (10mM HBS, pH 7.4). The dilutions of HFA were made in BSA-preblocked glass vials, prepared by incubating with 1% (w/v) BSA for 30 min, to minimize the sample loss due to non-specific adsorption on sample tube surfaces and/or effects due to altered immunogenicity [15].

## **4.4 Methods**

### **4.4.1 Surface cleaning of SIA Au chip and APTES functionalization**

The Au chip was cleaned with piranha etch [60  $\mu$ L of H<sub>2</sub>SO<sub>4</sub> (97.5%, v/v): 30  $\mu$ L of H<sub>2</sub>O<sub>2</sub> (30%, v/v)] for two minutes followed by extensive washing. Piranha treatment oxidizes the

gold surface, as evident by the contact angle, which is  $9.3^{\circ}$ . When the piranha-treated chips are washed with deionized water, the water molecules get strongly adsorbed on the surface thereby generating ‘hydroxyl’ groups [16, 17], as evident by the increase in contact angle to  $28^{\circ}$ - $32^{\circ}$ .

The chip was then incubated with 100  $\mu$ L of 2% (v/v) APTES for 1h at room temperature (RT) in a fume hood followed by five washes with UPW. Following this, different immobilization strategies were applied.

#### **4.4.2 EDC activation of anti-HFA antibody**

Anti-HFA antibody (990 $\mu$ L of 100  $\mu$ g/ml in HBS) was incubated at room temperature for 15 min with 10  $\mu$ L of cross-linking solution containing EDC (4 mg/mL) and sulfo-NHS (11 mg/mL) in 0.1 M MES buffer, pH 4.7. The procedure led to the activation of carboxyl groups on the anti-HFA antibody with EDC. The EDC-activated anti-HFA antibody was captured on the APTES-functionalized Au chip (previously described) for the covalent immobilization strategy.

Similarly, PrA was also activated with EDC and captured on the APTES-functionalized Au chip surface for the orientated strategy.

#### **4.4.3 Immobilization of anti-HFA antibody**

For the random antibody non-covalent immobilization strategy, 50  $\mu$ L of anti-HFA antibody (100  $\mu$ g/mL) was injected over all the four flow cells of an APTES-functionalized Au chip at a flow rate of 10  $\mu$ L/min and the baseline was allowed to stabilize. BSA (20  $\mu$ L of 1% (w/v)) was subsequently used for blocking.

For the covalent immobilization strategy, 50  $\mu\text{L}$  of the EDC-activated antibody (100  $\mu\text{g/mL}$ ) was injected over all the four flow cells of an APTES-functionalized Au chip, and BSA was used for blocking as previously described.

For orientated immobilization strategy, 50  $\mu\text{L}$  of the protein A (100  $\mu\text{g/mL}$ ) was injected over the four flow cells of piranha-treated Au chip at a flow rate of 10  $\mu\text{L/min}$ . Twenty microliters of 1% (w/v) BSA was then injected for blocking. After baseline stabilization, 50  $\mu\text{L}$  of anti-HFA antibody (100  $\mu\text{g/mL}$ ) diluted in 10 mM HBS, pH 7.4, was injected over all the flow cells at a flow rate of 10  $\mu\text{L/min}$ .

For the covalent-orientated immobilization strategy, 50  $\mu\text{L}$  of EDC-activated PrA was injected over all four flow cells of an APTES-functionalized Au chip at a flow rate of 10  $\mu\text{L/min}$ . The chip was blocked with BSA, as previously described, followed by the addition of anti-HFA antibody.

#### **4.4.4 Covalent-CM5-dextran immobilization strategy**

A CM5 dextran-functionalized Au chip was docked into BIAcore 3000 and primed. Pre-concentration studies were performed in order to obtain the optimum pH of the sodium acetate buffer for use with anti-HFA antibody immobilization (pH range of 4.0-5.0). Further activation was performed at a pH of 4.2 (optimum). Afterwards, the CM5-dextran chip was activated by injecting a 50  $\mu\text{L}$  solution containing 200  $\mu\text{g}$  of EDC and 550  $\mu\text{g}$  of SNHS in 0.1M MES buffer, pH 4.7, through all the flow cells at a flow rate of 10  $\mu\text{L/min}$ . Thereafter, the procedure employed for the random immobilization strategy was used, with the exception that blocking was initially performed with 20  $\mu\text{L}$  of 1M ethanolamine hydrochloride, pH 8.5, followed by 20  $\mu\text{L}$  of 1% (w/v) BSA. Ethanolamine hydrochloride

(1M), pH 8.5, blocks the unreacted ester groups in the CM5-dextran matrix, while BSA blocks the non-specific binding sites on the chip surface.

#### **4.4.5 HFA-detection**

Fifty microlitres of the dilution buffer (10mM HBS, pH 7.4) was passed through all the flow cells before HFA capture and the resultant changes in the SPR response units (RU) for each of the four flow cells were recorded. Fifty microlitres of HFA at six different dilutions (0.6, 1.2, 2.5, 5.0, 10.0 and 20.0 ng/mL) were then passed through the flow cells (sample volume was chosen arbitrarily). Subsequently, the RU values obtained for the blanks were subtracted from the RU values obtained for captured HFA of the corresponding flow cells.

All the experiments pertaining to different immobilization strategies were repeated three times in triplicates and the standard deviation was calculated. The SPR-based HFA detection curves were plotted with SigmaPlot software, version 11.2 based on a four parameter logistic. The analytical parameters such as  $EC_{50}$  and Hillslope, generated by the software analysis report, were then used to evaluate the analytical performance [18] of SPR immunoassays with the various antibody immobilization strategies.

#### **4.4.6 Complete regeneration of the APTES-functionalized gold surface**

##### **4.4.6.1 Siloxane bond lysis by acid treatment and O<sub>2</sub>-plasma**

The functionalized chips were subjected to acid-lysis of siloxane bonds [19-21] by HCl. The acid-mediated lysis based regeneration was optimized using various HCl strengths (5, 10, 12 and 15M), and exposure times (5, 10, 20 and 30 min). The O<sub>2</sub> plasma etching was also optimized at three different plasma powers *viz.* 12, 20 and 29W at different exposure times

of 3, 6, 9, 12 and 15 min. Subsequently, the combined HCl and O<sub>2</sub> plasma treatment procedure was optimized for Au surface regeneration.

Thickness of the APTES layer on Au chip was measured using UVISEL spectroscopic ellipsometer. The measurements of psi ( $\psi$ ) and delta ( $\Delta$ ) spectra were conducted at an incident angle of 70° over a wavelength range of 350-1000 nm. The silicon dioxide dispersion layer fitting model was then followed to determine the effective thicknesses of Au on glass, and of APTES on Au. This model was based upon fitting of the spectra on a 50 nm thick gold layer deposited on a glass base. The silane layer thickness was then predicted with this model. Each thickness obtained was an average of 50 measurements of the thickness at each given point.

Additional surface studies were performed using Rutherford backscattering (RBS) analysis. The APTES-functionalized SPR Au chip was loaded into the scattering chamber that was maintained under high vacuum conditions. A collimated beam of 2 MeV He<sup>+</sup> ions, generated by a 3.5 MV HVEE Singletron accelerator, was normally incident onto the sample. The ions backscattered at 101.25° scattering angle were collected and their energy was measured by an Ortec Ultra silicon solid-state detector. The resultant spectra were fitted using the SIMNRA software. The total Si areal density for each sample was extracted from the target structure that provides the best fit for the respective spectrum.

#### **4.4.6.2 SPR-based HFA immunoassay procedure**

Anti-HFA antibody (990  $\mu$ L of 100  $\mu$ g/mL reconstituted in HBS) was incubated for 15 min at RT with 10  $\mu$ L of the cross-linking solution containing EDC (4 mg/mL) and sulfo-NHS (11 mg/mL) in 0.1 M, pH 4.7 MES buffer. Later, 100  $\mu$ L of the resulting EDC-sulfo-NHS

activated antibody solution was passed over the silanized Au chip at 10  $\mu\text{L}/\text{min}$  to prepare anti-HFA antibody-coated chip. The anti-HFA antibody immobilized chip was then blocked using sulfo-NHS acetate, which reacts to free amino groups on the surface. This was followed by BSA-blocking in order to fill the void space on the chip thus, minimizing non-specific protein adsorption on the surface. Subsequently, the HFA at 0.6 to 20 ng/mL dilutions was assayed on the anti-HFA antibody immobilized chips for 30 cycles of regeneration.

#### **4.4.6.3 SPR-based reproducibility analysis of antibody immobilization on the regenerated Au chips**

The SPR Au chip was regenerated by treatment with 12 M HCl for 10 min followed by the 29 W  $\text{O}_2$ -plasma treatment for 5 min. The regenerated Au chips were re-functionalized with APTES as described and immunoassay was performed. This cycle of regeneration and antibody immobilization for immunoassay development was repeated over 30 cycles.

Surface properties such as hydrophilicity, amine-density and silane layer-thickness were monitored with contact angle, Rutherford back-scattering (RBS) and ellipsometry, respectively.

### **4.5 Results and Discussion**

#### **4.5.1 Comparison of antibody immobilization strategies as a function of antibody immobilization density**

The development of the APTES-functionalization of Au chips, used for various antibody immobilization strategies in this study, was optimized for APTES concentration, APTES functionalization time and APTES density (**Figure 4.2**).

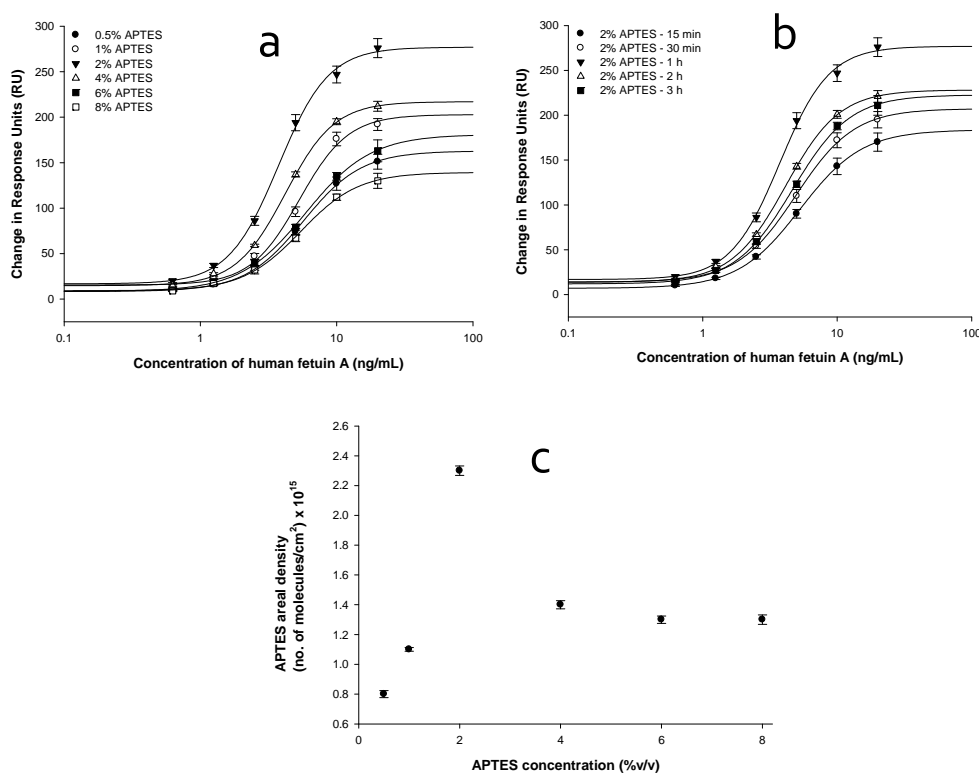


**Figure 4.2** Optimization of APTES functionalization of Au surface as a function of immunoassay performed for HFA detection with the anti-HFA antibodies immobilized on the surfaces exposed to (a) various concentrations of APTES; (b) Various incubation times of optimum APTES concentration (2% (v/v)); and, (c) APTES molecule density at different concentrations using Rutherford backscattering (RBS) method.

The effect of employing various antibody immobilization strategies in a SPR immunoassay was initially observed by determining the immobilization density of anti-HFA antibody on the SPR chip. The highest and lowest anti-HFA antibody immobilization densities, as shown in **Table 4.1**, were obtained with covalent-CM5-dextran immobilization and random immobilization strategies, respectively. The anti-HFA antibody immobilization densities were found in the decreasing order of covalent-CM5-dextran > covalent > covalent-

orientated > orientated > random strategies (**Figure 4.3a**), which were qualitatively analysed with atomic force microscopy (AFM) (**Figure 4.4**), qualitatively.

**Table 1** Determination of molecular densities of immobilized anti-HFA antibody and detected amount of HFA when different SPR immunoassay formats, based on various antibody immobilization strategies, were employed.

Antibody Immobilization Strategy	Immobilization of anti-HFA antibody			HFA***			
	$\Delta$ RU	Mass density* (ng/cm <sup>2</sup> )	Molecular Density** (molecules/cm <sup>2</sup> )	$\Delta$ RU	Mass density* (ng/cm <sup>2</sup> )	Molecular Density** (molecules/cm <sup>2</sup> )	EC <sub>50</sub> (ng/mL)
Random	816.0 ± 11.7	81.6 ± 1.2	3.3 × 10 <sup>11</sup>	63.0 ± 16	6.3 ± 1.6	(0.9 ± 0.2) × 10 <sup>11</sup>	5.7
Covalent	1536.0 ± 10.4	153.6 ± 1.0	6.1 × 10 <sup>11</sup>	149.0 ± 9.6	14.9 ± 1.0	(2.1 ± 0.1) × 10 <sup>11</sup>	3.8
Orientated	1112.0 ± 9.6	111.2 ± 1.0	4.4 × 10 <sup>11</sup>	113.0 ± 10.5	11.3 ± 1.0	(1.6 ± 0.1) × 10 <sup>11</sup>	4.0
Covalent-orientated	1457.0 ± 8.8	145.7 ± 1.0	5.8 × 10 <sup>11</sup>	194.0 ± 9.5	19.4 ± 1.0	(2.8 ± 0.1) × 10 <sup>11</sup>	3.7
Covalent-CM5-dextran	1728.0 ± 12.4	172.8 ± 1.2	6.9 × 10 <sup>11</sup>	138.0 ± 10.4	13.8 ± 1.0	(1.9 ± 0.1) × 10 <sup>11</sup>	4.1

#### Space here

**$\Delta$ RU:** Change in resonance units (RU) caused by binding

\*Calculated using the commonly used conversion factor i.e. 1000 RU=100 ng/cm<sup>2</sup> [13, 14].

\*\*Calculated by [Mass density (ng/cm<sup>2</sup>) / Molecular weight (in ng)]. Molecular weight of anti-HFA antibody and HFA were 150 kDa and 43.5 kDa, respectively. In order to calculate molecular weight in SI units, the conversion factor 1 kDa = 1000 Da = 1000 g was used. The molecular weight of anti-HFA antibody and HFA are 24.9×10<sup>-11</sup>ng and 7.0×10<sup>-11</sup>ng, respectively.

\*\*\*Calculations were performed for the detection of 5 ng/mL of HFA i.e. the concentration just above the EC<sub>50</sub>.

The immobilization densities were calculated using a conversion factor i.e. 1 ng/mm<sup>2</sup> of biomolecule corresponds to a change of 1000 RU [22-24]. The lowest antibody immobilization density in the random immobilization strategy was attributed to the irregular and uncontrolled binding of the antibody over the surface mainly by electrostatic and hydrophobic interactions [23]. Additionally, many other factors, such as molecular spreading and inter-molecular interactions, may affect the immobilization-density of adsorbed antibodies at the interface [24, 25], which, in turn, determines the functionality of adsorbed antibodies [25]. However, the introduction of PrA molecules enables the orientated

immobilization of antibodies in a site-directed fashion. The anti-HFA immobilization density of the orientated immobilization strategy was greater than that of the random immobilization strategy as PrA binds very strongly to the Au surface, which is the main reason that it has been used extensively for biosensing applications in various biosensor formats.

The capture ratio of 1:1 for anti-HFA antibody bound to PrA is in line with previous findings, which state that one PrA molecule can bind to a maximum of two antibody molecules based on conformational and intermolecular restrictions [26]. However, the anti-HFA antibody immobilization density was lower than that of the covalent-orientated immobilization strategy. This might be because PrA molecules adsorbed in the orientated format still have a tendency to undergo conformational changes and/or leaching off the surface. The higher antibody immobilization density of the covalent-orientated strategy may be due to the fact that covalently bound PrA molecules could resist leaching whilst maintaining their active conformation for binding.

The antibody immobilization density of the covalent strategy was higher than that of covalent-orientated strategy and this may be due to the fact that the total number of amino groups available for antibody crosslinking was significantly higher than the binding sites available on covalently immobilized PrA molecules. Therefore, there is a higher probability for an antibody to be directly crosslinked to the amino groups on the surface in comparison to binding in an orientated fashion to the covalently bound PrA molecules.

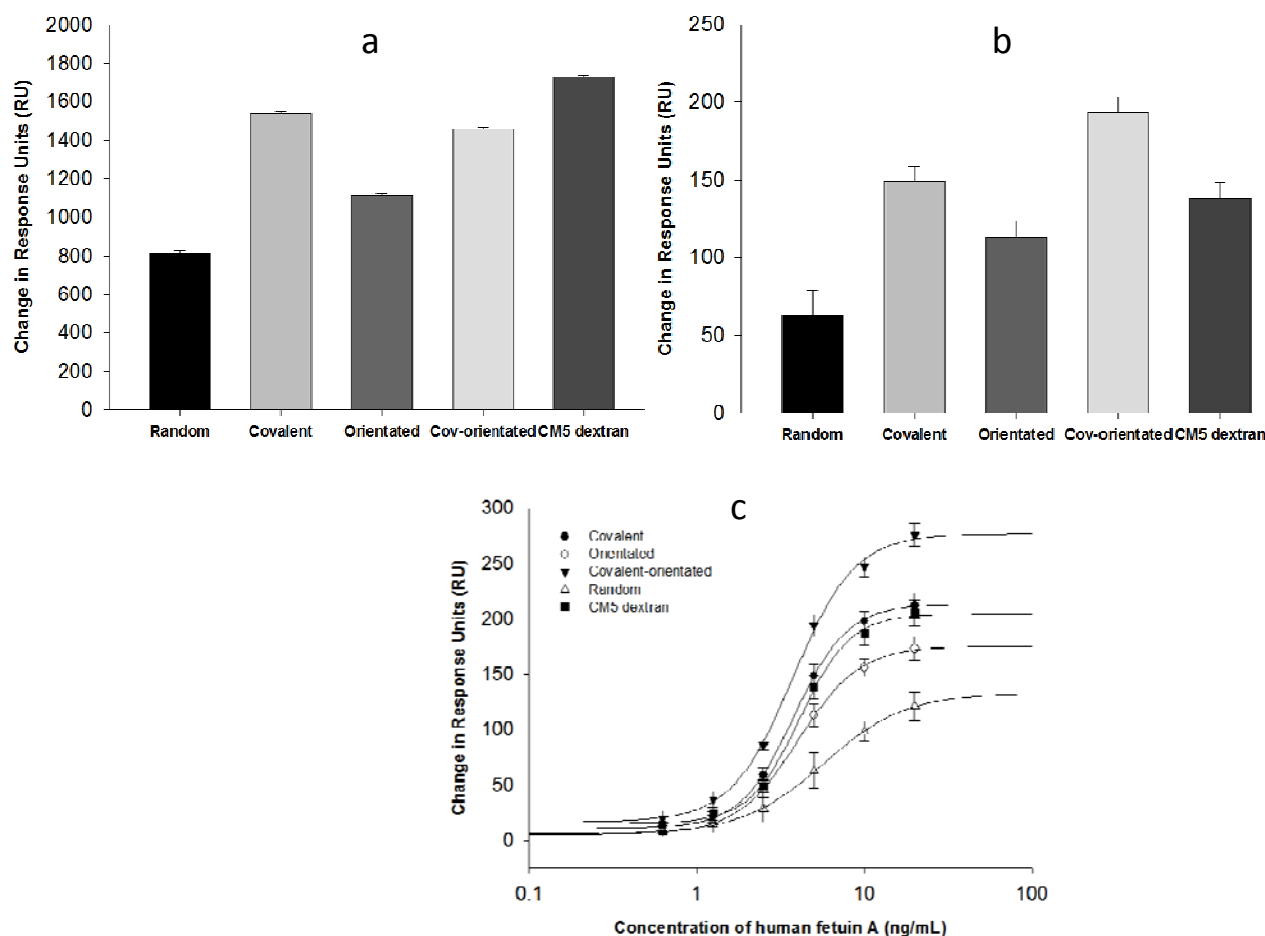


**Figure 4.3** Analysis of performance of the antibody immobilization strategies. (a) anti-HFA antibody capture-density as a function of change in relative response units. Antibody was captured in an increasing order of random, oriented, cov-oriented, covalent and CM5-dextran. (b) Capture efficiency analysis of immobilized anti-HFA antibody as a function of ratio of the amount of HFA captured and amount of antibody immobilized by the respective strategy. Highest amount of HFA was captured by the antibodies immobilized in cov-oriented format. (c) Performance of immunoassay for HFA detection (0.6-20 ng/mL) in each format. 'Cov' represents covalent.

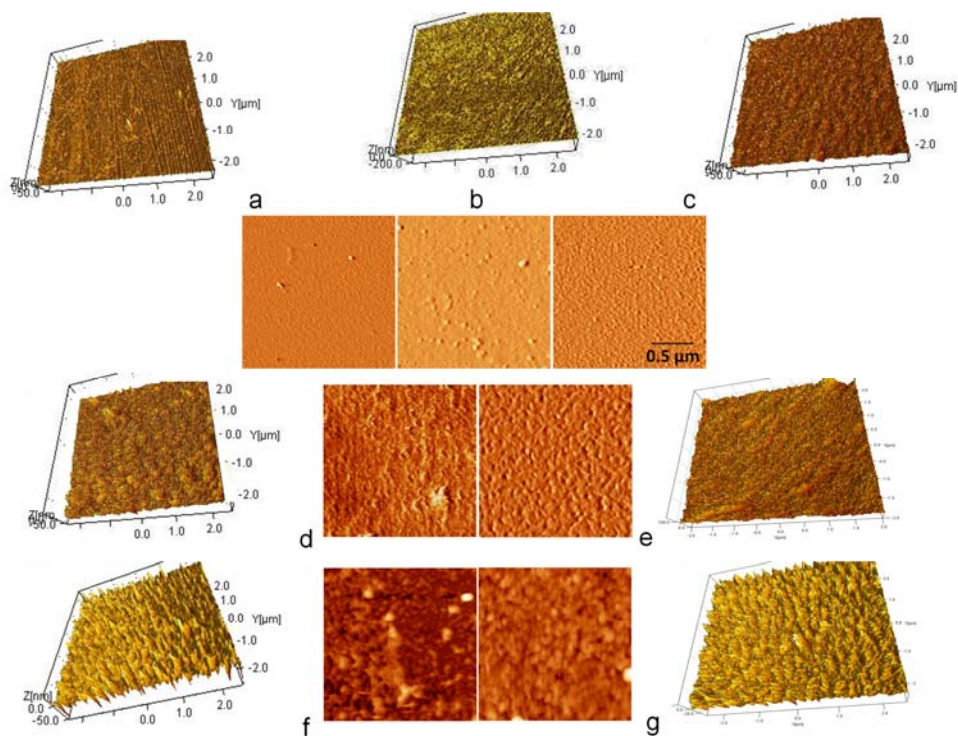


**Figure 4.4** Qualitative analysis of the surface for various steps of silane functionalization [bare Au (a), piranha activated Au (b), and APTES-coated Au surface (c)]. The surface analysis of antibody immobilized in various formats [random (d), oriented (e), covalent (f), and cov-oriented (g)] at a Z-scale of 150 nm in a scan area of 2  $\mu\text{m}$  X 2  $\mu\text{m}$  revealed that antibody distribution over the surface in oriented formats was highly uniform in comparison to non-oriented formats. Each section in main panel depicts an upside view numbered a-g and their corresponding 3D image. ‘Cov’ represents covalent.

On the other hand, the covalent-CM5-dextran immobilization strategy had the highest anti-HFA antibody density, which may be due to the fact that CM5-dextran has a long hydrophilic polymer chain with a large number of available carboxyl groups on the side chains. Moreover, apart from the increased effective surface area provided by the CM5-dextran, electrostatic interactions of the positively-charged amino groups on anti-HFA antibody towards the negatively-charged carboxyl functional groups on the surface of CM5 dextran can also occur.

Our results are very similar to the findings reported by Kausaite and colleagues in 2010 [27], where it was observed that a carboxymethyl dextran hydrogel-based immobilization strategy had a very high antibody immobilization density in comparison to random and orientated immobilization strategies. Here the random immobilization strategy was based on the passive immobilization of antibodies on a self-assembled monolayer (SAM) formed by 11-mercaptopundecanoic acid (MUA) whereas, the orientated immobilization strategy employed the capture of antibodies on the layer of covalently immobilized Protein G on the MUA SAM-functionalized surface.

#### **4.5.2 Comparison of antibody immobilization strategies as a function of HFA capture densities**

Anti-HFA antibodies bound to SPR Au chips, prepared by various antibody immobilization strategies, were employed for the detection of different concentrations of HFA (0.6-20.0 ng/mL), as shown in **Figure 4.3b**. The blank for the assay was the running buffer i.e. 10 mM HBS, pH 7.4. The RU of the blank in each flow cell was then subtracted from the RU value corresponding to the detection of a particular concentration of HFA in that flow cell.

All immobilization strategies used were evaluated using an HFA concentration of 5 ng/mL, which was the HFA concentration just above the  $EC_{50}$  of the random immobilization strategy. It was highest for the covalent-orientated strategy and lowest for the random strategy. The mass densities of HFA detected by the various antibody immobilization strategies were in the decreasing order of covalent-orientated > covalent > covalent-CM5-dextran > orientated > random. The  $EC_{50}$  of covalent-oriented strategy based anti-HFA bound SPR chip for HFA detection was also found to be the lowest (**Table 4.1**), which indicates that it was the most sensitive immunoassay format. The mass density of HFA

detected while using the covalent-orientated strategy was the highest of all the immobilization strategies employed. Conversely, the covalent-orientated strategy, which had a lower anti-HFA antibody mass density in comparison to the covalent-CM5-dextran and covalent strategies, had the highest response units for HFA capture and thus, the highest mass density. This clearly demonstrates that the total amount of antibody immobilized does not necessarily equate with maximum antigen (HFA) capture. The antigen-detection ability of adsorbed antibodies can be significantly compromised [24, 28]. It had been previously demonstrated that covalently-bound antibodies capture higher amount of antigen than adsorbed antibodies under the same set of conditions [3]. Therefore, the adsorption of antibodies can introduce certain conformational changes that may impact their antigen-recognition behaviour, thereby ultimately resulting in reduced antigen detection. The results shown in **Figure 4.3c** demonstrate that the effectiveness of an immunoassay is clearly dependent on the antibody immobilization strategies.

Our findings show that the covalent-orientated strategy, based on the binding of PrA to the chip and the orientated immobilization of capture antibodies, is ideal for the SPR-based immunoassay for HFA. There was no evidence of biofouling even after continuous HFA detection cycles or extended storage at 4°C (**Figure 4.5**).

#### **4.5.3 Regeneration studies of the APTES functionalized Au surface**

Various silane-based Au surface modification strategies have been employed for immunoassays; however, their use for SPR applications is fairly recent [25, 29]. There are reports claiming the successful regeneration of thiol terminal silane-functionalized Au surfaces [30]. It was observed that strong acid treatment such as HCl can dissolve the siloxane bonds and remove upto the second APTES layer as the first APTES layer on the Au

surface was very strongly bound through Au- thiol interactions.

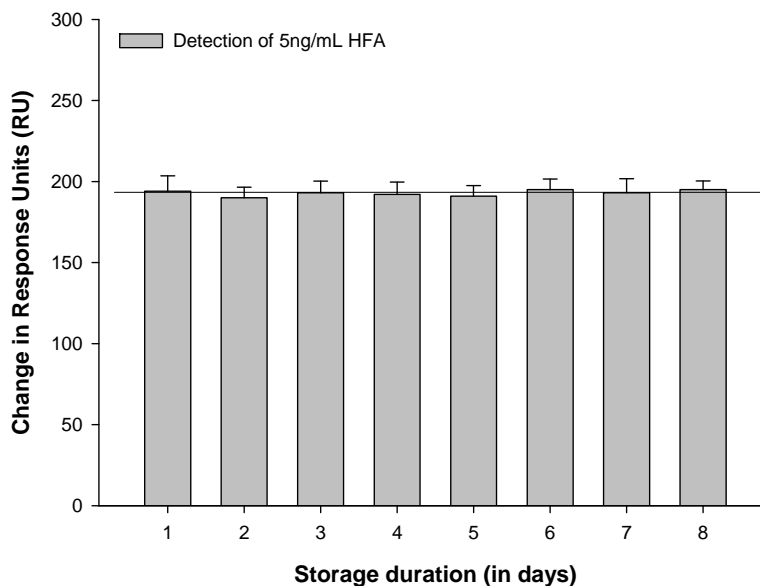


**Figure 4.5** Analysis of the biofouling properties of functionalized Au surfaces to determine the any non-specific protein interaction with the surface over a period of 8 days at 4 °C.

However, there was no critical assessment of reusability and functional characterization of SPR Au chip. In addition, HCl may also affect the homogeneity of Au coating. Here, a simple strategy, based on consecutive treatments with HCl and O<sub>2</sub>-plasma, for the complete regeneration of Au surface was developed.

The regeneration studies, as depicted in schematic **Figure 4.6**, were performed on the Au chips that were (a) functionalized with APTES, and (b) bound to anti-HFA antibody after APTES-functionalization. The thickness of APTES self-assembled monolayer (SAM) and the areal density of APTES on the bare, silanized and regenerated Au chip surfaces were determined by ellipsometry and RBS, respectively (**Figure 4.7a**).

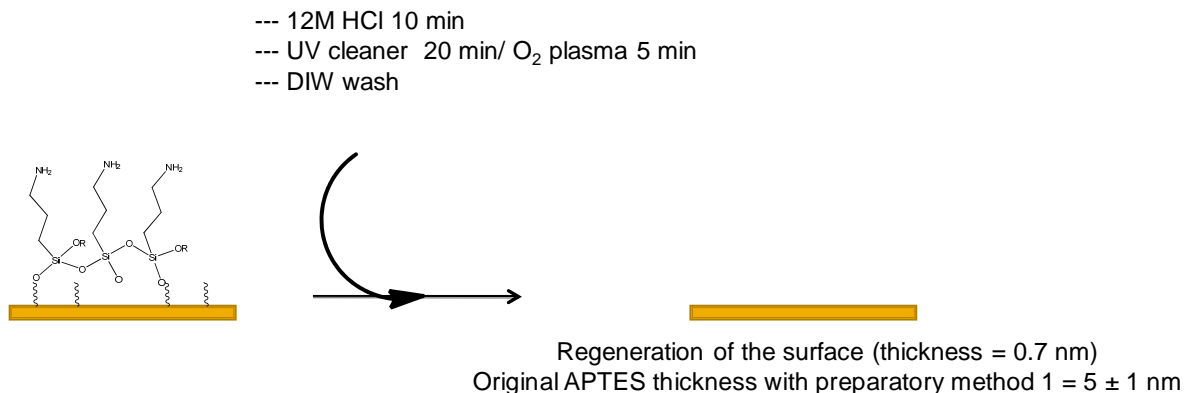


**Figure 4.6** Schematic representation of complete regeneration of the silane-functionalized Au surface by acid and/ or plasmolysis of the siloxane bonds. The surface was characterized with ellipsometry and Rutherford back scattering (RBS) analysis for detection of any residual APTES on the surface.

Twenty chips were APTES-functionalized and different regions on each chip (four spots in the corner and one spot in the centre) were analyzed to assess the homogeneity of silane layer. A SAM thickness of  $5 \text{ nm} \pm 1 \text{ nm}$  was obtained in all the repeats. The thickness was calculated with the instrument software, which generates a differential reflection profile [designated as psi ( $\psi$ ) and delta ( $\Delta$ )] for each corresponding layer.

The contact angle of water was obtained for the SAM of APTES on Au surface was  $59^\circ \pm 1^\circ$ , which is consistent with previous findings [31]. The contact angle obtained for piranha-treated bare Au was  $25^\circ$ , which was in agreement with previous reports that claimed the contact angle of cleaned Au in the range of  $0\text{--}30^\circ$  [32]. The regeneration of Au surface by the developed procedure was confirmed by RBS (**Figure 4.7b**) based on the absence of APTES signal on the regenerated SPR chip. XPS is routinely used for characterizing surface properties but due to poor spatial resolution and inability for absolute quantification of the species on the surface, the expected error would be less than 10%. Therefore, RBS was employed, which is capable of quantifying species to levels as low as 5%. XPS is useful

with thicker surface layers, but in this work 2-4 nm silane layers were only employed and, therefore, RBS, even with poor depth resolution was chosen to obtain silane layer quantification with less error. The areal density of APTES after APTES functionalization on the regenerated SPR Au chip was similar to that on the fresh SPR chip, which shows the complete regeneration of Au surface. During 30 consecutive HFA immunoassays, the areal density of APTES was highly-reproducible; this may imply that the developed regeneration procedure might not have any corrosive effect on the Au layer, hence maintaining its native surface properties.

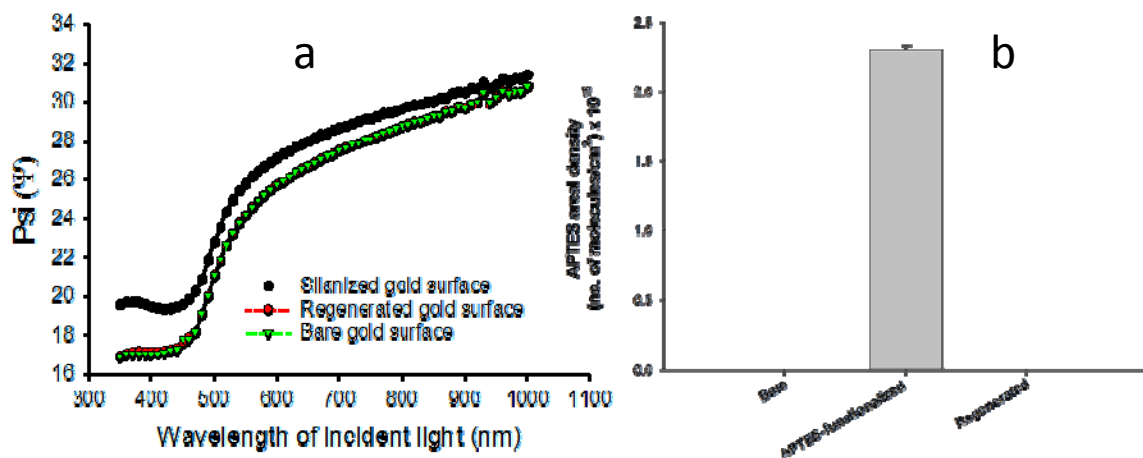


**Figure 4.6** (a) Evaluation of Au surface regeneration in SPR Au chips on the basis of thickness determination by ellipsometry. The data were recorded at 70° in the wavelength range of 300-1000 nm. A model was defined where gold on glass was used as the control to define the thickness of silane layer on 50 nm thick Au surface. Thickness values obtained were an average of 50 measurements at a given point. (b) Evaluation of areal density of APTES on bare, APTES-functionalized and regenerated Au surfaces by Rutherford back scattering (RBS). Error bars are standard deviation.

The developed Au surface regeneration procedure was optimized by determining the appropriate strength and treatment time of HCl and O<sub>2</sub>-plasma (individually in the initial

stages, and in combination thereafter). Initially the efficiency of regeneration was assessed by treating with 5, 10, 12 and 15 M of HCl for varied duration i.e. 5, 10, 20 and 30 min. The treatment with 15 M HCl for 30 min was found to be most appropriate for regenerating down to 1.7 nm thickness (**Figure 4.8a**). However, the acid treatment does not regenerate the surface completely due to the role played by the respective anions generated by acid treatment in the dissolution of siloxane bonds [33]. These anions, such as hydroxyl ( $\text{OH}^-$ ), sulfate ( $\text{SO}_4^{2-}$ ) and chloride ( $\text{Cl}^-$ ), potentially destabilize the siloxane frame work in the presence of water. However, the acidic environment enhances the polymerization of silanes, which is responsible for incomplete regeneration. Therefore, our intial acid-treatment approach was followed by  $\text{O}_2$ -plasma scrapping/ etching [34].

A plasma is a distinct yet complex state of matter, which is similar to a gas but contains ionized/charged species such as positive and negative ions and free radicals. Therefore, plasma can be described as an ionized state of gas where ionization can be achieved by exposing the gas to a strong electromagnetic field. The presence of considerable number of charges in plasma makes it suitable for various applications ranging from fusion power to plasma ashing. In addition, the nature of high energy charged particles and free radicals can be manipulated by breaking a specific gas such as oxygen, nitrogen and argon in plasma. Therefore, plasmas have the potential to break the molecular bonds of almost any solid support such as glass or polymers. Therefore, these plasmas have potential applications in surface chemistry and can be employed for regenerating the functionalized surfaces especially with an  $\text{O}_2$ -plasma that contains highly reactive oxygen ions/radicals. The  $\text{O}_2$ -plasma discharges are known to ionize the siloxane bonds present in the liquid phase hence breaking the silanol bonds with surface [34]. Therefore, along with HCl treatment,  $\text{O}_2$ -

plasma was also incorporated. The O<sub>2</sub>-plasma scrapping was done at plasma strengths of 12, 20 and 29W for 3, 6, 9, 12 and 15 min such that 29W O<sub>2</sub> plasma treatment for 12 min was most effective and regenerated down to 1.3 nm thickness (**Figure 4.8b**).

Finally, the surface regeneration was checked with various combinations of HCl and O<sub>2</sub> plasma. For the initial HCl treatment step, 12 M and 15 M HCl was used for 10, 20 and 30 min; whereas, for the O<sub>2</sub> plasma scrapping, 29W O<sub>2</sub> plasma was employed for 5, 10, 12 and 15 min. The complete regeneration of Au surface was obtained by treating it with 12 M HCl for 10 min followed by O<sub>2</sub>-plasma scrapping for 5 min, which completely removed the APTES coating. This was confirmed by the absence of silicon peak due to APTES functionalization on the Au surface by RBS. A negative ninhydrin test and a contact angle of 28° cross-validated the absence of silane on the surface.

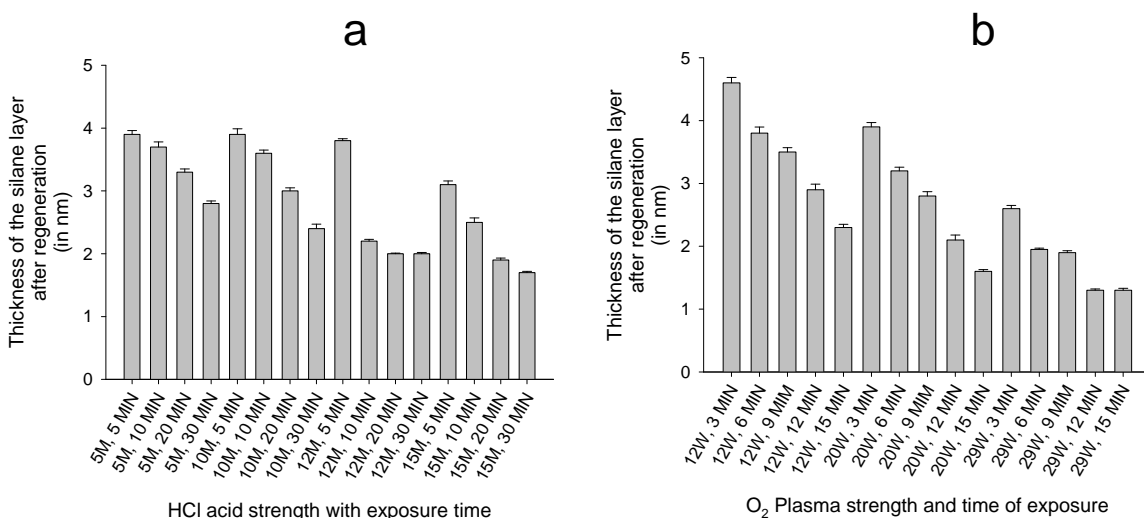


**Figure 4.8** Optimization of siloxane bond lysis at various acid (HCl) (a) and O<sub>2</sub> plasma (b) strengths as a function of exposure time (min). Thickness for each set was monitored using ellipsometry. Significant surface regeneration was obtained individually with 12 and 15M HCl strengths, and 29W plasma strength. However, complete surface regeneration was achieved with 12M HCl exposure for 10 min in conjunction with 29W plasma for 5 min.

The regenerated SPR Au chip was reused 30 times for SPR-based HFA immunoassay following the same bioanalytical procedure i.e. APTES-functionalization, anti-HFA antibody immobilization, HFA detection and surface regeneration. The reproducibility of APTES functionalization in each cycle was confirmed by ellipsometry and RBS, as discussed previously. The areal density of APTES after APTES functionalization was consistently uniform in each detection cycle. The immobilization density of anti-HFA antibody and the subsequent detection of HFA was also highly reproducible in each cycle, as confirmed by the SPR response (**Figure 4.9**).

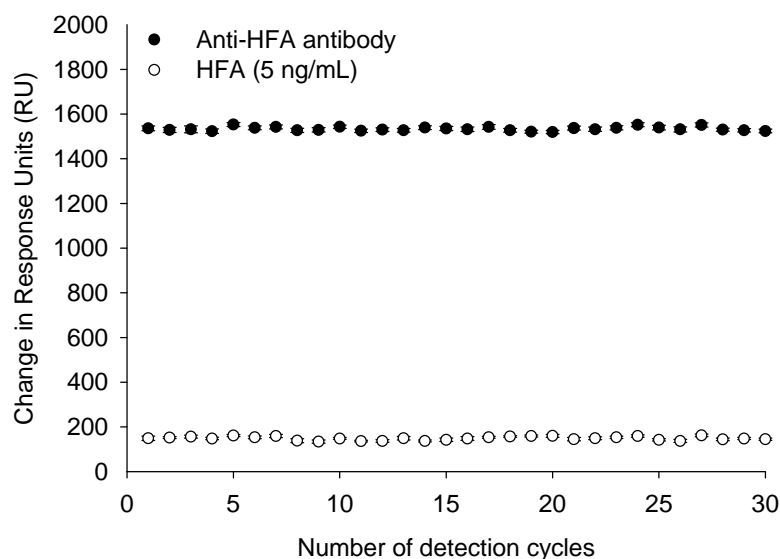


**Figure 4.9** Reproducibility of antibody immobilization and antigen detection on the SPR Au chip, which was reused 30 times after regenerating the Au surface using the developed procedure. The black dots correspond to the SPR signal obtained for anti-HFA antibody binding on the regenerated and re-functionalized Au surface whereas, the white dots represent the detection of HFA by anti-HFA antibody immobilized on such Au chip.

The percentage coefficient of variance in APTES functionalization, anti-HFA immobilization and HFA detection, during 30 consecutive HFA immunoassays on the same SPR chip after regeneration, were 3-5, 4-6 and 2-4%, respectively. The developed Au surface regeneration procedure completely regenerates the Au surface without affecting its surface properties. It has increased the cost-effectiveness of expensive SPR gold chip as the same SPR chip can be reused many times without any loss of activity.

#### **4.6 Conclusions**

A robust Au surface functionalization method was developed for SPR-based immunoassay applications. The developed strategy was optimized and employed to study the effect of various antibody immobilization strategies, i.e. random, covalent, orientated, covalent-orientated and covalent-CM5-dextran, on the analytical performance of a SPR-based immunoassay for HFA. The highest anti-HFA antibody immobilization density was obtained with covalent-CM5-dextran, whereas the highest amount of HFA was captured with the covalent-orientated strategy. Therefore, the orientation of the antibody plays an important role in the analytical performance of the SPR immunoassay. The relative molar density of HFA detected, which corresponds to the functional antibody immobilization density, is a more reliable indicator of analytical performance than the total antibody immobilization density. Additionally, a novel strategy, based on the acid and/ or plasmolysis of the siloxane bonds, was developed to regenerate the APTES-functionalized Au surface completely allowing the reuse of same Au chip for performing multiple cycles of functionalization and immunoassay development.

#### **4.7 References**

1. Skottrup P, Hearty S, Frøkiær H, Leonard P, Hejgaard J, O'Kennedy R, Nicolaisen M, Justesen AF: Detection of fungal spores using a generic surface plasmon resonance immunoassay. *Biosens Bioelectron* 2007, 22(11):2724-2729.
2. Stapleton S, Bradshaw B, O'Kennedy R: Development of a surface plasmon resonance-based assay for the detection of *Corynebacterium pseudotuberculosis* infection in sheep. *Anal Chim Acta* 2009, 651(1):98-104.
3. Dixit CK, Vashist SK, O'Neill FT, O'Reilly B, MacCraith BD, O'Kennedy R: Development of a high sensitivity rapid sandwich elisa procedure and its comparison with the conventional approach. *Anal Chem* 2010, 82(16):7049-7052.
4. Vashist SK, O'Sullivan SA, O'Neill FT, Holthofer H, O'Reilly B, Dixit CK: Modified ELISA Plate. 2010, PCT/ IE2009/ 000072 (WO 2010/ 044083 A2).
5. Snopok B, Boltovets P, Rowell F: Effect of the local environment and state of the immobilized ligand on its reaction with a macromolecular receptor. *Theor Exp Chem* 2006, 42(4):217-223.
6. Kausaite-Minkstimiene A, Ramanaviciene A, Ramanavicius A: Surface plasmon resonance biosensor for direct detection of antibodies against human growth hormone. *Analyst* 2009, 134(10):2051-2057.
7. Danczyk R, Krieder B, North A, Webster T, HogenEsch H, Rundell A: Comparison of antibody functionality using different immobilization methods. *Biotechnol Bioeng* 2003, 84(2):215-223.

8. Gedig ET: Surface chemistry in SPR technology. In *Handbook of Surface Plasmon Resonance*. Ed. Richard BMS, Anna JT. RSC Publishing, Cambridge, UK; 2008: 173-218.
9. Aslan K, Lakowicz JR, Geddes CD: Plasmon light scattering in biology and medicine: new sensing approaches, visions and perspectives. *Curr Opin Chem Biol* 2005, 9(5):538-544.
10. Yuan Y, He H, Lee LJ: Protein A-based antibody immobilization onto polymeric microdevices for enhanced sensitivity of enzyme-linked immunosorbent assay. *Biotechnol Bioeng* 2009, 102(3):891-901.
11. Holmberg A, Blomstergren A, Nord O, Lukacs M, Lundeborg J, Uhlen M: The biotin-streptavidin interaction can be reversibly broken using water at elevated temperatures. *Electrophoresis* 2005, 26(3):501-510.
12. Svitel J, Boukari H, Ryk DV, Willson RC, Schuck P: Probing the functional heterogeneity of surface binding sites by analysis of experimental binding traces and the effect of mass transport limitation. *Biophys J* 2007, 92(5):1742-1758.
13. Conti M, Falini G, Samorì B: How Strong is the coordination bond between a histidine tag and  $\text{Ni}^{+2}$  - nitrilotriacetate? an experiment of mechanochemistry on single molecules. *Angew Chemie Int Ed* 2000, 39(1):215-218.
14. Dixit CK, Vashist SK, MacCraith BD, O'Kennedy R: Multisubstrate-compatible ELISA procedures for rapid and high-sensitivity immunoassays. *Nat Protocols* 2011, 6(4):439-445.

15. Dixit CK, Vashist SK, MacCraith BD, O'Kennedy R: Evaluation of apparent non-specific protein loss due to adsorption on sample tube surfaces and/or altered immunogenicity. *Analyst* 2011, 136(7):1406-1411.
16. Palasantzas G, Svetovoy VB, van Zwol PJ: Influence of ultrathin water layer on the van der Waals/Casimir force between gold surfaces. *Phys Rev B* 2009, 79(23):235434.
17. Pan L, Jung S, Yoon R-: Effect of hydrophobicity on the stability of the wetting films of water formed on gold surfaces. *J Colloid Interface Sci* 2011, 361(1):321-330.
18. Kurtinaitiene B, Ambrozaite D, Laurinavicius V, Ramanaviciene A, Ramanavicius A: Amperometric immunosensor for diagnosis of BLV infection. *Biosens Bioelectron* 2008, 23(10):1547-1554.
19. Mitsyuk B: Mechanism of silica dissolution and state of silicic acid in hydrothermal solutions. *Theor Exp Chem* 1984, 19(5):554-559.
20. Vasant EF, Voort P, Vrancken K: Characterization and chemical modification of the silica surface: Amsterdam. In *Studies in surface science and catalysis Vol.93*: Elsevier Science & Technology; 1995.
21. Cypryk M, Apeloig Y: Mechanism of the acid-catalyzed si-o-si bond cleavage in siloxanes and siloxanols. a theoretical study. *Organometallics* 2002, 21(11):2165-2175.
22. Jonsson U, Fagerstam L, Ivarsson B, Johnsson B, Karlsson R, Lundh K, Lofas S, Persson B, Roos H, Ronnberg I: Real time biospecific interaction analysis using surface plasmon resonance and a sensor chip technology. *Biotechniques* 1991, 11(5):620-627.

23. Tang Y, Mernaugh R, Zeng X: Nonregeneration protocol for surface plasmon resonance: study of high-affinity interaction with high-density biosensors. *Anal Chem* 2006, 78(6):1841-1848.
24. Willard FS, Siderovski DP: Covalent immobilization of histidine-tagged proteins for surface plasmon resonance. *Anal Biochem* 2006, 353(1):147-149.
25. Spencer MJS, Nyberg GL: Adsorption of silane and methylsilane on gold surfaces. *Surf Sci* 2004, 573(2):151-168.
26. Jung A, Gronewold TMA, Tewes M, Quandt E, Berlin P: Biofunctional structural design of SAW sensor chip surfaces in a microfluidic sensor system. *Sens Act B: Chem* 2007, 124(1):46-52.
27. Kausaite-Minkstiniene A, Ramanaviciene A, Kirlyte J, Ramanavicius A: Comparative study of random and oriented antibody immobilization techniques on the binding capacity of immunosensor. *Anal Chem* 2010, 82(15):6401-6408.
28. Snopok BA, Kostyukevich EV: Kinetic studies of protein surface interactions: A two-stage model of surface-induced protein transitions in adsorbed biofilms. *Anal Biochem* 2006, 348(2):222-231.
29. Jung A, Gronewold TMA, Tewes M, Quandt E, Berlin P: Biofunctional structural design of SAW sensor chip surfaces in a microfluidic sensor system. *Sens Act B: Chem* 2007, 124(1):46-52.

30. Corrado DN (Ed): *Proceedings of the Sensors and Microsystems: Proceedings of 8<sup>th</sup> Italian Conference, Trento: 2004*, World Scientific Publishing Co. Pte Ltd. Singapore. Pp 45-69.
31. Siqueira Petri DF, Wenz G, Schunk P, Schimmel T: An improved method for the assembly of amino-terminated monolayers on sio<sub>2</sub> and the vapor deposition of gold layers. *Langmuir* 1999, 15(13):4520-4523.
32. Smith T: The hydrophilic nature of a clean gold surface. *J Colloid Interf Sci* 1980, 75(1):51.
33. Bai S, Urabe S, Okaue Y, Yokoyama T: Acceleration effect of sulfate ion on the dissolution of amorphous silica. *J Colloid Interf Sci* 2009, 331(2):551.
34. Leu GF, Brockhaus A, Engemann J: Diagnostics of a hexamethyldisiloxane/oxygen deposition plasma. *Surf Coatings Technol* 2003, 174-175:928.

## **Chapter 5**

Development of conjugates of Dye-doped  
Silica nanoparticle and anti-CD41 antibody  
for efficient platelet probing

(Published in Langmuir, 2010, 26(17), 13741–13746)

## 5.1 Abstract

Aminopropyltriethoxy silane (APTES)-based dye-doped silica nanoparticle (Si NP)-functionalization strategy was developed that was intended to conjugate anti-CD41 antibody for imaging platelets. The functionalization of NIR664 dye-doped Si NP was optimized for duration of functionalization, APTES concentration to obtain maximum NP dispersion and stability. Various chemical and physical parameters were monitored using techniques like Fourier Transform infrared spectroscopy (FTIR), Zeta potential measurement, fluorescent lifetime correlation spectroscopy, transmission-electron, scanning-electron and confocal microscopy. Afterwards, a microtitre plate-based fluorescent immunoassay (FIA) was performed to characterize the assay potential of the developed NP-anti-CD41 antibody conjugates.

## 5.2 Introduction

The use of fluorescence based nanoparticles (NPs) as high-brightness labels in the field of nanobiophotonics has potential in the broad area of clinical diagnostics [1]. The essential criterion to construct an efficient high-brightness label is the tuning of primarily two major properties (i) the brightness and (ii) the target specificity. Silica NPs have advantages such as high brightness compared to single dye molecule probes, tunability of size, ease of surface functionalization and relative biocompatibility. These properties are advantageous to design efficient bioassays with decreased limit of detection (LOD), [2] as well as the use of the NPs as cellular probes [3]. There are two main approaches to the synthesis of highly fluorescent silica NPs, the Stöber sol-gel process, [4] and the reverse micro emulsion [5] approach which is the approach used here. In our system, the near infrared dye, 4,5-Benzo-5'-(iodoacetaminomethyl)-1',3,3,3',3'-pentamethyl-1-(4-sulfobutyl)indodicarbocyanine (NIR664) has been covalently encapsulated in the silica NPs by the micro-emulsion method. The cyanine-based dyes are very efficient sensors of chemical environment because of their strong fluorescence response to the hydrophobicity of the immediate microenvironment [6] that actually alters the equilibrium between the monomer and aggregate state of the dye, having distinct absorption peaks at 665 and 615nm, respectively. While encapsulated inside a nanoparticle, the dye is distributed in two distinct populations and thus any significant alteration at the immediate micro-environment of the dye doped nanoparticle, can be sensed by this dynamic equilibrium.

The latter is achieved by functionalizing [7] the NP with appropriate surface chemistry that could facilitate the conjugation of the relevant ligand such as antibody to develop NP-based immunosensing [8, 9]. Standard conjugation strategies normally involve covalent linker-

based attachment chemistry. Various surface functionalization strategies are available such as amination, carboxylation, thiolation and epoxylation particularly using silanization approach [10-12]. The approach used in this study was based upon the amine functionalization using aminopropyl tri-ethoxy silane (APTES) self-assembled layer (SAL) strategy [13]. The availability of free hydroxyl groups on the silica surface facilitates the reaction initiation of alkoxy groups with the hydroxyl of surface (**Figure 5.1**). Conversely, specificity of antibody-NP conjugates could be enhanced by monitoring the surface's functional morphology and antibody's leach-proof functional conjugation to NPs. Optimum conjugation is obtained when the layer containing functional groups on the surface is evenly distributed over the surface/highly-ordered, [8, 9] which enables the antibody capture with proper orientation maintaining a functional conformation so as to avoid steric hindrance of binding to the target antigen.

Techniques like ellipsometry, [14, 15] Contact angle goniometry, [15] X-ray photoelectron spectroscopy (XPS) [16] are useful to measure the amine layer thickness on a flat surface, more popularly on the glass surface or silicon wafers [17]. But these techniques fall short for nanoparticle based systems because of the curved nature of the surface, along with possibility of NP agglomeration that could be recorded as the thickness. Therefore, Fourier-transform infrared spectroscopy (FTIR) was used as a basic strategy to determine functionalization [18, 19]. To elucidate the dynamics of APTES-based amine layer growth on NPs, FTIR in conjunction with FCS and FLCS were also employed [20].

### **5.3 Material**

NIR664 (1.6 mg), 1-hexanol (99%), Mercaptopropyltri-ethoxy silane (MPTES), Triton X-100, cyclohexane, hexanol, tetraethoxy silane,  $\text{NH}_4\text{OH}$ , absolute ethanol (EtOH),

aminopropyltriethoxy silane (APTES) and anti-CD41 antibody were procured from Sigma Aldrich, Blessington, Co. Wicklow, Ireland. PBS (sachet), 1-ethyl-3-[3-dimethylaminopropyl]carbodiimide hydrochloride (EDC), N-hydroxysulfosuccinimide (SNHS) and bovine serum albumin (BSA) were obtained from Thermo Fisher Ireland. The formvar carbon-coated copper grids for TEM experiments were procured from Agar Scientific.

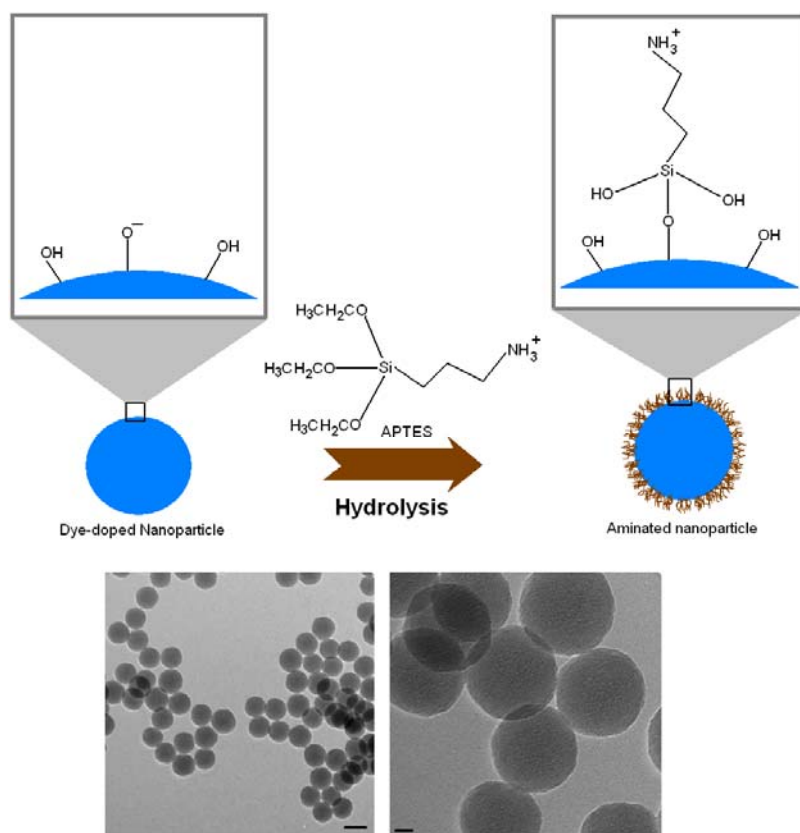


**Figure 5.1** A schematic representation of the amine-silanization reaction with the TEM image of the aminated NP having scale bar of 100 and 20nm length for the left and right image, respectively. Mechanism of APTES-mediated functionalization has been discussed in Chapter 2 in detail.

## 5.4. Methods

### 5.4.1 Synthesis of dye-doped NPs

The dye-doped silica nanoparticles were synthesized within our group and details could be found in the mentioned reference [21].

#### **5.4.2 Amine-silanization of the NPs**

The kinetics study was performed in order to study silanization behaviour of APTES on NPs. Silanization was performed with 2% (v/v) APTES prepared in absolute ethanol in a set of five different time points *viz.* 1, 2, 3, 5 and 12 h, considering non-functionalized NP as the control for this study (0 hr). Each sample set was fed with a starter batch of NP sample at a concentration of 10 mg/mL. Additionally, a set of NP functionalization with various amine concentrations was performed in order to find out the optimum working amine concentration. These NPs were subjected to 0.5, 1, 2, 3 and 4% APTES in absolute ethanol for the optimized period from the previous set of experiments, again with reference to un-functionalized NPs as the control (0% (v/v) APTES).

#### **5.4.3 Bioassay performance to determine the efficiency of antibody-NP conjugation**

Aminated NPs were conjugated to anti-CD41 antibody produced in mouse by using conventional carbodiimide linker chemistry. NP (10 mg/mL) were incubated with 2% (v/v) APTES over five different durations that is 1, 2, 3, 5 and 12 h. The NP-APTES solution was continuously stirred for corresponding durations. Each set of NP-APTES solution was subjected to centrifugation (1260 X g) followed by washing with absolute ethanol (five times) and finally with 0.1M PBS (pH 7.2). The anti-CD41 (900  $\mu$ L of 15  $\mu$ g/mL in 0.1M PBS, pH 7.2) was incubated with a 100  $\mu$ L pre-mixed solution of EDC (4 mg/mL) and SNHS (11 mg/mL) for 15 min at 37 °C. The resulting EDC-activated antibody solution was added to the APTES-functionalized NPs suspended in 0.1M PBS (pH 7.2) and incubated for 1 h at RT. The IgG-conjugated NP solution was washed five times with 0.1M PBS, pH 7.2.

The platelet (obtained as a donation from healthy subject at School of Nursing, DCU) was physisorbed in chemically-activated microtitre plate [22] wells by incubating for 2 h at 37 °C. Afterwards, the plate wells were washed five times with 0.1M PBS (pH 7.2) and blocked for 30 min with 1% (v/v) BSA in 0.1M PBS, pH 7.2 at 37°C. The plate was washed five times with PBS. The anti-CD41-conjugated NPs were incubated in the corresponding plate wells for 1 h at 37 °C followed by five PBS washes. The fluorescence was recorded using Tecan Safire2 monochromator-based microplate reader (Tecan GmbH, Austria) at excitation and emission wavelengths of 660 and 700 nm, respectively. Relevant controls were employed for each study.

#### **5.4.4 Characterization of the aminated NPs**

##### **5.4.4.1 Zeta potential for the measurement of interfacial charge**

Zeta potential for the aminated samples was measured by a Beckman Coulter Instrument by using the flow cell. The averages obtained from three measurement sets were analyzed by the DelsaNano software in the result section where each measurement was the average of 50 individual measurements performed at various positions (10 measurements each in 5 positions) in the flow cell that is set as default. However, size of the NPs could also be measured using the same instrument but with dynamic light scattering (DLS) settings.

##### **5.4.4.2 Fourier Transform Infra Red spectroscopic studies**

Liquid FT-IR (Thermo Nicolet Corporation, Madison, USA) was used to characterize the chemical nature of the functionalization on the NPs. NPs were re-suspended in two sets, one in absolute ethanol and the other in toluene at a concentration of 2 mg/ml in both cases. This was done in order to assess the effect of the solvent-based environment on the FT-IR spectral analysis. The functionalized samples from each set were subjected to FT-IR and

transmittance (%T) was recorded. The measurements were baseline-corrected with corresponding solvents. All these samples were later analyzed using various peaks in the transmission spectra.

#### **5.4.4.3 Miscellaneous physical characterization**

For UV-visible spectroscopy, a Cary 50 scan UV-visible spectrophotometer (Varian) was used. For fluorescence spectroscopy, a Fluoromax spectrophotometer was used. Regarding TEM measurement, a Hitachi 7000 transmission electron microscope was operated at 100kV. Image capture was performed digitally by a Megaview 2 CCD camera. Specimens were prepared by putting a drop of the ethanolic solutions of the nanoparticles on to a formvar carbon-coated copper grid. In conjunction with all these techniques, ninhydrin assay was also employed to determine the amination of the NPs.

#### **5.4.5 Antibody conjugation to the nanoparticle and characterization**

Bicinchoninic acid (BCA) assay of protein estimation was employed to characterize the antibody conjugation to the NPs and to quantify the amount/ number of antibodies on the NP surface. Fresh BCA solution was prepared according to the manufacturer's recommendations. A known weight of antibody-NP conjugate was reconstituted in water and freshly prepared BCA solution was added to it in recommended ratio and the sample was incubated at 37 °C for 1 h. Additionally, anti-CD41 that was serially half-diluted from 20 µg/mL to 20 ng/mL was also subjected to the BCA assay under the same conditions. The solution containing antibody-NP conjugates incubated in BCA was centrifuged (1260 X g) in order to obtain BCA solution without NPs. Later, conjugates and standard anti-CD41 samples were subjected to spectrophotometry at a wavelength of 562 nm. A calibration curve was prepared with the standards such that at least five antibody dilutions are in the

linear range of the curve. The absorbance obtained for conjugates was then plotted on the standard curve in order to deduce the exact concentration of antibody that was conjugated to nanoparticle. The obtained concentration of antibody was then converted into the number of molecules in the given mass. Additionally, based on the mass density of silica in NPs, average volume and weight of the NP subjected to BCA assay, the number of Si NP was calculated. Therefore, an approximate number of anti-CD41 antibody per NP can be calculated as a ratio of total number of antibody present in the given sample and NPs.

## **5.5 Results and Discussion**

Silica NPs were employed for this study because they are easy to develop. The current Si NP development methods also allow manipulation of NP morphology, such as size and shape. In addition, the most important property of these Si NPs is that there is a plethora of strategies to conjugate high-efficiency dyes to the core or surface of these NPs, which significantly increases their application.

### **5.5.1 Zeta potential measurement to measure surface charge**

During the amine-silanization reaction of the NPs by APTES, the negative charge of Si NPs was replaced by a positive charge due to the presence of amine groups. This charge transition on the nanosurface can effectively be measured as zeta potential. The zeta potential results are shown in **Figure 5.2a**. The unmodified nanoparticle shows an average zeta potential of -35.8 mV. The NP sample collected after 1 h of incubation with APTES shows a sharp increase of the zeta potential value to -8 mV. It continues to increase until it reaches saturation at 3 hr with a much higher positive value of over +35 mV signifying the stable deposition of the amine group all over the surface of the NPs. Additionally, higher the numerical value of the zeta potential of NPs, higher will their stability in a given solvent. However, although this technique is straightforward enough to report the effective

deposition of the positively charged amine groups on the negatively charged silica nanosurface, the finer details of the APTES deposition and the formation of the amine monolayer and cross linked super structures cannot be elucidated. The reason is attributed to the fact that upon reaching a critical value of the zeta potential (saturation point), any further conjugation of APTES to the nanosurface is involved in either cross-linking or intermolecular hydrogen bondings engaging the primary amine groups with -OH groups (nanosurface silanol group or -OH groups of surface attached APTES molecules) and thus limiting a further increase of positive zeta potential value.

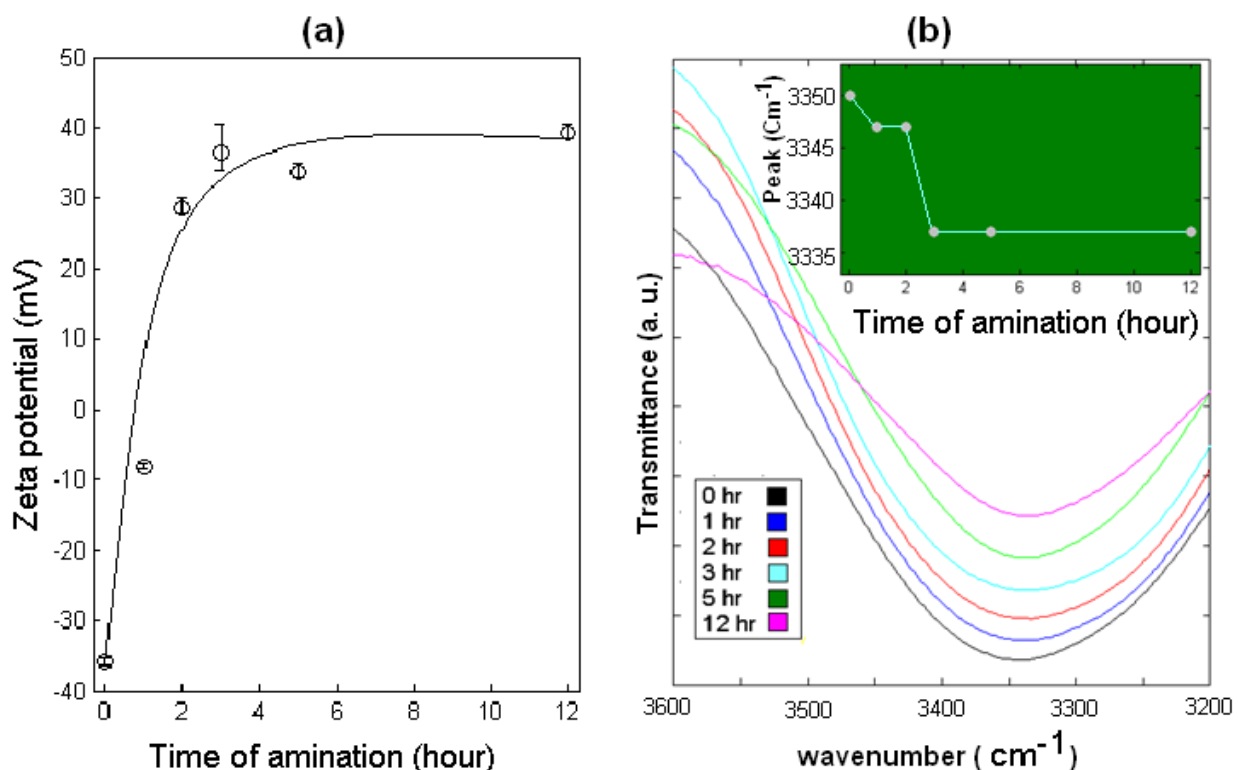


**Figure 5.2.** (a) A plot of incubation time for APTES with aminated NP suspension versus the zeta potential, and (b) FTIR spectra for the same samples where the inset shows peak shift versus time of amine-silanization.

### 5.5.2. Confirmation of the amine-functionalization of silica nanoparticles by Fourier Transform Infra Red spectroscopic measurement

FTIR has been performed in two solvents, ethanol and toluene, to investigate two different aspects of the silica nanosurface. In ethanol, the emphasis is given towards the replacement kinetics of the silanol (Si-OH) group by the amine group as a result of the siloxane bond formation and deposition of the protonated amine group on the nanosurface. In the toluene environment, however, the fine structure of the surface stabilized amine groups has been studied to make a detailed account of the whole process as there is no interference from the -OH groups of the ethanol. Firstly, in the presence of ethanol the overall amine-silanization process was studied by following the gradual disappearance of the surface siloxane (Si-OH) bond and the corresponding appearance of the amine group for the NPs suspended in ethanol. Both the hydroxyl and amine groups are closely placed at the far end of the FTIR spectrum from 3300 to 3600  $\text{cm}^{-1}$  signified by a broad peak in this region. But, there was a significant kinetic effect to monitor the amine-silanization by assessing the shift of the peak value of the broad peak from 3350  $\text{cm}^{-1}$  to 3337  $\text{cm}^{-1}$  as observed in **Figure 5.2b** (and inset). When this value of the wave number for the corresponding peaks was plotted against the time of NPs incubation with APTES, time kinetics was obtained showing saturation after 3 h which is shown in the inset of **Figure 5.2b**. Hence, like the zeta potential measurement, FTIR indicates saturation kinetics after 3h of reaction.

FTIR studies performed on the NPs suspended in toluene have shown several fine structures arising from the amine groups attached to the nanosurface and the attachment between the silica surface and the APTES moiety. Therefore, all subsequent FTIR characterizations were performed in toluene. The FTIR spectrum has been divided in two major parts to analyse the kinetics; the first segment to be discussed is the region between 1200 and 1800  $\text{cm}^{-1}$ , which

deals with various responses from the amine groups and the second region spans from 900 to 1200  $\text{cm}^{-1}$ , which mainly deals with the covalent attachment of the silica surface with the APTES. **Figure 5.3a** shows the response of the 900 to 1200  $\text{cm}^{-1}$  region. Its depicted in the FTIR curve, appearance of the 1110  $\text{cm}^{-1}$  peak indicates that Si-O bonds began to form from the first hour of reaction. But, the effective conjugation has started from the 2<sup>nd</sup> h of the reaction with the appearance of the conjugation peaks like Si-O-Si at 1030  $\text{cm}^{-1}$  and ethoxy group ( $-\text{OCH}_2\text{CH}_3$ ) at 1080  $\text{cm}^{-1}$ . Looking at the reaction steps of the amine-silanization given in the cartoon in **Figure 5.3b**, it is evident that the first step is the conjugation of surface  $-\text{OH}$  group with the hydrolyzed APTES which is followed by Si-O-Si bond formation between surface-attached APTES molecules to form the amine monolayer. This agrees well with the data. It can be seen that the rate of Si-O-Si peak formation is much higher up to the 3 h. For the NPs with higher APTES incubation time (i.e. 5 and 12 h) there is a steep increase of the ethoxy group ( $-\text{OCH}_2\text{CH}_3$ ) at 1080  $\text{cm}^{-1}$  signifying incomplete hydrolysis of APTES and significant increase in siloxane groups (Si-O-Si) at 1110  $\text{cm}^{-1}$  implying cross linking between the surface bound and free APTES leading to multiple inhomogeneous layers of amine groups on the nanosurface. In addition, the broad shoulder starting from 1125  $\text{cm}^{-1}$  signifies the polymerized and/or physically adsorbed APTES on the nanosurface that is very prominent in the 12 h incubation sample. A cartoon based on these detailed features during the amine-silanization process is presented in **Figure 5.3b**. In order to study the detailed amine group kinetics during this amine-silanization reaction the 1200 to 1800  $\text{cm}^{-1}$  spectrum of the aminated NPs was studied in detail and is shown in **Figure 5.4**. The characteristic FTIR peaks of the amine groups have been identified in detail. The asymmetric and symmetric deformation modes of amine groups due to the surface adsorbed APTES molecules have been observed at 1610 and 1510  $\text{cm}^{-1}$  respectively. These two peaks

originate from the interaction between the acidic silanol group on the nanosurface and basic amino group of the APTES.

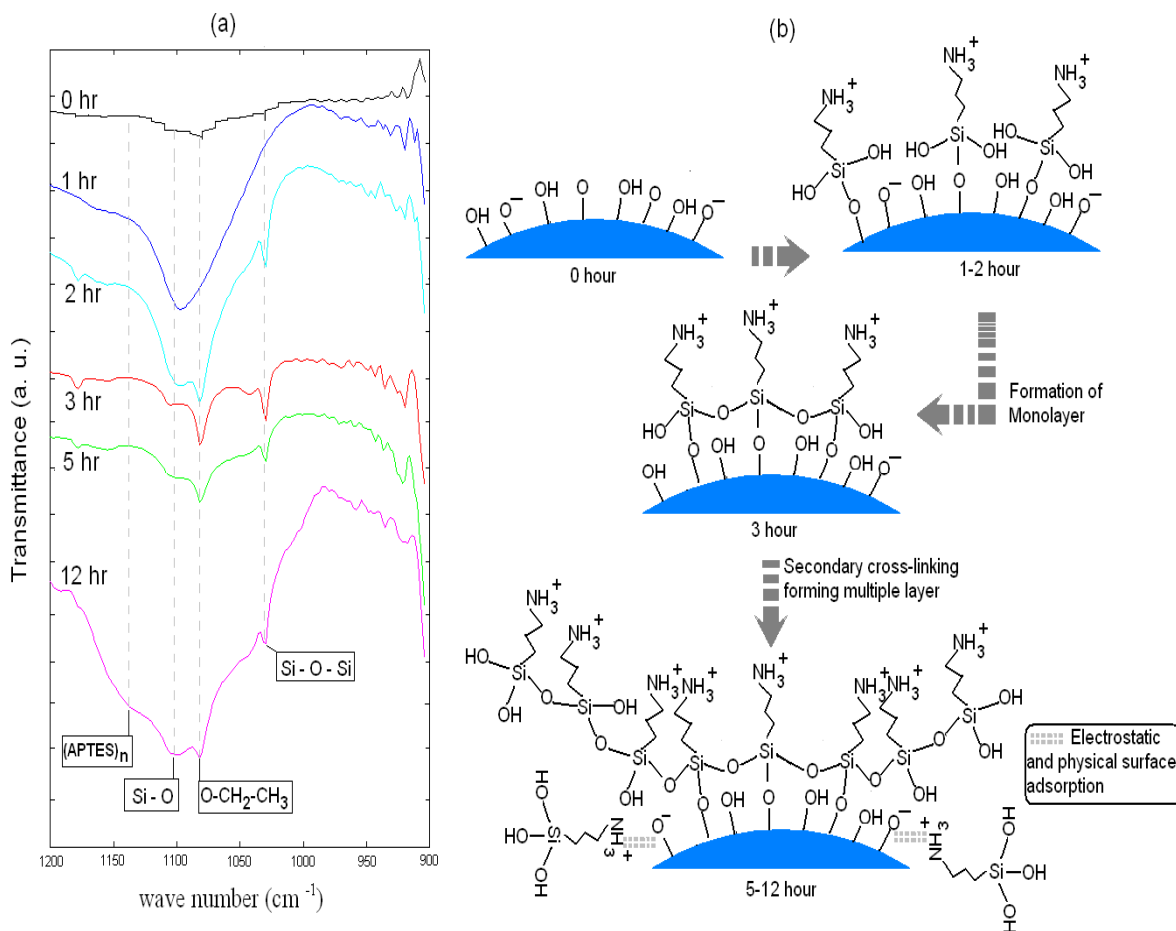


**Figure 5.3.** (a) The FTIR signature of the aminated NP (suspended in toluene) for various reaction times for the 900-1200 cm<sup>-1</sup> region is described to show the conjugation of APTES on the nanosurface, and (b) based on that, a diagram is presented to depict the APTES deposition as a function of reaction time.

The deformation modes of amine groups at 1575 and 1493 cm<sup>-1</sup>, which appear due to the hydrogen bond formation by the amine group presumably with atmospheric carbon dioxide, increase with the time of APTES incubation and show significantly higher density in the 12 h aminated NPs, with the 1575 cm<sup>-1</sup> band showing a more significant increase. The physical nature of the interaction is evident from the  $\omega(\text{CH}_3)$  mode, i.e. the -CH<sub>3</sub> wagging mode of

the APTES backbone at  $1300\text{cm}^{-1}$ . The two distinct peaks at  $1440$  and  $1390\text{ cm}^{-1}$  represent the asymmetric and symmetric deformation mode for the methyl ( $-\text{CH}_3$ ) groups from the ethoxy group ( $-\text{OCH}_2\text{CH}_3$ ) of the APTES indicating the incompleteness of the hydrolysis.

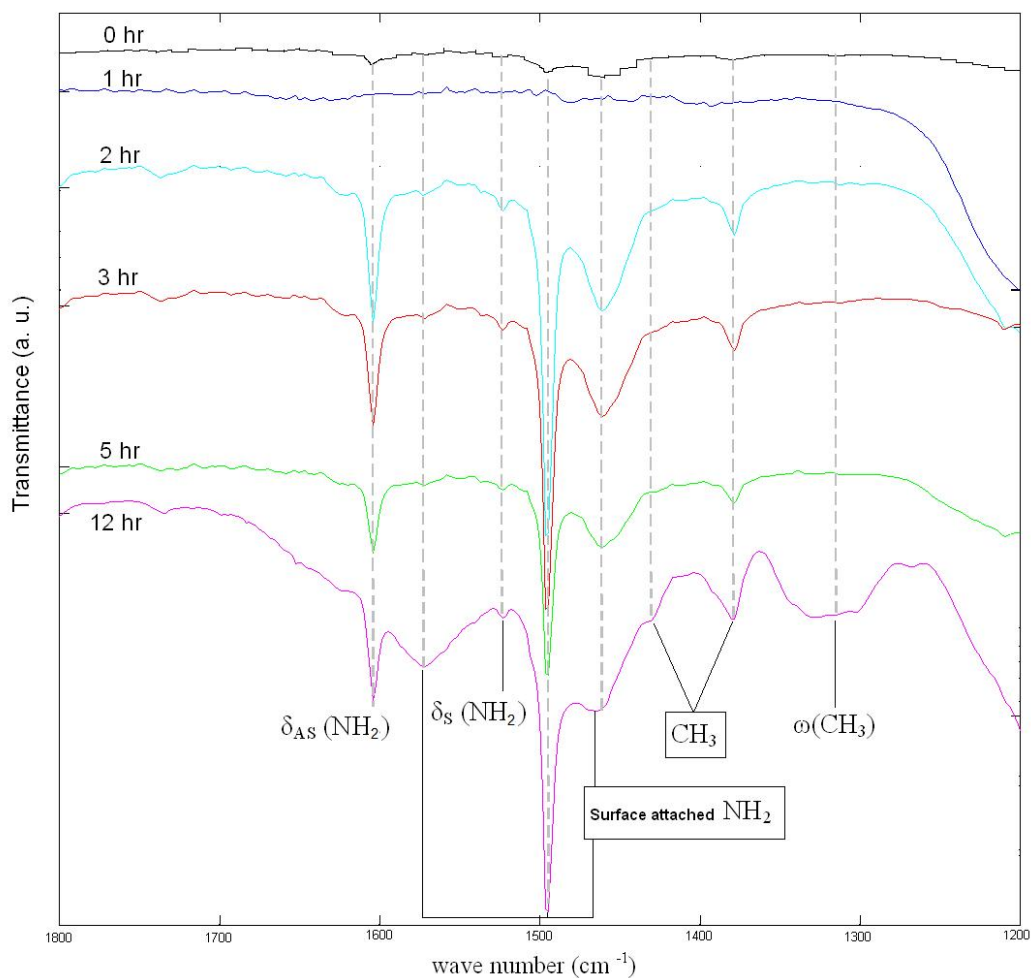


**Figure 5.4.** The FTIR signature of the aminated NP (suspended in toluene) for various reaction times for the  $1200\text{-}1800\text{ cm}^{-1}$  region is described to show the evolution of various populations of amine peaks.

### 5.5.3 Antibody conjugation and bioassay performance

The optimum reaction time for NP surface amine-silanization has been validated by assaying the antibody conjugation efficiency of the aminated NPs. The anti-CD41-NP

conjugates prepared with NPs of reported functionalization durations were incubated with platelet-adsorbed microtitre plate wells and characterized for their conjugation efficiency as a function of the fluorescence intensity (of the conjugated dye NIR664) at 694nm upon excitation at 660nm.

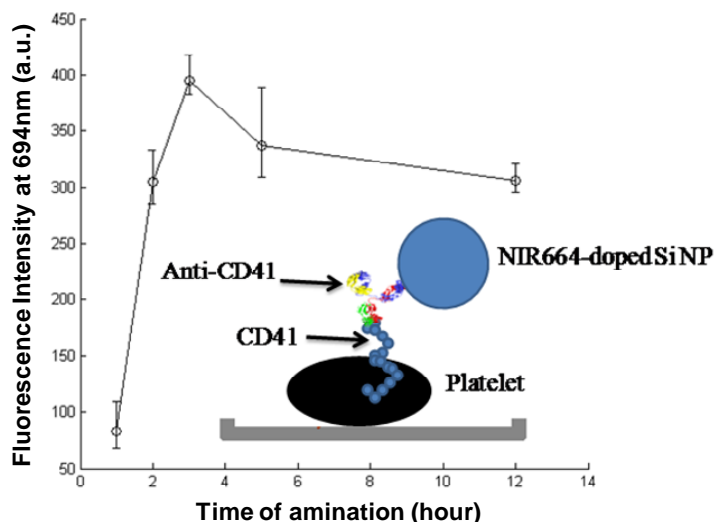


**Figure 5.5** A plot of NP fluorescence at 694nm (excited at 660nm) versus amine-silanization time is shown for a plate based direct binding assay that reports the binding between surface attached IgG and anti-IgG conjugated with the aminated NP.

The dependence of antibody binding on the ordering of the amine layer deposited on NP is depicted in **Figure 5.5** shows. The plot of fluorescence intensity vs. time of amine-silanization for the NPs shows an increase of the intensity up to 3 h reaction time followed by a steady decrease for longer times. Therefore the maximum antibody attachment occurred on the NPs having the 3 h amine-silanization. This shows the importance of monolayer of functional groups on a nanosurface for biomolecular conjugation.

For the 5 and 12 h amine-silanization sample, the multiple layering of cross linked APTES poses a marked inhibition for antibody attachment compared to the 3 h data. Firstly, during the longer time of amine-silanization reaction it is likely that the primary amine group of the

nanosurface bound APTES molecule can interact with the hydroxyl group of unbound APTES molecule via hydrogen bonding. Furthermore, the reverse interaction, i.e. hydrogen bond formation between the hydroxyl group of the surface bound APTES molecule and the primary amine group of a nearby unbound APTES molecule can significantly limit the number of free primary amine groups in spite of the longer extent of APTES exposure. In addition to that, the steric hindrance posed by the bulky amine layer composed of a cross-linking-driven mesh structure is likely to restrict the antibody attachment.

The optimum antibody-NP conjugate that was obtained from various characterization strategies performed was also characterized by visualizing under SEM (**Figure 5.6**) and confocal microscopy (**Figure 5.6 d, e**) for its specificity of labelling, distribution across the platelet and imaging performance. The data obtained indicate a highly non-homogeneous distribution of the conjugates across the platelet surface particularly along the periphery where the distribution of CD41 is reported to be dense. However, the agglomeration was found prominent in few instances, suggesting a poly-dispersed conjugate population. Further work is under investigation in order to obtain better poly-dispersity. On the contrary, conjugates were found highly specific to platelets as indicated in the confocal micrographs (**Figure 5.6 d, e**).

## **5.6 Conclusion**

This work has successfully demonstrated the optimization of functionalization of Si NP and, most importantly, the use of FL and FCS to monitor the surface modification process of silica NPs in conjunction with conventional techniques like zeta potentiometry and FTIR spectroscopy. An optimum reaction time of 3 h was found suitable to functionalize Si NP with APTES. This could be a generic regimen for all types of silane, as the underlying chemistry of silanization will remain the same. However, other contributing factors such as

the chemistry involved with functional groups of silanes like amine, thiol or carboxy may have some impact. Further experimentation is required to solve the surface-associated agglomeration of conjugates in order to improve dispersion of these NP conjugates in solution.

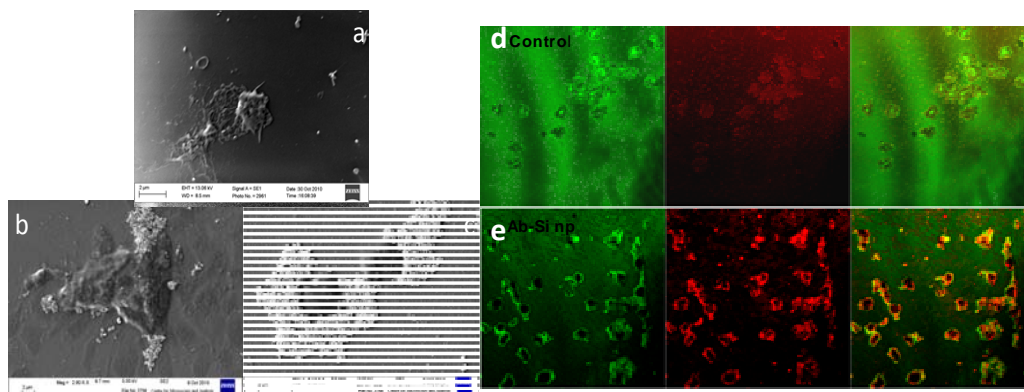


**Figure 5.6** Scanning electron micrographs illustrating (a) a platelet; (b) and (c) the interaction of anti-CD41-NP conjugates of the same stock with the platelet. The strong agglomeration tendency as depicted in ‘c’ micrographs indicates that further optimization of the conjugates is required to improve the solubility and dispersion in optimized PBS strength and pH. (d, e) A confocal micrograph of platelet imaging tendency of the NP- anti-CD41 antibody conjugates. Horizontally, upper panel depicts the control NPs conjugated to mouse IgG that is not targeted for CD41, whereas, the lower panel illustrates the anti-CD41-conjugated NPs, which are specifically labeling the platelet. Vertically, left, central and right panels correspond to imaging in the red and green component channels in order to abnegate the auto-fluorescence of platelets.

## 5.7 References

1. Wang L, Tan W: Multicolor FRET Silica nanoparticles by single wavelength excitation. *Nano Lett* 2006, 6(1):84-88.

2. Hun X, Zhang Z: Fluoroimmunoassay for tumor necrosis factor-[alpha] in human serum using Ru(bpy)<sub>3</sub>Cl<sub>2</sub>-doped fluorescent silica nanoparticles as labels. *Talanta* 2007, 73(2):366-371.
3. Bakalova R, Zhelev Z, Aoki I, Masamoto K, Mileva M, Obata T, Higuchi M, Gadjeva V, Kanno I: Multimodal silica-shelled quantum dots: Direct intracellular delivery, photosensitization, toxic, and microcirculation effects. *Bioconjug Chem* 2008, 19(6):1135-1142.
4. Nakamura M, Shono M, Ishimura K: Synthesis, characterization, and biological applications of multifluorescent silica nanoparticles. *Anal Chem* 2007, 79(17):6507-6514.
5. Wu H, Huo Q, Varnum S, Wang J, Liu G, Nie Z, Liu J, Lin Y: Dye-doped silica nanoparticle labels/protein microarray for detection of protein biomarkers. *Analyst* 2008, 133(11):1550-1555.
6. West W, Pearce S: The dimeric state of cyanine dyes. *J Phys Chem* 1965, 69(6):1894-1903.
7. Giaume D, Poggi M, Casanova D, Mialon G, Lahlil K, Alexandrou A, Gacoin T, Boilot J: Organic functionalization of luminescent oxide nanoparticles toward their application as biological probes. *Langmuir* 2008, 24(19):11018-11026.
8. Pei X, Zhao Y, Zhao X, Xu H, Chen B, Gu Z: Multiplex Chemiluminescent immunoassay based on silica colloidal crystal beads. *J Nanosci Nanotechnol* 2009, 9(11):6320-6325.
9. Wang Y, Liu B: Conjugated polymer as a signal amplifier for novel silica nanoparticle-based fluoroimmunoassay. *Biosens Bioelectron* 2009, 24(11):3293.

10. Shen G, Anand MFG, Levicky R: X-ray photoelectron spectroscopy and infrared spectroscopy study of maleimide-activated supports for immobilization of oligodeoxyribonucleotides. *Nucleic Acids Res* 2004, 32(20):5973-5980.
11. Kommareddy S, Amiji M: Preparation and evaluation of thiol-modified gelatin nanoparticles for intracellular dna delivery in response to glutathione. *Bioconjug Chem* 2005, 16(6):1423-1432.
12. Vejayakumaran P, Rahman IA, Sipaut CS, Ismail J, Chee CK: Structural and thermal characterizations of silica nanoparticles grafted with pendant maleimide and epoxide groups. *J Colloid Interf Sci* 2008, 328(1):81-91.
13. Gao F, Luo F, Yin J, Wang L: Preparation of aminated core-shell fluorescent nanoparticles and their application to the synchronous fluorescence determination of  $\hat{\text{I}}^3$ -globulin. *Luminescence* 2008, 23(6):392-396.
14. Miksa D, Irish ER, Chen D, Composto RJ, Eckmann DM: Dextran Functionalized surfaces via reductive amination: morphology, wetting, and adhesion. *Biomacromolecules* 2006, 7(2):557-564.
15. Lee MH, Brass DA, Morris R, Composto RJ, Ducheyne P: The effect of non-specific interactions on cellular adhesion using model surfaces. *Biomaterials* 2005, 26(14):1721-1730.
16. Wang Y, Yuan K, Li Q, Wang L, Gu S, Pei X: Preparation and characterization of poly(N-isopropylacrylamide) films on a modified glass surface via surface initiated redox polymerization. *Mater Lett* 2005, 59(14-15):1736-1740.

17. Flink S, van Veggel FCJM, Reinhoudt DN: Functionalization of self-assembled monolayers on glass and oxidized silicon wafers by surface reactions. *J Phys Organ Chem* 2001, 14(7):407-415.
18. Chiang C, Ishida H, Koenig JL: The structure of [gamma]-aminopropyltriethoxysilane on glass surfaces. *J Colloid Interf Sci* 1980, 74(2):396-404.
19. Pena-Alonso R, Rubio F, Rubio J, Oteo J: Study of the hydrolysis and condensation of  $\gamma$ -Aminopropyltriethoxysilane by FT-IR spectroscopy. *J Mater Sci* 2007, 42(2):595-603.
20. Roy S, Dixit CK, Woolley R, MacCraith BD, O'Kennedy R, McDonagh C: Novel multiparametric approach to elucidate the surface amine-silanization reaction profile on fluorescent silica nanoparticles. *Langmuir* 2010, 26(23):18125-18134.
21. Roy S, Woolley R, MacCraith BD, McDonagh C: Fluorescence lifetime analysis and fluorescence correlation spectroscopy elucidate the internal architecture of fluorescent silica nanoparticles. *Langmuir* 2010, 26(17):13741-13746.
22. Dixit CK, Vashist SK, O'Neill FT, O'Reilly B, MacCraith BD, O'Kennedy R: Development of a high sensitivity rapid sandwich elisa procedure and its comparison with the conventional approach. *Anal Chem* 2010, 82(16):7049-7052.

## **Chapter 6**

Analysis and reduction of process-induced  
aggregation of NIR-664 dye-doped silica  
nanoparticles

## 6.1 Abstract

NIR664 dye-doped silica nanoparticles (Si NP) were intended to be employed for probing platelets under various physiological conditions. However, aggregation was observed in aminopropyltriethoxy silane (APTES)-functionalized NPs after optimization of silanization conditions as described in **Chapter 5**. Therefore, aggregation susceptibility as a function of zeta potential was studied for unfunctionalized, amine and carboxy-functionalized NPs under various physico-chemical conditions such as nature of the solvent, ionic strength of the dispersion medium and pH. In addition, impact of antibody cross-linking with the functionalized NPs was also analysed. A consistent relation was obtained for salt strength and pH of the solvent. However, zeta potential of the antibody-cross-linked NPs was highly variable without any chemical or physical surface blocking. Conversely, no significant improvement could be registered even after chemical blocking with ethylenediamine (EDA) followed by physical blocking with BSA.

## 6.2 Introduction

Nanoparticles (NPs) in the form of homogenous solutions have numerous applications in the field of biomedical diagnostics and therapeutics [1-3]. However, the tendency of nanoparticles to aggregate has imposed restrictions to their applications in solvent [2, 4]. This aggregation is governed by multiple factors and most critical are the chemical and physical nature of these NPs. In a given system the stability of bare (unfunctionalized) NPs is predicted as a function of overall charge (**Figure 6.1**), which is an inherent property of the nanoparticle, such that the higher the charge the more stable and dispersed will be the system [5].

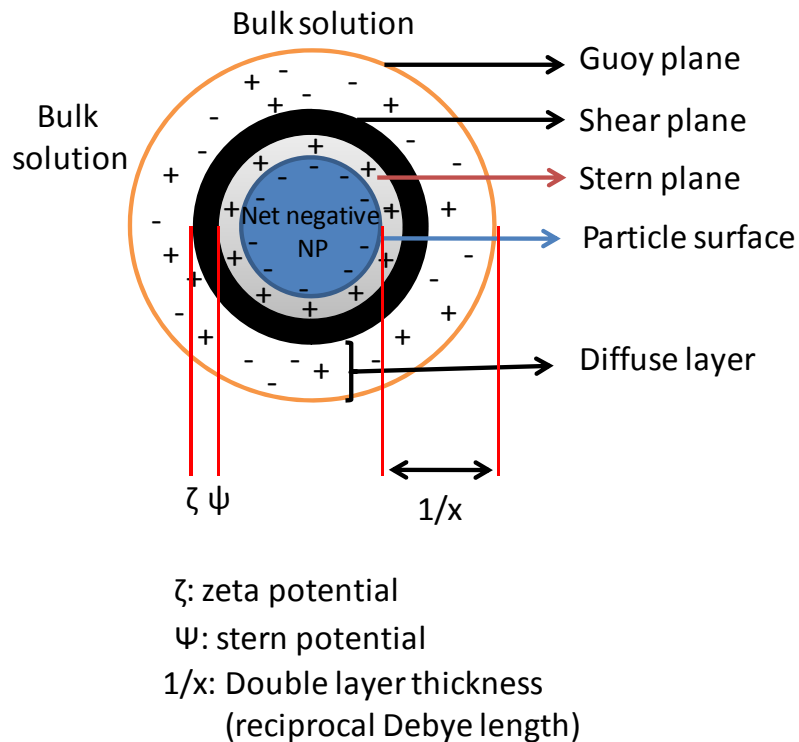


**Figure 6.1** Representation of charge distribution along various planes surrounding the NP and origin of zeta potential. Adapted from Somasundaram et al. (2009) [5].

The chemistry and surface properties of nanoparticles are affected by the surrounding chemical environment. Therefore, the overall charge-based stability might be compromised resulting in NP aggregation. Many novel surface modification strategies have been developed that claimed to minimize the aggregation behavior of NPs [4, 6-9]. Conversely, there are various interactions that prevail in the functionalized nanoparticles. Examples of such interactions could be inter-nanoparticle hydrogen bonding, hydrophobicity of the nanoparticle core, bipolar interface (shear plane; **Figure 6.1**) and others [10]. We speculate that the nanoparticle functionalization also introduces multivalency to the existing interactions by replicating the total number of reactive chemical species on the surface of nanoparticles. This aggregation model becomes more complicated when proteins are captured on the functionalized nanoparticles by chemical methods. A native antibody (model protein), which is not chemically modified, has multiple amine and carboxyl groups on its surface. Therefore, an antibody activated for either of these functional groups will have multiple activated sites, which increases the possibility of an antibody interacting with multiple nanoparticles. This could result in large aggregates of antibody-nanoparticle conjugates. In addition, this aggregation pattern will be more complicated if the activated antibodies react with other such antibodies prior to reacting with the functionalized nanoparticles in a multiple-nanoparticle binding behavior [10].

This study attempts to develop a better understanding of the aggregation behavior of the NIR664 dye-doped silica nanoparticles having an average size of  $95 \pm 5$  nm with the final aim of using these nanoparticles for probing platelet surface markers [11]. Bare and functionalized (carboxy and amine) nanoparticles were subjected to different physical environments i.e. pH and ionic strengths of phosphate buffer. The effect of antibody

crosslinking with the amine and carboxy-functionalized nanoparticles was also analyzed along with assessing the effect of physical and chemical surface blocking of the antibody conjugated nanoparticles. Further, an attempt was also made to reduce the heterogeneity in the size distribution of antibody-nanoparticle conjugates by gradual centrifugation. A method was attempted for separating out the aggregates from other antibody-conjugated nanoparticles as a function of centrifugal force and time.

### **6.3 Materials**

NIR664 (1.6 mg), 1-hexanol (99%), Mercaptopropyltri-ethoxy silane (MPTES), Triton X-100, cyclohexane, hexanol, tetraethoxy silane, ammonium hydroxide (NH<sub>4</sub>OH), absolute ethanol (EtOH), aminopropyltriethoxy silane (APTES) and anti-CD41 antibody were procured from Sigma Aldrich, Blessington, Co. Wicklow, Ireland. PBS (sachet), 1-ethyl-3-[3-dimethylaminopropyl]carbodiimide hydrochloride (EDC), N-hydroxysulfosuccinimide (SNHS) and bovine serum albumin (BSA) were obtained from Thermo Fisher Ireland.

### **6.4 Methods**

#### **6.4.1 Defining aggregation tendency in terms of zeta potential**

There is no direct measurement of nanoparticle aggregation. However, by measuring the surface charge properties and the nature of surface functional groups, the stability of the nanoparticle core could be predicted. This is a highly probabilistic approach that could have strong variability associated with it.

Therefore, zeta potential was employed as an indicative marker for the stability of the NPs. Zeta potential is the interfacial voltage or difference in the electrical potential of the solvent medium in bulk phase (dispersion media) that is interacting/ attached to the surface of

dispersed NPs. This is an absolute property associated with a given colloidal system. NP stability, on the basis of zeta potential, is defined as in **Table 6.1** [12].

**Table 6.1** Stability characteristics of colloidal particles as a function of zeta potential

<b>Zeta potential (mv)</b>	<b>Stability characteristics</b>
<b>± 10</b>	Highly instable (rapid aggregation)
<b>± 10-30</b>	Instable (slow flocculation)
<b>± 30-40</b>	Moderate stability (high solvent dependence)
<b>± 40-60</b>	Stable
<b>Above ± 60</b>	Highly stable

#### **6.4.2 Nanoparticle functionalization**

Prior to functionalization, NIR664 dye-doped silica nanoparticles were centrifuged and dried under a stream of nitrogen to evaporate any traces of solvent (ethanol). Afterwards, nanoparticles were weighted and a concentration of 20 mg/mL was prepared in the desired solvent as will be described. The optimization of silane-mediated functionalization of NIR664 dye-doped silica nanoparticles has already been reported from this laboratory [11].

##### **6.4.2.1 Functionalization with amino-silane**

NPs were functionalized according to the protocol described (Chapter 5, section 5.4.2, page 150). NPs, at a concentration described previously, were incubated in a solution of 3-aminopropyltriethoxy silane (APTES) (2% (v/v) in 90% (v/v) ethanol with deionized water) for 3 h. The functionalized NPs were washed five times with ethanol by repeated centrifugation. Functionalized nanoparticles obtained after the last wash were stored in ethanol for further analysis.

##### **6.4.2.2 Functionalization with carboxy-silane**

Nanoparticle stock was dissolved in deionized water because of the insolubility of carboxy silane in ethanol. Similar to amine functionalization, the dispersed nanoparticles were

incubated with carboxyl silane (2% (v/v)) for a period of three hours. These nanoparticles were also processed accordingly and were stored in ethanol.

### **6.4.3 Storage stability**

#### **6.4.3.1 Effect of solvent**

Bare, amine and carboxy-functionalized NPs were incubated in DIW and ethanol along with three different saline strengths of PBS (*viz.* 1, 10 and 100mM), pH 7.2. These solvents were selected on the basis of their use in the preparatory phases of the NPs and antibody-NP adducts.

#### **6.4.3.2 Effect of NP incubation at different pHs**

In order to study the effect of pH, bare and functionalized (amino and carboxy) NPs were incubated in DIW at pH 4, 7 and 10. The zeta potential was recorded after 24h of sample incubation.

#### **6.4.3.3 Effect of antibody cross-linking strategy and surface blocking methods**

In order to assess the effect of antibody immobilization strategy and surface blocking method of the antibody-conjugated NPs on their storage stability, two different schemes namely carboxy silane and amine silane-based functionalization, were performed (**Figure 6.2**). Functionalized NPs were subjected to antibody conjugation.

##### **6.4.3.3.1 Amine surface blocking strategy for antibody-cross-linked-amine-functionalized NP adducts**

Three different surface blocking strategies were employed for this study. Those were (i) physical blocking of surface with 1% (w/v) BSA in 1mM PBS, pH 7.2, (ii) chemical blocking of EDC-activated anti-CD41 antibody with ethylenediamine (EDA), and (iii) chemical blocking with EDA followed by surface blocking with BSA. The anti-CD41

antibody (900  $\mu$ L of 15  $\mu$ g/mL diluted in optimized buffer strength of PBS (pH 7.2) was incubated with a 100  $\mu$ L pre-mixed solution of EDC (4 mg/mL) and SNHS (11 mg/mL) for 15 min at 37  $^{\circ}$ C. The resulting EDC-activated antibody solution was added to the APTES-functionalized NPs (15 mg/mL), suspended in optimized buffer strength of PBS (pH 7.2) and incubated for 1 h at RT with continuous mild stirring. This antibody-conjugated NP solution was then washed five times with optimized buffer strength of PBS, pH 7.2, by repeated centrifugation (750 X g). Afterwards, the antibody-NP adduct was dispersed in optimized buffer strength of PBS, pH 7.2.

The prepared solution of antibody-conjugated NP was then incubated with 1% (w/v) BSA in PBS for 2h with continuous mild stirring. This solution was then washed as described and stored for further study. However, for chemical blocking experiments, after allowing cross-linking of EDC-activated antibody with NPs for 10 min, 10  $\mu$ L of EDA diluted in four different molar concentrations (*viz.* 50, 10, 0.1 and 0mM) was added to the reaction mixture. This reaction solution was allowed to further cross-link for 1h with continuous mild stirring followed by washing (centrifugation at 750 X g). A fraction of EDA-blocked solution was stored for further analysis; whereas, the other fraction was incubated with 1% (w/v) BSA as per the description.

#### **6.4.3.3.2 Carboxy surface blocking strategy for antibody-cross-linked-carboxy-functionalized NP adducts**

Similarly, all the three described surface blocking strategies were also employed for carboxy-functionalized NPs. Those were physical blocking of surface with 1% (w/v) BSA in optimized buffer strength of PBS, pH 7.2, chemical blocking of EDC-activated carboxy-NPs with ethylenediamine (EDA), and chemical blocking with EDA followed by surface

blocking with BSA. The carboxy groups on the functionalized NPs (1.8 mL of 15 mg/mL) were activated by incubating with 200  $\mu$ L EDC (4 mg/mL) and SNHS (11 mg/mL) for 15 min at RT with continuous mild stirring. The EDC-activated nanoparticles were centrifuged at 750 X g for 15 min in order to remove any unreacted excess EDC. These EDC-activated NPs were reconstituted in optimized buffer strength of PBS, pH 7.4 and anti-CD41 antibody (900  $\mu$ L of 15  $\mu$ g/mL) was added to it and incubated for 1 h at RT with continuous mild stirring. This antibody-conjugated NP solution was then washed with PBS (optimized buffer strength), pH 7.2, for five times by repeated centrifugation (750 X g). Afterwards, the antibody-NP adduct was dispersed in optimized buffer strength of PBS, pH 7.2.

The prepared solution of antibody-conjugated NP was then incubated with 1% (w/v) BSA in PBS for 2h with continuous mild stirring. This solution was then washed as described and stored for further study. However, for chemical blocking experiments, after allowing cross-linking of EDC-activated NPs with antibody for 10 min, 10  $\mu$ L of EDA diluted in four different molar concentrations (*viz.* 50, 10, 0.1 and 0mM) was added to the reaction mixture. This reaction solution was allowed to further cross-link for 1h with continuous mild stirring followed by washing (centrifugation at 750 X g). A fraction of EDA-blocked solution was stored for further analysis; whereas, the other fraction was incubated with 1% (w/v) BSA as per the description.

#### **6.4.4 Characterization of NP stability using Surface charge (zeta potential) measurement**

Zeta potential for the aminated samples was measured by a Beckman Coulter Instrument by using the flow cell. The averages obtained from three measurement sets were analyzed by the DelsaNano software in the result section where each measurement was the average of 50

individual measurements performed at various positions (10 measurements each in 5 positions) in the flow cell that is set as default.

## **6.5 Results and Discussion**

Stability of a colloidal system is described according to the DLVO theory [5]. According to this theory the stability of a colloidal system is dependent on the extent of attractive van der Waals and repulsive electrical double layer forces. These two forces predominantly govern the intermolecular interactions of NPs in Brownian motion. Therefore, the higher the double layer forces the better will be the dispersion of NPs in the colloid. Unfunctionalized Si NPs have a net negative charge of -35 to -60 mV, which indicates that strong repulsive double layer forces are significantly higher in comparison to the van der Waals interaction. Therefore, the unfunctionalized NPs are highly stable. In addition, size of the NPs is also a critical parameter in governing their stability. NPs having a smaller size have lower surface area to charge ratio, which indicates that high amount of charge is distributed over a smaller double-layer, indicating better dispersion and stability. NPs employed in this study are moderately sized (~ 95 nm) and therefore these have a moderate stability as also indicated by their zeta potential (~ -35 mV). However, after functionalizing a NP with carboxy or amine groups, the surface charge distribution is significantly changed. This causes a disruption of the pre-existing double layer forces. In this study, the effects of various factors that NPs are exposed to, during various preparatory phases, are assessed to determine their stability as a function of their respective zeta potentials.

### **6.5.1 Effect of solvent**

The nature of a solvent governs the strength of double layer forces at the interface of solvent and NP [13-15]. The zeta potential obtained for NPs incubated in DIW, ethanol and three

saline strengths of PBS, pH 7.2 is shown in **Figure 6.2**. The zeta potential obtained for unfunctionalized NPs suspended in DIW and ethanol was not significantly different; whereas, a significant shift toward positive scale was obtained for all the samples incubated in PBS, regardless of the salt concentration. The rationale to this significant increase in the zeta potential of the Si NP samples in PBS may be the disruption of the double layer at the interface due to the presence of additional salt-induced charges [16].

Following the concept of planes (i.e. shear and stern planes) in the measurements of zeta potential, the charge density around the NP changes the inter-molecular distance. An exponential decrease in the charge away from the shear plane is the critical parameter which is important in the NP stability, where the shear plane is the NP environment around it which interacts with the solvent. Debye double layer thickness (an inverse of the exponential charge decrease) is the space that holds the 'shear' plane. It is a function of available salt concentration/ ion strength of the given solution, such that with increasing salt concentration the double layer thickness decreases until the double layer repulsive forces are overcome by van der Waals attractive forces, resulting in aggregation (salting out effect) [17]. To this effect, a positive shift in zeta at increasing salt concentrations of PBS could also be justified. In addition to the double layer interaction behavior of the bare NPs, stability of the functionalized NPs is governed by the nature of the surface functional groups, as evident from the results obtained for amine and carboxy-functionalized NPs (**Figure 6.2**). A decrease in the zeta was registered for amine-functionalized NPs suspended in the solvents in the order of DIW, ethanol, PBS 1mM, PBS 10mM and PBS 100mM. However, the decrease was insignificant for DIW and ethanol dispersed NPs, where ethanol (polarity index: 5.2) is less polar than water (polarity index: 9) [18]. Functionalization of highly

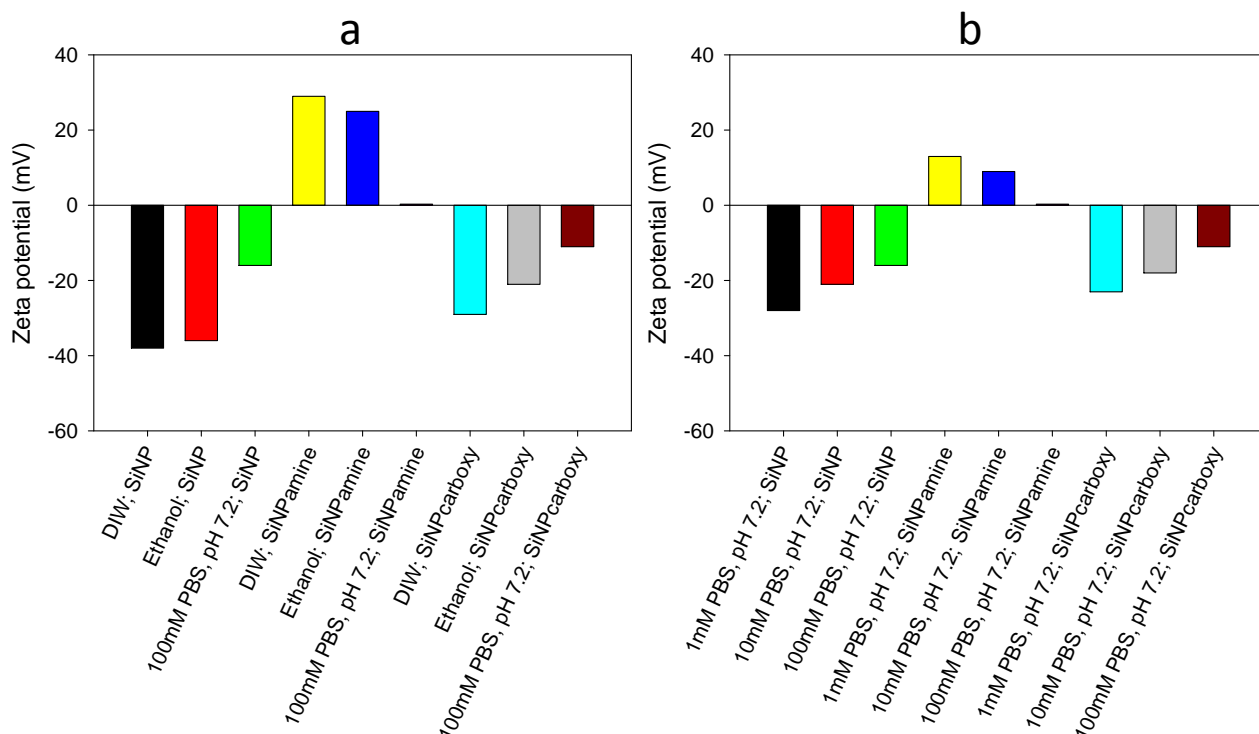


**Figure 6.2** Zeta potential of unfunctionalized, and carboxy and amine functionalized NPs as a function of nature of (a) solvent and (b) ionic strength of phosphate buffered saline. There was no significant effect on zeta potentials of NPs in DIW (polarity index: 9) and ethanol (polarity index: 5.2); whereas considerable decrease in zeta was registered for samples incubated in PBS. Zeta potential was found to have an inverse relation with the ionic strength of the dispersion media. DIW is de-ionized water; SiNP is silica nanoparticle followed the nature of functionalization as suffix. Amine and carboxy represents the respective functional groups on SiNP.

negative Si NPs with amino silane induces two basic changes in the composition of the NP. These are, decreasing the net negative charge of the NP core by engaging most of its pendant 'OH' groups and increasing its size by 5.6Å (for a monolayer). This results in a decreased 'stern' capacity of functionalized NPs where, 'stern' capacity is the amount of charge that can be adsorbed on the negative NP core, which migrates with the particle in the solvent. In addition, the possible role of hydrogen bonding between the hydrogen of amines

and oxygen of the unreacted hydroxyl groups of NPs could not be excluded in aggregation. Therefore, theoretically, the amine-functionalized NP should be unstable. The results obtained with zeta potential suggested the same for amine-functionalized NPs and flocculation could be observed even at a zeta of +29 mV. In addition, it is possible that functionalized NPs are actually a mixture of functionalized, partially and completely unfunctionalized NPs. Therefore, it may be speculated that this mixed colloid, which possesses all the abilities to induce aggregation, might be the plausible reason of NP instability.

Conversely, a shift in zeta potential further towards the negative scale for the carboxy functionalized NPs dispersed in DIW, ethanol and PBS (1mM ionic strength) was obtained. However, this negative shift was insignificant. The most negative zeta obtained with PBS, pH 7.2 might be the effect of pH (**Figure 6.3**), which is more basic than DIW and ethanol. However, the effect of salt concentration on carboxy-functionalized NPs was similar to the PBS dispersed amine-NPs.

Also, 1mM PBS, pH 7.2 was found to be a suitable replacement as a dispersion medium for DIW and ethanol for antibody conjugation and storage.

### **6.5.2 Effect of pH**

The zeta potential values of bare Si NP (pI 5.8) samples incubated in DIW at different pH, i.e. 5, 7 and 10, suggest that negative charge on the unfunctionalized NPs in solution was increasing with the increasing pH (**Figure 6.3**).

The rationale for this behaviour could be that with stronger alkaline dispersion medium the number of hydroxyl groups in the solution and on the surface might increase [19, 20]. These findings are consistent with the reports claiming to study the effect of various pH on the bare

Si NPs [21, 22]. In addition these results suggest that there is an inverse relation between the charge on NPs and pH of the dispersion medium. However, aminated NP samples with a net ‘+’ charge were found to be moderately stable (slow flocculation zone) at an acidic pH.

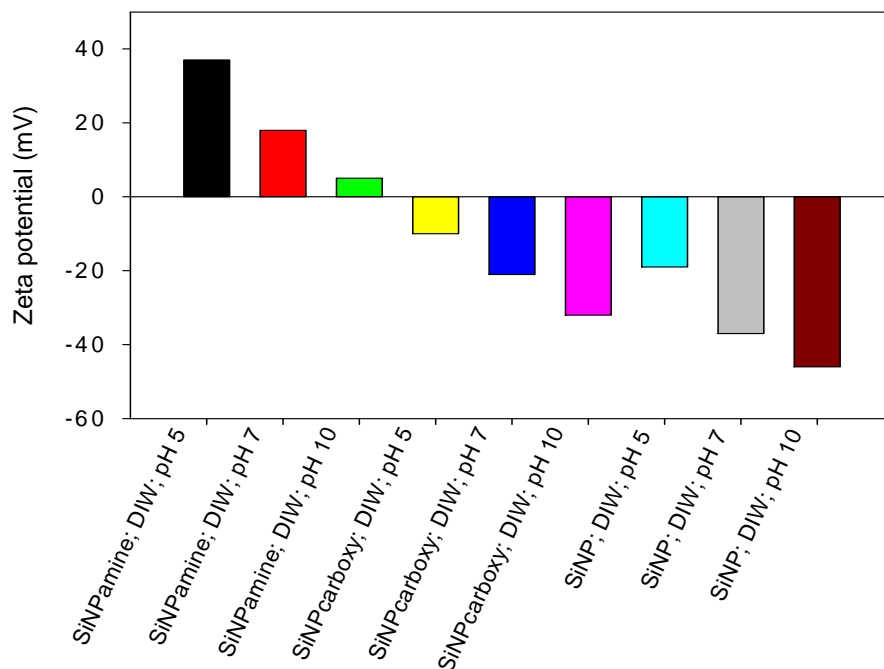


**Figure 6.3** Zeta potential of unfunctionalized, carboxy and amine functionalized NPs as a function of pH. There was a significant decrease/ negative shift in zeta for unfunctionalized NPs (SiNPunf) along with the increase in the alkalinity of the dispersion media. Similarly, carboxy and amine-functionalized NPs followed the decreasing trend with increasing alkalinity of the medium. Zeta potential was found to have an inverse relation with the alkali strength in the dispersion media. DIW is de-ionized water; SiNP is silica nanoparticle followed the nature of functionalization as suffix; amine and carboxy represents the respective functional groups on SiNP.

The zeta potential of aminated NPs decreases with increasing alkalinity of the solvent. The rationale is that the number of hydroxyl ions is significantly higher which could efficiently disrupt the orderly arrangement of ‘+’ surface charge. Conversely, when pH decreases, the

number of charged amine species will be higher in accordance of their respective pI values resulting in an ordered inter-particle repulsion that might contribute to the stability of aminated Si NPs under acidic conditions. Similarly, the net charge on the carboxy-functionalized NPs was also found to decrease more toward the basic pH. It could be simply explained as a function of number of hydroxyl groups present in the solvent. With increasing alkalinity, the number of hydroxyl groups significantly increases. This results in increased ionization of carboxy groups to carboxyl ions. This ionization increases the total negative charge inducing an ordered distribution of negative charge in the system, increasing the repulsive forces and overall stability of the system. However, there are reports that claim the possibility of the self-assembly of carboxy and amine silane-functionalized NPs due to intermolecular interactions of various carboxyl and amine groups [23, 24] implying that even at moderate zeta potentials these NPs are susceptible to flocculation.

### **6.5.3 Effect of antibody crosslinking**

It was hypothesized that a typical IgG antibody possessing multiple carboxy (approx. 37) and amine groups (approx. 80) (Entrez protein seq: AAA02914) could react with multiple antibodies and multiple NPs (**Section 6.2**) in an uncontrolled manner that could result in big aggregates of (antibody)<sub>n</sub>-(NP)<sub>n</sub>. Therefore, apart from non-covalent interaction-induced flocculation, the biggest challenge toward generating well dispersed antibody-NP adducts is to perform the covalent reaction in a controlled manner in order to minimize multimerization of the single NP and antibodies (individual) covalently bound to its surface. Several chemical and physical blocking experiments were performed. Chemical blocking was based upon blocking of EDC-activated carboxy groups on either antibody or NPs with

ethylenediamine (EDA). The activated carboxy groups were blocked with different molar concentrations of EDA with or without subsequent BSA blocking (physical).

The results obtained (**Figure 6.4**) showed that there was no EDA concentration dependence in either amine or carboxy functionalized NPs.

In the case of amine functionalized NPs, there was a decrease in the zeta potential (shift towards negative axis) for all the antibody-conjugated samples with EDA-based blocking with or without BSA. A plausible reason for this decrease could be the addition of protein (antibody) that might change the slipping plane of the NPs. In addition, the interaction of antibody with the NPs in the solution, which is a mixture of functionalized and unfunctionalized NPs, could have decreased the overall surface charge as their respective zeta potentials were found to be in the instability zone of the negative axis [8]. However, the decrease in zeta potential was comparatively more in the case of blocking with EDA in conjunction with BSA, which is an amine-rich globular protein. There could only be one plausible explanation for this increase in the negative charge with BSA-blocking. Each molecule of BSA has 89 primary free amines and 98 free carboxyl groups [25]. Considering that NPs are positively charged, if BSA blocks the surface with hydrophobic, ionic and van der Waals interactions then there will be a decrease in overall negative charge due to the reduction in the number of free carboxyl groups on BSA. However, as evident from **Figure 6.4**, the overall negative charge has increased following the BSA-blocking. Therefore, it may be proposed that the BSA coating on the surface might be as a result of non-ionic and non-covalent interactions, as a result of which there is significantly high number of free carboxyl groups of BSA on the surface resulting in an overall negative charge [8, 26].

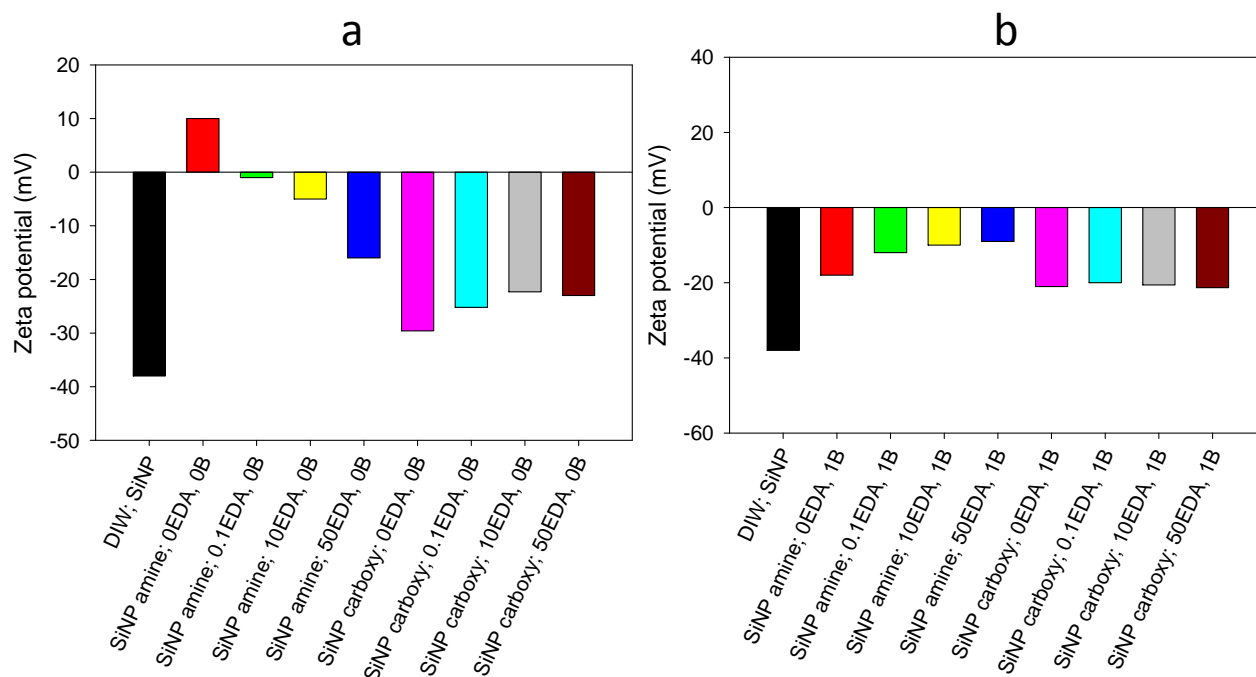


**Figure 6.4** Effect of antibody cross-linking and surface blocking strategies on their respective zeta potentials. Zeta potential registered for (a) EDA-based blocking of the EDC-activated carboxy groups, and (b) EDA-based blocking in tandem with physical blocking of the surface with BSA. There was no correlation between antibody conjugation strategies and their respective zeta potentials. EDA is ethylenediamine and B is BSA. The prefix with EDA and BSA represents their molar and weight percent concentrations, respectively. SiNP followed by suffix amine and carboxy represents silica NPs with respective functionalization.

It was proposed prior to the experiments that addition of EDA should reduce the aggregation induced by uncontrolled cross-linking. However, for carboxyl NPs the ‘charge reversal’ due to the blocking of carboxyl groups (negative) with EDA (positive) increased the zeta potential towards the positive axis. This positive shift of zeta was not significant enough to induce a stable positive charge. Moreover, this increase in zeta resulted in decreasing the stability of carboxy NPs. The anomalous charge imparting behaviour obtained for BSA-based blocking of amine-functionalized NPs was also observed for carboxy NPs. BSA-based

blocking of the surface was found to impart a positive shift in zeta unlike in amine NPs where a negative shift was obtained.

A visible flocculation in all the antibody conjugates was observed. It is important to mention here is that the aggregation behaviour of protein-conjugated NPs is very complex and it is a challenging task to design a model for analysing the nature of aggregation and forces that are playing crucial role in aggregation. There are many variables in antibody-NP conjugates that increase the possibilities of aggregation in these samples (**Figure 6.5**). Considering EDA and BSA blocking as an efficient method for minimizing aggregation due to covalent cross-linking of many antibody-NPs complexes, the potential participants in these aggregation events could be non-covalent interaction of proteins with other proteins or functional groups of NPs and vice versa. In addition, EDA, which is a homobifunctional blocker, could bind to two antibodies or NPs at the same time, one from each of its ends. This EDA-mediated cross-linking of antibodies and NPs with each other could result in a big complex of antibody-NP conjugates. However, EDA is a small molecule and steric hindrance created by the charge at the interphase and NP size could interfere with EDA-mediated cross-linking. Conversely, it is also important to mention that EDA is a prominent chelating agent and a precursor to polymers such as dendrimer polyamidoamine (PAMAM). Therefore, its potential role in crosslinking-mediated NP aggregation might not be neglected and further studies are required to understand the behaviour obtained with EDA and BSA-based surface blocking. In addition, the role of various colloid dispersants should also be studied.

## 6.6 Conclusions

A stability profile of the functionalized and unfunctionalized Si NPs employed for designing platelet diagnostics was generated as a function of dispersion media (solvent), salt

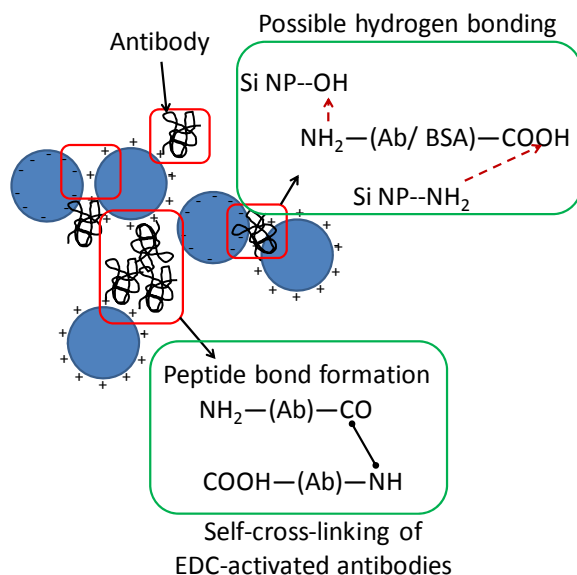


**Figure 6.5** A hypothetical model depicting various possible interactions that may have crucial role in nanoparticle aggregation. However, their individual roles in aggregation are not known. The main type of interactions that were speculated to play some role are (i) ionic and hydrophobic interactions along with hydrogen bonding between functional groups of an antibody (conjugated to a nanoparticle) with other nanoparticle; (ii) binding of nanoparticles to self-cross-linked antibodies (many antibodies cross-linked during the process of EDC activation); and, (iii) interaction of functionalized and bare nanoparticles with each other. The positively charged nanoparticles are amine functionalized; whereas, negatively charged nanoparticles are bare or partially functionalized.

concentration and pH of the solvent. A correlation was obtained between zeta potential-ionic strength and zeta potential-pH, as expected. However, for the stability profiling of these NPs after antibody conjugation and surface blocking with EDA and BSA, a clear relationship could not be established between zeta and conjugation strategies employed. This could imply to the complex nature of aggregation and involvement of various type of ionic, non-

ionic-non-covalent and covalent interactions in the underlying mechanisms of aggregate formation. And, it is a scientific challenge to model such a complex physical process. The choice of chemical blocker was also critical. EDA is reactive from both of its terminals and possibility of its reaction to two NPs from its each end may not be overlooked. Therefore, in further studies ethanolamine has been chosen as a chemical blocker. In addition further complex analysis should be performed in order to obtain a relevant information that could be employed to devise an efficient NP-based platelet diagnostics.

## 6.7 References

1. Schiestel T, Brunner H, Tovar GEM: Controlled surface functionalization of silica nanospheres by covalent conjugation reactions and preparation of high density streptavidin nanoparticles. *J Nanosci Nanotechnol* 2004, 4(5):504-511.
2. Bergman L, Rosenholm J, Ost A, Duchanoy A, Kankaanpaa P, Heino J, Linden M: On the complexity of the electrostatic suspension stabilization of the functionalized silica nanoparticles for biotargeting and imaging applications. *J Nanomater* 2008, Article ID 712514.
3. Kneuer C, Sameti M, Haltner EG, Schiestel T, Schirra H, Schmidt H, Lehr C: Silica nanoparticles modified with aminosilanes as carriers for plasmid DNA. *Int J Pharm* 2000, 196(2):257-261.
4. Bagwe RP, Hilliard LR, Tan W: Surface modification of silica nanoparticles to reduce aggregation and nonspecific binding. *Langmuir* 2006, 22(9):4357-4362.

5. Somasundaran P, Mehta S, Yu X, Krishnakumar S: Colloid systems and interfaces stability of dispersions through polymer and surfactant adsorption. In *Handbook of surface and colloid chemistry* (ed. 3). Ed. by Birdi K. CRC Press, Taylor and Francis Group; Florida, USA: 2009:155-196.
6. Moon JH, Shin JW, Kim SY, Park JW: Formation of uniform aminosilane thin layers: an imine formation to measure relative surface density of the amine group. *Langmuir* 1996, 12(20):4621-4624.
7. Rosenholm JM, Linden M: Wet-chemical analysis of surface concentration of accessible groups on different amino-functionalized mesoporous SBA-15 Silicas. *Chem Mater* 2007, 19(20):5023-5034.
8. Bharti B, Meissner J, Findenegg GH: Aggregation of silica nanoparticles directed by adsorption of lysozyme. *Langmuir* 2011, 27(16):9823-9833.
9. Rosen JE, Gu FX: Surface functionalization of silica nanoparticles with cysteine: a low-fouling zwitterionic surface. *Langmuir* 2011, 27(17):10507-10513.
10. Nel AE, Madler L, Velegol D, Xia T, Hoek EMV, Somasundaran P, Klaessig F, Castranova V, Thompson M: Understanding biophysicochemical interactions at the nano-bio interface. *Nat Mater* 2009, 8(7):543-557.
11. Roy S, Dixit CK, Woolley R, MacCraith BD, O'Kennedy R, McDonagh C: Novel Multiparametric Approach to elucidate the surface amine-silanization reaction profile on fluorescent silica nanoparticles. *Langmuir* 2010, 26(23):18125-18134.

12. Delgado A, Gonzalez-Caballero F, Hunter R, Koopal L, Lyklema L: Measurement and interpretation of electrokinetic phenomenon (IUPAC technical report). *Pure Appl Chem* 2005, 77(10): 1753-1805.
13. Abuin E, Lissi E, Jara P: Effect of the organic solvent on the interfacial micropolarity of aot-water reverse micelles. *J Chilean Chem Soc* 2007, 52:1082-1087.
14. Vorobyov I, Allen TW: The electrostatics of solvent and membrane interfaces and the role of electronic polarizability. *J Chem Phys* 2010, 132(18):185101.
15. Ioanid A, Mircea R, Ciuceanu TM.: Static dielectric electrolyte permittivity in electric double layer. *Digest J Nanomater Biostruc* 2011, 6(3):1427-1434.
16. Matsui J, Yamamoto K, Inokuma N, Orikasa H, Kyotani T, Miyashita T: Fabrication of densely packed multi-walled carbon nanotube ultrathin films using a liquid-liquid interface. *J Mater Chem.* 2007, 17(36):3806-3811.
17. Galindo-Rodriguez S, Allemann E, Fessi H, Doelker E: Physicochemical Parameters associated with nanoparticle formation in the salting-out, emulsification-diffusion, and nanoprecipitation methods. *Pharm Res* 2004, 21(8):1428-1439.
18. Zimmermann Y, El-Sayed M, Prause S, Spange S: The solvent-like nature of silica particles in organic solvents. *Monatshefte fur Chemie/Chemical Monthly* 2001, 132(11):1347-1361.
19. Yu JC, Jiang Z, Liu H, Yu J: Influence of solvation interactions on the zeta potential of titania powders. *J Colloid Interf Sci* 2003, 262(1):97.

20. Carnal F, Stoll S: Adsorption of weak polyelectrolytes on charged nanoparticles. impact of salt valency, pH, and Nanoparticle charge density. Monte Carlo simulations. *J Phys Chem, B* 2011, 115(42):12007-12018.
21. Xiao H, Cezar N: Organo-modified cationic silica nanoparticles/anionic polymer as flocculants. *J Colloid Interf Sci* 2003, 267(2):343.
22. Ma X, Lee N, Oh H, Kim J, Rhee C, Park K, Kim S: Surface modification and characterization of highly dispersed silica nanoparticles by a cationic surfactant. *Colloids Surf Physicochem Eng Aspects* 2010, 358(1-3):172.
23. Mahalingam V, Onclin S, Peter M, Ravoo BJ, Huskens J, Reinhoudt DN: Directed self-assembly of functionalized silica nanoparticles on molecular printboards through multivalent supramolecular interactions. *Langmuir* 2004, 20(26):11756-11762.
24. An Y, Chen M, Xue Q, Liu W: Preparation and self-assembly of carboxylic acid-functionalized silica. *J Colloid Interf Sci* 2007, 311(2):507.
25. Valencia JV, Weldon SC, Quinn D, Kiers GH, DeGroot J, TeKoppele JM, Hughes TE: Advanced glycation end product ligands for the receptor for advanced glycation end products: biochemical characterization and formation kinetics. *Anal Biochem* 2004, 324(1):68.
26. Chibowski E, Szcze A, Houysz L: Changes of zeta potential and particles size of silica caused by DPPC adsorption and enzyme phospholipase A<sub>2</sub> presence. *Adsorption* 2010, 16(4):305-312.

# **Chapter 7**

## Conclusions and future work

## 7.1 Conclusions

A generic strategy was required that could be employed to activate a wide range of solid support materials to increase stability of oxidized surface with a higher degree of homogeneity. Therefore, a surface modification strategy was successfully developed and optimized using potassium hydroxide and oxygen-plasma treatment-based surface activation followed by amino-terminal silane-based functionalization. The developed method can also be performed using silanes with carboxy- or epoxy-functionalities because the basic functionalization chemistry of the silane remains the same irrespective of the terminal functional groups present on it. This creates many practical applications of the surface activation and functionalization strategy described in this thesis such as (a) development of high sensitivity immunoassays on various polymeric and metallic supports as demonstrated in this thesis, and (b) development of customized biosensor surfaces for potential label-free detection along with microarray and microfluidic platforms.

This strategy was employed to modify a range of polymeric surfaces, such as polystyrene, polymethylmethacrylate, cellulose acetate, poly carbonate and polycyclo-olefins. A high sensitivity immunoassay was developed and optimized using HFA as the model antigen system. The sensitivity of this immunoassay was 38 pg/mL, which was eight to ten-fold more sensitive than conventional immunoassays (based on adsorption of the antibody on the surface). The same strategy was later employed to develop several commercially relevant immunoassays for proprietary analytes of Bristol Myers Squibb, Syracuse, NY, USA.

The potential of the developed strategy could be realized as the technology was transferred to Bristol Myers Squibb, and VTT, a leading Finnish research institute. In addition, this strategy

was employed for functionalizing other polymer-based bioanalytical platforms for microarray and fluorescence assay developments with fluorocap.

In the course of this research understanding of several important processes was analyzed and developed. The most important is determination of the loss of analyte during sample preparation, which is often overlooked in routine analysis. Minimizing such losses is an important issue because it could have significant effects on the overall immune/bioassay performance. A model describing the nature of analyte loss was developed, which was very useful in predicting the nature of such losses and calculating their amounts. However, this model has certain limitations and is strictly based upon the model situation examined. Therefore, many additional parameters may have to be considered. Adsorption and loss of conformation of analyte were predominant factors contributing to the loss of analyte. BSA-based pre-treatment of sample tubes was developed to minimize such effects. This pre-treatment step significantly lessens these losses. In addition, the impact of storing temperature was also established as a contributing factor to such losses and it was found that storage at 4 °C reduces these losses. Therefore, it is suggested that sample preparation be performed in pretreated tubes and, when required, they should be stored at 4 °C.

The other major area was the assessment and modelling of the various possibilities of aggregation of silica nanoparticles following chemical functionalization. However, this model has significant limitations as it was strictly based upon the assumption that crosslinking might have a significant role in aggregation of these NPs along with other non-covalent (van der Waals forces) and ionic interactions. Various factors, such as self-interaction of unfunctionalized and functionalized silican nanoparticles, self-conjugation of silica nanoparticles after chemical activation, antibody-antibody interactions in the antibody-conjugated silica nanoparticles, and

the tendency of an antibody to conjugate to many nanoparticles were identified as contributing parameters in silica nanoparticle aggregation. Further studies are ongoing to other contributing parameters. In addition, with optimum antibody conjugation strategies, these NPs could prove to be efficient probes for a range of biological systems. Their high probing efficiency (~ 95%) and specificity (~ 100%) was demonstrated with anti-CD41 antibody-conjugated NPs for detecting CD41 surface marker on the platelets.

Therefore, this research contributes significantly to understanding the various basic parameters for enhancing the sensitivities and probing the efficiencies of immobilized antibody systems and could have tremendous influence on the bioassay performance. In addition, the strategies developed could be employed to generate commercially relevant immunoassays.

## **7.2 Future work**

Further development of the research described in this thesis should involve the following issues

### **7.2.1 Sorting NPs as a function of their charge using a self-developed NP sorter**

Functionalization of NPs is a method with partial efficiency and only a certain percentage of the actual mass of NPs is grafted with desired functional groups. It was speculated that a mixed population of NPs might be the most significant reason for aggregation of the functionalized NPs (without antibody conjugation), which have a zeta potential in the range of moderate stability. Therefore, a prototype should be designed for separating out NPs on the basis of their net charge. This will allow study of the charge-based aggregation behavior of these dye-doped NPs. However, this sorter will only be useful for amine functionalized NPs, which have a net '+' charge and could be separated using the electric field migration property of NPs.

### **7.2.2 Replacing ethylenediamine (EDA) with ethanolamine (EA)**

EDA is a homobifunctional blocker having amine at both the terminals. Initially, EDA was selected for quenching the activated carboxy-groups due to its high reactivity. However, it was later realized that due to the presence of two amino groups (bivalency) on EDA this could also be involved in aggregation as a result of binding two NPs or antibodies in a cascade fashion. Therefore, EDA will be replaced by EA for future studies despite its low reactivity toward carboxyl groups in comparison to EDA.

### **7.2.3 Gradual centrifugation as an aggregate sorting procedure**

Aggregation in protein-conjugated NPs is inevitable under the current experimental conditions. Therefore, a gradual centrifugation model will also be employed in tandem with the above strategies. This model is based on subjecting the antibody-conjugated NPs as a function of (i) centrifugal force, and (ii) time of centrifugation. It is anticipated from this model that aggregates will be removed from the solvent medium according to their sizes and a much more homogeneous and dispersed solution of antibody-conjugated NPs could be obtained.

# **Appendix I**

## **Publications**

# Development of a High Sensitivity Rapid Sandwich ELISA Procedure and Its Comparison with the Conventional Approach

Chandra Kumar Dixit,<sup>†,‡</sup> Sandeep Kumar Vashist,<sup>†,§,¶</sup> Feidhlim T. O'Neill,<sup>†</sup> Brian O'Reilly,<sup>†</sup> Brian D. MacCraith,<sup>†,§</sup> and Richard O'Kennedy<sup>\*,†,‡,§</sup>

Centre for Bioanalytical Sciences (CBAS), National Centre for Sensor Research, Applied Biochemistry Group, School of Biotechnology, and Biomedical Diagnostics Institute (BDI), Dublin City University, Dublin 9, Ireland, and Bristol-Myers Squibb (BMS), Swords Laboratories, Watery Lane, Swords, Co. Dublin, Ireland

This text redacted due to 3rd party copyright  
This text redacted due to 3rd party copyright  
This text redacted due to 3rd party copyright  
This text redacted due to 3rd party copyright  
This text redacted due to 3rd party copyright  
This text redacted due to 3rd party copyright  
This text redacted due to 3rd party copyright  
This text redacted due to 3rd party copyright  
This text redacted due to 3rd party copyright  
This text redacted due to 3rd party copyright  
This text redacted due to 3rd party copyright  
This text redacted due to 3rd party copyright  
This text redacted due to 3rd party copyright  
This text redacted due to 3rd party copyright  
This text redacted due to 3rd party copyright  
This text redacted due to 3rd party copyright  
This text redacted due to 3rd party copyright  
This text redacted due to 3rd party copyright  
This text redacted due to 3rd party copyright

[illegible]

[illegible]

[illegible]



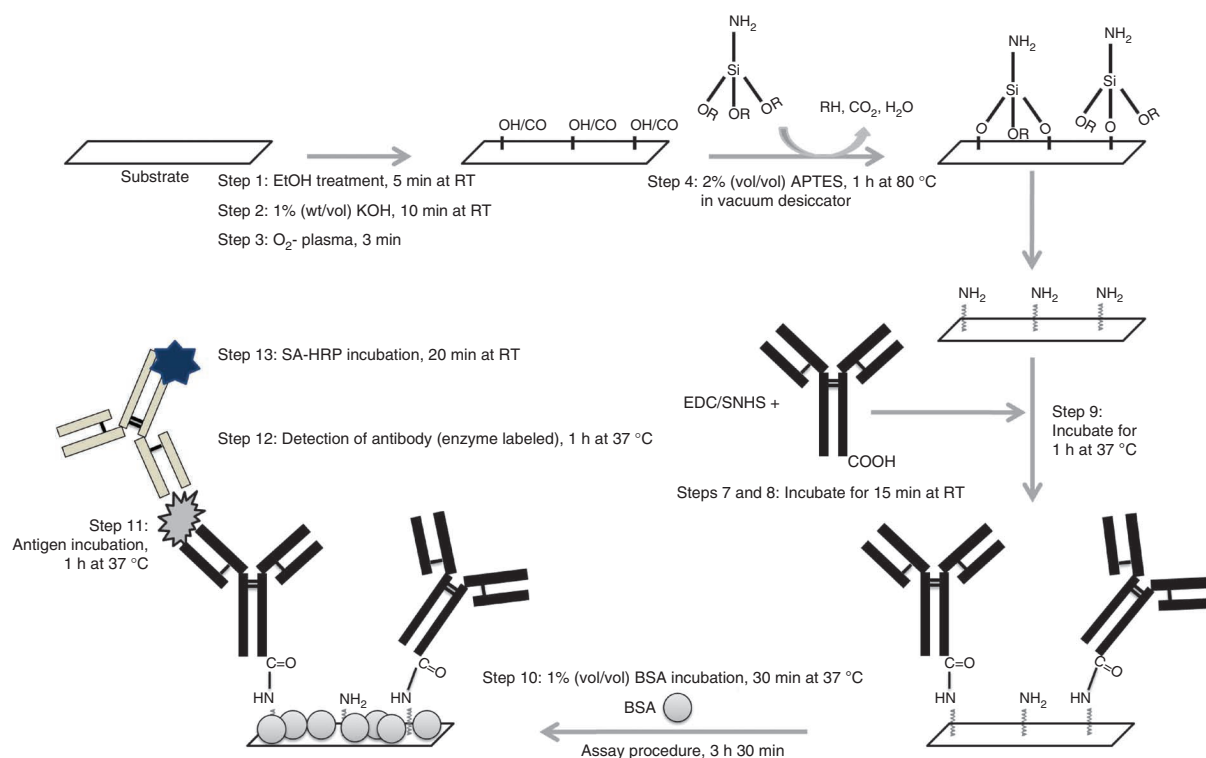


**Figure 1** | Schematic representation of the optimized surface modification and antibody immobilization strategy. The method involves 1% (wt/vol) KOH treatment that generates OH/CO groups on the polymeric surfaces, depending on their chemical nature; this facilitates the reaction of amine-terminal silane (APTES). Antibody was conjugated to the amino groups of the functionalized surface. These steps were followed with a standardized ELISA procedure with optimized blocking, washing and incubation steps. SA-HRP, streptavidin-HRP; SNHS, SulfoNHS.

Nevertheless, silane functionalization can be performed at room temperature (RT; ~25 °C) in a fume hood, thereby obviating the need for use of a vacuum pump and an oven. The use of this alternative approach will certainly affect various analytical parameters such as limit of detection (LOD) and effective concentration for half-maximum response ( $EC_{50}$ ), but the performance may still be better than the conventional method, particularly when the silanization time is increased.

## Experimental design

**Silanization.** Silanization requires a vacuum desiccator and oven. The oven should be preset to 80 °C for at least 20 min for temperature equilibration, and vacuum should then be applied. It is advantageous to equilibrate the desiccator before generating the vacuum. Various parameters such as APTES concentration and silanization time were also optimized in this study (**Supplementary Fig. 1**). The characterization of APTES functionalization was monitored with Fourier transform infrared (FTIR) spectroscopy (**Supplementary Fig. 2**). The silane has a marked tendency for multimerization, as it contains both nucleophilic and electrophilic centers. This makes the duration of silanization a critical parameter, as formation of randomized multilayers of silane can occur over extended time periods. This will eventually result in random antibody capture, which will directly affect overall immunoassay performance. Reports suggest that APTES forms multilayers after 3 h of incubation<sup>25,26</sup>. Therefore, we fully optimized our protocol, both for the duration of silanization and the concentration of APTES used (**Supplementary Fig. 1**).

**Immunoassay optimization.** In immunoassay development, all the components were commercially obtained as lyophilized samples and were checked for quality of performance before use. A number of process controls relevant to the reported procedure were included to optimize the ELISA and are shown in **Supplementary Figure 3**. Process controls included were also designed to test the cross-reactivity of kit components. HFA (standard positive control) and standards were supplied with the kit. The relevant analyte (fetuin for this study) obtained from various sources and additional control biomolecules that may present cross-reactivity challenges, such as human fetuin B in the assay developed for HFA, must also be used as controls. In this study, 1% (vol/vol) BSA in 0.1 M PBS was used as a blank. Different HFA dilutions were prepared and subjected to ELISA in the developed and conventional assay formats in order to define various analytical parameters. In addition, a number of assay dilutions were selected such that the lowest and highest concentrations followed the sigmoidal curve and were required to have at least five concentrations in the linear range on the standard curve. An irrelevant analyte, such as albumin, was routinely used as a negative control.

**Result analysis.** The  $EC_{50}$  (ref. 26) is the half-maximal effective concentration of antigen/ligand that induces 50% of the maximum detectable signal on the linear working range of an assay. Therefore,  $EC_{50}$  provides quantitative details of the analyte detection ability of an assay. Theoretically, it could be calculated by using four- or five-parameter curve fitting equations<sup>27</sup>. Most of the analysis systems determine the value of  $EC_{50}$  using four-parameter logistic-based



standard curve analysis. We have used SigmaPlot 11.0 software to analyze the various parameters such as  $EC_{50}$  and Hill slope (Supplementary Fig. 4).

LOD or assay sensitivity is the ability of the assay to detect the lowest possible analyte concentration present in the solution. There are many stringent ways to calculate LOD<sup>28</sup>. However, the most common and widely used method to determine LOD is signal of blank  $\pm 3$  s.d. The procedure for the calculation of LOD is given in the Supplementary Methods section.

**Microtiter plate assembly to develop assays on different polymeric supports.** The design and assembly of microtiter plates with

different solid supports is summarized in **Supplementary Figure 5**. A patterned, double-sided, pressure-sensitive adhesive was designed and developed such that the hole pattern at the bottom of microtiter plate corresponds to that on the adhesive. This adhesive was applied to the pre-blocked bottomless microtiter plates and the desired polymeric support was then attached. Afterward, pressure was applied with a press. More details about this strategy can be found in Vashist *et al.*<sup>24</sup> and also in **Supplementary Figure 5**. Microtiter plates prepared using the described method differ from the commercially available plates in having a different polymeric solid support. Therefore, these plates can be used in the PROCEDURE in the same manner as that of commercial microtiter plates.

## MATERIALS

### REAGENTS

- Anti-HRP antibody (Sigma-Aldrich, cat. no. P2419-2ML)
- HRP (Sigma-Aldrich, cat. no. P8375)
- Human fetuin A ELISA kit (R&D Systems, cat. no. DY1184e) **! CAUTION** Store the reconstituted antibody and antigen at 4 °C only if they are to be used within 2 months, otherwise, aliquot out and store at –80 °C for up to 6 months. The kit contains mouse anti-HFA capture antibody (720  $\mu$ g ml<sup>–1</sup>); HFA/ $\alpha$ -2-HS glycoprotein (AHSG) (90 ng ml<sup>–1</sup>); biotin-labeled goat anti-HFA detection antibody; and HRP-conjugated streptavidin **! CAUTION** Streptavidin is light-sensitive. Store in the dark.
- Blocker BSA (10 $\times$ , pH 7.4, 10% (wt/vol); Thermo Scientific, cat. no. 37525) **! CRITICAL** Filter before use to remove microbial contamination. This is critical for surface blocking.
- Absolute ethanol (Sigma-Aldrich, cat. no. 02856) **! CAUTION** It is highly flammable. Keep the container tightly closed. Keep away from sources of ignition. Alcohol vapors may be harmful to soft tissues such as the eyes or the respiratory tract. Use in a safety cabinet or a fume cupboard.
- Sulfuric acid (H<sub>2</sub>SO<sub>4</sub>; Sigma-Aldrich, cat. no. 339741) **! CAUTION** It is strongly corrosive and an irritant. Avoid contact with any part of the body. Wear suitable protective clothing and safety glasses during handling. Handle in a safety cabinet or a fume cupboard. In case of skin contamination, wash immediately with acid neutralizers and seek medical advice immediately.
- KOH pellets (99.99%, semiconductor grade; Sigma-Aldrich, cat. no. 306568) **! CAUTION** It can cause severe burns. Avoid contact with skin and eyes. Wear appropriate protection and handle in a safety cabinet. **! CRITICAL** The concentration of KOH must be exactly 1% (wt/vol) in autoclaved deionized water (DIW, 18  $\Omega$ ). It can affect the surface properties and can affect antibody immobilization.
- 3-Aminopropyltriethoxysilane (3-APTES; Sigma-Aldrich, cat. no. A3684) **! CAUTION** It is a skin and eye irritant. It is potentially toxic to the kidneys. **! CRITICAL** Prepare in autoclaved DIW (18  $\Omega$ ; see REAGENT SETUP).
- BupH phosphate-buffered saline (PBS) packs (0.1 M sodium phosphate and 0.15 M sodium chloride (pH 7.2); Thermo Scientific, cat. no. 18372) **! CAUTION** Avoid inhaling the powder. **! CRITICAL** Prepare in autoclaved DIW (18  $\Omega$ ; see REAGENT SETUP).
- BupH MES-buffered saline packs (0.1 M MES (2-(*N*-morpholino)ethane sulfonic acid), 0.9% (wt/vol) sodium chloride (pH 4.7); Thermo Scientific, cat. no. 28390) **! CAUTION** Avoid inhalation. **! CRITICAL** Prepare in autoclaved DIW (18  $\Omega$ ; see REAGENT SETUP).
- 1-Ethyl-3-(3-dimethylaminopropyl)-carbodiimide hydrochloride (EDC; Thermo Scientific, cat. no. 22981) **! CAUTION** It is an irritant. Handle inside a fume cupboard. EDC is hygroscopic, absorbs moisture and may lose activity. Equilibrate to RT before opening the container **! CRITICAL** Store at recommended temperature (–20 °C). Reconstitute in 0.1 M MES (pH 4.7; see REAGENT SETUP).
- Sulfo-*N*-hydroxysuccinimide (SulfoNHS; Thermo Scientific, cat. no. 24525) **! CRITICAL** Store at the recommended temperature (4 °C). Reconstitute in 0.1 M MES (pH 4.7; see REAGENT SETUP).
- TMB substrate kit (Thermo Scientific, cat. no. 34021). The kit contains TMB solution (0.4 g l<sup>–1</sup>) **! CAUTION** It is a skin, eye and lung irritant. In case

of skin contact, wash with plenty of water **! CRITICAL** TMB to peroxide ratio is critical for color development. Maintain it in the ratio 1:1; peroxide solution (containing 0.02% (vol/vol) H<sub>2</sub>O<sub>2</sub> in citric acid buffer; Thermo Scientific) **! CAUTION** It is a strong oxidizing agent. It is harmful if swallowed and also poses severe risk of damage to eyes. Rinse immediately with plenty of water in case of contact and seek medical attention. Wear suitable protection and work in safety cabinet or fume cupboard.

- Deionized water (18  $\Omega$ , DIW)

### EQUIPMENT

- Freezer (–70 °C, operating range –60 to –80 °C; New Brunswick)
- Refrigerator (2–8 °C; Future)
- ELISA plate reader (Tecan)
- Mini incubator (Labnet)
- Harrick plasma cleaner (Harrick Plasma; model number PDC-002)
- PVC fume cupboard (Chemflow range; CSC)
- Nunc microwell 96-well polystyrene plates (flat bottom (non-treated), sterile; Sigma-Aldrich, cat. no. P7491)
- PMMA (Poly(methyl methacrylate)) polycarbonate, cellulose acetate polymer (in the form of 1-mm-thick sheets) and zeonex polymer (1.5-mm-thick slides; Microfluidic ChipShop)
- Desiccator with vacuum control nozzle (Lennox)
- Vacuum source
- Eppendorf microtubes (1.5 ml; Sigma-Aldrich, cat. no. Z 606340)
- SigmaPlot software bundle version 11.0 from Systat for detailed assay analysis

### REAGENT SETUP

**PBS** Each sachet (BupH phosphate-buffered saline (PBS) packs) contains 0.1 M phosphate and 0.15 M NaCl and yields a volume of 500 ml in the pH range 6.8–7.4. Add a sachet to 100 ml of autoclaved DIW and dissolve. Finally, adjust the volume up to 500 ml. This can be stored at RT for 2 weeks. Check pH before use.

**MES** Each sachet (BupH MES-buffered saline packs) contains 0.1 M MES and 0.9% (wt/wt) NaCl and yields a volume of 500 ml at pH 4.7. Add a sachet to 100 ml of autoclaved DIW and dissolve. Adjust the final volume up to 500 ml. Check the pH and adjust it to 4.7 if necessary. This can be stored at RT for 2 weeks. Check pH before use.

**APTES** The solution is supplied at 99% purity. Reconstitute in autoclaved DIW to produce an effective 2% (vol/vol) solution. Prepare a fresh solution for each functionalization.

**EDC** Each pack contains 25 g EDC. Reconstitute in 0.1 M MES buffer (pH 4.7), at a concentration of 8 mg ml<sup>–1</sup>. Mix it with equal volumes of sulfoNHS solution (22 mg ml<sup>–1</sup>). Aliquots can be stored effectively for 6 months at –20 °C.

**SulfoNHS** Each pack contains 5 g sulfoNHS. Reconstitute in 0.1 M MES (pH 4.7), at a concentration of 22 mg ml<sup>–1</sup>. Mix with equal volumes of EDC (8 mg ml<sup>–1</sup>). Aliquots can be stored effectively for 6 months at –20 °C.

**H<sub>2</sub>SO<sub>4</sub>** The concentrated solution is 37 N. Add 2.7 ml of 37 N H<sub>2</sub>SO<sub>4</sub> to 97.3 ml of DIW to produce a 1 N solution. Reaction of acid and water is exothermic; therefore, acid should always be added to water. This solution can be stored indefinitely at RT.

## PROTOCOL

### PROCEDURE

#### Surface activation and amine functionalization ● TIMING ~1 h 30 min

1| Incubate the surface of the plate well with 100  $\mu$ l of absolute ethanol for 5 min and wash extensively with DIW (minimum five times with 300  $\mu$ l DIW per well). Washing can also be performed with an automatic plate washer or squeeze bottles.

2| Incubate the surface of the plate well with 100  $\mu$ l of 1% (wt/vol) KOH in DIW for 10 min and wash extensively with DIW (as described in Step 1).

▲ **CRITICAL STEP** KOH treatment should not be longer than the optimized time, because it may cause strong aberrations in the surface and may change the surface properties.

3| Treat the KOH-activated surface with  $O_2$  plasma in the plasma cleaner set at a plasma strength of 29.6 W. The total input power of the instrument is 200 W. Vacuum pump with a pump speed of  $0.83 \text{ ft}^3 \text{ min}^{-1}$  was used to generate a pressure of 0.27 mbar. Monitor the process of plasma development in the chamber.

▲ **CRITICAL STEP** Flush the plasma cabinet with  $O_2$  to generate an oxidizing environment. Keep the vacuum pump switched on during the whole process. The duration of plasma treatment (3 min) is critical.

#### ? TROUBLESHOOTING

4| Incubate the plasma-oxidized plate well surface with 100  $\mu$ l of 2% (vol/vol) APTES in DIW.

▲ **CRITICAL STEP** Place the APTES-added plates in the desiccator and create vacuum. Incubate the vacuum desiccator at 80 °C for 1 h.

5| Equilibrate the desiccator to RT after incubation.

! **CAUTION** Open the desiccator in a fume cupboard to avoid APTES fumes. Use a fume cupboard and wear protective clothing and safety glasses.

▲ **CRITICAL STEP** Equilibrating the desiccator stops the APTES vaporization and enhances the uniformity of functionalization.

#### ? TROUBLESHOOTING

6| Wash the APTES-modified plate well surface extensively five times with DIW (as described in Step 1).

#### Antibody immobilization ● TIMING ~1 h

7| Dissolve 0.4 mg of EDC and 1.1 mg of sulfoNHS in 100  $\mu$ l of 0.1 M MES (pH 4.7).

▲ **CRITICAL STEP** The ratio of EDC and sulfoNHS is important for optimal cross-linking. Use the recommended ratios of EDC and sulfoNHS or optimize this ratio.

#### ? TROUBLESHOOTING

8| Incubate 990  $\mu$ l of the antibody to be immobilized with 10  $\mu$ l of EDC-sulfoNHS solution for 15 min at RT.

9| Incubate the activated antibody in the APTES-modified plate well surface for 1 h at 37 °C and wash five times with 300  $\mu$ l of 0.1 M PBS (pH 7.4).

#### ? TROUBLESHOOTING

#### ELISA ● TIMING ~3 h 30 min (sandwich format)

10| To carry out the HFA ELISA (sandwich format), block the antibody-immobilized surface with 300  $\mu$ l of 1% (vol/vol) BSA for 30 min at 37 °C; follow this by five washings with PBS, as described in Step 9.

▲ **CRITICAL STEP** Use filtered BSA or filter the BSA solution before use to remove any microbial or other contaminants.

#### ? TROUBLESHOOTING

11| Add 100  $\mu$ l of HFA (range from  $4.8 \text{ pg ml}^{-1}$  to  $20 \text{ ng ml}^{-1}$ ) in triplicate to BSA-blocked wells and incubate for 1 h at 37 °C; follow with five PBS washings, as described in Step 9.

#### ? TROUBLESHOOTING

12| Incubate 100  $\mu$ l of biotin-conjugated detection antibody in each of the antigen-captured wells for 1 h at 37 °C, and follow by five PBS washings, as described in Step 9.

#### ? TROUBLESHOOTING

13| Add 100  $\mu$ l of streptavidin-HRP conjugate and incubate for 20 min; follow with five PBS washings, as described in Step 9.

#### ? TROUBLESHOOTING

14| Add 100  $\mu$ l of TMB- $H_2O_2$  mixture to each of these wells and incubate for 20 min at RT to develop color.

#### ? TROUBLESHOOTING

**15** Stop the enzyme-substrate reaction with addition of 50  $\mu\text{l}$  of 1 N  $\text{H}_2\text{SO}_4$  to each well.

**16** Record the absorbance at a primary wavelength of 450 nm and secondary wavelength of 540 nm in the Tecan ELISA plate scanner.

**▲ CRITICAL STEP** Determine the absorbance within 10 min of stopping the enzyme-substrate reaction.

## ? TROUBLESHOOTING

Troubleshooting advice can be found in **Table 1**.

**TABLE 1** | Troubleshooting table.

Step	Problem	Possible reason	Solution
3	No violet color	High $\text{O}_2$ content in the chamber	Restart the plasma etching procedure. Flush less $\text{O}_2$ into the chamber
5	No color development in the enzyme-substrate reaction of the ELISA procedure, whereas the passively adsorbed control plate developed color	Characterize with FTIR spectroscopy to determine whether there is any characteristic amine peaks. If not, then APTES may be degraded (hydrolyzed). If yes, proceed to next troubleshooting step	Use a different batch of APTES
7	Same as in Step 5	Check as in Step 5; if the problem is not resolved after replacing APTES, then the EDC may be degraded/hydrolyzed	Use a new EDC stock. If the problem still persists, check the next troubleshooting step
9, 11, 12	No color development in the enzyme-substrate reaction of the ELISA procedure	Capture or detection antibody and/or antigen may have lost functionality	Proteins, such as antibodies or many antigens, are highly susceptible to temperature or storage conditions. Avoid repeated freeze-thaw cycles and store appropriately
10	High background	Check quality of BSA	Use different BSA stock and make up fresh solution in PBS
13	No color development in the enzyme-substrate reaction of the ELISA procedure	Degraded streptavidin	Streptavidin should be stored in the dark. Reconstitute fresh solution and store in the dark
14	Same as in Step 13	TMB or $\text{H}_2\text{O}_2$ may be degraded	Use fresh TMB and/or $\text{H}_2\text{O}_2$ solution

## ● TIMING

Steps 1–6, Surface activation: ~1 h 30 min

Steps 7–9, Antibody immobilization: ~1 h

Steps 10–16, Sandwich format: ~3 h 30 min

## ANTICIPATED RESULTS

The developed procedure was demonstrated using HFA as the antigen. With this improved method, a 16-fold increase in assay sensitivity was achieved (**Fig. 2**) in comparison with the conventional assay format. The analytical sensitivity of the developed sandwich ELISA procedure was  $39 \text{ pg ml}^{-1}$ , with an  $\text{EC}_{50}$  of  $3 \text{ ng ml}^{-1}$ , whereas the sensitivity and  $\text{EC}_{50}$  of the

**Figure 2** | Assay performance with the developed and conventional ELISA procedure. A concentration range of HFA/AHSG ( $0\text{--}20,000 \text{ pg ml}^{-1}$ ) was subjected to ELISA on different plates with either covalently immobilized or passively adsorbed antibody. The results shown are the mean  $\pm$  s.d. The  $\text{EC}_{50}$  represents the concentration of the analyte/ligand that generates 50% of the maximum signal obtained in the linear working range on a standard curve. This is also known as half-maximum effective concentration. The LOD is the minimum amount of the analyte that is detected when the analyte is subjected to an assay. % CV denotes the variability in measuring a specific analyte concentration in a given number of assay repeats.

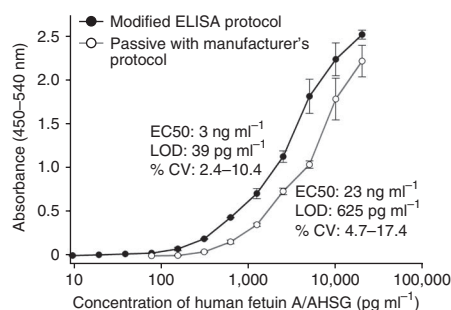
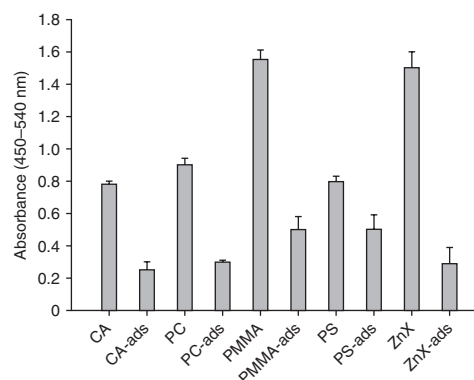


**Figure 3** | The performance of the developed procedure on a range of polymeric solid support matrices. The assay was performed at a HFA concentration of  $1.25 \text{ ng ml}^{-1}$  and a comparison was made. CA, PC, PMMA, PS and ZnX correspond to signals obtained for the assays performed on amine-functionalized cellulose acetate, polycarbonate, polymethyl methacrylate, polystyrene and zeonex, respectively. The suffix '-ads' after the polymer abbreviation (on x axis) corresponds to the assay performed with antibody adsorbed on the respective unmodified polymeric matrix, e.g., CA-ads corresponds to signal obtained for the assay performed with antibody adsorbed on unmodified cellulose acetate polymer.



conventional assay were  $625 \text{ pg ml}^{-1}$  and  $23 \text{ ng ml}^{-1}$ , respectively. The working/dynamic range for the developed sandwich ELISA was  $10\text{--}20,000 \text{ pg ml}^{-1}$ , whereas for conventional assay it was  $150\text{--}20,000 \text{ pg ml}^{-1}$  (ref. 11). This was mainly because of the higher retention rate of the covalently immobilized antibody, whereas the physisorbed antibody in conventional assays could leach out or be lost because of protein exchanges<sup>3–6</sup>. Another advantage of this strategy is the long-term storage stability of the capture antibody-coated microtiter plates, which can be useful for the development of commercial diagnostics. The developed protocol also enables the utilization of a number of different solid support matrices, irrespective of their chemical nature, as depicted in **Figure 3**. The developed procedure was demonstrated by performing ELISA on different polymeric matrices, such as cellulose acetate, polystyrene, PMMA and polycyclo-olefin (Zeonex), in a modified microtiter plate format<sup>11,24</sup>. Thus, the newly developed procedure has considerable advantages over the existing procedure, which will enable this protocol to find wide applications as an analytical tool in industrial, clinical and research settings.

Note: Supplementary information is available via the HTML version of this article.

**ACKNOWLEDGMENTS** We acknowledge Bristol-Myers Squibb (BMS), Syracuse, USA and Industrial Development Agency, Ireland for the financial support under the Centre for Bioanalytical Sciences (CBAS) project code 116294. This material is based on work supported in part by the Science Foundation Ireland under grant 05/CE3/B754.

**AUTHOR CONTRIBUTIONS** C.K.D., S.K.V. and R.O. conceived, designed and refined the method; C.K.D., S.K.V. and R.O. wrote this manuscript; S.K.V., R.O. and B.D.M. supervised the work.

**COMPETING FINANCIAL INTERESTS** The authors declare no competing financial interests.

- Jia, C.-P. *et al.* Nano-ELISA for highly sensitive protein detection. *Biosens. Bioelectron.* **24**, 2836–2841 (2009).
- Andrade, G., Barbosa-Stancioli, E.F., Mansur, A.A.P., Vasconcelos, W.L. & Mansur, H.S. Design of novel hybrid organic–inorganic nanostructured biomaterials for immunoassay applications. *Biomed. Mater.* **1**, 221–234 (2006).
- Ball, V., Huetz, P., Elaissari, A., Cazenava, J.P., Voegel, J.C. & Schaaf, P. Kinetics of exchange processes in the adsorption of proteins on solid surfaces. *Proc. Natl Acad. Sci. USA* **91**, 7330–7334 (1994).
- Huetz, P., Ball, V., Voegel, J.C. & Schaaf, P. Exchange kinetics for a heterogeneous protein system on a solid surface. *Langmuir* **11**, 3145–3152 (1995).
- Essa, H., Magner, E., Cooney, J. & Hodnett, B.K. Influence of pH and ionic strength on the adsorption, leaching and activity of myoglobin immobilized onto ordered mesoporous silicates. *J. Mol. Catal. B* **49**, 61–68 (2007).
- Wang, X., Wang, Y., Xu, H., Shan, H. & Lu, J.R. Dynamic adsorption of monoclonal antibody layers on hydrophilic silica surface: a combined study by spectroscopic ellipsometry and AFM. *J. Colloid Interface Sci.* **323**, 18–25 (2008).
- Kaur, J., Boro, R.C., Wangoo, N., Singh, K.R. & Suri, C.R. Direct hapten-coated immunoassay format for the detection of atrazine and 2,4-dichlorophenoxyacetic acid herbicides. *Anal. Chim. Acta* **607**, 92–99 (2008).
- Mansur, H., Palhares, R., Andrade, G., Piscitelli-Mansur, A. & Barbosa-Stancioli, E. Improvement of viral recombinant protein-based

immunoassays using nanostructured hybrids as solid support. *J. Mater. Sci. Mater. Med.* **20**, 513–519 (2009).

- Gomez-Serrano, V., Acedo-Ramos, M., Valenzuela-Calahorra, C. & Lopez-Peinado, A.J. Regeneration of activated carbon after contact with sulfuric acid solution. *J. Chem. Technol. Biotechnol.* **75**, 835–839 (2000).
- Vasconcellos, A.S., Oliveira, J.A.P. & Baumhardt-Neto, R. Adhesion of polypropylene treated with nitric and sulfuric acid. *Eur. Polym. J.* **33**, 1731–1734 (1997).
- Dixit, C.K., Vashist, S.K., O'Neill, F.T., O'Reilly, B., MacCraith, B.D. & O'Kennedy, R. Development of a high sensitivity rapid sandwich ELISA procedure and its comparison with the conventional approach. *Anal. Chem.* **82**, 7049–7052 (2010).
- Patel, G.N. & Bolikal, D. Single step pre-swelling and etching of plastics for plating. US patent no. 5,049,230 (1991).
- Patel, G.N. & Patel, S.H. Etching plastics with nitrosyls. US patent no. 5,591,354 (1997).
- Park, S. & Jung, W. Effect of KOH activation on the formation of oxygen structure in activated carbons synthesized from polymeric precursor. *J. Colloid Interface Sci.* **250**, 93–98 (2002).
- Vijayendran, R.A. & Leckband, D.E. A quantitative assessment of heterogeneity for surface-immobilized proteins. *Anal. Chem.* **73**, 471–480 (2001).
- Park, S., Seo, M., Ma, T. & Lee, D. Effect of chemical treatment of Kevlar fibers on mechanical interfacial properties of composites. *J. Colloid Interface Sci.* **252**, 249–255 (2002).
- Svarnas, P., Spyrou, N. & Held, B. Polystyrene thin films treatment under DC point-to-plane low-pressure discharge in nitrogen for improving wettability. *Eur. Phys. J. Appl. Phys.* **28**, 105–112 (2004).
- Laib, S. & MacCraith, B.D. Immobilization of biomolecules on cycloolefin polymer supports. *Anal. Chem.* **79**, 6264–6270 (2007).
- Raj, J. *et al.* Surface immobilisation of antibody on cyclic olefin copolymer for sandwich immunoassay. *Biosens. Bioelectron.* **24**, 2654–2658 (2009).
- Boulares-Pender, A., Prager-Duschke, A., Elsner, C. & Buchmeiser, M.R. Surface-functionalization of plasma-treated polystyrene by hyperbranched polymers and use in biological applications. *J. Appl. Polym. Sci.* **112**, 2701–2709 (2009).
- North, S.H., Lock, E.H., Cooper, C.J., Franek, J.B., Taitt, C.R. & Walton, S.G. Plasma-based surface modification of polystyrene microtitre plates for covalent immobilization of biomolecules. *Appl. Mater. Interface* **2**, 2884–2891 (2010).

22. Kaur, J., Singh, K.V., Raje, M., Varshney, G.C. & Suri, C.R. Strategies for direct attachment of hapten to a polystyrene support for applications in enzyme-linked immunosorbent assay (ELISA). *Anal. Chim. Acta.* **506**, 133–135 (2004).
23. Lacy, A. *et al.* Rapid analysis of coumarins using surface plasmon resonance. *J. AOAC Int.* **89**, 884–892 (2006).
24. Vashist, S.K., O'Sullivan, S.A., O'Neill, F., Holthofer, H., O'Reilly, B. & Dixit, C.K. A multiwell plate for biological assays. WIPO, Publication no. W02010/044083 (2010).
25. Song, Y., Hildebrand, H. & Schmuki, P. Optimized monolayer grafting of 3-aminopropyltriethoxysilane onto amorphous, anatase and rutile TiO<sub>2</sub>. *Surf. Sci.* **604**, 346–353 (2010).
26. Cass, T. & Ligler, F.S. *Immobilized Biomolecules in Analysis: A Practical Approach* (Oxford University Press, 1998).
27. Armbruster, D.A., Schwarzhoff, R.H., Hubster, E.C. & Liserio, M.K. Enzyme immunoassay, kinetic microparticle immunoassay, radioimmunoassay, and fluorescence polarization immunoassay compared for drugs-of-abuse screening. *Clin. Chem.* **39**, 2137–2146 (1993).
28. Armbruster, D.A., Tillman, M.D. & Hubbs, L.M. Limit of detection (LOD)/limit of quantitation (LOQ): comparison of the empirical and the statistical methods exemplified with GC-MS assays of abused drugs. *Clin. Chem.* **40**, 1233–1238 (1994).

Cite this: *Analyst*, 2011, **136**, 1406

www.rsc.org/analyst

PAPER

# Evaluation of apparent non-specific protein loss due to adsorption on sample tube surfaces and/or altered immunogenicity†

Chandra K. Dixit,<sup>‡,ab</sup> Sandeep K. Vashist,<sup>‡,§,ac</sup> Brian D. MacCraith<sup>ad</sup> and Richard O'Kennedy<sup>\*abd</sup>

Received 5th September 2010, Accepted 16th December 2010

DOI: 10.1039/c0an00689k

The non-specific loss of protein analytes can have a major effect on assay results particularly where the concentrations of such analytes are extremely low and the matrix is complex. This report assesses how the protein incubated in sample tubes may be lost due to adsorption. Use of proteins, such as bovine serum albumin (BSA), may be used to pre-treat tubes to reduce such losses. However, such losses may also be associated with structural perturbations leading to changes in immunogenicity (as a result of alterations in specific epitope-related conformations). This can lead to erroneous results or lack of comparability with a range of methodologies such as the bicinchoninic protein assay and immunoassays or when surface plasmon resonance (SPR)-based approaches are used. A model system to evaluate these phenomena is proposed.

## Introduction

Analytical techniques such as surface plasmon resonance (SPR) and enzyme-linked immunosorbent assay (ELISA) may involve sample preparation<sup>1–5</sup> and long incubation periods of analyte in sample tubes. Thus, there is a possibility of analyte loss due to non-specific binding to matrix-associated interferants or adsorption of protein molecules onto the surface of the tubes or onto devices used in the preparation procedure.<sup>6–14</sup> This may result in a low analyte recovery and/or a considerable decrease in the signal obtained with specific techniques (*e.g.* antibody-based methods such as ELISA). Therefore, it is critically important to prevent such analyte loss, particularly for the antigens that are present at very low concentrations (such as cardiac troponins, tumor biomarkers or cytokines).<sup>15</sup> The use of relevant controls and standards can be used to compensate for some losses due to this phenomenon. However, it can have very significant effects if the technique or assay used is no longer able to detect the low

levels of the analyte present, due to the amount lost in the pre-analysis steps.

This report describes analyte losses both as a function of duration of incubation and due to the chemical nature of the tube material. The model analytes employed for this study were human fetuin A (HFA) and HRP-labeled mouse IgG. Analyte loss was characterized by comparative analysis of sampling performed in tubes that were either treated with blocking proteins such as BSA or were used without any prior treatment (untreated). Known quantities of the analyte were incubated in BSA-treated and untreated tubes made of polypropylene (PP) and low protein-adsorbing chrome-coated glass (GT) (customized for SPR studies) for 0, 0.5 and 12 h. The analyte loss was characterized as a function of decrease in absorbance obtained with the bicinchoninic acid (BCA) assay (which is a direct method for calculation of total protein concentration in solution and hence, to quantitate protein recovery). After confirming protein analyte loss with the BCA assay, enzyme-linked immunoassay (ELIA) and surface plasmon resonance (SPR) were employed to determine the apparent concentration of the targeted analytes. Our findings indicated that in immunoassay-based analyses the reduction in concentration may be due to a combination of losses associated with non-specific adsorption and structural changes that may result in altered epitope conformation leading to reduced immunogenicity.

## Experimental

### Materials

1-Ethyl-3-(3-dimethylaminopropyl)carbodiimide (EDC), sulfo-*N*-hydroxysuccinimide (SNHS), phosphate buffered saline (PBS, 0.1 M, pH 7.4), 2-(*N*-morpholino)ethanesulfonic acid (MES,

<sup>a</sup>Centre for Bioanalytical Sciences (CBAS), National Centre for Sensor Research, Dublin City University, Dublin 9, Ireland. E-mail: richard.okennedy@dcu.ie; Fax: +353 1 700 7810; Tel: +353 1 700 5412

<sup>b</sup>Applied Biochemistry Group, School of Biotechnology, Dublin City University, Dublin 9, Ireland

<sup>c</sup>Bristol-Myers Squibb (BMS), Swords Laboratories, Watery Lane, Swords, Co., Dublin, Ireland

<sup>d</sup>Biomedical Diagnostics Institute (BDI), Dublin City University, Dublin 9, Ireland

† Electronic supplementary information (ESI) available: Supplementary Theory & Analysis: Details of ELIA (EC50), SPR and BCA assay performance for analyte incubations. See DOI: 10.1039/c0an00689k

‡ Authors contributed equally.

§ Current address: Nanoscience and Nanotechnology Initiative (NUSNNI) Nanocore, National University of Singapore, T-Lab level 11, 5A Engineering Drive 1, 117580, Singapore.

pH 4.7), tetramethylbenzidine (TMB) substrate kit, BCA assay kit and bovine serum albumin (BSA) were purchased from Fischer Scientific (Ireland), Ballycoolin, Dublin, Ireland. HRP-labeled mouse IgG, goat anti-mouse IgG, potassium hydroxide (KOH), 3-APTES, absolute ethanol, Nunc 96-well polystyrene plates (P7491) and Eppendorf polypropylene (PP) microtubes were obtained from Sigma-Aldrich, Tallaght, Dublin, Ireland. SIA gold chips (BR-1004-05) and glass vials (BR-1002-09) were obtained from GE Healthcare, Buckinghamshire, HP7 9NA, UK. Human fetuin A/AHSG duoset kit, with all human fetuin A assay components, was procured from R&D Systems Europe, Abingdon, Oxon, UK. The kit consisted of the capture anti-human fetuin A/AHSG (anti-HFA) antibody from mouse, human fetuin A/AHSG standard, biotinylated goat anti-HFA detection antibody and streptavidin–HRP. All the assay components were reconstituted in 0.15 M PBS, pH 7.4, with 1% (w/v) BSA. All buffers and solutions were prepared using Milli-Q deionised water (DIW). The dilution of BSA was made in 0.15 M PBS, pH 7.4, whereas KOH and 3-APTES were diluted in DIW. EDC and SNHS were reconstituted in 0.1 M MES buffer, pH 4.7.

### Tube-blocking

Polypropylene (PP) and glass (GT) tubes were treated with 1% (w/v) BSA for 30 min followed by extensive washing with PBS (0.15 M, pH 7.4; Sigma-Aldrich, Ireland). The tubes were dried under nitrogen ( $N_2$ ).

### Sampling

HFA (0–20 000 pg mL<sup>-1</sup>) and HRP-labeled mouse IgG (0–1210 ng mL<sup>-1</sup>) were reconstituted in 0.15 M PBS, pH 7.4. All samples were incubated in BSA-treated and untreated tubes (PP and GT) for 0, 0.5 and 12 h at room temperature (RT). Additionally, HFA was also incubated in BSA (1% (w/v))-treated and untreated tubes at 4 °C for analysis essential to quantify the contribution of sample incubation conditions to the altered immunogenicity. ‘Blank’ controls for this study had zero analyte concentration and were incubated for 0 h in blocked PP and GT tubes. These controls also facilitate the detection of any BSA leaching into solution from the tube surfaces following blocking.

### Analytical

ELIA was performed over the stated concentration range of analytes for all sets of sampling, whereas the BCA and SPR assays were performed at concentrations of 10 ng mL<sup>-1</sup> and 300 ng mL<sup>-1</sup> for HFA and HRP-labeled mouse IgG, respectively. The BCA assay, performed according to the manufacturer's instructions, was used to determine the HFA recovery in the samples incubated for different durations. ELIA was performed with covalently immobilized anti-HFA antibody, as previously described.<sup>16</sup> The microtiter plate wells were activated using 1% (w/v) KOH. The amine-functionalization was performed with 3-aminopropyltriethoxy silane (APTES). The anti-HFA antibody was conjugated to the aminated surface *via* EDC chemistry.

For SPR (Biacore 3000) analysis each flow-cell of the amine-activated gold chip had approximately 5000 response units of anti-HFA antibody immobilised, using EDC chemistry. The

sample buffer (HEPES, pH 7.0) was passed over all the flow-cells serving as a blank. Four different concentrations of HFA (1.25–10 ng mL<sup>-1</sup>) in two sets were incubated in BSA-treated and untreated tubes and were then subjected to SPR analysis. The corresponding control values were deducted from each signal value. The absorbance and RU signals obtained for ELIA and SPR were analysed and reported as the % analyte loss, where the % signal loss for each set of experiment was calculated as a loss relative to the 0 h sampling performed in blocked (B) tubes and discussed in detail in the Theory and analysis section. Similarly, goat anti-mouse IgG was immobilized on the chip and HRP-labeled mouse IgG was assayed at a concentration of 300 ng mL<sup>-1</sup> (concentration just above the EC<sub>50</sub> value). SPR was performed on all samples that were used in the BCA assay and ELIA.

### Theory and analysis

The model developed is an attempt to capture key elements that can impinge on the accuracy and potential sensitivity of an assay and to suggest approaches that may help to quantitate and minimise the sample loss. It is also the case that there are inherent limitations in the analytical methods used but the model attempts to take these into consideration.

The model describing various theoretical considerations is presented in Fig. 1. The model follows the sequence of events according to the ‘A–B’ rule, where the contributing factors are calculated by deducting individual fractions at each step from the total. All the calculations performed with the results obtained from BCA, ELIA and SPR were based on an assumption that there was no significant analyte loss for the samples incubated in blocked tubes for 0 h incubation. The difference in signals obtained for samples incubated for various durations in blocked and unblocked tubes with respect to those in blocked tubes at 0 h quantifies the adsorption-based analyte loss (% $\Delta S$ ). This is summarized as eqn (1).

$$\% \Delta S = [1 - (S_t / S_{0h\ B})] \times 100 \quad (1)$$

where  $S_t$ : signal obtained for the HFA or HRP-labeled mouse IgG samples at a given incubation time and  $S_{0h\ B}$ : signal obtained for the HFA or HRP-labeled mouse IgG sample incubated in BSA-treated tubes at 0 h incubation (equivalent to 100% signal).

The loss was expressed as the relative percentage signal loss (Table 1, marked with \*), where the signal corresponds to the absorbance (for ELIA-based analysis) or response units (for SPR-based analysis) for each set of sampling performed in either PP or GT tubes.

Similarly, the signal loss contributed by the reduced analyte immunogenicity (% $\Delta S_{\text{immunogenicity-associated}}$ ) was calculated as the difference in signals obtained with the samples incubated for 12 h in blocked tubes at RT with respect to those in blocked tubes for 12 h at 4 °C. This is shown in eqn (2). This assumption was based on the fact that when protein molecules in solution are adsorbed onto surfaces, their conformation may become more unstable and a loss of structural integrity can occur.<sup>17–21</sup> There may also be aggregation-dependant activity loss where the aggregation may either be due to solvent<sup>22,23</sup> or temperature effects.<sup>24</sup> Additionally, an increase in protein adsorption occurs

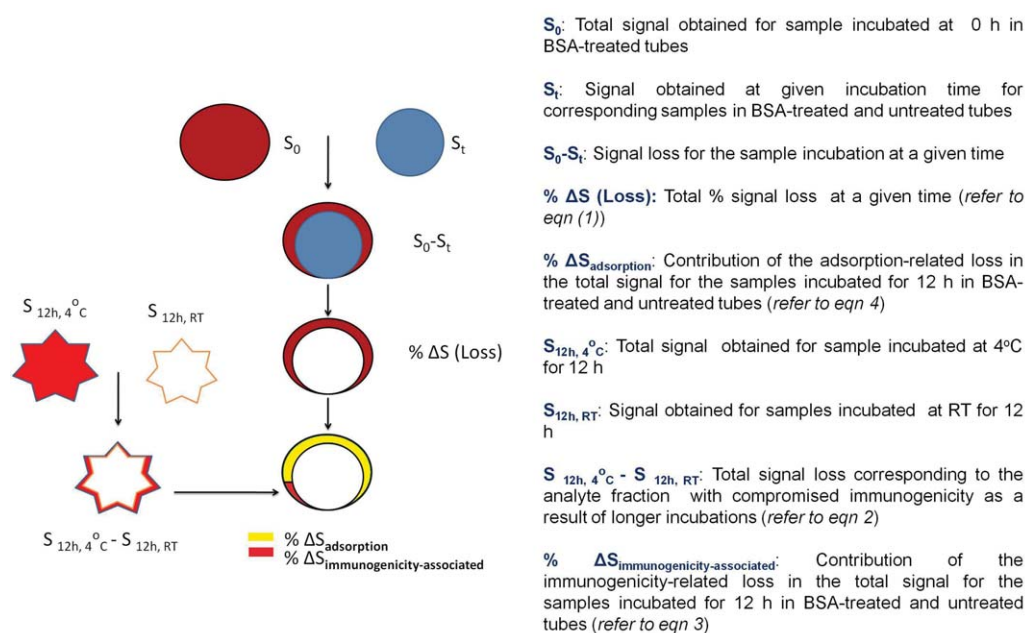


**Fig. 1** This model is designed to illustrate that the losses in the analyte (e.g. HFA) concentration, as determined by antibody-based methods, result from a combination of both adsorption on the tube surfaces and loss of the conformation-related immunogenicity and that these increase over the time of incubation and also are temperature dependent.

in the temperature range 20–40 °C. However, at lower temperatures there is a significant reduction in adsorption.<sup>25,26</sup>

For this study, the analyte samples were incubated in the BSA-treated tubes under two conditions: (a) at RT and (b) at 4 °C with the same experimental set-up. The percentage fraction of the signal loss relative to the samples incubated at 4 °C for 12 h was calculated using the following eqn (2)

$$\% \Delta S_{\text{immunogenicity-associated}} = [1 - (S_{12h, RT} / S_{12h, 4^\circ C})] \times 100 \quad (2)$$

where  $S_{12h, RT}$ : signal of the HFA or HRP-labeled mouse IgG samples incubated for 12 h at RT and  $S_{12h, 4^\circ C}$ : signal of the

corresponding sample incubated for 12 h at 4 °C in BSA-treated tubes (equivalent to the estimate of the signal loss contributed mainly by adsorption in blocked tubes only).

This fraction, as exemplified by eqn (2), corresponds to losses associated with the altered immunogenicity in samples due to longer incubations. However, the total analyte loss (eqn (1)) for 12 h incubation at RT is consisted of two different loss fractions corresponding to adsorption and the altered immunogenicity. Therefore, in order to obtain how much the compromised immunogenicity (eqn (2); Table 2, marked with \*\*) contributes toward the total signal loss we have devised eqn (3).

**Table 1** Determination of the total HFA loss due to non-specific adsorption and the conformation-related immunogenicity changes<sup>a</sup>

Incubation time/h	Sample tube	Percentage signal loss* relative to samples of 0 h incubation time in blocked tubes		Correlation studies BCA vs. ELIA
		ELIA	BCA	
0 RT	BSA-treated PP	0	0	BSA-treated PP <sup>b</sup> , $r^2 = 1.00$ ( $p = 0.76$ ) and untreated PP, $r^2 = 0.78$ ( $p = 0.48$ )
	Untreated PP	7	5	
0.5 RT	BSA-treated PP	11	2	
	Untreated PP	23	7	
12 RT	BSA-treated PP	34 (24**)	24	
	Untreated PP	65 (49**)	30	
12 (4 °C)	BSA-treated PP	24***	9	
	Untreated PP	48***	24	

<sup>a</sup> \* The percentage signal loss for each set of HFA samples at a defined incubation time was calculated using eqn (1). The control for this used blocking performed at 0 h incubation. \*\* The fraction of the total signal loss contributed by adsorption-based non-specific losses and calculated using eqn (4). \*\*\* The percentage signal loss obtained for sampling performed at 12 h in BSA-treated and untreated tubes (\*\*) after deducting the fraction corresponding to the immunogenicity loss (marked with \*\* in Table 2) corresponds closely with the percentage signal loss obtained for the samples incubated in BSA-treated and untreated tubes at 4 °C for 12 h. This indicates that the immunogenicity-related losses in HFA samples were minimized for incubations at 4 °C. <sup>b</sup> PP stands for polypropylene tubes. <sup>c</sup>  $r^2$  is the coefficient of determination of the techniques used for cross-validation and the  $p$ -value (at 95% confidence) represents the level of significance between the analysis performed with both the experimental approaches used. The  $r^2$  and  $p$ -values for this study were calculated using SigmaPlot software version 11.0.

$$\%(\Delta S/\Delta S_{\text{immunogenicity-associated}}) = [(B_n)(A_n)] \quad (3)$$

where  $B_n$ : the altered immunogenicity-associated loss ( $\% \Delta S_{\text{immunogenicity-associated}}$ ) for 'n' h of incubation at RT,  $A_n$ : the total signal loss ( $\% \Delta S$ ) in the samples for the corresponding incubation time (as calculated using eqn (1)).

Similarly, the adsorption-associated analyte loss can be obtained by deducting the altered immunogenicity fraction (eqn (3)) from the total analyte loss corresponding to 100% loss (eqn (1)). The percentage fraction of the total signal loss corresponding to the loss due to non-specific adsorption (Table 1, marked with \*\*) was calculated using eqn (4),

$$[(100 - B_n)A_n] \quad (4)$$

Furthermore, these equations are explained in detail with an example in the Theory and analysis section of the ESI†.

Moreover, the immunogenicity-associated loss in untreated tubes could also be determined by eqn (5) (Table 2). A comparison of samples incubated in untreated tubes for 12 h at RT with the samples in untreated tubes for 12 h at 4 °C is informative (eqn (5), Table 2). The fractions corresponding to loss due to adsorption and immunogenicity are listed in Table 1.

## Results and discussions

### Evaluation of the protein loss in unblocked PP tubes

The loss of HFA (initial concentration ( $C_0$ ) = 10 ng mL<sup>-1</sup>) and HRP-labeled mouse IgG (initial concentration ( $C_0$ ) = 300 ng mL<sup>-1</sup>) over the time was quantified by the BCA assay (Fig. 2). The relative loss was calculated as a difference between the initial ( $C_0$ ) and recovered ( $C_T$ ) concentrations of the analyte in solution [ $C_0 - C_T$ ]. The analyte loss obtained with the BCA assay was also compared and correlated with SPR and ELIA (Fig. 2, Table 1 and Fig. S1a and c, ESI†). However, the analyte loss shown with the BCA assay was considerably lower than that found with SPR and ELIA.

This difference in loss calculated using the BCA assay with respect to ELIA and SPR is due to the nature of the analytical approach. BCA measures the total protein content in the solution and does not distinguish the conformationally compromised analyte from its active form. Therefore only the protein loss attributed to adsorption is accountable in the case of BCA assay. However, ELIA and SPR are highly sensitive approaches and

losses due to both adsorption and the analyte conformation changes are detectable. This results in a higher % signal loss due to analyte loss. There was no significant loss obtained with the BCA assay for the samples incubated in untreated tubes for 0 h and 0.5 h. Whereas, a consistent increase in the percentage loss was obtained with ELIA and SPR as a function of the increasing incubation time.

The protein loss was higher in GT tubes in comparison to PP tubes (Fig. S2, ESI†). This differential analyte loss behaviour was attributed to the chemical nature of the tube material used. The data obtained for HFA were validated with a HRP-labeled mouse IgG-based two component system (Fig. S3, ESI†). Similar results were obtained with the HRP-labeled mouse IgG and were in accordance with the previous reports on the loss of immunoglobulin from the solution.<sup>27</sup> However, HFA (59 kDa) is

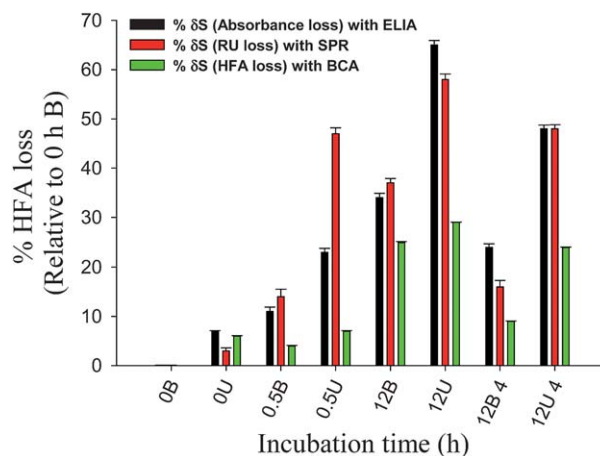


**Fig. 2** Analysis of the protein analyte (HFA) loss due to non-specific adsorption and the conformation-related immunogenicity as a function of percentage signal loss. The BCA assay was employed initially to quantify the HFA loss (initial concentration ( $C_0$ ) of 10 ng mL<sup>-1</sup>) in the BSA-treated (B) and untreated (U) sample tubes (the numerical value before B and U corresponds to the time of incubation in hours). The findings of the BCA assay were cross-validated to immunoassay formats with a sandwich ELIA and SPR. The '12B 4' and '12U 4' correspond to the 12 h incubation of HFA performed at 4 °C in BSA-treated and untreated tubes, respectively. Error bars represent the standard deviation. The % loss was expressed relative to the signal obtained for samples incubated in blocked tubes at 0 h incubation (equivalent to 100% signal) and was calculated using eqn (1).

**Table 2** Determination of the immunogenicity-associated loss for HFA samples incubated in BSA-treated and untreated tubes for 12 h at 4 °C<sup>a</sup>

	In BSA-treated tubes (eqn (2))	In untreated tubes (eqn (5))
$\% \Delta S_{\text{immunogenicity-associated}}$	30*	28*
Immunogenicity-associated loss as a % of the total loss	10**	18**

<sup>a</sup> \* The calculations pertaining to the immunogenicity-associated analyte loss were performed using either eqn (2), or the modified version of eqn (2), as mentioned in eqn (5).  $\% \Delta S_{\text{immunogenicity-associated}}$  in untreated tubes =  $[\{1 - (S_{12h \text{ U RT}}/S_{12h \text{ U } 4^\circ\text{C}})\} - \{1 - (S_{12h \text{ B RT}}/S_{12h \text{ B } 4^\circ\text{C}})\}] \times 100$  eqn (5) determines the compromised immunogenicity-associated loss in untreated tubes by comparing samples incubated in untreated tubes for a 12 h duration at 4 °C and RT. This comparison will provide the losses due to the altered immunogenicity by deducting adsorption-associated losses in unblocked tubes. Fraction  $[\{1 - (S_{12h \text{ U RT}}/S_{12h \text{ U } 4^\circ\text{C}})\}]$  in eqn (5) corresponds to the loss due to the altered immunogenicity and adsorption but the fraction  $[\{1 - (S_{12h \text{ B RT}}/S_{12h \text{ B } 4^\circ\text{C}})\}]$  corresponds to adsorption losses. Therefore, by deducting adsorption losses from the earlier will give the altered immunogenicity-associated losses in untreated tubes. \*\* Contribution of  $\% \Delta S_{\text{immunogenicity-associated}}$  toward total signal loss (Table 1, \*\*) was calculated using eqn (3).

a relatively smaller molecule in comparison to the HRP-labeled mouse IgG molecule (194 kDa). This significant size difference between HFA and the mouse IgG–HRP conjugate significantly changes the adsorption behaviour although the loss behaviour follows the same pattern for both analytes.

### Effect of tube-blocking on the protein analyte loss

The tube surface was treated with 1% (w/v) bovine serum albumin (BSA), which is a routine blocking agent for various immunoassays. Tubes were incubated with 1% (w/v) BSA for 30 min followed by washing with 0.15 M PBS, pH 7.4, and dried under  $N_2$ .

The percentage signal loss (protein analyte loss) in the blocked tubes was analyzed using the same procedure as described previously for the untreated tubes. A comparative analysis was made for the analyte loss obtained for test samples incubation in BSA-treated and untreated tubes over a 12 h incubation period (Fig. 2).

A significant decrease ( $p \leq 0.05$ ) in the amount of protein loss was achieved by blocking the tubes with 1% (w/v) BSA. However, it is advisable to optimize the surface blocking as a function of BSA concentrations and tube-treatment times for all types of polymers as the adsorption kinetics of the blocking proteins are dependent on the chemical nature of the surface to be treated.

The tube treatment significantly improved the available antigen concentration in solution and, hence, various analytical features of the assays (Table S1, ESI†). However, while a certain amount of analyte loss was observed in the BSA-treated tubes with 12 h incubation, it was significantly less ( $p \leq 0.05$ ), in comparison to the untreated tubes (Fig. S1a–d, ESI†). This signal loss in blocked tubes may be due to the nature of BSA, which has a tendency to bind reversibly to a variety of potential analytes, thus developing a dynamic interaction between the BSA adsorbed on the tube surface and the free analyte in solution.<sup>28,29</sup>

The effect of tube-blocking was also analyzed in a direct assay format by incubating HRP-labeled mouse IgG in the untreated and BSA-treated tubes, and assaying with immobilized goat anti-mouse IgG (Fig. S3, ESI†). The results obtained were found to correspond to those with HFA.

### Evaluation of the contribution of the HFA fraction with conformation-related impaired immunogenicity

The loss of protein activity as a result of conformational changes on solid–liquid interfaces<sup>29–32</sup> or due to molecular flattening/spreading<sup>33</sup> has already been demonstrated. However, analysis of protein losses due to these phenomena and their effects on the bio/immunoassay performance have not been reported. It was shown that adsorption may be a potential source of conformational stress on protein molecules, which may result in a compromised immunogenicity. Therefore, in this study an attempt was made to assess the contribution of the immunogenicity loss to the loss of signal in samples incubated for 12 h at room temperature. This fraction of signal loss was quantified by calculating the difference in the signals obtained for samples incubated in BSA-treated and untreated tubes at room

temperature and comparing them with samples incubated in BSA-treated tubes at 4 °C using eqn (2). These calculations were initially based upon previous reports stating that the conformation-associated activity of a protein is retained at lower temperatures in the order of 4 °C > RT > 37 °C.<sup>34–38</sup> Therefore, the signal loss contributed by the fraction of HFA with the impaired immunogenicity will be minimal for the samples incubated in BSA-blocked tubes at 4 °C. There was a substantial signal loss due to this phenomenon, which was significantly greater in the samples incubated in untreated tubes. As claimed in many studies<sup>29–33</sup> the compromised immunogenicity loss may be a result of the conformational stress/change induced either by solid–liquid interface or by molecular spreading of proteins in physisorbed systems that increases over the period of incubation.

The adsorption-associated loss ( $\% \Delta S_{\text{adsorption}}$ ) obtained for samples incubated at RT and the total loss ( $\% \Delta S$ ) in samples incubated at 4 °C for 12 h were equivalent ( $p \leq 0.001$ ) (Tables 1 and 2). These findings justify our assumption that there were significant reductions in the losses due to the impaired immunogenicity of the HFA samples incubated at 4 °C for a duration of 12 h. One explanation may be that the kinetics of proteins in solution reduces significantly at lower temperatures. Therefore, with less movements in the solution, the probability of analyte interactions with the surface is also reduced.

The results obtained indicate that epitope-conformation changes and related immunogenicity alterations contribute significantly to the apparent loss of analytes during sample preparation and processing, and may be significantly minimized by using BSA-blocked tubes at 4 °C.

### Evaluation of the signal loss due to the nature of tube material

The dependence of the protein loss on the chemical composition of the sample tubes (PP and glass (GT)) was analyzed. The % signal losses obtained for HFA sampling in BSA-treated and untreated PP tubes were significantly lower than the corresponding values obtained in GT tubes even though GT tubes were customized for low protein adsorption. This protein adsorption behaviour strongly supports the previous reports, where hydrophilic self-assembled monolayers (SAMs) were found to be more active in terms of protein adsorption than hydrophobic SAMs.<sup>10,39,40</sup> A similar finding was also reported for silica-based nanoparticulate material.<sup>41</sup> However, the BSA-treatment significantly reduced the analyte losses due to non-specific adsorption in both type of tubes (Fig. S4, ESI†). Therefore, the use of pre-treated sample tubes significantly reduced analyte losses and this is of major significance to generate accurate assay results, minimise the loss of analytes and leads to a greater reproducibility in immunoassays based on different assay/biosensor formats.

### Conclusions

In the design of any assay involving protein analytes it is necessary to carefully select the tubes used and it may be necessary to pre-treat (block) them to minimise losses due to non-specific adsorption or alterations in the immunogenicity. Careful selection of temperature is also required. It is advisable to optimise these parameters in relation to each protein studied.

A model approach was developed to assist in the rationale understanding of the issues involved.

## Acknowledgements

We acknowledge Bristol-Myers Squibb (BMS), Syracuse, USA and the Industrial Development Authority, Ireland, for financial support under the CBAS project code 116294. This material is based in part on works supported by the Science Foundation Ireland (Grant 05/CE3/B754), and the Biomedical Diagnostics Institute (BDI), all of which are gratefully acknowledged.

## References

- 1 M. Horie, K. Nishio, K. Fujita, S. Endoh, A. Miyauchi, Y. Saito, H. Iwahashi, K. Yamamoto, H. Murayama, H. Nakano, N. Nanashima, E. Niki and Y. Yoshida, *Chem. Res. Toxicol.*, 2009, **22**, 543–553, DOI: 10.1021/tx800289z.
- 2 D. H. Krieter and B. Canaud, *Nephrol., Dial., Transplant.*, 2003, **18**, 651–654, DOI: 10.1093/ndt/gfg054.
- 3 N. Tomisawa and A. Yamashita, *J. Artif. Organs*, 2009, **12**, 194–199, DOI: 10.1007/s10047-009-0469-0.
- 4 R. Walsh and M. Coles, *Clin. Chem. (Washington, D. C.)*, 1980, **26**, 496–498.
- 5 C. C. Wu and G. C. Chen, *Anal. Biochem.*, 1989, **177**, 178–182, DOI: 10.1016/0003-2697(89)90036-5.
- 6 S. J. Bark and V. Hook, *J. Proteome Res.*, 2007, **6**, 4511–4516, DOI: 10.1021/pr070294o.
- 7 D. Dutta, S. K. Sundaram, J. G. Teeguarden, B. J. Riley, L. S. Fifield, J. M. Jacobs, S. R. Addleman, G. A. Kaysen, B. M. Moudgil and T. J. Weber, *Toxicol. Sci.*, 2007, **100**, 303–315, DOI: 10.1093/toxsci/kfm217.
- 8 C. A. Haynes and W. Norde, *Colloids Surf., B*, 1994, **2**, 517–566.
- 9 C. A. Haynes and W. Norde, *J. Colloid Interface Sci.*, 1995, **169**, 313–328, DOI: 10.1006/jcis.1995.1039.
- 10 B. Menaa, M. Herrero, V. Rives, M. Lavrenko and D. K. Eggers, *Biomaterials*, 2008, **29**, 2710–2718, DOI: 10.1016/j.biomaterials.2008.02.026.
- 11 B. Menaa, C. Torres, M. Herrero, V. Rives, A. R. W. Gilbert and D. K. Eggers, *Biophys. J.*, 2008, **95**, L51–L53.
- 12 K. Nakanishi, T. Sakiyama and K. Imamura, *J. Biosci. Bioeng.*, 2001, **91**, 233–244, DOI: 10.1016/S1389-1723(01)80127-4.
- 13 L. F. Waanders, K. Chwalek, M. Monetti, C. Kumar, E. Lammert and M. Mann, *Proc. Natl. Acad. Sci. U. S. A.*, 2009, **106**, 18902–18907, DOI: 10.1073/pnas.0908351106.
- 14 N. Weib, W. Wente and P. Muller, *Eppendorf Applications*, 2008.
- 15 B. McDonnell, S. Hearty, P. Leonard and R. O’Kennedy, *Clin. Biochem.*, 2009, **42**, 549–561, DOI: 10.1016/j.clinbiochem.2009.01.019.
- 16 C. K. Dixit, S. K. Vashist, F. T. O’Neill, B. O’Reilly, B. D. MacCraith and R. O’Kennedy, *Anal. Chem.*, 2010, **82**, 7049–7052, DOI: 10.1021/ac101339q.
- 17 M. Wahlgren and T. Arnebrant, *Trends Biotechnol.*, 1991, **9**, 201, DOI: 10.1016/0167-7799(91)90064-O.
- 18 S. Sui, H. Wu, J. Sheng and Y. Guo, *J. Biochem. (Tokyo)*, 1994, **115**, 1053–1057.
- 19 V. Hlady and J. Buijs, *Curr. Opin. Biotechnol.*, 1996, **7**, 72, DOI: 10.1016/S0958-1669(96)80098-X.
- 20 A. M. Moulin, S. J. O’Shea, R. A. Badley, P. Doyle and M. E. Welland, *Langmuir*, 1999, **15**, 8776–8779, DOI: 10.1021/la990416u.
- 21 P. Roach, D. Farrar and C. C. Perry, *J. Am. Chem. Soc.*, 2005, **127**, 8168–8173, DOI: 10.1021/ja042898o.
- 22 C. Pérez-Rodríguez, N. Montano, K. Gonzalez and K. Griebenow, *J. Controlled Release*, 2003, **89**, 71, DOI: 10.1016/S0168-3659(03)00074-9.
- 23 K. Goyal, L. J. Walton and A. Tunnacliffe, *Biochem. J.*, 2005, **388**, 151–157, DOI: 10.1042/BJ20041931.
- 24 P. Capasso, M. Aliprandi, G. Ossolengo, F. Edenhofer and A. de Marco, *BMC Biotechnol.*, 2009, **9**, 80, DOI: 10.1186/1472-6750-9-80.
- 25 J. Satulovsky, M. A. Carignano and I. Szleifer, *Proc. Natl. Acad. Sci. U. S. A.*, 2000, **97**, 9037–9041.
- 26 R. M. A. Azzam, P. G. Rigby and J. A. Krueger, *Phys. Med. Biol.*, 1977, **22**, 422–430.
- 27 C. M. Alves, R. L. Reis and J. A. Hunt, *J. R. Soc., Interface*, 2010, **7**, 1367–1377, DOI: 10.1098/rsif.2010.0022.
- 28 Y. L. Jeyachandran, J. A. Mielczarski, E. Mielczarski and B. Rai, *J. Colloid Interface Sci.*, 2010, **341**, 136–142, DOI: 10.1016/j.jcis.2009.09.007.
- 29 K. C. Kwok, K. M. Yeung and N. H. Cheung, *Langmuir*, 2007, **23**, 1948–1952, DOI: 10.1021/la061779e.
- 30 C. S. Lee and G. Belfort, *Proc. Natl. Acad. Sci. U. S. A.*, 1989, **86**, 8392–8396.
- 31 W. Norde and J. P. Favier, *Colloids Surf.*, 1992, **64**, 87–93.
- 32 M. Rabe, D. Verdes, J. Zimmermann and S. Seeger, *J. Phys. Chem. B*, 2008, **112**, 13971–13980, DOI: 10.1021/jp804532v.
- 33 G. Raffaini and F. Ganazzoli, *Langmuir*, 2010, **26**, 5679–5689, DOI: 10.1021/la903769c.
- 34 É. Kiss, *Colloids Surf., A*, 1993, **76**, 135, DOI: 10.1016/0927-7757(93)80071-L.
- 35 A. Kondo and H. Fukuda, *J. Colloid Interface Sci.*, 1998, **198**, 34, DOI: 10.1006/jcis.1997.5278.
- 36 S. Balamurugan, L. K. Ista, J. Yan, G. P. Lopez, J. Fick, M. Himmelhaus and M. Grunze, *J. Am. Chem. Soc.*, 2005, **127**, 14548–14549, DOI: 10.1021/ja054156g.
- 37 X. Cheng, H. E. Canavan, D. J. Graham, D. G. Castner and B. D. Ratner, *Biointerphases*, 2006, **1**, 61–72, DOI: 10.1116/1.2187980.
- 38 N. E. Idenyi, C. E. Ekuma and A. E. Umahi, *Biotechnology*, 2006, **5**, 429–435.
- 39 V. Silin, H. Weetall and D. J. Vanderah, *J. Colloid Interface Sci.*, 1997, **185**, 94–103, DOI: 10.1006/jcis.1996.4586.
- 40 Q. Wang, J. Wang, P. H. Geil and G. W. Padua, *Biomacromolecules*, 2004, **5**, 1356–1361, DOI: 10.1021/bm049965r.
- 41 B. Menna, F. Menna, C. Aiolfi-Guimaraes and O. Sharts, *Int. J. Nanotechnol.*, 2010, **7**, 1–45.

## Novel Multiparametric Approach to Elucidate the Surface Amine-Silanization Reaction Profile on Fluorescent Silica Nanoparticles

Shibsekhar Roy,<sup>†</sup> Chandra K. Dixit,<sup>‡</sup> Robert Woolley,<sup>†</sup> Brian D. MacCraith,<sup>†</sup>  
Richard O'Kennedy,<sup>‡</sup> and Colette McDonagh<sup>\*,†</sup>

<sup>†</sup>National Biophotonics and Imaging Platform, School of Physical Sciences and <sup>‡</sup>School of Biotechnology,  
Dublin City University, Glasnevin, Dublin 9, Ireland

Received August 12, 2010. Revised Manuscript Received October 18, 2010

This Article addresses the important issue of the characterization of surface functional groups for optical bioassay applications. We use a model system consisting of spherical dye-doped silica nanoparticles (NPs) that have been functionalized with amine groups whereby the encapsulated cyanine-based near-infrared dye fluorescence acts as a probe of the NP surface environment. This facilitates the identification of the optimum deposition parameters for the formation of a stable ordered amine monolayer and also elucidates the functionalization profile of the amine-silanization process. Specifically, we use a novel approach where the techniques of fluorescence correlation spectroscopy (FCS) and fluorescence lifetime measurement (FL) are used in conjunction with the more conventional analytical techniques of zeta potential measurement and Fourier transfer infrared spectroscopy (FTIR). The dynamics of the ordering of the amine layer in different stages of the reaction have been characterized by FTIR, FL, and FCS. The results indicate an optimum reaction time for the formation of a stable amine layer, which is optimized for further biomolecular conjugation, whereas extended reaction times lead to a disordered cross-linked layer. The results have been validated using an immunoglobulin (IgG) plate-based direct binding assay where the maximum number of IgG-conjugated aminated NPs were captured by immobilized anti-IgG antibodies for the NP sample corresponding to the optimized amine-silanization condition. Importantly, these results point to the potential of FCS and FL as useful analytical tools in diverse fields such as characterization of surface functionalization.

### 1. Introduction

The use of fluorescence-based nanoparticles (NPs) as high brightness labels in the field of nanobiophotonics has potential in the broad area of clinical diagnostics.<sup>1</sup> The essential criteria to construct an efficient high brightness label involves the tuning of primarily two major properties (i) the brightness and (ii) the target specificity. The latter, which is the focus of this Article, is achieved by functionalizing<sup>2</sup> the NP with appropriate surface chemistry, which facilitates the conjugation of the relevant biomolecule, for example, an antibody in the case of NP-based immunosensing.<sup>3,4</sup> For this attachment, several surface functionalization strategies are available such as amine-silanization,<sup>5</sup> thiol-silanization,<sup>6</sup> and epoxylation.<sup>7</sup> Optimum conjugation requires a well-ordered surface,<sup>8</sup> which enables conjugation of the antibody with proper functional conformation so as to avoid steric hindrance of binding to the target antigen.

Silica NPs have advantages such as high brightness compared with single dye molecule probes, tunability of size, ease of surface functionalization, and relative biocompatibility. These properties are advantageous to design efficient bioassays with decreased limit

of detection (LOD)<sup>9</sup> as well as the use of the NPs as cellular probes.<sup>10</sup> There are two main approaches to the synthesis of highly fluorescent silica NPs, the Stöber sol–gel process,<sup>11</sup> and the reverse microemulsion<sup>12</sup> approach, which is the approach used here.

Standard conjugation strategies normally involve covalent linker-based attachment chemistry. The approach used here involves an amine functionalization strategy using aminopropyl triethoxy silane (APTES).<sup>13</sup> The availability of free hydroxyl groups on the silica surface facilitates the surface functionalization of the NP. The ability of silanes such as APTES to form siloxane bonds by reacting with the silanol hydroxyl groups, makes them useful in silica functionalization. In this work, to achieve a homogeneous, ordered amine surface layer, we adopted an APTES-based self-assembly approach.

Techniques like ellipsometry,<sup>14,15</sup> contact-angle goniometry,<sup>15</sup> and X-ray photoelectron spectroscopy<sup>16</sup> are useful to measure the amine layer thickness on a flat surface, more popularly on the glass surface<sup>15–17</sup> or silicon wafers,<sup>17</sup> but these techniques fall short

\*Corresponding author. E-mail: Colette.McDonagh@dcu.ie.

(1) Wang, L.; Tan, W. *Nano Lett.* **2006**, *6*, 84–88.  
(2) Giaume, D.; Poggi, M.; Casanova, D.; Mialon, G.; Lahlil, K.; Alexandrou, A.; Gacoin, T.; Boilot, J. *Langmuir* **2008**, *24*, 11018–11026.  
(3) Pei, X.; Zhao, Y.; Zhao, X.; Xu, H.; Chen, B.; Gu, Z. *J. Nanosci. Nanotechnol.* **2009**, *9*, 6320–6325.  
(4) Wang, Y.; Liu, B. *Biosens. Bioelectron.* **2009**, *24*, 3293–3298.  
(5) Shen, G.; Horgan, A.; Levicky, R. *Colloids Surf., B* **2004**, *35*, 59–65.  
(6) Kommareddy, S.; Amiji, M. *Bioconjugate Chem.* **2005**, *16*, 1423–1432.  
(7) Vejayakumaran, P.; Rahmana, I. A.; Sipaut, C. S.; Ismail, J.; Chee, C. K. *J. Colloid Interface Sci.* **2008**, *328*, 81–91.  
(8) Tsukruk, V. V.; Rinderspacher, F.; Bliznyuk, V. N. *Langmuir* **1997**, *13*, 2171–2176.

(9) Hun, X.; Zhang, Z. *Talanta* **2007**, *73*, 366–371.  
(10) Bakalova, R.; Zhelev, Z.; Aoki, I.; Masamoto, K.; Mileva, M.; Obata, T.; Higuchi, M.; Gadjeva, V.; Kanno, I. *Bioconjugate Chem.* **2008**, *19*, 1135–1142.  
(11) Nakamura, M.; Shono, M.; Ishimura, K. *Anal. Chem.* **2007**, *79*, 6507–6514.  
(12) Wu, H.; Huo, Q.; Varnum, S.; Wang, J.; Liu, G.; Nie, Z.; Liu, J.; Lin, Y. *Analyst* **2008**, *133*, 1550–1555.  
(13) Gao, F.; Luo, F.; Yin, J.; Wang, L. *Luminescence* **2008**, *23*, 392–396.  
(14) Miksa, D.; Irish, E. R.; Chen, D.; Composto, R. J.; Eckmann, D. M. *Biomacromolecules* **2006**, *7*, 557–564.  
(15) Lee, M. H.; Brass, D. A.; Morris, R.; Composto, R. J.; Ducheyne, P. *Biomaterials* **2005**, *26*, 1721–1730.  
(16) Wang, Y.; Yuan, K.; Li, Q.; Wang, L.; Gu, S.; Pei, X. *Mater. Lett.* **2005**, *59*, 1736–1740.  
(17) Flink, S.; van Veggel, F. C. J. M.; Reinhoudt, D. N. *J. Phys. Org. Chem.* **2001**, *14*, 407–415.

for NP-based systems because of the very small thickness of the amine layer<sup>15,17</sup> on the NP surface compared with the NP diameter. This significantly limits the detection by the aforesaid methods. Another important technique, FTIR, has also been used<sup>18,19</sup> to elucidate the dynamics of APTES-based amine layer growth on a planar silica surface, but the dynamics as well as the time course of the reaction on the nanosurface have not yet been reported in detail to our knowledge. In this Article, we have not only extended the study of the amine-silanization profile to the nanosurface of dye-doped silica NPs but also introduced fluorescence lifetime (FL)<sup>20</sup> and fluorescence correlation spectroscopy (FCS)<sup>21,22</sup> to complement the conventionally used techniques for NPs like zeta potential measurement and FTIR to construct a complete reaction profile for the surface amine-silanization of the NPs. The advantage of fluorescence-based techniques lies in high sensitivity detection. In our system, the near-infrared dye, 4,5-benzo-5'-(iodoacetaminomethyl)-1',3,3,3',3'-pentamethyl-1-(4-sulfobutyl)-indodicarbocyanine (NIR664), has been covalently encapsulated in the silica NPs by the microemulsion method. The cyanine-based dyes are very efficient sensors of chemical environment because of their strong fluorescence response to the hydrophobicity of the immediate microenvironment<sup>23</sup> that actually alters the equilibrium between the monomer and aggregate states of the dye, having distinct absorption peaks at 665 and 615 nm, respectively. While encapsulated inside a NP, the dye is distributed in two distinct populations, and thus any significant alteration at the immediate microenvironment of the dye doped NP can be sensed by this dynamic equilibrium. Hence, we have applied the fluorescence-based techniques of FCS and FL measurement to probe the behavior of the dye under the influence of the immediate microenvironment of the aminated NP surface. The dual component FL behavior of the dye in the NP has recently been reported by our group, which describes smaller (say t1) and larger (say t2) components as representative for the core fraction and a more solvent accessible, that is, a peripheral fraction.<sup>24</sup> This has been used here as a useful tool for characterizing the surface functionalization.

Regarding FCS, several parameters have been reported to be critical in describing some key biomolecular reactions by various groups. Flomenbom et al. have reported on the stretching of fluorescence correlation decay to elucidate a protease activity.<sup>25</sup> Kohl et al. also used fluorescence cross-correlation to determine protease activity and presented relative cross-correlation as an interesting tool to investigate the reaction kinetics.<sup>26</sup> Later, Prakash et al. addressed the fluctuation of enzymatic catalysis by using the autocorrelation function (ACF).<sup>27</sup> Recently, protein folding dynamics has been addressed by FCS.<sup>28</sup> Of late, the important application of this versatile technique in the field of nanoprobe

characterization has been published by the Wiesner group,<sup>29</sup> who have shown the FCS signatures of dye within a NP. We have extended the application of this technique to probe the surface functionalization of the NP, in particular, to elucidate the detailed structure of the amine functional layer as a function of APTES exposure.

A key achievement of this work is the use of multiple characterization techniques, including some novel approaches, to achieve an optimized ordered amine layer. The model system used is a dye-doped silica NP where the dye fluorescence is sensitive to the NP surface environment. This enables the use of novel techniques such as FL and FCS, in combination with FTIR and other techniques, to monitor the growth and conformation of amine groups on the surface.

## 2. Experimental Section

**2.1. Synthesis of Dye-Doped NPs.** NIR664 (1.6 mg, Sigma Aldrich) solubilized in 1-hexanol (Sigma Aldrich) was reacted with 1  $\mu$ L of mercaptopropyl triethoxy silane (MPTES, Sigma Aldrich) in a nitrogen atmosphere with constant stirring at room temperature for 3 to 4 h. The iodoacetamide part drives the reaction by interacting with the thiol group to form covalent conjugation. For the particle synthesis, we prepared a microemulsion by mixing 3.78 g Triton X-100 (Sigma Aldrich), 15 mL of cyclohexane (Sigma Aldrich), 1.6 mL of hexanol (Sigma Aldrich), 2 mL of the conjugated dye, and 0.96 mL of Milli-Q water by stirring for 5 min. After the microemulsion was formed, 200  $\mu$ L of TEOS (Sigma Aldrich) was added to it and stirred for 30 min. Then, 120  $\mu$ L of  $\text{NH}_4\text{OH}$  (Sigma Aldrich) was added to start the alkaline hydrolysis for 24 h. Then, a further 150  $\mu$ L of TEOS was added to the reaction mixture to make a compact silica shell at the exterior of the NP. It was then washed four times with ethyl alcohol (Sigma Aldrich) in 9000 rpm for 25 min and finally resuspended in ethyl alcohol. The TEM picture of the  $\sim$ 80 nm NP can be found in Figure s1 of the Supporting Information.

**2.2. Amine-Silanization of the NPs.** The kinetics study was performed to study silanization behavior of APTES (Sigma Aldrich, Ireland) on NPs. Silanization was performed with 2% (v/v) APTES prepared in absolute ethanol in a set of five different time points viz. 1, 2, 3, 5, and 12 h, considering nonfunctionalized NP as the control for this study (0 h). Each sample set was fed with a starter batch of NP sample at a concentration of 6 mg/mL. Additionally, a set of NP functionalization with various amine concentrations was performed to find out the optimum working amine concentration. These NPs were subjected to 0.5, 1, 2, and 3% APTES in absolute ethanol for the optimized period from the previous set of experiments again with reference to nonfunctionalized NPs as the control (0% APTES).

**2.3. Thiol-Silanization of the NPs.** For comparison, NPs from the same batch were modified with 2% (v/v) thiol-terminal mercaptopropyltrimethoxysilane (MPTMS) under similar conditions for the same time period at which amine-silanization of NPs was performed. The extent of thiol-silanization was checked spectrophotometrically by using Ellman's reagent (Thermo Fischer, Dublin, Ireland; see Figure s2 of Supporting Information for details).

**Assay Details.** Aminated NPs were conjugated to mouse IgG by using conventional linker chemistry for attaching mouse IgG. NPs (10 mg/mL) were incubated with 4% (v/v) APTES over five different durations, that is, 1, 2, 3, 5, and 12 h. The NP-APTES solution was continuously stirred for corresponding durations. Each set of NP-APTES solution was subjected to centrifugation (15000 rpm) wash with absolute ethanol five times and finally with 0.01 M PBS (pH 7.4). The mouse IgG (990  $\mu$ L of 3  $\mu$ g/mL in 0.1 M PBS, pH 7.4; Sigma Aldrich, Ireland) was incubated with a

(18) Chiang, C.; Ishida, H.; Koenig, J. L. *J. Colloid Interface Sci.* **1980**, *74*, 396–404.

(19) Pena-Alonso, R.; Rubio, F.; Rubio, J.; Oteo, J. L. *J. Mater. Sci.* **2007**, *42*, 595–603.

(20) Berndt, M.; Lorenz, M.; Enderlein, J.; Diez, S. *Nano Lett.* **2010**, *10*, 1497–1500.

(21) Digman, M. A.; Gratton, E. *Wiley Interdiscip. Rev.: Syst. Biol. Med.* **2009**, *1*, 273–282.

(22) Ray, K.; Zhang, J.; Lakowicz, J. R. *Anal. Chem.* **2008**, *80*, 7313–7318.

(23) West., W.; Pearce., S. J. *Phys. Chem.* **1965**, *69*, 1894–1903.

(24) Roy, S.; Woolley, R.; MacCraith, B. D.; McDonagh *Langmuir* **2010**, *26*, 13741–13746.

(25) Flomenbom, O.; Velonia, K.; Loos, D.; Masuo, S.; Cotlet, M.; Engelborghs, Y.; Hofkens, J.; Rowan, A. E.; Nolte, R. J. M.; Van der Auweraer, M.; de Schryver, F. C.; Klafter, J. *Proc. Natl. Acad. Sci. U.S.A.* **2005**, *102*, 2368–2372.

(26) Kohl, T.; Haustein, E.; Schwille, P. *Biophys. J.* **2005**, *89*, 2770–2782.

(27) Prakash, M. K.; Marcus, R. A. *Proc. Natl. Acad. Sci. U.S.A.* **2007**, *104*, 15982–15987.

(28) Neuweiler, H.; Johnson, C. M.; Fersht, A. R. *Proc. Natl. Acad. Sci. U.S.A.* **2009**, *106*, 18569–18574.

(29) Larson, D. R.; Ow, H.; Vishwasrao, H. D.; Heikal, A. A.; Wiesner, U.; Webb, W. W. *Chem. Mater.* **2008**, *20*, 2677–2684.

10  $\mu$ L premixed solution of 1-ethyl-3-[3-dimethylaminopropyl]-carbodiimide hydrochloride (EDC; Thermo Fischer, previously Pierce) (4 mg/mL) and *N*-hydroxysulfosuccinimide (SNHS; Thermo Fischer) (11 mg/mL) for 15 min at 37 °C. The resulting EDC-activated IgG solution was added to the APTES-functionalized NPs, suspended in 0.01 M PBS (pH 7.4), and incubated for 1 h at RT. The IgG-conjugated NP solution was washed five times with 0.01 M PBS pH 7.4. The goat anti-IgG (10  $\mu$ g/mL; Sigma Aldrich) was physisorbed in the microtiter plate wells by incubating for 2 h at 37 °C. Afterward, the plate wells were washed five times with 0.1 M PBS (pH 7.4) and blocked for 30 min with 1% (v/v) bovine serum albumin (BSA; Thermo Fischer) in 0.1 M PBS, pH 7.4 at 37 °C. The plate was subjected to a wash with PBS five times. The IgG-conjugated NPs were incubated in the corresponding anti-IgG immobilized plate wells and incubated for 1 h at 37 °C, followed by five PBS washes. The fluorescence was recorded with Tecan (GmbH, Austria). A 96-well plate was used to incubate goat antimouse IgG on its surface. Unbound anti-IgG was washed away. IgG-conjugated NPs of equal concentrations were added to the anti-IgG plate (in triplicate). After 30 min, the unbound NPs were washed away. The plate was excited at 660 nm and was read at 690 nm.

#### 2.4. Characterization of the Aminated Nanoparticles.

**Zeta Potential Measurement.** The zeta potential for the aminated samples was measured by a Beckman Coulter Instrument by using the flow cell. The average obtained from three measurement sets was analyzed by the DelsaNano software in the Results and Discussion section, where each measurement was the average of 50 individual measurements performed at various positions (10 measurements each in 5 positions) in the flow cell that is set as default.

**FTIR Study.** Liquid FT-IR (Thermo Nicolet Corporation, Madison, WI) was used to characterize the chemical nature of the functionalization on NPs. NPs were resuspended in two sets, one in absolute ethanol and the other in toluene at a concentration of 2 mg/mL for both of the cases. This was done to assess the effect of the solvent-based environment on the FT-IR spectral analysis. The functionalized samples from each set were subjected to FT-IR, and transmittance (%*T*) was recorded. The measurements were baseline-corrected with corresponding solvents. All of these samples were later analyzed using various peaks in the transmission spectra.

**Measuring FL and FCS.** FL and FCS measurements were performed on a MicroTime 200 inverse time-resolved fluorescence microscope (MT200, PicoQuant, Berlin, Germany). The microscope body comprised a modified Olympus IX71 equipped with a 60 $\times$  water immersion lens (UPlanSApo 60 $\times$  1.2 water/CC1.48, Olympus). Sample illumination was achieved using a horizontally polarized 640 nm pulsed diode laser (LDH-P-C640, PicoQuant) operated at 20 MHz. For FL and FCS, a pulsed laser is used to provide the fluorescence excitation, and the detection was performed on two different time scales. The shorter time scale is the picosecond-to-nanosecond one, where the distance between the exciting laser pulses and the photon detection events is tagged with time, whereas the larger time scale of detection is in the range of hundreds of nanoseconds to seconds. The FL is calculated from the decay of the photon intensity. The absolute arrival time recorded for the detected photons is used for calculating the ACF. However, the ACF function is inversely proportional to the number of particles in the illumination volume. Fluorescence was separated from excitation using a 535/640 nm dichroic filter (z532/635rpc, AHF/Chroma) and passed through a 690/70 M emission filter (HQ690/70M, AHF/Chroma). NP suspensions were placed on cleaned microscope coverslips (Sigma) before mounting on the microscope stage. Objective correction collar settings were optimized for minimum sample illumination volumes with maximum detection levels, and all NP lifetime recordings were performed 20  $\mu$ m above the coverslip surface with a recording time of 120 s per sample. Emitted light passed through a polarization independent

50/50 beam splitter (Olympus) and focused onto two single-photon avalanche detectors (SPADs, Micro Photon Devices). Illumination was maintained at 0.2  $\mu$ W at the detectors for all samples. More than 10 000 counts were recorded for each sample, and the resulting lifetime histograms were tail-fit immediately to correct for the influence of the machine response function using double exponential fits. Data were recorded in the time-tagged, time-resolved format (TTTR) format that enabled both lifetime and FCS to be performed on the same data set. All data were analyzed using SymPhoTime (PicoQuant).

**Theoretical Aspects of the Correlation Study.** The fluorescence ACF is denoted by  $G_a$  in eq 1, where  $I_a$  is the fluorescence intensity from channel 1,  $\tau$  is the time delay, and the brackets ( $\langle \rangle$ ) represent the time average (of time  $t$ ) of the bracketed term.

$$G_a(\tau) = \frac{\langle I_a(t)I_a(t+\tau) \rangle}{\langle I_a(t) \rangle \langle I_a(t) \rangle} \quad (1)$$

However, the ACF performed on the solution has been observed to include the instrument response function (IRF) at the beginning of the time scale contributed by both channels 1 and 2. To compensate for the effect of the IRF, the intensities from channels 1 and 2 have been cross-correlated, and the cross-correlation function (CCF), denoted by  $G_{ab}$ , is defined in eq 2, where  $I_a$  and  $I_b$  are the fluorescence intensities of channels 1 and 2, respectively, and the other terms are the same as those in eq 1. Significant improvement of the correlation function is obtained after the ACF is replaced by the CCF, where the CCF acts as a filter for the IRF. For our fluorescence correlation study, CCF has been performed and discussed below.

$$G_{ab}(\tau) = \frac{\langle I_a(t)I_b(t+\tau) \rangle}{\langle I_a(t) \rangle \langle I_b(t) \rangle} \quad (2)$$

Another important advantage of CCF in the application field lies in its ability to quantify the process more accurately as the amplitude of the CCF is proportional to the fluorophore concentration, which can be estimated by applying eq 3, where  $V_{\text{eff}}$  is the effective volume. To equilibrate different sets of aminated NPs, we have normalized the fluorophore concentration by dividing the amplitude of CCF by the amplitude of the ACF for the channel having a smaller fluorophore count. This is referred to as the relative cross-correlation factor to channel 'a' ( $CC_{ra}$ ), as shown in eq 4.<sup>26</sup> For the ACF calculation, the channel having a lower count is chosen over its high counting counterpart. The choice is so because the photon counts, which correlate with the number of fluorophores in the confocal volume, may suffer significantly from fluorescence quenching for a very high concentration of the fluorophore, leading to inaccurate concentration parameters.

$$\langle C_{ab} \rangle = \frac{G_{ab}(0)}{V_{\text{eff}}G_a(0)G_b(0)} \quad (3)$$

$$CC_{ra} = \frac{\langle C_{ab} \rangle}{\langle C_a \rangle} = \frac{G_{ab}(0)}{G_a(0)} \quad (4)$$

A reaction like surface amine-silanization that manipulates the immediate microenvironment of the nanosurface significantly affects the FCS decay by introducing relaxation to the decay time. In this system of reacting molecules, the reaction system is composed of two primary components, the NP surface and hydrolyzed APTES. During the initial stages of this reaction, the nanosurface is considered to be nonhomogeneous because of the incompleteness of the reaction leading to a variety of distributions of surface-attached APTES molecules on the NPs. This heterogeneous distribution of surface-attached APTES is sensed as a disordered microenvironment by the chemically sensitive monomer–aggregate equilibrium of the encapsulated dye, slowing down the correlation decay. It leads to the hypothesis that the decrease in the decay constant can be utilized to monitor the whole reaction with

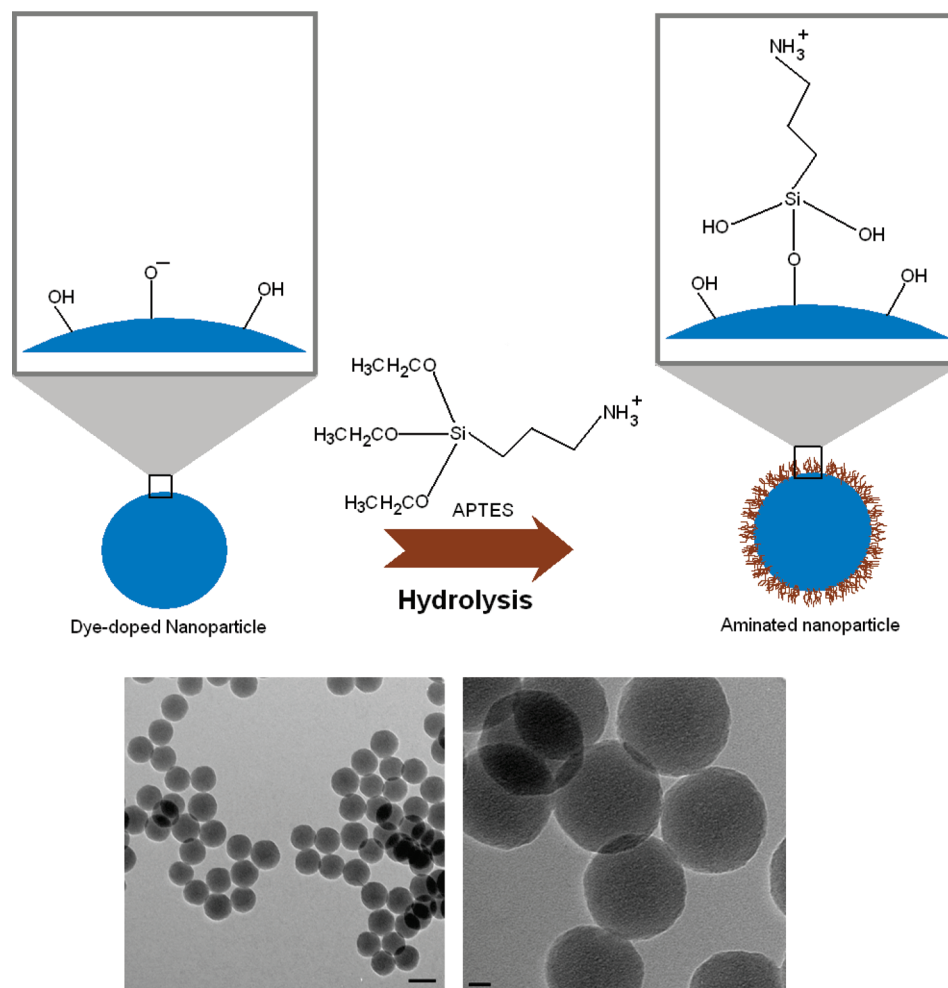


**Figure 1.** Cartoon depicting the amine-silanization reaction with the TEM image of the aminated NP having size bar of 100 and 20 nm length for the left and right images, respectively.

reference to the initial state (i.e., reaction at time 0) with respect to the ordering phenomena of the whole system. The parameter  $\alpha_{\text{cor}}$  is introduced to correlate the decay constants, as shown in eq 5, where  $\alpha_0$  and  $\alpha_t$  are the decay constants at time 0 and  $t$  (hours), respectively. Hence, the parameter  $\alpha_{\text{cor}}$  works as a correlator between the state of the reaction at time,  $t$ , and the initial state of a reaction.

$$\alpha_{\text{cor}} = \frac{\alpha_0 - \alpha_t}{\alpha_0} \quad (5)$$

**Other Characterization Techniques.** For UV–visible spectroscopy, a Cary 50 scan UV–visible spectrophotometer (Varian) was used. For fluorescence spectroscopy, a Fluoromax spectrophotometer was used. Regarding TEM measurement, a Hitachi 7000 transmission electron microscope was operated at 100 kV. Image capture was performed digitally by a Megaview 2 CCD camera. We prepared specimens by putting a drop of the ethanolic solutions of the NPs on a Formvar carbon-coated copper grid (Agar Scientific).

### 3. Results and Discussion

**3.1. Zeta Potential Measurement to Measure Surface Charge.** During the amine-silanization reaction of the NPs by APTES, the negatively charged hydroxyl groups are replaced by the positively charged amine groups (Figure 1). This charge transition on the nanosurface can effectively be measured with zeta

potential measurement. The zeta potential results are shown in Figure 2a. The unmodified NP shows an average zeta potential of  $-35.8$  mV. The NP sample collected after 1 h of incubation with APTES shows a sharp increase of the zeta potential value to  $-8.1$  mV. It continues to increase until it reaches saturation at 3 h with a much higher positive value of  $> 35$  mV signifying the stable deposition of the amine group all over the surface of the NPs. Additionally, the high numerical value of the zeta potential demonstrates the solvent stability of the NPs. However, although this technique is straightforward enough to report the effective deposition of the positively charged amine groups on the negatively charged silica nanosurface, the finer details of the APTES deposition and the formation of the amine monolayer and cross-linked super structures cannot be elucidated. The reason for that is attributed to the fact that upon reaching a critical value of the zeta potential (here, the saturation value), any further conjugation of APTES to the nanosurface is involved in either cross-linking or intermolecular hydrogen bonding engaging the primary amine groups with  $-\text{OH}$  groups (nanosurface silanol group or  $-\text{OH}$  groups of surface-attached APTES molecules), thus limiting a further increase in positive zeta potential value.

**3.2. FTIR Measurement Demonstrates Amine Functionalization.** FTIR has been performed in two solvents, ethanol and toluene, to investigate two different aspects of the silica nanosurface. In ethanol, the emphasis is given toward the replacement kinetics of the silanol ( $\text{Si}-\text{OH}$ ) group by the amine group as a

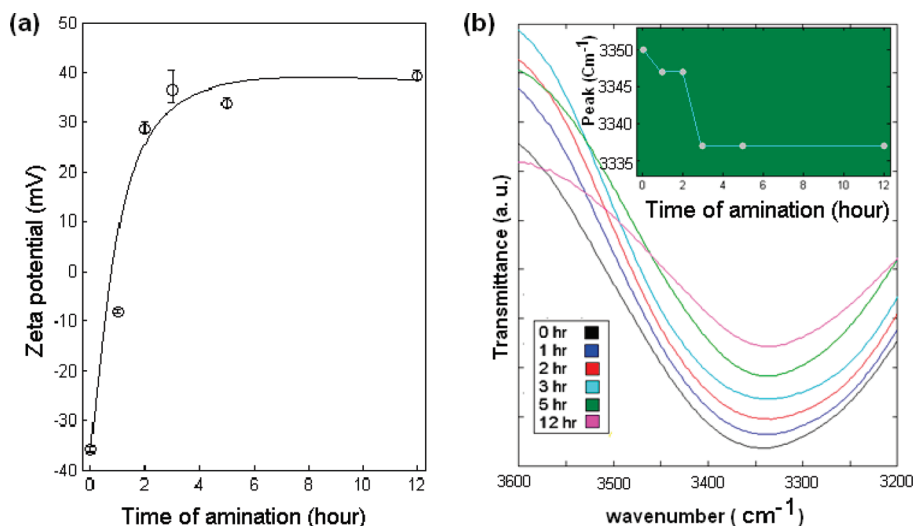


**Figure 2.** (a) Plot of incubation time for APTES with aminated NP suspension versus the zeta potential. (b) FTIR spectra for the same samples where the inset shows peak shift versus time of amine-silanization.

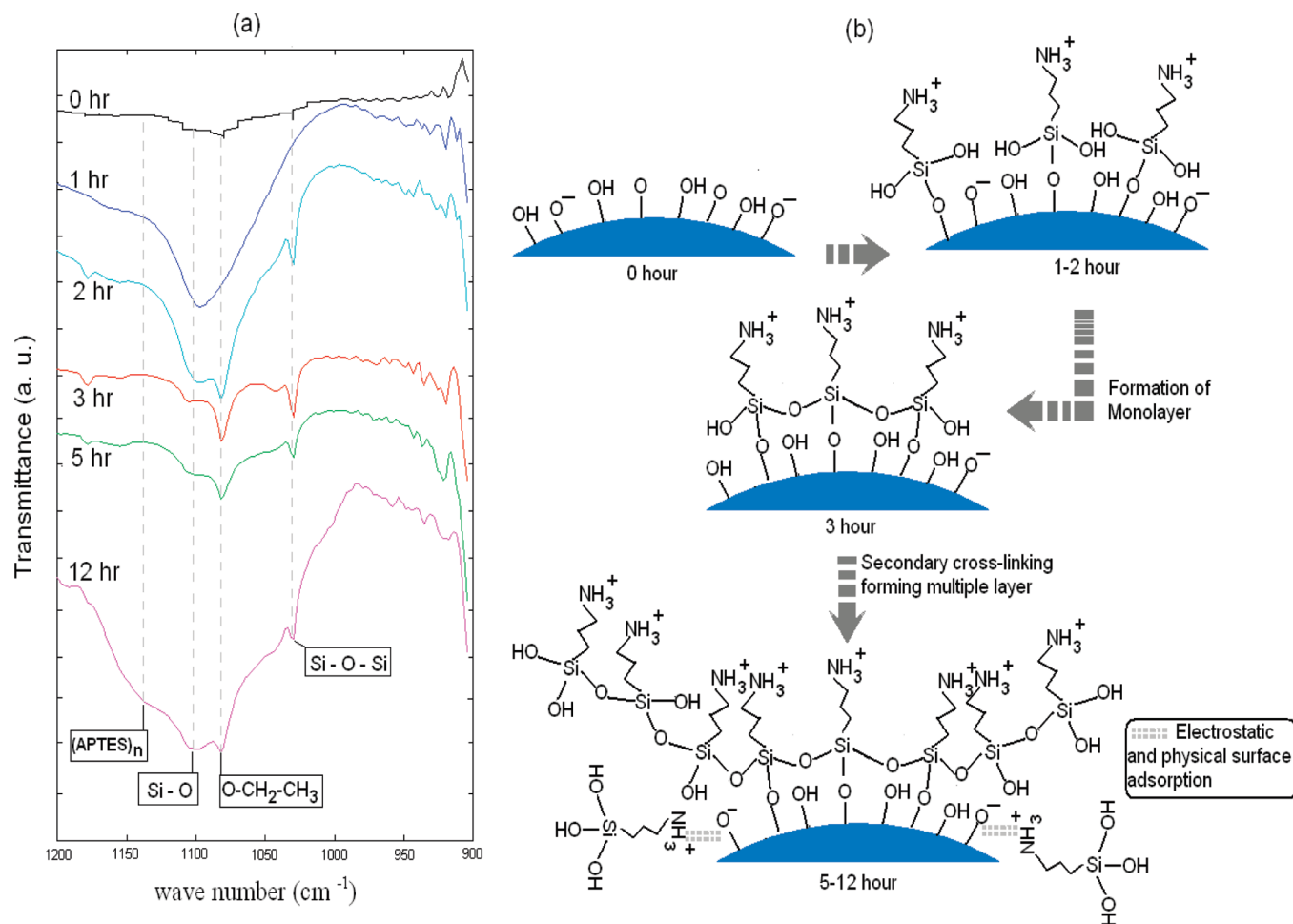


**Figure 3.** (a) FTIR signature of the aminated NP (suspended in toluene) for various reaction times for the 900–1200 cm<sup>-1</sup> region is described to show the conjugation of APTES on the nanosurface. (b) Based on that a cartoon is presented to depict the APTES deposition as a function of reaction time.

result of the siloxane bond formation and deposition of the protonated amine group on the nanosurface. In the toluene environment, however, the fine structure of the surface-stabilized amine groups has been studied to make a detailed account of the whole process because there is no interference from the -OH

groups of the ethanol. First, in the presence of ethanol, the overall amine-silanization process was studied by following the gradual disappearance of the surface siloxane (Si-OH) bond and the corresponding appearance of the amine group for the NPs suspended in ethanol. Both the hydroxyl and amine groups are closely placed

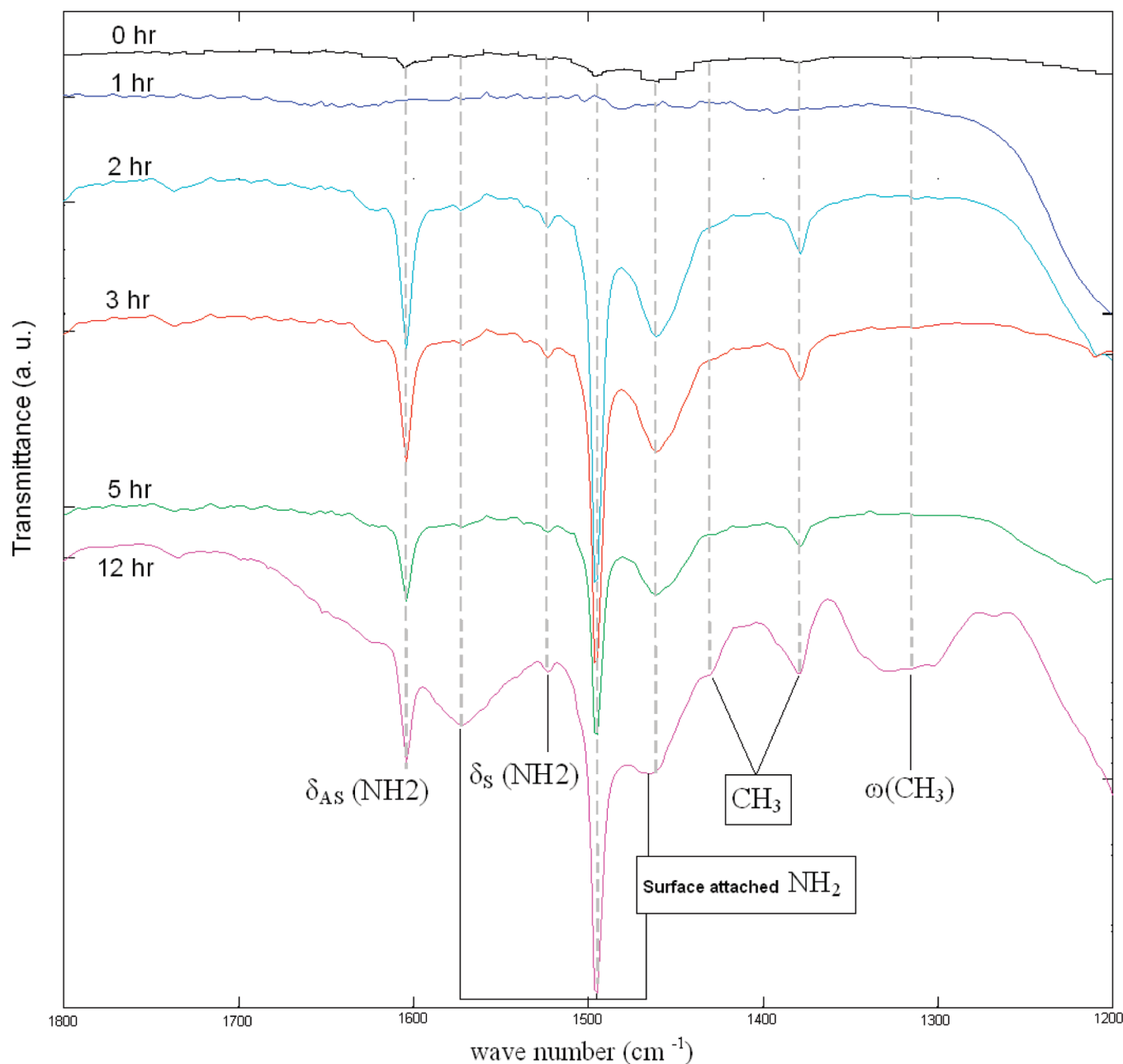


**Figure 4.** FTIR signature of the aminated NP (suspended in toluene) for various reaction times for the 1200–1800  $\text{cm}^{-1}$  region is described to show the evolution of various populations of amine peaks.

at the far end of the FTIR spectrum from 3300 to 3600  $\text{cm}^{-1}$ , signified by a broad peak in this region, but there was a significant kinetic effect to monitor the amine-silanization by assessing the shift of the peak value of the broad peak from 3350 to 3337  $\text{cm}^{-1}$ , as observed in Figure 2b. When this value of the wavenumber for the corresponding peaks was plotted against the time of NPs incubation with APTES, time kinetics was obtained, showing saturation after 3 h, which is shown in the inset of Figure 2b. Therefore, like the zeta potential measurement, FTIR indicates saturation kinetics after 3 h of reaction.

FTIR studies performed on the NPs suspended in toluene have shown several fine structures arising from the amine groups attached to the nanosurface and the attachment between the silica surface and the APTES moiety. The FTIR spectrum has been divided into two major parts to analyze the kinetics; the first segment to be discussed is the region between 1200 and 1800  $\text{cm}^{-1}$ ,

which deals with various responses from the amine groups, and the second region spans from 900 to 1200  $\text{cm}^{-1}$ , which mainly deals with the covalent attachment of the silica surface with the APTES. Figure 3a shows the response of the 900 to 1200  $\text{cm}^{-1}$  region. It shows that the Si–O bonds began forming from the first hour of reaction from the 1110  $\text{cm}^{-1}$  peak, but the effective conjugation has started from the second hour of the reaction with the appearance of the conjugation peaks like Si–O–Si at 1030  $\text{cm}^{-1}$  and ethoxy group ( $-\text{OCH}_2\text{CH}_3$ ) at 1080  $\text{cm}^{-1}$ . Looking at the reaction steps of the amine-silanization given in the cartoon in Figure 3b, it is evident that the first step is the conjugation of surface –OH group with the hydrolyzed APTES, which is followed by Si–O–Si bond formation between surface-attached APTES molecules to form the amine monolayer. This agrees well with the data. It can be seen that the rate of Si–O–Si peak formation is much higher up to the third hour. For the NPs with higher APTES

incubation time (i.e., 5 and 12 h), there is a steep increase in the ethoxy group ( $-\text{OCH}_2\text{CH}_3$ ) at  $1080\text{ cm}^{-1}$  signifying incomplete hydrolysis of APTES and significant increase in siloxane groups ( $\text{Si}-\text{O}-\text{Si}$ ) at  $1110\text{ cm}^{-1}$ , implying cross-linking between the surface bound and free APTES leading to multiple inhomogeneous layers of amine groups on the nanosurface. In addition, the broad shoulder starting from  $1125\text{ cm}^{-1}$  signifies the polymerized or physically adsorbed APTES on the nanosurface that is very prominent in the 12 h incubation sample. A cartoon based on these detailed features during the amine-silanization process is presented in Figure 3b.

To study the detailed amine group kinetics during this amine-silanization reaction, we studied the  $1200$  to  $1800\text{ cm}^{-1}$  spectrum of the aminated NPs in detail, which is shown in Figure 4. The characteristic FTIR peaks of the amine groups have been identified in detail. The asymmetric and symmetric deformation modes of amine groups due to the surface-adsorbed APTES molecules have been observed at  $1610$  and  $1510\text{ cm}^{-1}$ , respectively. These two peaks originate from the interaction between the acidic silanol group on the nanosurface and basic amino group of the APTES. The deformation modes of amine groups at  $1575$  and  $1493\text{ cm}^{-1}$ , which appear because of the hydrogen bond formation by the amine group presumably with atmospheric carbon dioxide, increase with the time of APTES incubation and show significantly higher density in the 12 h aminated NPs, with the  $1575\text{ cm}^{-1}$  band showing a more significant increase. The physical nature of the interaction is evident from the  $\omega(\text{CH}_3)$  mode, that is, the  $-\text{CH}_3$  wagging mode of the APTES backbone at  $1300\text{ cm}^{-1}$ . The two distinct peaks at  $1440$  and  $1390\text{ cm}^{-1}$  represent the asymmetric and symmetric deformation mode for the methyl ( $-\text{CH}_3$ ) groups from the ethoxy group ( $-\text{OCH}_2\text{CH}_3$ ) of the APTES, indicating the incompleteness of the hydrolysis.

**3.3. Fluorescence Lifetime Studies of the Aminated NP Surface.** NIR664-doped NPs show two distinct FLs corresponding to the solvent-insensitive core fraction of the conjugated dye located in the NP interior and the solvent-accessible dye population located near the nanosurface. The smaller component of the FL (denoted as  $t_1$ ) represents the core fraction, and the large fraction (denoted as  $t_2$ ) represents the solvent accessible fraction. The values of the  $t_1$  and  $t_2$  for the unmodified NPs are  $0.534$  and  $0.967\text{ ns}$ , respectively. Figure 5a shows the behavior of both components of the FLs with the time of amine-silanization. These data show that both lifetime components reach a maximum at 3 h of reaction and then drop for longer times (The normalized TCSPC data can be observed in Figure S3 of the Supporting Information). This behavior is attributed to the efficient sensing of the chemical microenvironment by the entrapped dye.<sup>23,24</sup> The intensity decay of the fluorophore is sensitive to the dye environment, in this case the deposition of the ordered amine layer on the NP surface. The amine monolayer formation that takes place in 3 to 4 h of amine-silanization is correlated to the peak of the FL trend in Figure 5a, whereas the decrease in the FL on the higher time scale denotes the deterioration of layer coherence due to the secondary cross-linking between the amine monolayer with the unbound APTES, slowing the intensity decay and resulting in the decrease in the FL.

This FL technique has been extended to evaluate its potential to estimate the extent of amine-silanization on the nanosurface. NPs were functionalized with different APTES concentrations, as described in the Experimental Section, for 3 h to achieve a monolayer distribution of the amine groups. Then, they were tested by FL measurement. The result, demonstrated in Figure 5b, shows the dependence of the FL on the APTES concentration. It clearly shows that both lifetimes ( $t_1$  and  $t_2$ ) sense the surface

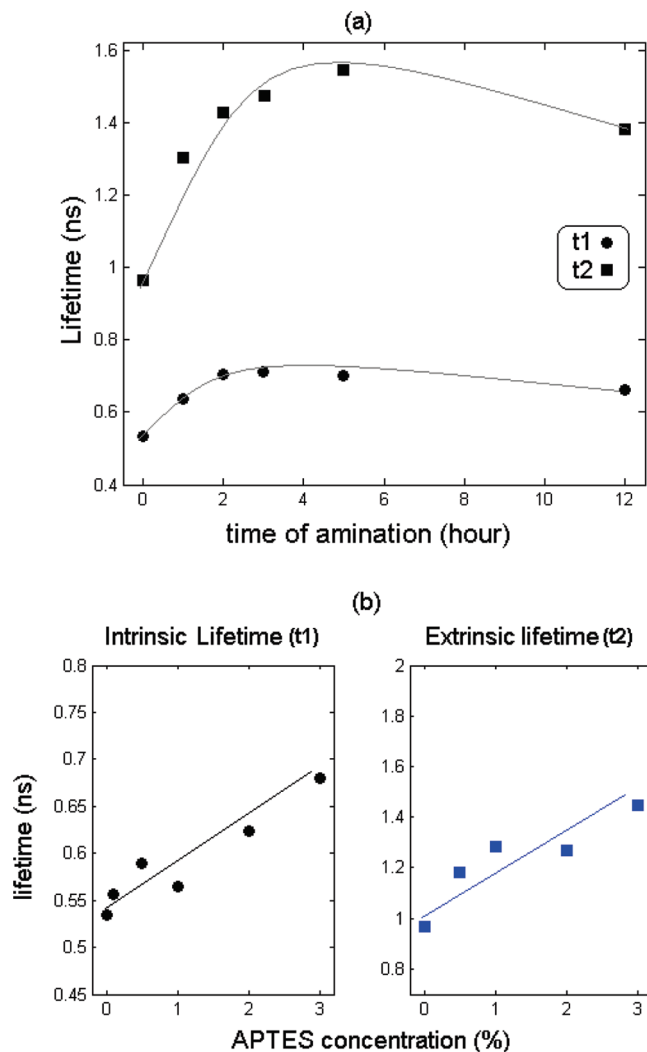


**Figure 5.** (a) Dependence of FL on the duration of amine-silanization reaction and (b) the dependence of the FLs (smaller and higher component in left and right panel, respectively) of aminated NPs on the reacting APTES concentration.

microenvironment and there is a linear relationship between lifetime and APTES concentration.

To test the universality of this technique, we have also tested it on thiolated NPs. NPs with different extents of thiol-silanization have shown some dependency of the FL on the MP TES concentration (results can be found in the Supporting Information), but the linear fit was not as good as that for the aminated NPs (Figure S4 in Supporting Information). This difference in dye sensitivity with various surface functionalization chemistries can be explained by the chemical stability of the functional group. Thiol ( $-\text{SH}$ ) groups are much more prone to aerial oxidation to form disulfide linkage ( $-\text{S}-\text{S}-$ ) between surface-attached or unbound MP TES molecules, making the thiol monolayer irregular and less-ordered compared with the much more stable amine monolayer.<sup>30</sup>

**3.4. FCS Study of the Aminated NPs.** The cross-correlograms of the NPs in the various stages of the amine-silanization reaction were calculated by cross-correlating the ACFs obtained from both channels, as described in the Experimental Section. The CCF was further normalized to nullify the concentration effect, that is, the number of fluorophores present in the confocal volume.

(30) Bravo-Osuna, I.; Teutonico, D.; Arpicco, S.; Vauthier, C.; Ponchel, G. *Int. J. Pharm.* **2007**, *340*, 173–181.

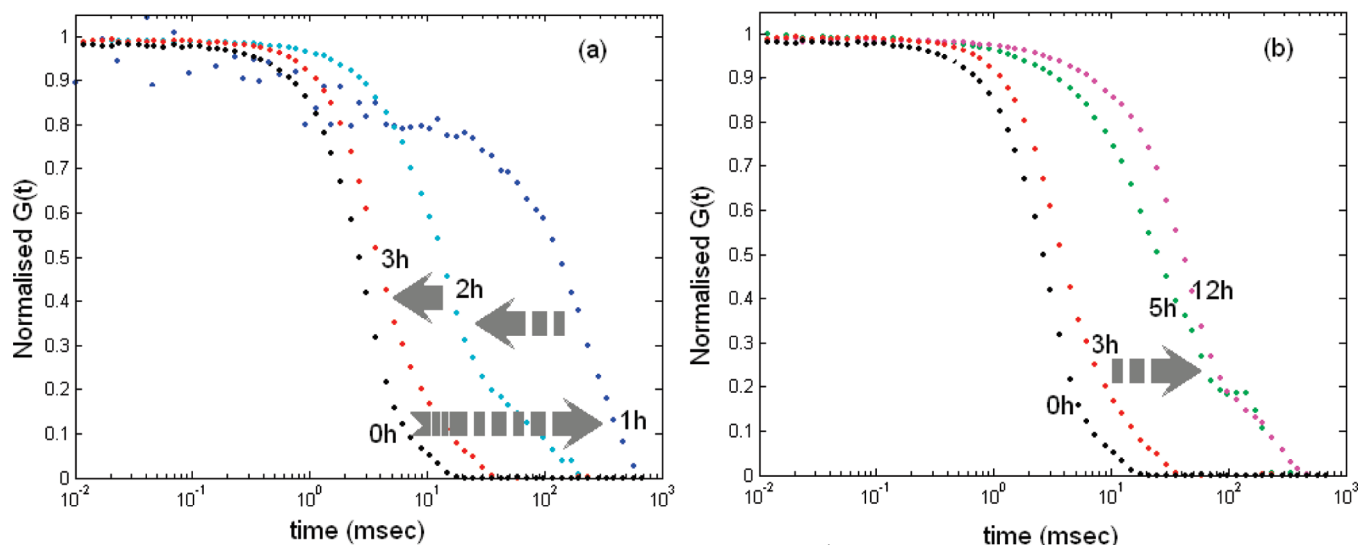


**Figure 6.** Normalized fluorescence cross correllogram for aminated NPs is shown in two panels, (a) the 0–3 h kinetics and (b) 5–12 h observations with respect to 0 and 3 h CCFs.

**Table 1.** Decay Constants of the Normalized CCFs for Aminated NP Samples

time of amine-silanization reaction (h)	single exponential fit $Gn(t) = ae^{-\alpha t}$		biexponential fit $Gn(t) = ae^{-\alpha t} + be^{-\beta t}$			
	a	$\alpha$	a	$\alpha$	b	$\beta$
0	1.004	0.2647	−1.248	1.392	2.25	0.1875
1	0.72	0.0048	−0.007	0.006	0.72	0.0048
2	0.9959	0.0467	1.036	0.0467	−0.04	0.047
3	1.006	0.1639	−4.757	0.1639	5.76	0.1379
5	0.9837	0.0232	0.985	0.0230	−0.0012	0.007
12	0.9897	0.0157	<b>0.969</b>	0.0157	<b>0.0198</b>	0.0163

The normalized correllogram for the NPs, shown in Figure 6, is categorized in two time windows relating to the different stages of amine-silanization; Figure 6a shows the correllogram from 0 to 3 h, and Figure 6b shows the same for higher reaction times, that is, 5 and 12 h. Here Figure 6a represents the formation of the amine monolayer and Figure 6b shows the secondary cross-linking phenomenon between surface-attached and unbound APTES, which was previously discussed. The decay time of this cross-correllogram is strongly correlated with the ordering of the APTES molecules on the NP surface. The unbound NP (at time 0 h) is the most ordered state characterized by homogeneously populated silanol (Si–OH) groups throughout the surface. At the start of the reaction, the system gets the maximum disordered configuration after 1 h when very few APTES molecules are chemically bound to the surface, and some of them are physically adsorbed as unhydrolyzed APTES molecules. There is a 35 times increase in the CCF decay time from 20 to 700 ms for the first hour of reaction. This significantly high decay time reflects the nonhomogeneity of the immediate surface environment due to the incompleteness of the reaction, which is effectively sensed by the dynamic monomer–aggregate equilibrium of the encapsulated dye. This smaller extent of reactivity during the first hour mark also fits well with the FTIR results discussed earlier. In the second hour of the reaction, the CCF decay time decreased to 200 ms, and in the third hour, it decreases to 35 ms, which is very close to that of the initial state. Therefore, the maximum stabilization during amine-silanization is achieved during the ordered monolayer formation, which gives a decay time closest to the initial state. On the higher time scale, shown in Figure 6b, the decay time increases again

to as high as 500 ms for both 5 and 12 h. This increment shows the reappearance of the disordered state signifying the formation of secondary cross-linking between surface-attached APTES with the free APTES molecule. It is also important to note that the maximum of the FL versus reaction time curve (Figure 2c) was observed during the ordered monolayer formation, where the chemical-ordering-driven alteration of the microenvironment is sensed efficiently by the entrapped dye population. While investigating the basic principle behind the sensing method, it has been found that the surface functionalization drives the monomer–aggregate equilibrium of NIR664 more toward the aggregate state, which is evident from the absorption spectra of the NPs (Figure S5 in Supporting Information).

Further analysis of the CCF data can give even more information about the reaction states of the amine-silanization pathway. The normalized CCFs ( $Gn(t)$ ) were fitted with a single exponential decay (in a  $R^2$  range of 0.93 to 0.99), where  $\alpha$  is the decay constant. The variation of these decay constants for different fitting conditions is given in Table 1. At the start of the reaction, the value of  $\alpha$  decreases sharply in the first hour and returns to a maximum at 3 h before further decreasing at longer times. Importantly, the bulk deposition of the amine layer after 12 h is indicated by the emergence of a biexponential fit with both pre-exponential factors (shown in Table 1) having positive values indicating two distinct chemical microenvironments effectively sensed by the fluorophore. However, it can be hypothesized that the ratio of the two exponents is probably a function of the ratio of the thickness of amine layer and NP radius.

A comparative study between amplitudes of ACF and CCF was carried out to probe the stabilization of the amine layer on the nanosurface. Figure 7a gives the profiles of ACF and CCF in different stages of amine-silanization. The degree of similarity of the amplitudes of these two correlations is indicative of the overall order of the system. The correllogram in the first hour shows a large difference of the amplitude between the two correlation decays, indicating a lesser extent of stable monolayer formation. As described in the Experimental Section, this stabilization of the amine layer on the nanosurface has been examined with the variation of normalized cross-correlation amplitude ( $CC_{ra}$ ) with time on a scale where fully unbound and completely stable layers are set as 0 and 1, respectively. The first hour of amine-silanization shows a very low value of  $CC_{ra}$  (just over 2%). This value increases

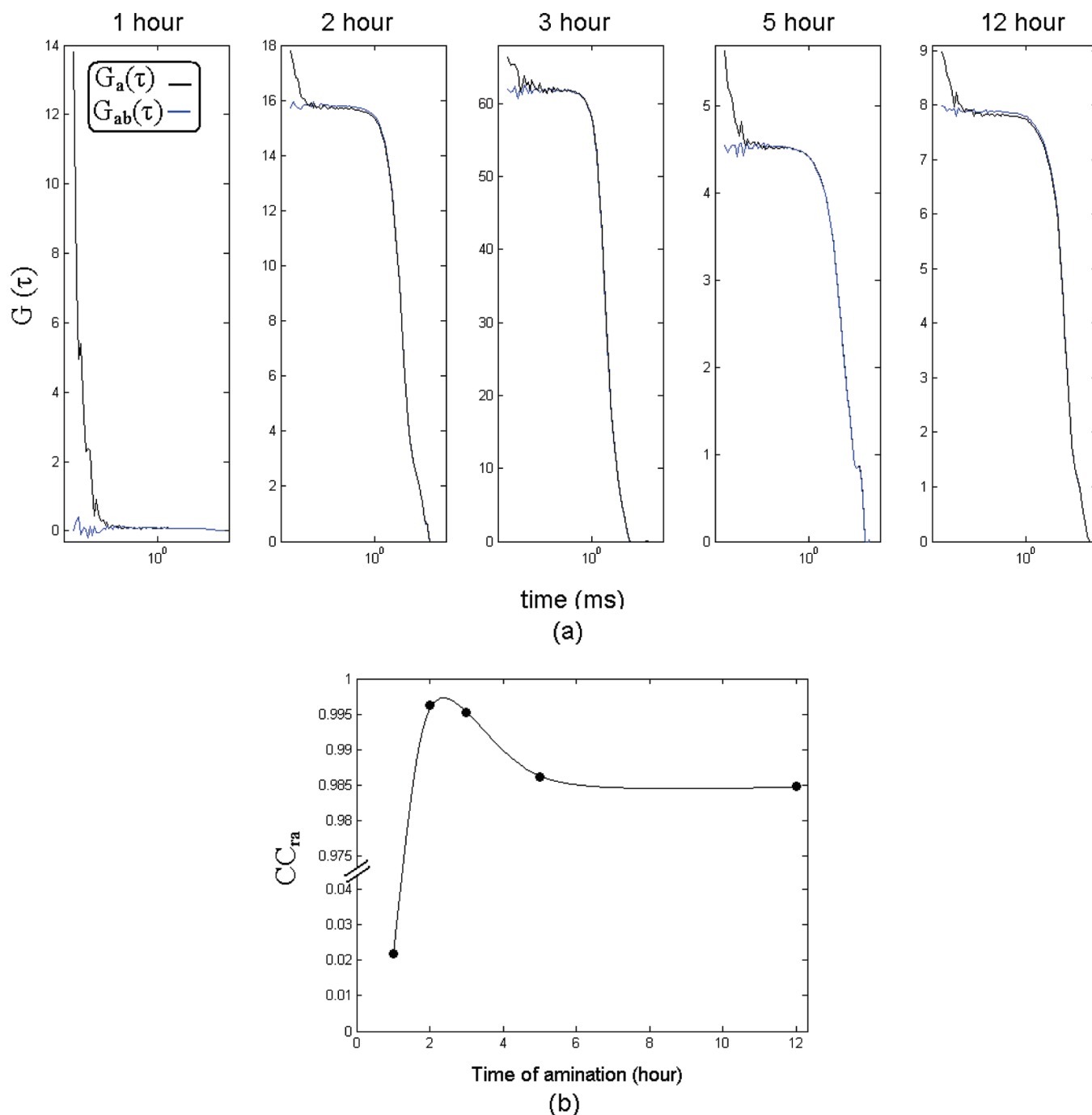


**Figure 7.** Plots of ACF and CCF for each set of aminated NPs have been presented (a) and the dependence of  $CC_{ra}$  on the amine-silanization time is presented to construct the reaction profile (b).

significantly in the second hour. The maximum is reached at  $\sim 3$  h before decreasing at higher time scales. This stabilization landscape, as shown in Figure 7b, denotes the formation of the stable monolayer of surface-attached APTES molecule up to 3 h, followed by destabilizing secondary cross-linking by surface-bound and free APTES molecules at longer times.

This monolayer formation and secondary cross-linking-driven multiple APTES layer has been constructed by designing the reaction coordinate based on the correlation between the single exponential decay constant for different stages of amine-silanization with that of the initial reaction stage, as described in eq 5. In Figure 8, a spline was generated on the basis of a hypothesis presented in the Experimental Section with the experimental  $\alpha_{cor}$

values to form a close approximation to the energy landscape for the amine-silanization reaction on NP surface. Hence, the minima and the maxima of the curve represent the most ordered and disordered states of the reaction, respectively. Here the two maximum points, that is, in a very early stage ( $\sim 1$  h) and in later stages ( $\sim 12$  h), represent the most disordered states of the reaction because of the heterogeneously distributed nanosurface-attached APTES molecules for the former and formation of secondary bulky amine layers via cross-linking and H-bonding for the latter. The minimum of the curve during the reaction occurs after 3 h of reaction time denoting the amine monolayer formation, the most ordered state during the reaction having the minimum distance with the initial stage in the reaction coordinate.

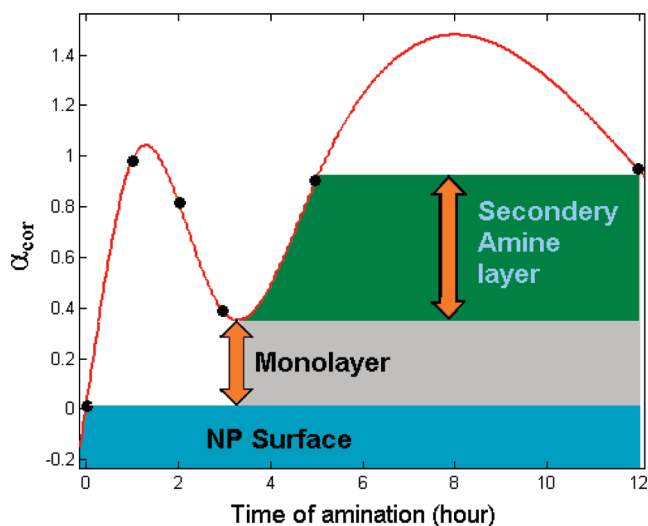


**Figure 8.** Construction of a reaction profile for the nanosurface amine-silanization on the basis of chemical ordering, described by the correlation parameter  $\alpha_{\text{cor}}$  that measures the correlation distance between different states of the reaction and the initial state.

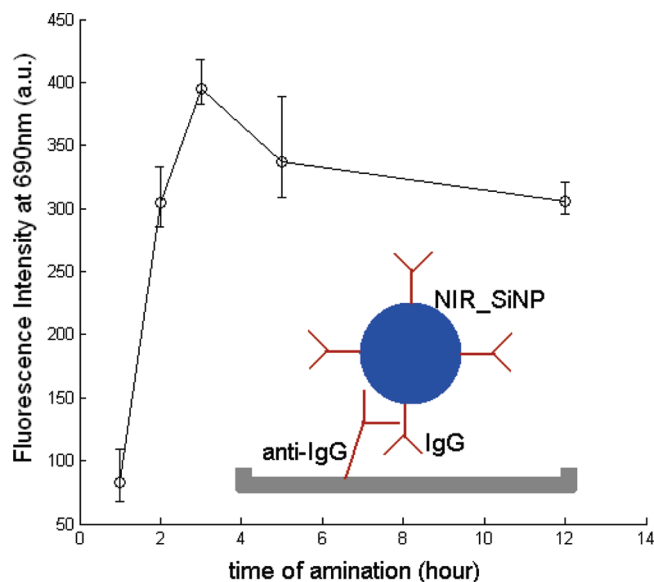


**Figure 9.** Plot of NP fluorescence at 700 nm (excited at 660 nm) versus amine-silanization time is shown for a plate-based direct binding assay that reports the binding between surface attached IgG and anti-IgG conjugated with the aminated NP.

**3.5. Direct Binding Immunoassay.** The optimum reaction time for NP surface amine-silanization has been validated by assaying the antibody conjugation efficiency of the aminated NPs. As described in the Experimental Section, the binding between anti-IgG- and IgG-conjugated aminated NP was studied by measuring the fluorescence intensity (of the conjugated dye NIR664) at 700 nm upon excitation at 660 nm. Figure 9 shows the dependence of antibody binding on the ordering of the amine layer deposited on the NP. The plot of fluorescence intensity versus time of amine-silanization for the NPs shows an increase in the intensity up to 3 h reaction time, followed by a steady decrease for longer times. Therefore, the maximum antibody attachment occurred on the

NPs having the 3 h amine-silanization. This shows the importance of an ordered monolayer of functional groups on a nanosurface for biomolecular conjugation. For the 5 and 12 h amine-silanization sample, the multiple layering of cross-linked APTES poses a marked inhibition for antibody attachment compared with the 3 h data. First, during the longer time of amine-silanization reaction, it is likely that the primary amine group of the nanosurface-bound APTES molecule can interact with the hydroxyl group of unbound APTES molecule via hydrogen bonding. Furthermore, the reverse interaction, that is, hydrogen bond formation between the hydroxyl group of the surface bound APTES molecule and the primary amine group of a nearby unbound APTES molecule, can significantly limit the number of free primary amine groups despite the longer extent of APTES exposure. In addition to that, the steric hindrance posed by the bulky amine layer composed of a cross-linking driven mesh structure is likely to restrict the antibody attachment.

#### 4. Conclusions

In this work, we have successfully demonstrated the application of FL and FCS to monitor the surface-modification process of silica NPs as well as optimized the surface layer structure for efficient conjugation of biomolecules. Conventional techniques like zeta potentiometry and FTIR spectroscopy can indicate the bulk amine group deposition and the altered chemical signatures on the nanosurface, respectively. The FTIR analysis identified an optimum time of 3 h for the formation of an ordered amine monolayer and the formation of a disordered secondary APTES cross-linked layer at longer reaction times. The superior sensitivity of fluorescence, in particular, FLs, coupled to the sensitivity of the encapsulated dye to the NP surface environment, facilitated the elucidation of the details of the amine-silanization reaction and the evolution of the amine layer structure in different stages of the reaction. This is manifested as a variation in FL value as a function of amine-silanization reaction time, which, in agreement with the FTIR analysis, indicates an optimum reaction time of 3 h. The power of FCS as a novel probe of functional layer structure has also been demonstrated. Analysis of both the normalized CCF function,  $G_{\text{ab}}$ , and the relative cross-correlation factor,  $CC_{\text{ra}}$ , indicates an optimum amine-silanization reaction time of 3 h in agreement with the FL analysis. Furthermore, an in-depth analysis of the FCS decay constant variation further validated the above conclusions. Finally, a direct binding assay was carried out that indicated that maximum antibody–antigen binding occurs on the ordered amine monolayer corresponding to 3 h of reaction time. This work clearly demonstrates the potential of FL and FCS to complement and supplement other more conventional characterization techniques toward the elucidation of nanosurface functional layer structure and kinetics.

**Acknowledgment.** This work was supported through the National Biophotonics and Imaging Platform, Ireland, and funded by the Irish Government's Programme for Research in Third Level Institutions, Cycle 4, National Development Plan 2007-2013.

**Supporting Information Available:** TEM picture of the NPs, characterization and FL assay of the thiolated NPs, normalized TCSPC results, and UV/visible spectra of silanized NPs. This material is available free of charge via the Internet at <http://pubs.acs.org>.

Cite this: *Analyst*, 2011, **136**, 4431

www.rsc.org/analyst

PAPER

# Effect of antibody immobilization strategies on the analytical performance of a surface plasmon resonance-based immunoassay†

Sandeep Kumar Vashist,<sup>‡§ab</sup> Chandra Kumar Dixit,<sup>§ac</sup> Brian D. MacCraith<sup>ad</sup> and Richard O'Kennedy<sup>\*acd</sup>

Received 18th April 2011, Accepted 26th July 2011

DOI: 10.1039/c1an15325k

Antibody immobilization strategies (random, covalent, orientated and combinations of each) were examined to determine their performance in a surface plasmon resonance-based immunoassay using human fetuin A (HFA) as the model antigen system. The random antibody immobilization strategy selected was based on passive adsorption of anti-HFA antibody on 3-aminopropyltriethoxysilane (APTES)-functionalized gold (Au) chips. The covalent strategy employed covalent crosslinking of anti-HFA antibody on APTES-functionalized chips using 1-ethyl-3-[3-dimethylaminopropyl]carbodiimide (EDC) and sulfo-*N*-hydroxysuccinimide (SNHS). The orientation strategy used passive adsorption of protein A (PrA) on Au chips, with subsequent binding of the anti-HFA antibody in an orientated fashion *via* its fragment crystallisable (Fc) region. In the covalent-orientated strategy, PrA was first bound covalently, to the surface, which in turn, then binds the anti-HFA antibody in an orientated manner. Finally, in the most widely used strategy, covalent binding of anti-HFA antibody to carboxymethyldextran (CM5-dextran) was employed. This immobilization strategy gave the highest anti-HFA antibody immobilization density, whereas the highest HFA response was obtained with the covalent-orientated immobilization strategy. Therefore, the covalent-orientated strategy was the best for SPR-based HFA immunoassay and can detect 0.6–20.0 ng/mL of HFA in less than 10 min.

## Introduction

Immunoassays based on the immobilization of antibodies on a substrate have been widely used in different biosensing or bioanalytical techniques for the detection of specific antigens. Surface plasmon resonance (SPR)-based immunosensors are 'real-time' and 'label-free' rapid assay formats that provide highly useful information on biomolecular interactions<sup>1,2</sup> and provide highly reproducible immunoassays.

The immobilization of antibodies on sensor chips plays a very important role in the analytical performance of a SPR-based immunoassay. The affinity, orientation and stability of the antibodies are often affected by the immobilization strategy

employed.<sup>3,4</sup> In addition, the size of the antibodies/fragments used and their surface distribution and the size of the analyte are of significance in relation to the minimization of steric hindrance, which may affect the immunoassay performance. Antibodies present in the solution phase have three dimensional freedom of movement and maintain their native structure. Immobilization of antibodies at an interface restricts their freedom of movement and may impact on their three dimensional conformation.<sup>5</sup> Therefore, a critical understanding of the interactions between macromolecular receptor and ligand is important.<sup>5</sup>

A large number of chemistries are available for immobilizing antibodies on biosensor surfaces, however, those introducing orientation<sup>6</sup> and maintaining native antibody conformation<sup>7</sup> are of major importance. CM5-dextran is often used where the antibody is linked *via* its amine groups to the EDC-NHS-activated carboxyl groups of CM5 by heterobifunctional cross-linking and this chemistry leads to a high density of antibody immobilization. However, immobilization using this strategy can result in interference with the antigen detection capability if the antibody is inadvertently captured *via* amine groups of or adjacent to the antigen binding site.<sup>8</sup>

In another format, poly-histidine tagged antibodies are bound to nitriloacetic acid (NTA)-modified surfaces. However, problems may arise from the strong non-specific adsorption of other metal-binding proteins to the poly-histidine tag and continuous leaching of the bound ligand.<sup>9,10</sup> Biotin-avidin systems have also

<sup>a</sup>Centre for Bioanalytical Sciences (CBAS), National Centre for Sensor Research, Dublin City University, Dublin 9, Ireland. E-mail: richard.okennedy@dcu.ie; Fax: +353 1 700 5412; Tel: +353 1 700 7810

<sup>b</sup>Bristol-Myers Squibb (BMS), Swords Laboratories, Watery Lane, Swords, Co. Dublin, Ireland

<sup>c</sup>Applied Biochemistry Group, School of Biotechnology, Dublin City University, Dublin 9, Ireland

<sup>d</sup>Biomedical Diagnostics Institute (BDI), Dublin City University, Dublin 9, Ireland

† Electronic supplementary information (ESI) available. See DOI: 10.1039/c1an15325k

‡ Current Address: NUSNNI-NanoCore, National University of Singapore, T-Lab Level 11, 5A Engineering Drive 1, Singapore 117580

§ These authors contributed equally

been used for immobilization in SPR assays. Streptavidin-coated SPR chips are preferred for the site-directed immobilization of biotinylated antibodies. This strategy introduces steric freedom along with site-directed orientation. However, as with other proteins, immobilization of streptavidin on the surface may introduce conformational-stress that may reduce its binding affinity for biotin. This can also occur with other physical parameters such as temperature.<sup>11</sup> Conversely, strategies employing thiols, which can be immobilized on the gold surface with high-affinity and without any prior surface modification, provide strong site-directed orientation. This strategy is useful if the antibody naturally has free thiol groups. However, if the thiol group is introduced chemically, involving reaction with the antibody's amine groups, then this can affect activity.

A high degree of orientation for the capture antibody on a sensor surface can be attained with a sub-layer of proteins such as protein A or protein G.<sup>12</sup> These proteins are specific for binding the Fc region of the antibodies, which keeps the fragment antigen-binding (Fab) region free for antigen binding thus obviating the need of any chemical modification of the antibody. However, randomly immobilized Fc-binding protein molecules may affect the orientation of antibody to some degree but this is significantly lower in comparison to the degree of orientation actually achieved. Nevertheless, due to steric considerations, a maximum of two antibodies may only be accommodated by each of these protein binding molecules.<sup>7</sup> Drawbacks associated with random immobilization and the introduction of conformational strain will not affect, to a significant degree, the antibody molecules captured on the sub-layer of Fc-binding proteins. Moreover, Fc-binding protein-antibody interaction is generally regenerative.<sup>13</sup>

The present study is aimed at determining the effect of various antibody immobilization strategies, *i.e.* random, orientated, covalent, covalent-orientated and covalent-CM5-dextran on a SPR-based immunoassay for HFA. Recently we reported a multi-substrate compatible novel antibody immobilization strategy,<sup>14</sup> which is based on the APTES functionalization of the surface and the covalent binding of antibodies to it by EDC-SNHS heterobifunctional crosslinking. Various optimization parameters associated to APTES functionalization of the Au chip are described in the supplementary section Figure S1 & S2.† The same strategy was employed for SPR immunoassays and the schematic representation of the strategy is depicted in Fig. 1. An alternate covalent-orientated strategy was also devised by introducing an additional step in the covalent strategy, where PrA was initially bound covalently and anti-HFA antibody was immobilized, thereafter, in an orientated manner. The random strategy employed the passive adsorption of anti-HFA antibody on APTES-functionalized chips, whereas the orientated strategy used the passive adsorption of PrA on SIA Au chips followed by the orientated immobilization of anti-HFA antibody. The covalent-CM5-dextran strategy employed the covalent binding of amino groups of anti-HFA antibody to the carboxyl groups of CM5-dextran using EDC-SNHS. Each strategy was compared on the basis of their SPR immunoassay performance, anti-HFA antibody immobilization density and mass-density of captured HFA. This study provides an insight as to how antibody orientation strategy may influence immunoassay performance.

## Materials and methods

### Reagents and materials

EDC, SNHS and 2-(*N*-morpholino)ethane sulfonic acid (MES, pH 4.7) were purchased from Thermo Scientific. 3-APTES (purity 98%, w/v), 4-(2-hydroxyethyl)-1-piperazineethanesulfonic acid (HEPES), Tween 20, H<sub>2</sub>O<sub>2</sub> (30%, v/v), H<sub>2</sub>SO<sub>4</sub> (97.5%, v/v), ethylenediaminetetraacetic acid (EDTA), NaCl and protein A (soluble, Cowan strain, recombinant, expressed in *Escherichia coli*) were procured from Sigma-Aldrich, Singapore. The human Fetuin A/AHSG kit with all the necessary components was obtained from R&D Systems Inc., USA. All buffers and solutions were prepared with 18MΩ Milli-Q ultrapure water (UPW) filtered through a 2-μm filter. Surface Plasmon Resonance was performed on BIAcore 3000 purchased from GE Healthcare, Uppsala, Sweden. The SIA kit (BR-1004-05) containing SPR Au chips, carboxymethyl dextran (CMD)-functionalized Au chips, and ethanolamine hydrochloride (1M, pH 8.5) were purchased from GE Healthcare, London, U.K.

The SPR Au chip was assembled according to the instructions supplied by the manufacturer. HEPES-buffered saline (HBS) buffer (10mM) pH 7.4, (running buffer for BIAcore) was made up, filtered through 0.2μm Millipore filter paper and degassed overnight in order to remove any air bubbles, which may cause interference with SPR analysis. All the sample dilutions were made in the running buffer (10mM HBS, pH 7.4). The dilutions of HFA were made in BSA-preblocked glass vials, prepared by incubating with 1% (w/v) BSA for 30 min, to minimize the sample loss due to non-specific adsorption on sample tube surfaces and/or effects due to altered immunogenicity.<sup>15</sup>

### Surface cleaning of SIA Au chip and APTES functionalization

The Au chip was cleaned with piranha etch [60 μL of H<sub>2</sub>SO<sub>4</sub> (97.5%, v/v): 30 μL of H<sub>2</sub>O<sub>2</sub> (30%, v/v)] for two minutes followed by extensive washing. Piranha treatment oxidizes the gold surface, as evident by the contact angle, which is 9.3°. When the piranha-treated chips are washed with deionized water, the water molecules get strongly adsorbed on the surface thereby generating 'hydroxyl' groups,<sup>16,17</sup> as evident by the increase in contact angle to 28°–32°.

The chip was then incubated with 100 μL of 2% (v/v) APTES for one hr at room temperature (RT) in a fume hood followed by five washes with UPW. Following this, different immobilization strategies were applied.

### EDC activation of anti-HFA antibody

Anti-HFA antibody (990μL of 100 μg/ml in HBS) was incubated at room temperature for 15 min with 10 μL of cross-linking solution containing EDC (4 mg/mL) and sulfo-NHS (11 mg/mL) in 0.1 M MES buffer, pH 4.7. The procedure led to the activation of carboxyl groups on the anti-HFA antibody with EDC. The EDC-activated anti-HFA antibody was captured on the APTES-functionalized Au chip (previously described) for the covalent immobilization strategy.

Similarly, PrA was also activated with EDC and captured on the APTES-functionalized Au chip surface for the orientated strategy.

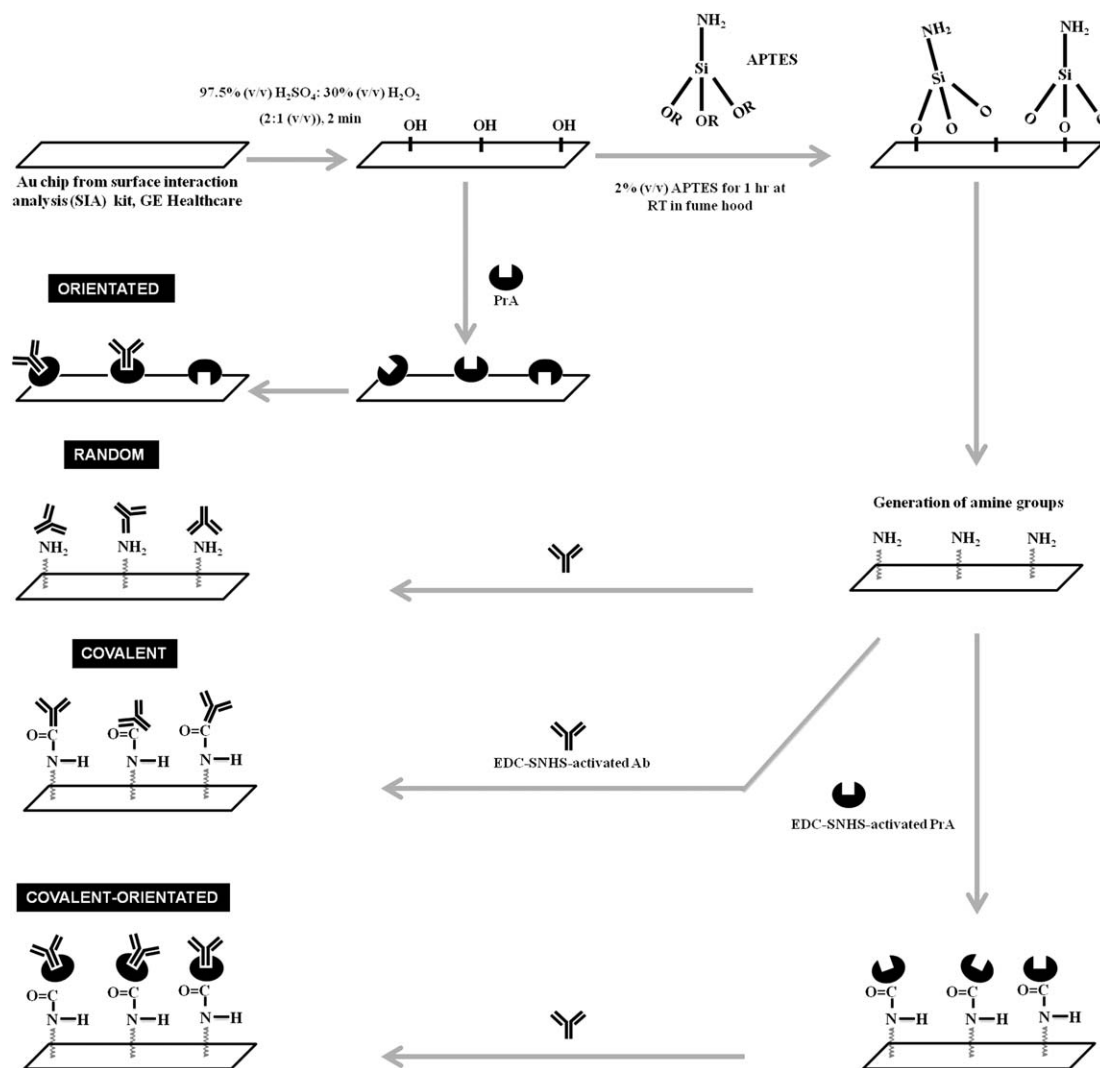


Fig. 1 Schematic representation of various immobilization strategies employed for the SPR-based HFA immunoassay. PrA is protein A.

### Immobilization of anti-HFA antibody

For the random antibody non-covalent immobilization strategy, 50  $\mu\text{L}$  of anti-HFA antibody (100  $\mu\text{g}/\text{mL}$ ) was injected over all the four flow cells of an APTES-functionalized Au chip at a flow rate of 10  $\mu\text{L}/\text{min}$  and the baseline was allowed to stabilize. BSA (20  $\mu\text{L}$  of 1% (w/v)) was subsequently used for blocking.

For the covalent immobilization strategy, 50  $\mu\text{L}$  of EDC-activated antibody (100  $\mu\text{g}/\text{mL}$ ) was injected over all the four flow cells of an APTES-functionalized Au chip, and BSA was used for blocking as previously described.

For orientated immobilization strategy, 50  $\mu\text{L}$  of protein A (100  $\mu\text{g}/\text{mL}$ ) was injected over the four flow cells of the piranha-treated Au chip at a flow rate of 10  $\mu\text{L}/\text{min}$ . Twenty microliters of 1% (w/v) BSA was then injected for blocking. After baseline stabilization, 50  $\mu\text{L}$  of anti-HFA antibody (100  $\mu\text{g}/\text{mL}$ ) diluted in 10 mM HBS, pH 7.4, was injected over all the flow cells at a flow rate of 10  $\mu\text{L}/\text{min}$ .

For the covalent-orientated immobilization strategy, 50  $\mu\text{L}$  of EDC-activated PrA was injected over all four flow cells of an APTES-functionalized Au chip at a flow rate of 10  $\mu\text{L}/\text{min}$ . The

chip was blocked with BSA, as previously described, followed by the addition of anti-HFA antibody.

### Covalent-CM5-dextran immobilization strategy

A CM5 dextran-functionalized Au chip was docked into BIAcore 3000 and primed. Pre-concentration studies were performed in order to obtain the optimum pH of the sodium acetate buffer for use with anti-HFA antibody immobilization (pH range of 4.0–5.0). Further activation was performed at a pH of 4.2 (optimum). Afterwards, the CM5-dextran chip was activated by injecting a 50  $\mu\text{L}$  solution containing 200  $\mu\text{g}$  of EDC and 550  $\mu\text{g}$  of SNHS in 0.1M MES buffer, pH 4.7, through all the flow cells at a flow rate of 10  $\mu\text{L}/\text{min}$ . Thereafter, the procedure employed for the random immobilization strategy was used, with the exception that blocking was initially performed with 20  $\mu\text{L}$  of 1M ethanolamine hydrochloride, pH 8.5, followed by 20  $\mu\text{L}$  of 1% (w/v) BSA. Ethanolamine hydrochloride (1M), pH 8.5, blocks the unreacted ester groups in the CM5-dextran matrix, while BSA blocks the non-specific binding sites on the chip surface.

## HFA-detection

Fifty microlitres of the dilution buffer (10mM HBS, pH 7.4) was passed through all the flow cells before HFA capture and the resultant changes in the SPR response units (RU) for each of the four flow cells were recorded. Fifty microlitres of HFA at six different dilutions (0.6, 1.2, 2.5, 5.0, 10.0 and 20.0 ng/mL) were then passed through the flow cells. Subsequently, the RU values obtained for the blanks were subtracted from the RU values obtained for captured HFA of the corresponding flow cells.

All the experiments pertaining to different immobilization strategies were repeated nine times and the standard deviation was calculated. The SPR-based HFA detection curves were plotted with SigmaPlot software, version 11.2 based on a four parameter logistic (eqn (1)). The analytical parameters such as  $EC_{50}$  and Hillslope, generated by the software analysis report, were then used to evaluate the analytical performance<sup>18</sup> of SPR immunoassays with the various antibody immobilization strategies.

$$y = \min + (\max - \min) / [1 + (x/EC_{50})^{(-Hillslope)}] \quad (1)$$

## Results and discussion

### Comparison of antibody immobilization strategies on basis of anti-HFA antibody immobilization density

The development of the APTES-functionalization of Au chips, used for various antibody immobilization strategies in this study, was optimized for APTES concentration, APTES functionalization time and APTES density (Supplementary Fig. S1 and S2).

The effect of employing various antibody immobilization strategies in a SPR immunoassay was initially observed by determining the immobilization density of anti-HFA antibody on the SPR chip. The highest and lowest anti-HFA antibody immobilization densities, as shown in Table 1, were obtained with covalent-CM5-dextran immobilization and random immobilization strategies, respectively. The anti-HFA antibody immobilization densities were found in the decreasing order of covalent-CM5-dextran > covalent > covalent-orientated > orientated > random strategies (Fig. 2). The immobilization

densities were calculated using a conversion factor *i.e.* 1 ng/mm<sup>2</sup> of biomolecule corresponds to a change of 1000 RU.<sup>19–21</sup> The lowest antibody immobilization density in the random immobilization strategy was attributed to the irregular and uncontrolled binding of the antibody over the surface mainly by electrostatic and hydrophobic interactions.<sup>21</sup> Additionally, many other factors, such as molecular spreading and inter-molecular interactions, may affect the immobilization-density of adsorbed antibodies at the interface,<sup>19,22</sup> which, in turn, determines the functionality of adsorbed antibodies.<sup>22</sup> However, the introduction of PrA molecules enables the orientated immobilization of antibodies in a site-directed fashion. The anti-HFA immobilization density of the orientated immobilization strategy was greater than that of the random immobilization strategy as PrA binds very strongly to the Au surface, which is the main reason that it has been used extensively for biosensing applications in various biosensor formats.

The capture ratio of 1 : 1 for anti-HFA antibody bound to PrA is in line with previous findings, which state that one PrA molecule can bind to a maximum of two antibody molecules based on conformational and intermolecular restrictions.<sup>23</sup>

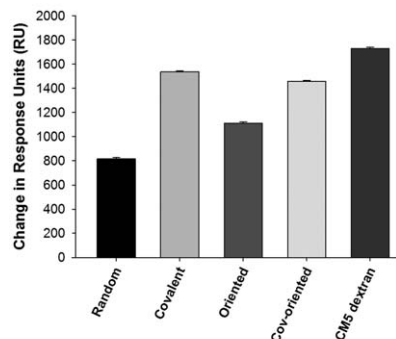


**Fig. 2** Change in response units caused by anti-HFA antibody immobilization when various antibody immobilization strategies were used for the SPR-based HFA immunoassay. Error bars represent standard deviation obtained from the nine repeats for each sample. Cov means covalent.

**Table 1** Determination of molecular densities of immobilized anti-HFA antibody and detected amount of HFA when different SPR immunoassay formats, based on various antibody immobilization strategies, were employed<sup>a</sup>

Antibody Immobilization Strategy	Immobilization of anti-HFA antibody			HFA <sup>d</sup>			
	$\Delta$ RU	Mass density <sup>b</sup> (ng/cm <sup>2</sup> )	Molecular Density <sup>c</sup> (molecules/cm <sup>2</sup> )	$\Delta$ RU	Mass density <sup>b</sup> (ng/cm <sup>2</sup> )	Molecular Density <sup>c</sup> (molecules/cm <sup>2</sup> )	$EC_{50}$ (ng/mL)
Random	816.0 ± 11.7	81.6 ± 1.2	3.3 × 10 <sup>11</sup>	63.0 ± 16	6.3 ± 1.6	(0.9 ± 0.2) × 10 <sup>11</sup>	5.7
Covalent	1536.0 ± 10.4	153.6 ± 1.0	6.1 × 10 <sup>11</sup>	149.0 ± 9.6	14.9 ± 1.0	(2.1 ± 0.1) × 10 <sup>11</sup>	3.8
Orientated	1112.0 ± 9.6	111.2 ± 1.0	4.4 × 10 <sup>11</sup>	113.0 ± 10.5	11.3 ± 1.0	(1.6 ± 0.1) × 10 <sup>11</sup>	4.0
Covalent-orientated	1457.0 ± 8.8	145.7 ± 1.0	5.8 × 10 <sup>11</sup>	194.0 ± 9.5	19.4 ± 1.0	(2.8 ± 0.1) × 10 <sup>11</sup>	3.7
Covalent-CM5-dextran	1728.0 ± 12.4	172.8 ± 1.2	6.9 × 10 <sup>11</sup>	138.0 ± 10.4	13.8 ± 1.0	(1.9 ± 0.1) × 10 <sup>11</sup>	4.1

<sup>a</sup>  $\Delta$ RU: Change in resonance units (RU) caused by binding. <sup>b</sup> Calculated using the commonly used conversion factor *i.e.* 1000 RU = 100 ng/cm<sup>2</sup>.<sup>13,14</sup>

<sup>c</sup> Calculated by [Mass density (ng/cm<sup>2</sup>)/Molecular weight (in ng)]. Molecular weight of anti-HFA antibody and HFA were 150 kDa and 43.5 kDa, respectively. In order to calculate molecular weight in SI units, the conversion factor 1 kDa = 1000 Da = 1000 g was used. The molecular weight of anti-HFA antibody and HFA are 24.9 × 10<sup>-11</sup>ng and 7.0 × 10<sup>-11</sup>ng, respectively. <sup>d</sup> Calculations were performed for the detection of 5 ng/mL of HFA *i.e.* the concentration just above the  $EC_{50}$ .

However, the anti-HFA antibody immobilization density was lower than that of the covalent-orientated immobilization strategy. This might be because PrA molecules adsorbed in the orientated format still have a tendency to undergo conformational changes and/or leaching off the surface. The higher antibody immobilization density of the covalent-orientated strategy may be due to the fact that covalently bound PrA molecules could resist leaching whilst maintaining their active conformation for binding.

The antibody immobilization density of the covalent strategy was higher than that of covalent-orientated strategy and this may be due to the fact that the total number of amino groups available for antibody crosslinking was significantly higher than the binding sites available on covalently immobilized PrA molecules. Therefore, there is a higher probability for an antibody to be directly crosslinked to the amino groups on the surface in comparison to binding in an orientated fashion to the covalently bound PrA molecules.

On the other hand, the covalent-CM5-dextran immobilization strategy had the highest anti-HFA antibody density, which may be due to the fact that CM5-dextran has a long hydrophilic polymer chain with a large number of available carboxyl groups on the side chains. Moreover, apart from the increased effective surface area provided by the CM5-dextran, electrostatic interactions of the positively-charged amino groups on anti-HFA antibody towards the negatively-charged carboxyl functional groups on the surface of CM5 dextran can also occur.

Our results are very similar to the findings reported recently,<sup>24</sup> where it was observed that a carboxymethyl dextran hydrogel-based immobilization strategy had a very high antibody immobilization density in comparison to random and orientated immobilization strategies. Here the random immobilization strategy was based on the passive immobilization of antibodies on a self-assembled monolayer (SAM) formed by 11-mercaptopundecanoic acid (MUA) whereas, the orientated immobilization strategy employed the capture of antibodies on the layer of covalently immobilized Protein G on the MUA SAM-functionalized surface.

#### Comparison of antibody immobilization strategies on basis of HFA capture densities

Anti-HFA antibodies bound to SPR Au chips, prepared by various antibody immobilization strategies, were employed for the detection of different concentrations of HFA (0.6–20.0 ng/mL), as shown in Fig. 3. The blank for the assay was the running buffer *i.e.* 10 mM HBS, pH 7.4. The RU of the blank in each flow cell was then subtracted from the RU value corresponding to the detection of a particular concentration of HFA in that flow cell.

All immobilization strategies used were evaluated using an HFA concentration of 5 ng/mL, which was the HFA concentration just above the  $EC_{50}$  of the random immobilization strategy. It was highest for the covalent-orientated strategy and lowest for the random strategy. The mass densities of HFA detected by the various antibody immobilization strategies were in the decreasing order of covalent-orientated > covalent > covalent-CM5-dextran > orientated > random. The  $EC_{50}$  of covalent-orientated strategy based anti-HFA bound SPR chip for HFA detection was also found to be the lowest (Table 1), which

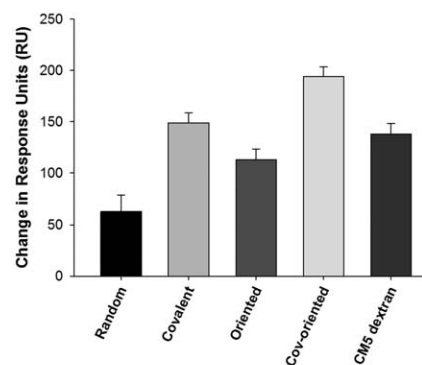


**Fig. 3** Change in response units caused by HFA detection at 5 ng/mL when various antibody immobilization strategies were used for the SPR-based HFA immunoassay. Error bars represent standard deviation obtained from the nine repeats for each sample. Cov means covalent.

indicates that it was the most sensitive immunoassay format. The mass density of HFA detected while using the covalent-orientated strategy was the highest of all the immobilization strategies employed. Conversely, the covalent-orientated strategy, which had a lower anti-HFA antibody mass density in comparison to the covalent-CM5-dextran and covalent strategies, had the highest response units for HFA capture and thus, the highest mass density. This clearly demonstrates that the total amount of antibody immobilized does not necessarily equate with maximum antigen (HFA) capture. The antigen-detection ability of adsorbed antibodies can be significantly compromised.<sup>19,25</sup> We previously demonstrated that covalently-bound antibodies capture higher amount of antigen than adsorbed antibodies under the same set of conditions.<sup>3</sup> Therefore, the adsorption of antibodies can introduce certain conformational changes that may impact their antigen-recognition behaviour, thereby ultimately resulting in reduced antigen detection. The results shown in Fig. 4 demonstrate that the effectiveness of an immunoassay is clearly dependent on the antibody immobilization strategies.

Our findings show that the covalent-orientated strategy, based on the binding of PrA to the chip and the orientated immobilization of capture antibodies, is ideal for the SPR-based

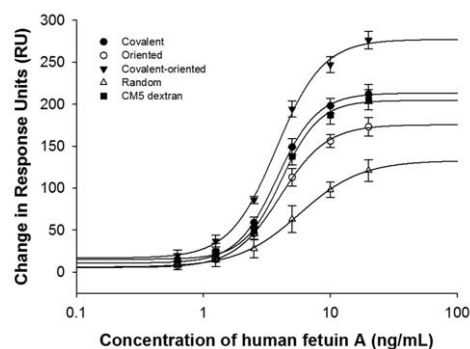


**Fig. 4** SPR-based immunoassay curves for HFA detection when various antibody immobilization strategies were employed. Error bars represent standard deviation obtained from nine assay repeats for each sample type.

immunoassay for HFA. There was no evidence of biofouling even after continuous HFA detection cycles or extended storage at 4 °C (Supplementary Fig. S2 and S3†).

## Conclusions

Various antibody immobilization strategies, *i.e.* random, covalent, orientated, covalent-orientated and covalent-CM5-dextran, were employed to determine their effect on the analytical performance of a SPR-based immunoassay for HFA. The highest anti-HFA antibody immobilization density was obtained with covalent-CM5-dextran, whereas the highest amount of HFA was captured with the covalent-orientated strategy. Therefore, the orientation of the antibody plays an important role in the analytical performance of the SPR immunoassay. The relative molar density of HFA detected, which corresponds to the functional antibody immobilization density, is a more reliable indicator of analytical performance than the total antibody immobilization density.

## Acknowledgements

We acknowledge Bristol Myers Squibb (BMS), Syracuse, USA and the Industrial Development Authority, Ireland, for the financial support under the CBAS project code 116294. This material is based in part on works supported by the Science Foundation Ireland (Grant 05/CE3/B754), and the Biomedical Diagnostics Institute (BDI), all of which are gratefully acknowledged.

## References

- 1 P. Skottrup, S. Hearty, H. Frøkiær, P. Leonard, J. Hejgaard, R. O'Kennedy, M. Nicolaisen and A. F. Justesen, *Biosens. Bioelectron.*, 2007, **22**, 2724.
- 2 S. Stapleton, B. Bradshaw and R. O'Kennedy, *Anal. Chim. Acta*, 2009, **651**, 98.
- 3 C. K. Dixit, S. K. Vashist, F. T. O'Neill, B. O'Reilly, B. D. MacCraith and R. O'Kennedy, *Anal. Chem.*, 2010, **82**, 7049.
- 4 S. K. Vashist, S. A. O'Sullivan, F. T. O'Neill, H. Holthofer, B. O'Reilly, C. K. Dixit. WO/2010/044083 (<http://www.wipo.int/pctdb/en/wo.jsp?WO=2010044083>).
- 5 B. A. Snopok, P. N. Boltovets and F. J. Rowell, *Theor. Exp. Chem.*, 2006, **42**, 217.
- 6 A. Kausaite-Minkstiniene, A. Ramanaviciene and A. Ramanavicius, *Analyst*, 2009, **134**, 2051.
- 7 R. Danczyk, B. Krieder, A. North, T. Webster, H. HogenEsch and A. Rundell, *Biotechnol. Bioeng.*, 2003, **84**, 215.
- 8 B. M. S. Richard, J. T. Anna (2008). *Handbook of Surface Plasmon Resonance*. RSC Publishing, Cambridge.
- 9 K. Aslan, J. R. Lakowicz and C. Geddes, *Curr. Opin. Chem. Biol.*, 2005, **9**, 538.
- 10 Y. Yuan, H. He and L. J. Lee, *Biotechnol. Bioeng.*, 2009, **102**, 891.
- 11 A. Holmberg, A. Blomstergren, O. Nord, M. Lukacs, J. Lundberg and M. Uhlén, *Electrophoresis*, 2005, **26**, 501.
- 12 J. Svitel, H. Boukari, D. V. Ryk, R. C. Willson and P. Schuck, *Biophys. J.*, 2007, **92**, 1742.
- 13 M. Conti, G. Falini and B. Samori, *Angew. Chem.*, 2000, **112**, 221.
- 14 C. K. Dixit, S. K. Vashist, B. D. MacCraith and R. O'Kennedy, *Nat. Protoc.*, 2011, **6**, 439.
- 15 C. K. Dixit, S. K. Vashist, B. D. MacCraith and R. O'Kennedy, *Analyst*, 2011, **136**, 1406.
- 16 G. Palasantzas, V. B. Svetovoy and P. J. V. Zwol, *Phys. Rev. B: Condens. Matter Mater. Phys.*, 2009, **79**, 235434.
- 17 L. Pan, S. Jung and R.-H. Yoon, *J. Colloid Int. Sci.*, 2011, **361**, 321.
- 18 B. Kurtinaitiene, D. Ambrozaite, V. Laurinavicius, A. Ramanaviciene and A. Ramanavicius, *Biosens. Bioelectron.*, 2008, **23**, 1547.
- 19 F. S. Willard and D. P. Siderovski, *Anal. Biochem.*, 2006, **353**, 147.
- 20 U. Jönsson, L. Fägerstam, B. Ivarsson, B. Johnsson, R. Karlsson, K. Lundh, S. Låfas, B. Persson, H. Roos, I. Rönnberg, S. Sjölander, E. Stenberg, R. Stahlberg, C. Urbaniczky, H. Ostlin and M. Malmqvist, *BioTechniques*, 1991, **11**, 620.
- 21 Y. Tang, R. Mernaugh and X. Zang, *Anal. Biochem.*, 2006, **78**, 1841.
- 22 M. J. S. Spencer and G. L. Nyberg, *Surf. Sci.*, 2004, **573**, 151.
- 23 A. Jung, T. M. A. Gronewold, M. Tewesb, E. Quandt and P. Berlin, *Sens. Actuators, B*, 2004, **124**, 46.
- 24 A. Kausaite-Minkistiniene, A. Ramanaviciene, J. Kirlyte and A. Ramanavicius, *Anal. Chem.*, 2010, **82**, 6401.
- 25 B. A. Snopok and E. V. Kostyukovich, *Anal. Biochem.*, 2006, **348**, 222.